The effect of changing climate and vegetation on the topographic evolution of catchments in the Chilean Coastal Cordillera over millennial timescales

Dissertation
der Mathematisch-Naturwissenschaftlichen Fakultät
der Eberhard Karls Universität Tübingen
zur Erlangung des Grades
eines Doktors der Naturwissenschaften
(Dr. rer. nat.)

vorgelegt von

Manuel Schmid

aus Ebersbach an der Fils

Tübingen
2019

Gedruckt mit Genehmigung der
Mathematisch-Naturwissenschaftlichen Fakultät der Eberhard
Karls Universität Tübingen.

Tag der mündlichen Prüfung	27.01.2020
Dekan	Prof. Dr. Wolfgang Rosenstiel
1. Berichterstatter	Prof. Dr. Todd Ehlers
2. Berichterstatter	Prof. Dr. Thomas Hickler

Abstract

The complex interplay between climate change, the composition and density of surface vegetation cover and physical surface processes has been a focus of scientific research in the field of geomorphology for the last few decades. The classical approach for explaining differences in topography only considers the influence of tectonic processes and lithological material constants as endogenic forcings and the effect of precipitation as an exogenic forcing, where the stabilizing effect of vegetation cover has mostly been neglected. To develop a more complete view of the complex topographic system and incorporate the dynamics between climate and vegetation, a numerical model framework consisting of a dynamic vegetation model (LPJ-GUESS) and a landscape evolution model (Landlab) was developed and tested against four different study areas situated in the Chilean Coastal Cordillera on the basis of, available paleoclimate data. These study areas were chosen based on homogeneous endogenic forcings, with a comparable tectonic uplift rate and the same granodioritic lithology, all of which allow for better parameterization of surface processes.

Three main simulation experiments were conducted: 1. LPJ-GUESS simulations, which gave insight about large-scale dynamic adjustments of vegetation cover and composition for the respective climate zones. 2. Landlab simulations which were designed to reproduce steady-state topographic metrics observed in the focus areas and to determine the reaction of the topographic system to transient, external changes in precipitation or vegetation cover 3. Coupled simulations with direct feedback during model-runtime between LPJ-GUESS and Landlab for the timeperiod since the last glacial maximum (21ka before present) to present day.

The experiments show a complex reaction of both vegetation and topography to climatic forcings, with absolute changes in vegetation cover not exceeding 10%, but large-magnitude adjustments of plant composition due to changes in climate. Simulations show magnitudes and time-scales of adjustment are highly dependent on initial catchment vegetation cover and amount of annual precipitation received. Coupled simulations show large short-term variations in catchment-mean erosion rates for very arid and very humid focus areas, while areas with mediterranean climate show lesser magnitude fluctuations but a more pronounced long-term decrease in mean erosion rates.

In summary, this thesis helps in understanding the complex climate-erosion interactions by showing the nature of the threshold-controlled system which governs the reactions of topography to natural changes in climate or vegetation cover.

Zusammenfassung

Die komplexen Zusammenhänge zwischen klimatischen Änderungen, der Vergesellschaftung und Wuchsdichte von Oberflächenvegetation und Erosionsprozessen sind schon seit Jahrzehnten ein Fokus der Geomorphologie. Der klassische Ansatz, Unterschiede in Topographischen Gegebenheiten zwischen einzelnen Gebieten zu erklären war meist nur gestützt auf die Auswirkungen von tektonischen Prozessen, lithologischen Materialkonstanten oder den erosiven Effekt von Niederschlag. Der stabilisierende Effekt einer Vegetationsbedeckung wurde hierbei meist vernachlässigt. Um eine allumfassendere Einsicht in das komplexe System von Topographien und die Zusammenhänge von Klima und Vegetation zu ermöglichen, wurde ein neues numerisches Modellsystem, bestehend aus einem dynamischen Vegetationsmodell (LPJ-GUESS) und einem Landschaftsevolutionsmodell (Landlab) entwickelt und anhand von vier verschiedenen Gebieten in den chilenischen Küsten-Kordilleren getestet. Diese Gebiete wurden ausgewählt anhand ihrer homogenen tektonischen Verhältnisse und derselben granodioritschen Lithologie, was eine genauere Quantifizierung der freien Modelparameter erlaubt.

Drei Simulationsexperimente wurden durchgeführt: 1. LPJ-GUESS Simulationen, welche Einblick in die großflächige Vegetationsdichte und Verteilung der Modelgebiete erlaubten. 2. Landlab Simulationen welche entwickelt wurden um den topographischen Gradienten zwischen den Modelgebieten darzustellen und die Reaktion der Topographien auf externe Änderungen des Niederschlags und der Vegetationsdichte zu bestimmen. 3. Gekoppelte Simulationen mit einer direkten Rückkopplung zwischen LPJ-GUESS und Landlab zur Simulationslaufzeit, für den Zeitraum zwischen dem letzten glazialen Maximum und den heutigen Bedingungen.

Die durchgeführten Experimente zeigen eine komplexe Reaktion von Vegetation und Topographien auf klimatische Einflüsse. Die maximalen Änderungen in kumulativer Vegetationsbedeckung überschreiten einen Wert von 10% nicht, während sich die relative Vergesellschaftung verschiedener Pflanzenarten stark anpasst. Weitergehend zeigen die Simulationen, dass sowohl das absolute Ausmaß als auch der Zeitraum, welcher benötigt wird um einen neuen Gleichgewichtszustand zu erreichen vom Initialzustand des Systems abhängt.

Zusammengefasst hilft diese Arbeit dabei die komplexen Zusammenhänge zwischen Klima und Erosion besser zu verstehen indem das Schwellenwert kontrollierte System welches die topographischen Reaktionen auf Änderungen in Klima und Vegetationsbedeckung tiefer erforscht.

Acknowledgments

Foremost I want to thank my supervisor Prof. Todd Ehlers. Thank you for giving me the chance to work on this project, which I can only describe as one of the hardest and most rewarding challenges I've been through so far. In this context I also want to thank the whole ESD - working group for productive discussions, more cool ideas than I will ever be able to process and an open ear, whenever I needed one. In this context I need to give Kirstin some special remarks, since you were not only part of my working group but also the person who coordinated most of the meetings that I went to and I think you were the main part why these meetings were always a very pleasant experience. Also I want to say a special thank you to Christian, my late-night python helpdesk, writing companion and all-around nice guy.

Thanks to Todd (again) and Friedhelm and all the other PI's which put such a great project together and worked relentlessly to get it funded. Thanks to the DFG who appreciated how great this project really is and finally funding it. Thanks to Daniel Hobley and the whole developer team behind Landlab for putting together such an awesome modelling framework which I could build upon.

Apart from this, I spent too much time in Tübingen to possibly thank all the important people I met during this time but I feel that I need to address some persons which were not only nice to have around but absolutely mandatory in keeping myself together. Writing this thesis has not been easy for me. It took a larger impact on my personal life than I ever thought it would and there certainly were more than enough times were I was ready to quit. Thank you Eva for being so tolerant on my time management the last few months and accepting that this is just something I need to finish and supporting me no matter what. Thank you Sasan, Jule, Sami and Jascha for regularly showing me what a good life can look like. Thank you Marius, Simon and Lennart for listening to me ramble on about how stressed I was, especially when it was after 2am in the morning. Thank you Karen for endless balcony sessions and life discussions. Thank you Miro for reminding myself what I am capable to do. Thank you Robin for spontaneous weekend escapes which helped keeping the adrenaline level high and the stress level low.

Last but not least, of course I need and want to thank my family. Without you, I would not be here today and only your great and ongoing support enabled me to pursue this road and do what I love.

Contents

List of Figures (excluding manuscripts)

List of Tables (excluding manuscripts)

1 Introduction

It has long been suspected that the appearance of biotic life on the Earth's surface had a considerable impact on the governing processes that determine the shape and structure on our present-day topography. Deciphering the laws which apply to the complex system of topographic evolution, is a step towards a more fundamental understanding about the nature of the world that we see around us and is also mandatory for gaining insight into a more sustainable approach of decision making to preserve the current state of the Earth.

While the general effect of vegetation cover as a ground stabilizing agent has been recognized by previous generations and has a long history of research within the fields of geomorphology, biogeography and agricultural engineering, the topic still poses a complex and difficult problem with a lot of unanswered questions and not very well constrained answers.

The main concept that anyone who wants to develop a integrated theory of the effect of biota on surface processes needs to address, is the feedback between climatic processes which have a direct and immediate effect on the erosion and transport of sediment, for example by increasing overland flow runoff through increasing precipitation, and the biotic processes, which have a indirect effect through accumulation of biomass on the Earth's surface and hence modulating the physical parameters of bedrock and sediment. This modulation is generally thought of as to increase resistance to external eroding agents.

This thesis aims to further the knowledge on this topic by investigating the effect that the introduction of vegetation cover has on the evolution of landscapes by integrated landscape evolution modelling of study areas in the Chilean Coastal Cordillera. For this purpose, a model framework was developed that encompasses both a dynamic vegetation model and a landscape evolution model which were used to understand the sensitivity of landscape topographies and erosion rates to both steady-state and transient forcings of precipitation and vegetation cover and composition.

The structure of the thesis incorporates an introductory chapter which aims to give an overview about the commonly accepted effects of vegetation cover on underlying landscapes, the state-of-science and general theory behind numerical landscape evolution modelling and dynamic vegetation modelling and the techniques and field areas that were utilized in this study. This is followed by a chapter which describes the hypothesis and research questions that were addressed during this study. The next chapter then shows the obtained results which were the outcome of the work done in the form of manuscripts, either published or in manuscript form. The last chapter then aims to summarize the obtained results and

revisits the previous stated hypothesis for a discussion of the obtained knowledge and an outlook for potential future work.

1.1 Effects of vegetation on surface processes

The effects that either a constant or a changing vegetation cover has on surface processes, always needs to be viewed in the context of coeval climate change. Changes in precipitation or temperature act as the drivers which create conditions that lead either to a steady-state vegetation cover, which does not show large fluctuations over time, or disturbances that lead to transient shifts in density, distribution and the composition of plant types within a catchment.

An exception of this is the case of human induced land-use change (e.g large-scale deforestation, monocultural agriculture) which lead to an increase in soil erosion rates since the neolithic revolution, in catchments with large anthropogenic overprint [Hewawasam, 2003, Anselmetti et al., 2007, Kaplan et al., 2009, Williams, 2009]. While these effects have a large impact on certain regions and are an important field of study on their own, this thesis focuses on the natural changes of vegetation cover which accompany the changes in climate since the last glacial maximum (21ka B.P) in the Chilean Coastal Cordillera.

The presence of vegetation influences the various physical or chemical processes either directly, where plants have an active feedback on the material properties of the land surface or indirectly, where the existence of vegetation leads to a modulation of other processes which influence erosion and sediment transport. The next few paragraphs describe these various direct and indirect mechanisms.

The most prominent direct feedback of vegetation on land surface is an increase in slope and streambank stability [Operstein and Frydman, 2000, Simon and Collison, 2002, Norris et al., 2008, Kokutse et al., 2016]. This is commonly attributed to root reinforcement of soil cohesion which increases the shear-stress resistance and therefore the resistance to erosion and transport of material [Kadlec, 1990, Roering et al., 2003, Fan and Su, 2008, Preti and Giadrossich, 2009, Liang et al., 2017]. This leads to a higher resistance of root penetrated surface material to both internal and external shear stresses which manifests in higher critical slope angles for vegetated surfaces compared to bare, non-vegetated slopes [Riestenberg and Sovonick-Dunford, 1983, Stokes et al., 2008, Eab et al., 2015]. In channels, the effect of increased shear stress resistance leads to an increase in channel relief and less lateral channel migration, due to higher stability of channel bank and bed material [Gran and Paola, 2001, Murray and Paola, 2003, Nikora et al., 2008]

Apart from this direct, mechanical effect that vegetation cover exercises on surface materials, there exists an associated indirect, ecohydrological influence of surface process modulation by vegetation. The existence of plants impacts the net water mass balance of a specific surface area by enhancing flux of water vapour into the atmosphere by evapotranspiration [Bosch and Hewlett, 1982, Costa and Foley, 1997, Zhang et al., 2001, Nachabe et al., 2005]. Through the increase of microporosity and microfractures by root stems, vegetation also increases the flux of water into subsurface water layers due to enhanced infiltration and therefore negatively impacting hortonian runoff production [Dunne et al., 1991, 1995, Descheemaeker et al., 2006]. In summary, these effects reduce water availability to overland flow, which is directly associated with the erosion and transport of sediment [Hairsine and Rose, 1992, Ludwig et al., 2005, Ebabu et al., 2019].

An additional indirect effect of vegetation cover, which is not directly linked to either mechanical or ecohydrological properties, is the impact on erosion and transport of material by stochastic processes which act on vegetated hillslopes. A ground covering canopy layer acts in two ways: it disperses incoming rain droplets, therefore modifying maximum drop size [Brandt, 1989] and it reduces impact velocity of rain droplets, if the canopy height is below 1m [Stocking and Elwell, 1976, Geißler et al., 2012]. This reduces the amount and distance of material transported by rainsplash erosion [Dunne et al., 2010, Saedi et al., 2016] which, when viewed over a hillslope length scale, decreases the sediment flux from hillslopes to adjacent river channels [Michaelides et al., 2009].

While there are other effects of vegetation cover on surface characteristics, e.g controls on dominant sediment grain size for different vegetation covers [Yang et al., 2008], the processes that were described in the previous paragraphs are the ones most dominantly used for explaining large scale landscape response to vegetation cover and are therefore in the focus of this thesis.

Among the first researchers to quantify the complex effect of vegetation cover on erosion processes were Langbein and Schumm [1958] who recognized that the annual sediment load of basins is a non-linear function of the mean annual precipitation that is received by the corresponding catchments (Fig. 1, left side).

This non-linear relationship between sediment yield and precipitation shows the complex interrelated processes which act on the surface of landscapes due to the constant competition between precipitation, which is known as an increasing agent of erosion and vegetation cover, which modifies ecohydrological properties and mechanical soil properties. The general shape of this relationship was reproduced by various other studies that explored denudation

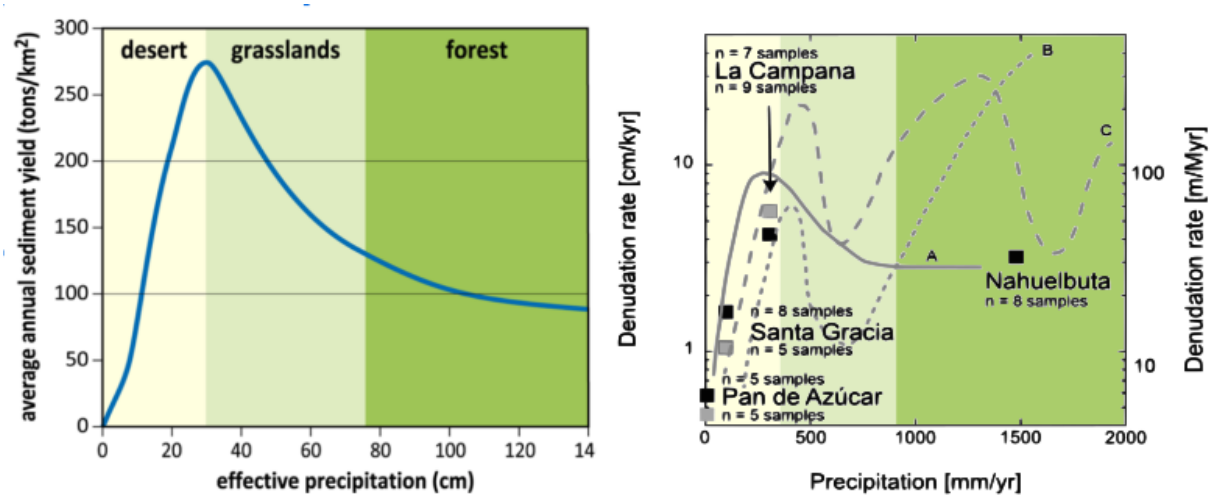

Figure 1: Average annual sediment yield for catchments with varying values of effective precipitation (after Langbein and Schumm [1958]). The data shows a distinct peak in sediment yield for values of effective annual precipitation of 300 mm, which marks the boundary between desertic conditions and grass dominated landscapes. Values of sediment yield decrease strongly for higher values of effective precipitation although the slope of the curve decreases going to more humid conditions. Right side shows depth-profile denudation rates modified from Schaller et al. [2018]. Colorcoding of biomes is equal to left panel. Data indicates same trend between denudation rates and precipitation for the Eartshape study areas as the average sediment yield data from Langbein and Schumm [1958]

rates across catchments situated in different climate zones (Fig. 1, right side; Schaller et al. [2018]) which gives evidence for a non-linear relationship which governs the interplay between surface processes and the combination of precipitation and vegetation cover.

Overall surface vegetation cover is, in most ecosystems, positively correlated with mean annual precipitation [Xin et al., 2008] for plant compositions that show water-limitation [Yu et al., 2003]. In certain bioecological systems, the density of vegetation cover is more controlled and limited by temperature [Kong et al., 2017] but mean annual precipitation and associated soil-moisture values always show a significant impact on growth rates and vegetation stability except for very humid ecosystems where rainfall variability over short time-scales does not lead to drying out of surface soil.

This interplay between the dependency of vegetation cover density to mean annual precipitation, leads to a threshold behaviour where the increase of precipitation that is required to significantly increase the surface vegetation cover gets larger for areas that are situated in a more humid climate with high initial values of vegetation, compared to sparsely-vegetated, arid areas [Schmid et al., 2018]. This is thought to lead to a in-

equilibrium between water availability to geomorphic processes, which enhances erosion, and an increase in surface vegetation cover, which restricts erosive processes and therefore leads to the proposed relationship depicted in Fig. 1. The research carried out and described in this thesis aims to give a better quantitative insight about the threshold behaviour of the vegetation-precipitation relationship and how catchments in different climate zones react to these boundaries.

In the next chapter, the methods that are used in this study are defined and the value of numerical modelling as a tool for answering complex questions in a controlled, synthetic environment is explained.

1.2 Landscape evolution modelling

As described in chapter 1.1, the interplay between climatic changes and changes in surface vegetation cover, is complex and highly non-linear, which makes it difficult to distinguish between the resulting topographic signals of individual processes that can be attributed to one or the other of these competing effects. The dawn of dating techniques, based on cosmogenic nuclides, that allow scientists to constrain erosion rates on short-timescales (10^3 - 10^5 yrs; Lal [1991], von Blanckenburg [2006]) for whole drainage systems makes it possible to gain information about mean erosion rates for catchments located in different climate zones and with varying climatic history. Since these erosion rates are still a composite of both the effects of climate change and associated vegetation changes, methods are needed to deconstruct those rates into their individual influences.

Numerical modelling has emerged as a valuable tool for not only understanding past topographic evolution based on tectonics, lithology and climate change [Howard, 1997, Willgoose, 2005, Tucker and Hancock, 2010] but also for understanding the effect of vegetation cover on topographies [Collins and Bras, 2004, Istanbulluoglu et al., 2004, Istanbulluoglu and Bras, 2005, Istanbulluoglu et al., 2008, Collins and Bras, 2010]. Process-based models for computing topographic changes lead to a more precise understanding of the time-sensitive evolution of landscapes, away from a purely descriptive, qualitative model approach to a more precise, quantitative approach of determining individual rates of changes within catchments (see Fig. 2).

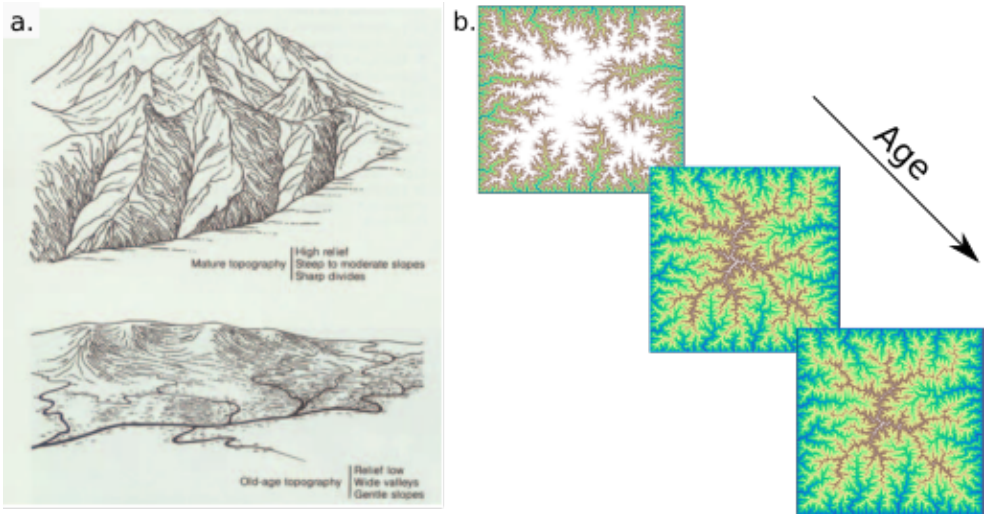

Figure 2: Left side of the figure (a.) shows a classic, conceptual form of qualitative landscape evolution model which utilizes a purely descriptive approach to distinguish between a mature (top) and old-age (bottom) landscape (modified from Tucker and Hancock [2010]). Right side (b.) shows exemplary output of a modern landscape evolution model (Landlab) and depicts the evolution of a landscape as a result of tectonic, fluvial and hillslope processes for different timeslices.

1.2.1 General model formulation

Landscape evolution models (LEM's) make use of mathematical descriptions of natural occurring processes to give insight about shape, patterns and rates within simulated model domains. While the specifications between different LEM's differ in terms of grid-meshing, minimum and maximum resolution and incorporated processes, which makes certain LEM's more effective for specific tasks, most LEM's can be described by three general equations:

- Mass Balance Equation
- Equation for erosion/transport by fluvial processes
- Equations for erosion/transport by diffusive hillslope processes

The mass balance equation therefore can be represented by a combination of these governing processes:

$$\frac{\delta z(x,y)}{\delta t} = U - \frac{\delta h(x,y)}{\delta t}|_{\text{fluvial}} - \frac{\delta h(x,y)}{\delta t}|_{\text{hillslope}} \tag{1}$$

where the term on the left is the overall topographic change over time, the first term on the right is the tectonic uplift rate, the second term on the right represents the amount

of elevation change over time due to fluvial processes and the last term on the right is the amount of elevation change over time due to processes linked to diffusive hillslope processes.

Fluvial processes

The erosion of material through fluvial processes is generally represented with the stream-power-model, which consists of a suite of equations, designated to provide a accessible, numerically stable and computational feasible solution, yet capturing enough complexity of the underlying processes to give testable, realistic answers. The basic equation of the stream-power-model is a power law function of excess shear stress [Howard and Kerby, 1983, Howard et al., 1994, Tucker and Slingerland, 1994, Howard, 1997, Ferguson, 2005]

$$E = k_e(\tau_b - \tau_c)^\alpha \tag{2}$$

where E is the incision rate of a bedrock channel, τ_b is the bed shear stress, τ_c is the threshold bed shear stress that needs to be exceeded for detachment of bedrock, α is a constant scaling exponent, which is depended on the main process of detachment of material and k_e is the the shear stress coefficient, which is used to describe the general efficiency of fluvial processes in a specific tectonic and lithological setting [Lague et al., 2000, Snyder et al., 2003, Robl et al., 2017]. Since the exact value of bed shear stress is hard to determine in a natural setting, it is generally formulated as a derivation of the mannings equation as a function of local bed slope and discharge [Istanbulluoglu et al., 2004]

$$\tau_b = \rho g n_b^\alpha Q^\alpha S^\beta \tag{3}$$

where ρ is the density of water, g is the acceleration of gravity, n_b is the mannings roughness coefficient which is a metric of surface resistance to overland flow, S is total bed gradient at each point in the channel and Q is the surface water discharge for each point in the channel which can be represented as the drainage area A of each node times the received precipitation ($Q = A * P$). Values α and β are positive, constant exponents. Combining equation 2 with equation 3 leads to the classic version of the stream-power equation [Stock and Montgomery, 1999]

$$\frac{\delta h(x,y)}{\delta t}|_{\text{fluvial}} = K_f(A * P)^m S^n \tag{4}$$

where K_f is the coefficient of incision ($K_f = k_e \rho g n_b^{\alpha}$), A and S are the drainage area and the bed slope for each node in the grid and m/n are process-dependent exponential parameters.

This set of basic equations was used for numerous studies in landscape evolution modelling and was tested to predict realistic results [Whipple et al., 1999, Lague, 2014, Harel et al., 2016] for reproducing longitudinal river profiles and erosion rates.

Hillslope processes

Material flux on hillslopes in evolving landscapes represents a complex system which encompasses a large variety of different processes that all tend to move sediment along the topographic gradient which is initially set by the river networks [Burbank et al., 1996, Larsen and Montgomery, 2012]. These processes are generally thought of as having a strong stochastic nature (e.g tree-throw, rainsplash, bioturbation, frost cracking; Furbish et al. [2009]) and differ in effectiveness between areas due to lithologic parameters and climatic limits [Jones, 2001].

The most-common approach to integrate this variety of processes in a computational effectice way for large-scale landscape evolution modelling is the formulation of hillslope flux as a diffusive process which is dependent on the local topographic slope:

$$-\frac{\delta h(x,y)}{\delta t}|_{\text{hillslope}} = \nabla q_{sd} \tag{5}$$

In the above equation, the term on the left side is the change in elevation at each point in the landscape which is a result of diffusive hillslope processes and the term on the right ∇q_{sd} is the divergence of sediment flux. This flux is most commonly denoted as being linear dependent on local slope so that q_{sd} can be formulated as a representation of Fick's law of diffusion

$$q_{sd} = K_d S \tag{6}$$

In this representation of diffusive processes, q_{sd} is equal to the sediment flux along a hillslope, K_d is the diffusivity parameter which describes the efficiency of material transport and S is the local slope, which is equal to the potential energy gradient, posed by differences in topographic elevation ($S = \frac{\delta z}{\delta x}$).

By combination of the fluvial and hillslopes erosion laws and substituting the respective term in the mass balance equation (Eq. 1), the general formulation of elevation change at each node per timestep can be derived:

$$\frac{\delta z(x,y)}{\delta t} = U - \nabla K_d S - K_f (A * P)^m S^n \tag{7}$$

In this formulation, the change of topography within a landscape is mostly dependent on the local slope S, the amount of precipitation P and the two parameters describing efficiency of erosion and transport by hillslope and fluvial processes K_d and K_f. The next chapter of the thesis goes into more detail about the possibilities to represent the effect of vegetation on these surface processes within this basic model framework and the resulting implications.

1.2.2 Representing vegetation in surface process equations

To enable researchers to make use of numerical models to predict landscape changes as a function of not only climate but also of a static or dynamic vegetation cover, it is necessary to formulate surface process equations which incorporate a metric that is related to the density of vegetation within a landscape. This density is mostly expressed by one of the following two metrics: leaf area index (LAI) or foliar projected vegetation cover (FPC). There are other metrics, related to the density and type of vegetation, which can be used to express individual physical processes (e.g root density and depth) [Baets et al., 2008], but these are difficult to constrain by remote sensing and are mostly used in smaller-scale engineering applications.

LAI gives a measurement of the total green leaf area per unit ground area ($LAI = Total\,Leaf\,Area\,/\,Total\,Ground\,Area$) which can be derived effectively as a function of the normalized difference vegetation index (NDVI) by various remote sensing techniques [Kerr and Ostrovsky, 2003, Peng Gong et al., 2003, Wang et al., 2005]. LAI is widely used in the fields of ecology to estimate net primary productivity (NPP) since it directly relates to the green above-ground biomass [Leverenz and Hinckley, 1990, Barigah et al., 1994, Clark et al., 2007].

FPC is defined as the ratio between the vertically projected area of vegetated ground to the total ground area ($FPC = Vegetated\,Area\,/\,Total\,Ground\,Area$) and ranges from 0% for barren, non-vegetated ground to 100% for completely vegetated ground. FPC can be derived from LAI values following the Lambert-Beer-Equation [Prentice et al., 1993]:

$$FPC[\%] = (1 - exp(-0.5LAI)) * 100 \tag{8}$$

The FPC value is commonly used in landscape evolution modelling due to its advantage of a more representative parameter-space with values ranging between 0% and 100%, while remote sensing derived LAI values do not fit in a fixed range of values and are therefore more complex to interpret. The following paragraphs give an overview how the surface process equations laid out in chapter 1.2.1 can be modified to incorporate FPC as a controlling factor for erosion/transport effectiveness.

FPC dependency of fluvial process equations

Deriving equations for a vegetation cover influence of fluvial erosion processes is commonly done by building on the formulation of bed-shear stress (Eq. 3) by expanding the concept of the mannings roughness parameter n_b. This parameter is derived from the original mannings equation which is used in surface hydrology to estimate the velocity of a fluid flowing through a defined cross-section [Manning, 1891]

$$V = \frac{1}{n} R_h^{2/3} S^{1/2} \tag{9}$$

With V being the average flow velocity, R_h being the hydraulic radius and S being the local slope. The parameter n is a way of describing the resistance of a certain channel or surface to the direct flow of a medium. n is dependent on a variety of factors including channel shape, medium grain size, bed-form and bed-cover and therefore includes vegetation. n has been empirically derived for different channel types and different vegetation covers [Chow, 1959] and can therefore be used for describing the effects vegetation cover on the effectiveness of erosion through overland flow. The n values for the total mannings roughness of a surface can be expressed as a linear combination of different roughness values for the according vegetation types, hence resulting in a value for n which encompasses all possible plant-types found in the area of interest:

$$n_{total} = n_{base} + n_{Veg.TypeI} + n_{Veg.TypeII} + ... \tag{10}$$

With n_{Base} being the determined roughness of the barren ground without vegetation and $n_{Veg.Type}$ being the mannings value for the respective types of vegetation. Following this approach, the combination of the mannings equation (Eq.9), the bed shear stress equation

(Eq.3) and the stream-power equation (Eq. 4) yields (for more detailed derivation see Collins and Bras [2004], Istanbulluoglu and Bras [2005], Schmid et al. [2018]):

$$\frac{\delta h(x,y)}{\delta t}|_{\text{fluvial}} = k_e \rho g n_{total}^m (\frac{n_{Base}}{n_{total}})^{3/2} (A * P)^m S^n \tag{11}$$

Which describes the change of elevation at each node not only as a function of the discharge and local slope (compare Eq.4) but also with a dependency of the mannings value at each node n_{total}. Since the mannings values for different vegetation types only give a way of describing flow resistance for a type of vegetation but not as a function of the density of vegetation cover, the total mannings value n_{total} is reformulated to be a function of FPC of specific plant types:

$$n_{total} = n_{base} + n_{Ref,Veg.TypeI} \frac{FPC_{Veg.TypeI}}{FPC_{Ref,Veg.TypeI}} + n_{Ref,Veg.TypeII} \frac{FPC_{Veg.TypeII}}{FPC_{Ref,Veg.TypeII}} + ... \tag{12}$$

Where n_{Base} is the mannings value for barren ground, the different values for n_{Ref} are mannings roughness values for a specific type of vegetation, values for FPC are surface vegetation cover values for the specific plant type and FPC_{ref} values are vegetation cover values for which the reference mannings roughness values are obtained (commonly choosen to be a fully vegetated surface, $FPC_{ref} = 100\%$). As with the standard formulation ob mannings values (Eq. 10), this equation can be linearly expanded to encompass different types of vegetation cover.

The combination of equations 11 and 12 gives a possibility to describe the fluvial erosion of material as a function of the percentage vegetation cover values of different types of vegetation and therefore provides a tool to numerically determine how the plant system within a catchment influences the erosion by overland flow and the river network itself with higher values of vegetation cover leading to less effective erosion of bedrock or sediment through increases in the total mannings coefficient.

FPC dependency of hillslope process equations

This section intends to give an overview about the vegetation effect of diffusive hillslope processes and how they can be represented in the equations for hillslope erosion laid out in chapter 1.2.1. Compared to the numeric representation of vegetation effects in the fluvial process equations with the mannings equation, there exists no common accepted framework or parameter which directly describes the hillslope erosion and transport as a function of

vegetation cover. Since the general accepted form of a hillslope transport law equals either a linear or non-linear diffusion equation with topographic slope as the main driving gradient (Eq. 5), it is possible to define a vegetation influence on the diffusivity parameter K_d, since this parameter as derived from the first fick's law of diffusion, gives a metric about the mobility of mass or particles along a gradient [Foufoula-Georgiou et al., 2010].

There is ongoing discussion about the effect that vegetation has on the hillslope diffusion coefficient. There is evidence that an increase in vegetation cover due to the stabilizing effects of an increase in soil cohesion leads to a less effective transport of material along a hillslope and therefore a negative relationship between K_d and FPC (see chapter 1.1, Jahn [1989], Istanbulluoglu and Bras [2005]).

Other studies suggest that soil creep rates are higher for densely vegetated forest areas, compared to arid areas with only sparse vegetation [Roering et al., 2002, Perron, 2017]. This is attributed to bioturbation and tree throw processes that have a higher occurrence interval for areas with larger vegetation cover and potentially higher values for soil creep initiated by rain splash, where the effect of higher precipitation outweighs the effect of canopy shielding from vegetation.

This thesis focuses on the first case, where an increase in vegetation is negatively correlated with the hillslope diffusivity factor K_d, since there exists better constrained evidence as a foundation for the numerical implementation [Prosser and Dietrich, 1995].

The assumption that an increase in surface vegetation cover decreases hillslope diffusivity is translated in a negative power law where K_d is a function of a baseline diffusivity K_b which represents the maximum diffusivity for a barren landscape without the presence of vegetation and an exponential which takes into account the FPC values for each node (for further information see Schmid et al. [2018]) and a scaling factor α:

$$K_d = K_b \exp^{-(\alpha * FPC)} \tag{13}$$

This results in a equation for the elevation change over time due to hillslope processes which is dependent on the local slope S and the percentage vegetation cover for each node:

$$-\frac{\delta h(x,y)}{\delta t}|_{\text{hillslope}} = -\nabla K_b \exp^{-(\alpha * FPC)} S \tag{14}$$

With the equations derived in this section for fluvial and hillslope processes as a function of vegetation cover, it is possible to numerically investigate the effect of vegetation cover on

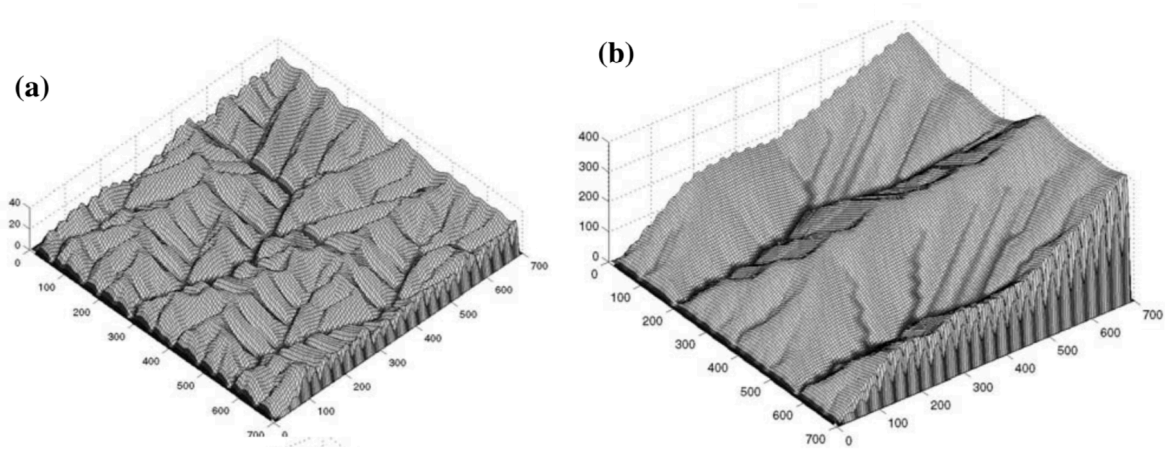

Figure 3: Example model output of landscape evolution model (CHILD) with vegetation implementation (from Istanbulluoglu and Bras [2005]). Left side shows simulation for unvegetated conditions and right side for simulation with vegetated ground. The unvegetated landscape shows a higher grade of dissection, lower slope and lower total elevation while the vegetated simulations shows lower drainage density, higher relief and slopes.

large scale landscape evolution over time (see Fig.3). Table 1 provides an overview about important parameters and their respective units.

1.3 Dynamic vegetation modelling

This section is designed to give an overview over common practices in dynamic vegetation modelling and the applications within geomorphology. Predicting the evolution of the density and composition of large-scale vegetation cover as a function of climate change, nutrients and physiological traits is of interest in a variety of different fields ranging from palaeontology, botany, agricultural engineering, climate research and geomorphology.

Especially in geomorphology, with the recent efforts to build a more extensive theoretical basis of the effect of vegetation on topographic evolution, the development of global dynamic vegetation models (GDVM's) helps by creating the possibility to simulate transient effects in the composition of vegetation types, vegetation structure, external vegetation dynamics (e.g tree-throw, fire) and biochemical cycles of nutrients and water between plants and soil [Fisher et al., 2010, Werner et al., 2018].

Table 1: Model Parameters used for derivation of main equations.

Parameter	Unit	Description
U	mm/yr	Tectonic Uplift
dx, dy	m	Node Spacing
FPC	%	Foliar projected vegetation cover
k_e	m/yr(kg/m yr^2)$^{-p}$	SPL scaling factor
τ_b	kg * m^{-1} * yr^{-2}	Bed Shear Stress
τ_c	kg * m^{-1} * yr^{-2}	Critical Shear Stress
ρ	kg/m^3	Water Density
g	m/s^2	Acceleration of Gravity
n_{base}	s/(m$^{(1/3)}$)	Base Mannings Coeffcient
n_{Ref}	s/(m$^{(1/3)}$)	Reference Mannings Coeffcient
n_{Total}	s/(m$^{(1/3)}$)	Total Mannings Coeffcient
Q	m^3/s	Water Discharge
A	m^2	Drainage Area
P	mm	Mean Annual Precipitation
S	m/m	Topographic Slope
α, β	-	Shear Stress Exponents
m, n	-	Stream Power Exponents
K_d	m^2 / yr	Hillslope Diffusivity
K_b	m^2 / yr	Baseline Diffusivity
K_f	1/m	Fluvial Erodibility

While there exist many versions of different GDVM's, this thesis focuses on a version of the Lund-Potsdam-Jena General Ecosystem Simulator (LPJ-GUESS, Smith et al. [2001]) which was used in obtaining the presented results. This thesis aims to give a overview about the general processes implemented into LPJ-GUESS and not a full explanation about the underlying equations.

LPJ-GUESS is a individual-based second-generation vegetation model which incorporates forest-gap dynamics [Smith et al., 2001, Sitch et al., 2003]. The plant composition within an model domain is simulated by means of plant functional types (PFT), which represents different classifications of non-phylogenetic groupings of different plant species that are classified by their reactions to external forcings, use of nutrients and resources, growth form and photosynthetic pathway (C_3 or C_4) (see Fig. 4; Box [1996], Duckworth et al. [2000]).

Biochemical processes (e.g plant respiration, photosynthesis, litter decomposition) and hydrologial processes (e.g water flux through soil hydrology and stomatal regulation) are

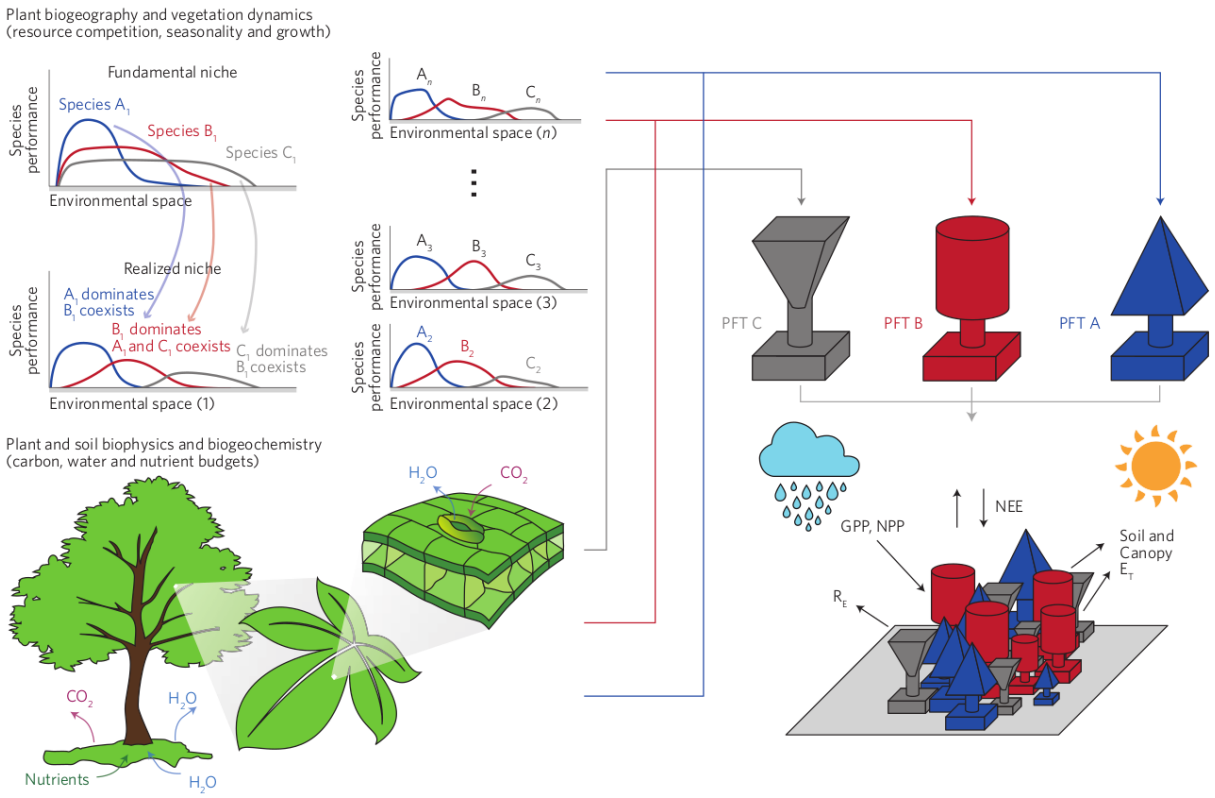

Figure 4: Example of plant functional type classification scheme (from Arneth et al. [2014]). Upper left shows the fundamental and realized species performance over an environmental space for different species. These niches are a function of cumulative plant traits (e.g stomata conductance, depicted in illustration bottom left). Plant functional types (PFT's) consist of a number of species which show similar growth characteristics (and therefore the same species performance in the same environmental space).

simulated on a daily timestep while larger-scale biotic processes (e.g plant establishment and mortality, biomass allocation) are modelled on a yearly timescale.

PFT population density in LPJ-GUESS is a function of the establishment rate of new individuals, the mortality rate of old individuals and loss of individuals through disturbances. Establishment rate is calculated on the PFT cohort level, which represents a new age-class of an individual PFT. Cohort establishment is dependent on a expected maximum rate and a function which determines the maximum potential productivity of the forest floor, which depends on shade that is cast on the floor by existing species, the soil water and nutrient content and temperature. Therefore cohort establishment is most effective either at the starting point of a simulation, with no large individuals present or after a disturbance which creates unshaded space to establish new individuals.

Mortality rate is determined as a stochastic function which determines the minimum background mortality rate as function of the PFT cohorts current age and and maximum expected life span of the observed PFT. Apart from the age-based mortality, a stress mortality is implemented to represent risk of PFT death by non-optimal growth conditions. This stress mortality is a function of a PFT-specific maximum potential productivity and the individual leaf area index, which is a metric describing how a PFT makes use of its growth potential.

Disturbances in LPJ-GUESS are manifold, ranging from draught to tree-throws and fires. These events are modelled as random events with a defined probability and therefore a case specific frequency distribution. Disturbance events kill all affected individuals and make room for the establishment of new species cohorts.

Since the highly stochastic nature of these modelled processes makes it difficult to make predictions for a specific modelled region, LPJ-GUESS simulates vegetation dynamics on a defined number of replicate patches. A patch size is defined so that a large individual of a PFT that is simulated still has influence over the defined area and usually has a value of 1000 m^2. While the individual patches can show large variations in PFT composition and density due to stochastic disturbances, the values of a sufficient number of patches will converge towards a mean value that is a function of input parameters and boundary conditions.

1.4 The Earthshape project

The research that is presented in this thesis was conducted within the framework of a integrative DFG-sponsored research project "Earthshape: Earth Surface Shaping by Biota" (*www.earthshape.net*), which focuses on the research questions of how different types of biotic life affect physical and chemical processes in the Earths critical zone and therefore contribute in shaping the Earth's surface.

The underlying goal of the Earthshape project is a synthesis from several sub-projects that work on different time and spatial scales, from small-scale, short-term microbiological processes to large-scale, long-term geomorphic processes. In order to achieve comparable results, all sampling for different sub-projects was performed in four study areas along the Chilean Coastal Cordillera (see Fig. 5).

The four study areas, chosen as research grounds, show traits that make them ideal for quantifying the respective scientific questions since they show a distinct North-South orientation along the Chilean Coast and span over approximately 15°latitude (approx. 1500

km) and therefore capture a large variation in climatic and ecological gradient. Furthermore they show no signs of recent glaciations since LGM conditions and no significant differences in the respective tectonic and lithologic setting. This allows topographic comparisons between the areas without the need to correct for or include glacial overprint, different uplift rates or physical and chemical material properties of the bedrock.

The Earthshape study areas include (from North to South): **Pan de Azucar** (26°S), which is situated near the city of Chanaral, is a arid, desertic environment with sparse vegetation, mainly consisting of cacti and shrubs and a total ground cover of approximately 10%. Present day mean annual precipitation and temperature is approximately 10 mm and 18°C.

The study area of **Santa Gracia** (30°S), located NE of the city of La Serena, is situated in a semi-arid climate zone with a mean annual precipitation of approximately 156 mm and a mean annual temperature of 14.9°C. Vegetation consists mainly out of shrubs and cacti with a total vegetative ground cover of approximately 30%.

La Campana study area (32°S) is located NW of Santiago de Chile. It is situated in a mediterranean climate zone with a approximate annual precipitation of 360 mm and a annual temperature of 14°C. Vegetation is dense with a ground cover of approximate 70% and a rich composition of species from evergreen sclerophyllus trees to a variety of shrubs and grasses.

Most southern area **Nahuelbuta**, located East of the city of Angol shows a temperate climate with a annual precipitation of 1400 mm and annual temperature of 8.1°C. Vegetation is very dense with an almost 100% ground cover and consists of a broad variety of trees, shrubs and grass.

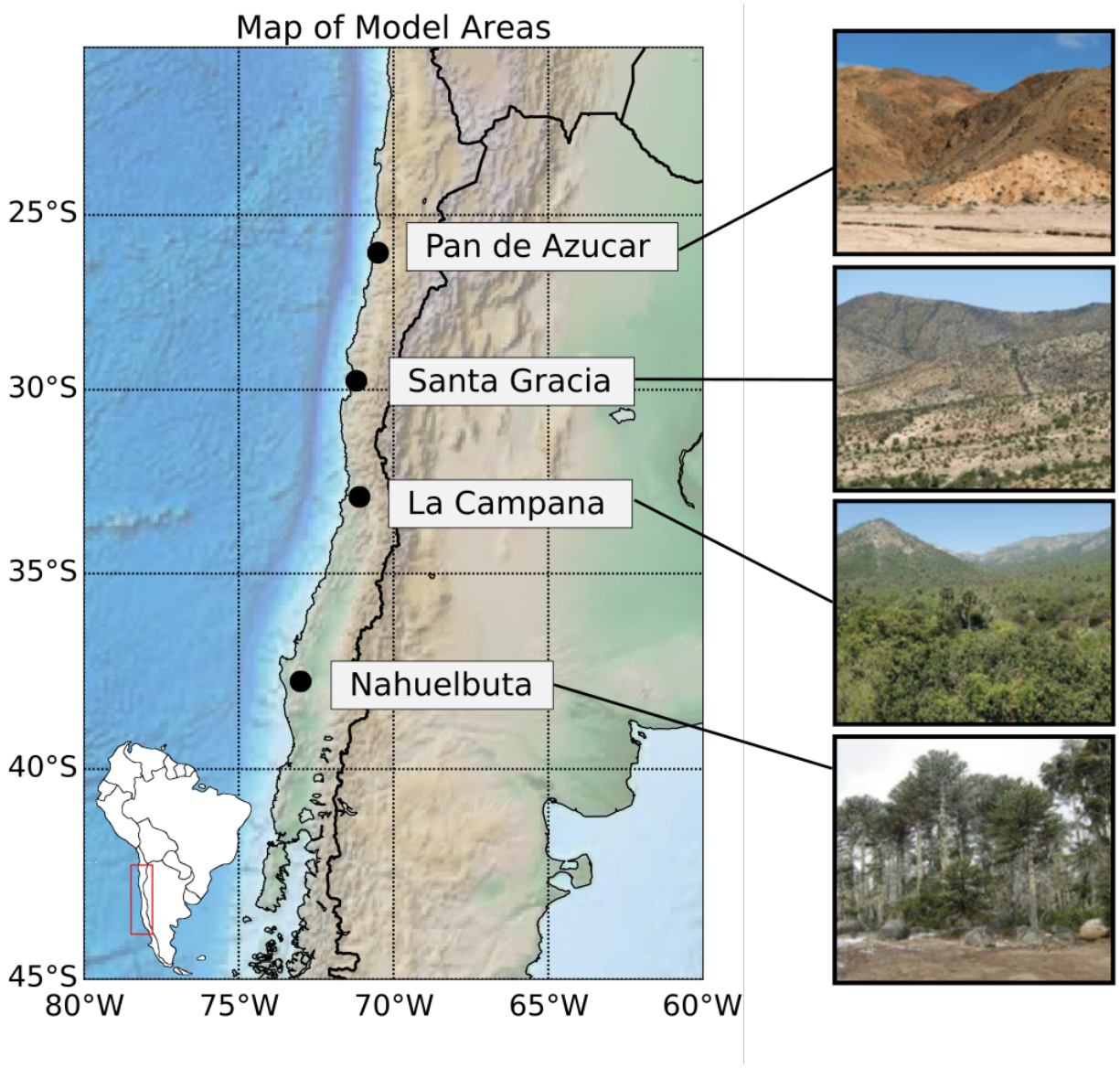

Figure 5: Map of Earthshape study areas that were used in this thesis. Northern area Pan de Azucar shows very arid, desertic environment with only sparse vegetation. Santa Gracia is situated in a semi-arid enviroment with patchy vegetation, mostly consistent of shrubs and cactii. La Campana area shows a mediterranean climate with forest-like vegetation. Southern area Nahuelbuta lies in a humid climate zone with very dense, nearly full, vegetation cover with a rich and diverse composition of different trees, shrubs and grasses.

2 Examined Hypothesis and conceptual approach

While the previous chapters explained the general concepts of biogeomorphology and the methods and study areas used in obtaining the presented results, this chapter gives explanations about the main hypothesis that were the foundation of this study and the conceptual approach that was used for determining the validity of the following hypothesis.

(I) The effects of vegetation cover on surface processes occur over temporal and spatial scales shorter than geologic processes (e.g. rock uplift, climate change). However, short term vegetation effects on topography are recorded over geologic timescales in the form of variations in different topographic metrics (e.g relief, slope, channel steepness)

(II) Climatic change since the last glacial maximum has lead to an increase in the density and changes in the composition of vegetation cover and has a measurable stabilizing effect on catchment properties such as mean erosion rates, relief or slope in the Chilean Coastal Cordillera.

In the next subsections, a more detailed view of the initial assumptions and the approach which was chosen for answering these hypothesis is given. The more complete outcome of the conducted research is given in chapter 3 in the form of two published manuscripts and one manuscript that is in preparation.

2.1 Hypothesis (I): Vegetation cover controls over topographic evolution

Steady State Catchment Conditions affected by Vegetation cover

The stabilizing effect of vegetation cover on the Earth's surface has long been recognized as was described in chapter 1.1. Although this knowledge was utilized widely within the fields of eco-engineering and agricultural engineering [Norris et al., 2008, Fattet et al., 2011, Vannoppen et al., 2017], the stabilizing effect that changes in vegetation cover exerts on topographies at the catchment level was so far mostly qualitatively described and the sensitivities of topographic forcings to shifts in the density and composition of vegetation cover were not constrained within the context of realistic climatic changes [Collins and Bras, 2004, Istanbulluoglu and Bras, 2005, Murray et al., 2008].

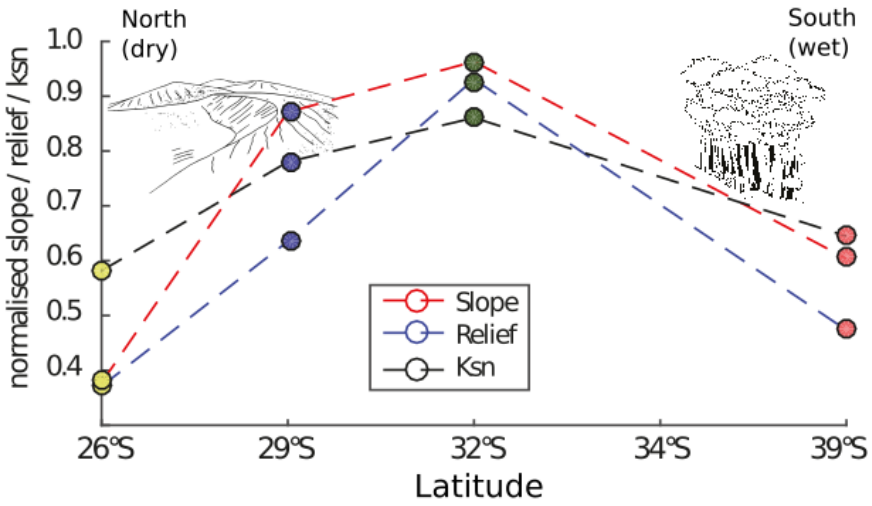

Figure 6: Normalized catchment-mean topographic metrics (Slope, Relief, Channel Steepness) for Earthshape focus areas. Topographies show increase in topographic metrics going from N to S with highest values for La Campana study area. Going further south, metrics decline towards Nahuelbuta study area.

This thesis aims to advance the understanding of the diverging effects of precipitation and surface vegetation cover on landscape evolution by exploring the assumption that **while the effects of vegetation cover on surface processes occur on shorter timescales than geologic processes, their resulting effects are still on a magnitude large enough to be recorded in different topographic metrics**.

This assumption is supported by the shape of the gradient of topographic metrics between the different Earthshape study areas (see Fig. 6) which shows a distinct peak in the observed topographic metrics (slope, relief and channel steepness). These occurring differences in topographies are generally attributed to changes in either tectonic uplift, lithologic parameters or large-scale fault processes. Since the Earthshape study areas are assumed to not differ drastically in these endogenic characteristics, the topographic gradient is proposed to be a result from exogenic forcings, specifically the competition between precipitation and vegetation cover.

The previous stated assumption was tested by incorporating realistic, satellite-derived values of vegetation cover and mean annual precipitation for each Earthshape study area into a landscape evolution model with modified algorithms to represent the rate of surface processes as a function of vegetation cover (presented in Schmid et al. [2018]). The resulting

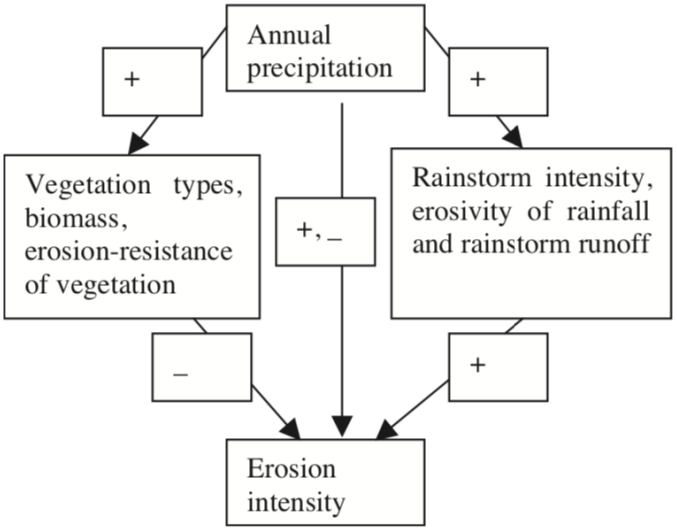

Figure 7: Conceptual model of the feedback loop between increases in mean annual precipitation, surface vegetation cover and erosion(from Jiongxin [2005]). Annual precipitation is positively correlated with the intensity and therefore erosivity of runoff. Precipitation is also positively correlated with ground biomass and vegetation cover which has a negative effect on erosion intensity, therefore the direct correlation between precipitation and erosion intensity can not clearly be defined since it depends on the individual dominating contributions of vegetation and precipitation.

topographic metrics of the synthetic model domains were analysed and compared to the satellite derived topographic metrics shown in Fig. 6

Threshold controlled reactions to transient changes in vegetation cover and precipitation

It is generally believed that the stabilizing effect of vegetation cover in combination with the eco-hydrological properties of a mature vegetation within a landscape lead to an decrease in drainage density and hillslope curvature and an increase in total and local relief and mean catchment slopes until a certain threshold in mean annual precipitation is reached, where the system goes from vegetation-dominated to discharge dominated [Collins and Bras, 2010, Schmid et al., 2018]. At this threshold value of precipitation, the plant ecosystem is not longer water-limited which leads to no significant increase in vegetation while precipitation increases [Asner et al., 2005]. This leads to an direct increase in overland flow and therefore capacity to erode and transport sediment and hence decreases in topographic relief and slope.

Figure 7 shows an generalized flowchart of the feedback loop between precipitation, vegetation and erosion intensity where + and - symbols indicate positive or negative correlation. Increases in annual precipitation generally show positive correlation with the growth of vegetation biomass and therefore the erosion-resistance of vegetation which in turn has a negative effect on erosion intensity. Simultaneously, an increase in precipitation has a positive correlation with the intensity of single, large precipitation events and therefore maximum runoff, which shows a large positive effect on erosion intensity [Dadson et al., 2003]. Therefore, the direct effect of changes in annual precipitation on erosion intensity can be positive or negative, depending on the threshold between vegetation dampening of erosion processes and runoff-induced increases in erosion rates. Therefore the assumption is stated that **the magnitude and direction of the reaction of catchment topography and erosion rates to transient changes in precipitation and associated changes in vegetation cover is a function of the initial climatic and vegetative conditions of a specific area.**

This assumption was tested by a two-way approach laid out in Werner et al. [2018] and Schmid et al. [2018] by conducting dynamic vegetation model runs to determine a realistic long-term value of vegetation cover change for the Earthshape study areas, which were then implemented into the landscape evolution model, with empirically derived associated precipitation changes to quantify the magnitude and rate of topographic changes and changes in erosion rates for different scenarios.

2.2 Hypothesis (II): LGM - PD climatic differences control catchment erosion rates

To gain insight knowledge about the long-term effect that climatic shifts exert on catchment topographies, it is important to derive topographic evolution as a function of realistic climate data and the associated changes in surface vegetation cover and composition to evaluate realistic magnitudes of topographic changes due to a climatic history. Since the derivation of a high resolution, large-scale dataset which contains histories of vegetation cover values for different global positions is non-trivial and most of the available datasets only cover biotic histories for shorter periods and show gaps, which are result of sedimentary conditions [Grosjean et al., 2003], a numerical approach for determination of vegetation cover within a catchment was chosen.

Climate change from the LGM to present day has been constrained using a combination of proxy-based reconstructions and different numerical climate simulations (see Fig. 8, Mutz

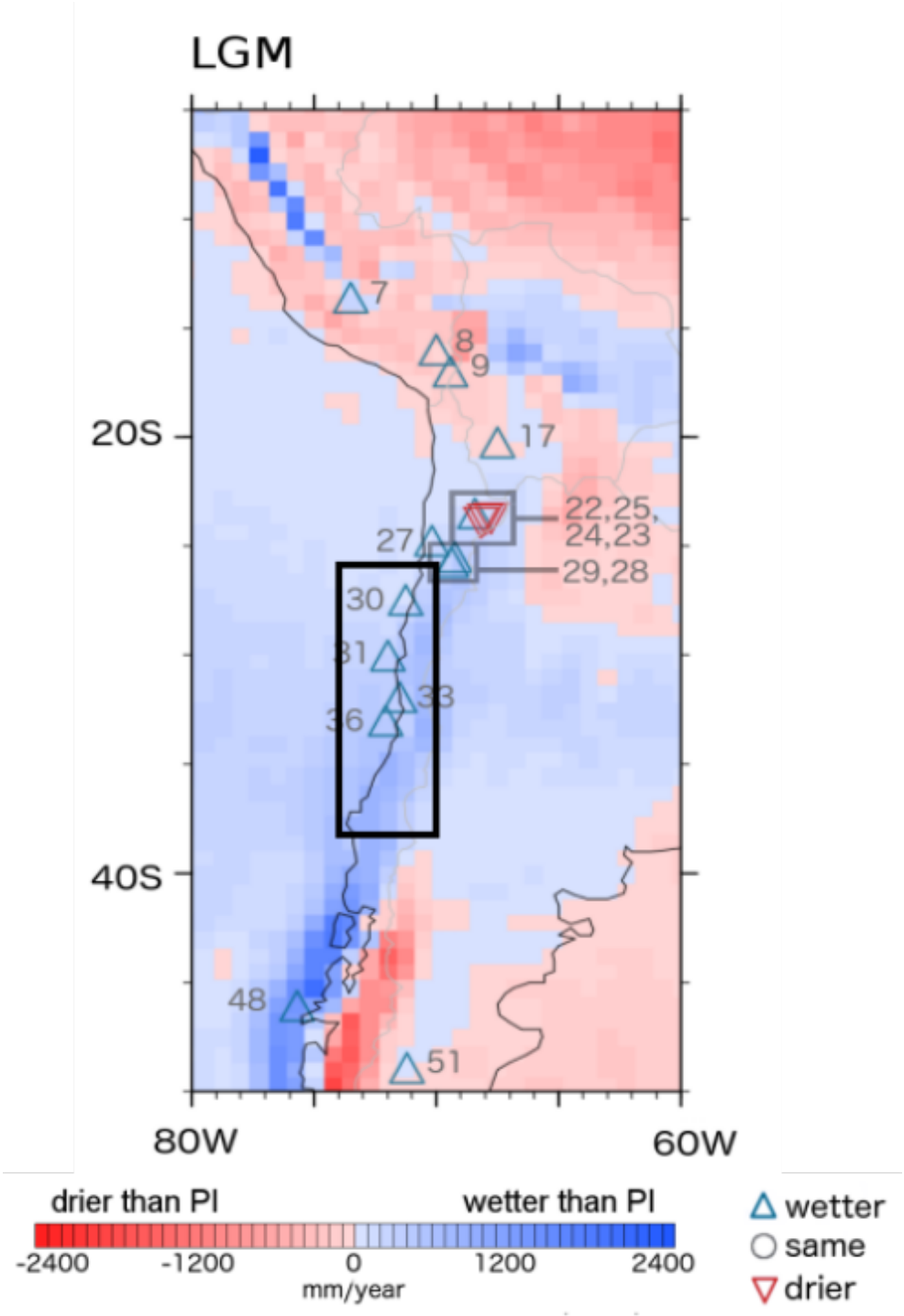

Figure 8: Simulated differences in mean annual precipitation for LGM to Pre-Industrial (PI) conditions for South America (modified from Mutz et al. [2018]). Symbols indicate proxy-based reconstructions which correspond with the model-predicted precipitation deviations. Black box outlines location of Earthshape study areas. Data shows wetter conditions for LGM timeslice compared to PI timeslice, with increasing intensity going from N to S

et al. [2018]). For the Earthshape study areas, these different methods predict a general trend of higher annual precipitation values for LGM conditions compared to pre-industrial (PI) times. The LGM-PI difference of annual preciptiation gets more pronounced going from N to S with with values of approximately 350 mm/yr more precipitation at LGM conditions at the northern boundary of the Earthshape study areas to approximately 800 mm/yr increase in LGM precipitation at the southern boundary. There is further evidence from Maldonado and Villagrán [2006] that the climatic variations in Chile (analyzed at 32°S) show large variations in the time interval between 9000 and 2000 years before present, which were accompanied by shifts in plant composition from arboreal types to open, shrub-land types.

Since this data suggests that the climatic conditions in Chile show not only a variation in mean annual precipitation and mean annual temperature [Mutz et al., 2018] but also in the composition and density of vegetation cover and these processes are known to affect the shape and formation of topographies, the assumption is stated that **there is a distinct, area-specific reaction of landscapes to the climatic change since the last glacial maximum and today, which is specific to the climatic and biotic setting the catchment is located in.**

To test this assumption, a fully coupled model framework was built which incorporates a full-cycle feedback between LPJ-GUESS and Landlab at each timestep of the model simulation. This gives insight about the dynamic allocation and spatial differences of vegetation cover within a landscape and the associated topographic shifts. Simulation were conducted for climate data from LGM to PD for four Earthshape study areas. The dedicated manuscript is in final stage of preparation and the latest version is attached in section 3.2.1

3 Scientific results

The following section presents the scientific results for the previously addressed hypothesis which were tested and analysed in three publications. Two of them are already accepted and published, a third one is currently in a late stage of preparation and soon to be submitted. The latest version of the manuscript is presented.

3.1 Vegetation cover controls over topographic evolution

3.1.1 Declaration of contributions to joint publication

This subsection of the dissertation has been published in *Earth Surface Dynamics* as part of a set of companion papers and is available online and through open-access under *https://doi.org/10.5194/esurf-6-829-2018* for Part 1 and *https://doi.org/10.5194/esurf-6-859-2018* for Part 2. The full citations of both companion publications are:

> *Werner, C., Schmid, M., Ehlers, T. A., Fuentes-Espoz, J. P., Steinkamp, J., Forrest, M., Liakka, J., Maldonado, A., and Hickler, T.: Effect of changing vegetation and precipitation on denudation –* ***Part 1: Predicted vegetation composition and cover over the last 21 thousand years along the Coastal Cordillera of Chile****, Earth Surf. Dynam., 6, 829-858, https://doi.org/10.5194/esurf-6-829-2018, 2018.*
>
> *Schmid, M., Ehlers, T. A., Werner, C., Hickler, T., and Fuentes-Espoz, J.-P.: Effect of changing vegetation and precipitation on denudation –* ***Part 2: Predicted landscape response to transient climate and vegetation cover over millennial to million-year timescales****, Earth Surf. Dynam., 6, 859-881, https://doi.org/10.5194/esurf-6-859-2018, 2018.*

The original manuscripts are provided in sections 3.1.2 and 3.1.3. In the following paragraphs, the exact author contributions for the respective publications are laid out.

Part 1: Predicted vegetation composition and cover over the last 21 thousand years along the Coastal Cordillera of Chile

Nine authors contributed to this joint work: Christian Werner (CW), Manuel Schmid (MS), Todd Ehlers (TE), Juan-Pablo Fuentes-Espoz (JF), Joerg Steinkamp (JS), Mathew Forrest (MF), Johan Liakka (JL), Antonio Maldonado (AM) and Thomas Hickler (TH). Todd Ehlers and Thomas Hickler build up the initial theoretical framework of this study and were primary investigator for the research grant. Christian Werner and Manuel Schmid build up the design of simulations and paper hypothesis. Christian Werner carried out the simulations and data preparation with help from Matthew Forrest, Johan Liakka and Antonio Maldonado. Christian Werner and Manuel Schmid performed data analysis and interpretation. Manuscript preparation was done by Christian Werner with help from Manuel Schmid and input from all co-authors. Detailed contributions are provided in table 2

Table 2: Author contribution (in %) of manuscript *Effect of changing vegetation and precipitation on denudation – Part 1: Predicted vegetation composition and cover over the last 21 thousand years along the Coastal Cordillera of Chile*. Paper has been published at 08.10.2018

Author	Author position	Scientific ideas [%]	Data generation [%]	Analysis & Interpretation [%]	Paper writing [%]
CW	1	30	60	50	60
MS	2	20	40	30	20
TE	3	30	0	0	5
JF	4	0	0	5	0
JS	5	0	0	5	0
MF	6	0	0	5	0
JL	7	0	0	0	5
AM	8	0	0	0	5
TH	9	20	0	5	5

Part 2 - Predicted landscape response to transient climate and vegetation cover over millennial to million-year timescales

Five authors contributed to this joint work: Manuel Schmid (MS), Todd Ehlers (TE), Christian Werner (CW), Thomas Hickler (TH) and Juan-Pablo Fuentes-Espoz (JF). Todd Ehlers and Thomas Hickler build up the initial theoretical framework of this study and were primary investigators for the research grant. Manuel Schmid build up on this by developing the numerical framework and the general modelling workflow. Simulation setup and post-processing and interpretation of results, including statistics and visualization was done by Manuel Schmid with input from Todd Ehlers and Christian Werner. Manuscript preparation was done by Manuel Schmid with input from Todd Ehlers, Christian Werner and Thomas Hickler. Detailed contributions are provided in table 3

Table 3: Author contribution (in %) of manuscript *Effect of changing vegetation and precipitation on denudation – Part 2: Predicted landscape response to transient climate and vegetation cover over millennial to million-year timescales.* Paper has been published at 08.10.2018

Author	Author position	Scientific ideas [%]	Data generation [%]	Analysis & Interpretation [%]	Paper writing [%]
MS	1	40	80	60	60
TE	2	40	10	30	20
CW	3	5	10	10	10
TH	4	10	0	0	5
JF	5	5	0	0	5

3.1.2 Paper: Part 1 - Predicted landscape response to transient climate and vegetation cover over millennial to million-year timescales

Earth Surf. Dynam., 6, 829–858, 2018
https://doi.org/10.5194/esurf-6-829-2018

Earth Surface Dynamics
Open Access
EGU

Effect of changing vegetation and precipitation on denudation – Part 1: Predicted vegetation composition and cover over the last 21 thousand years along the Coastal Cordillera of Chile

Christian Werner[1], Manuel Schmid[2], Todd A. Ehlers[2], Juan Pablo Fuentes-Espoz[3], Jörg Steinkamp[1], Matthew Forrest[1], Johan Liakka[4], Antonio Maldonado[5], and Thomas Hickler[1,6]

[1]Senckenberg Biodiversity and Climate Research Centre (BiK-F), Senckenberganlage 25, 60325 Frankfurt, Germany
[2]Department of Geosciences, University of Tuebingen, Wilhelmstrasse 56, 72074 Tuebingen, Germany
[3]Department of Silviculture and Nature Conservation, University of Chile, Av. Santa Rosa 11315, La Pintana, Santiago RM, Chile
[4]Nansen Environmental and Remote Sensing Center, Bjerknes Centre for Climate Research, Thormøhlens gate 47, 5006 Bergen, Norway
[5]Centro de Estudios Avanzados en Zonas Áridas (CEAZA), Raúl Bitrán 1305, La Serena, Chile
[6]Department of Physical Geography, Geosciences, Goethe University, Altenhoeferallee 1, 60438 Frankfurt/Main, Germany

Correspondence: Christian Werner (christian.werner@senckenberg.de)

Received: 7 February 2018 – Discussion started: 21 February 2018
Revised: 24 August 2018 – Accepted: 15 September 2018 – Published: 8 October 2018

Abstract. Vegetation is crucial for modulating rates of denudation and landscape evolution, as it stabilizes and protects hillslopes and intercepts rainfall. Climate conditions and the atmospheric CO_2 concentration, hereafter [CO_2], influence the establishment and performance of plants; thus, these factors have a direct influence on vegetation cover. In addition, vegetation dynamics (competition for space, light, nutrients, and water) and stochastic events (mortality and fires) determine the state of vegetation, response times to environmental perturbations and successional development. In spite of this, state-of-the-art reconstructions of past transient vegetation changes have not been accounted for in landscape evolution models. Here, a widely used dynamic vegetation model (LPJ-GUESS) was used to simulate vegetation composition/cover and surface runoff in Chile for the Last Glacial Maximum (LGM), the mid-Holocene (MH) and the present day (PD). In addition, transient vegetation simulations were carried out from the LGM to PD for four sites in the Coastal Cordillera of Chile at a spatial and temporal resolution adequate for coupling with landscape evolution models.

A new landform mode was introduced to LPJ-GUESS to enable a better simulation of vegetation dynamics and state at a sub-pixel resolution and to allow for future coupling with landscape evolution models operating at different spatial scales. Using a regionally adapted parameterization, LPJ-GUESS was capable of reproducing PD potential natural vegetation along the strong climatic gradients of Chile, and simulated vegetation cover was also in line with satellite-based observations. Simulated vegetation during the LGM differed markedly from PD conditions. Coastal cold temperate rainforests were displaced northward by about 5° and the tree line and vegetation zones were at lower elevations than PD. Transient vegetation simulations indicate a marked shift in vegetation composition starting with the past glacial warming that coincides with a rise in [CO_2]. Vegetation cover between the sites ranged from 13 % (LGM: 8 %) to 81 % (LGM: 73 %) for the northern Pan de Azúcar and southern Nahuelbuta sites, respectively, but did not vary by more than 10 % over the 21 000 year simulation. A sensitivity study suggests that [CO_2] is an important driver of vegetation changes and, thereby, potentially

Published by Copernicus Publications on behalf of the European Geosciences Union.

landscape evolution. Comparisons with other paleoclimate model drivers highlight the importance of model input on simulated vegetation.

In the near future, we will directly couple LPJ-GUESS to a landscape evolution model (see companion paper) to build a fully coupled dynamic-vegetation/landscape evolution model that is forced with paleoclimate data from atmospheric general circulation models.

1 Introduction

On the macroscale, it has been suggested that sediment yields from rivers exhibit a nonlinear relationship with changing vegetation (Langbein and Schumm, 1958). Although this relationship is controversial (e.g., Riebe et al., 2001; Gyssels et al., 2005), previous work highlights that vegetation is likely a first-order control on catchment denudation rates (Acosta et al., 2015; Collins et al., 2004; Istanbulluoglu and Bras, 2005; Jeffery et al., 2014). While relatively simple vegetation descriptions have been included in landscape evolution modeling (LEM) studies (Collins et al., 2004; Istanbulluoglu and Bras, 2005), these descriptions do not include explicit representations of plant competition for water, light, and nutrients or stand dynamics which are key to determining the progression of vegetation state.

Dynamic global vegetation models (DGVMs) were created as state-of-the-art tools for representing the distribution of vegetation types, vegetation dynamics (forest succession and disturbances by, e.g., fire), vegetation structure, and biogeochemical exchanges of carbon, water, and other elements between the soil, the vegetation, and the atmosphere (Prentice et al., 2007; Snell et al., 2014). Interactions with the climate system have been a special focus, including both the transient response to climatic changes and using DGVMs as land–surface schemes of Earth system models (i.e., Cramer et al., 2001; Bonan, 2008; Reick et al., 2013; Yu et al., 2016). DGVMs are instrumental for understanding the impact of future climate change on vegetation (i.e., Morales et al., 2007; Hickler et al., 2012) as well as studying feedbacks between changing vegetation and the climate (i.e., Raddatz et al., 2007; Brovkin et al., 2009). In addition, DGVMs have been utilized to better understand past vegetation changes, ranging from the Eocene (Liakka et al., 2014; Shellito and Sloan, 2006) and late Miocene (Forrest et al., 2015) to the Last Glacial Maximum (LGM; $\sim$ 21 000 BP) and the mid-Holocene (MH, $\sim$ 6000 BP) (i.e., Harrison and Prentice, 2003; Allen et al., 2010; Prentice et al., 2011; Bragg et al., 2013; Huntley et al., 2013; Hopcroft et al., 2017). Using these models, it has been shown that vegetation often responds with substantial time lags to changes in climate (Hickler et al., 2012; Huntley et al., 2013). Such transient changes are likely to influence erosion rates and catchment denudation. Acosta et al. (2015) showed that ^{10}Be-derived mean catchment denudation rates are lower for steeper but vegetated hillslopes in the Rwenzori Mountains and the Kenya Rift flanks than the erosion rates for sparsely vegetated, lower-gradient hillslopes within the Kenya Rift zone.

Jeffery et al. (2014) investigated how interdependent climate and vegetation properties affect central Andean topography. They found that the mean hill slope gradient correlates most strongly with the percent vegetation cover, and that climate influences on topography are mediated by vegetation. On a shorter timescale, Vanacker et al. (2007) determined that the removal of natural vegetation due to land use change significantly increases sediment yield from catchments, while catchments with high vegetation cover (natural or artificial) return to their natural benchmark erosion rates after reforestation.

However, past vegetation changes are not only the result of changes in climate. The atmospheric CO_2 concentration [CO_2] has varied substantially throughout Earth's history (i.e., Brook, 2008) and is an important factor limiting photosynthesis and plant growth (i.e., Hickler et al., 2015). A glacial [CO_2] of approx. 180 ppm is close to the CO_2 compensation point of about 150 ppm for C_3 plants (Lovelock and Whitfield, 1982), which implies that the majority of all plants on Earth were severely CO_2-limited in the LGM relative to present day (PD). Vegetation models tend to overestimate the forest cover during the last glacial if they do not account for the strong limiting effect of [CO_2] (Harrison and Prentice, 2003). Furthermore, changes in [CO_2] also affect stomatal conductance and, thereby, plant water stress, plant productivity, and the hydrological cycle (Gerten et al., 2005). Although the magnitude of so-called "CO_2 fertilization effects" is still highly debated (Hickler et al., 2015), the physiological effects of [CO_2] might be important drivers of landscape evolution.

While DGVMs are, in principle, very widely applicable, simulation setups do require modification and calibration for particular applications. For regional applications, DGVMs should be tested against present-day data in the study region and process representations should be adapted to specific conditions (Hickler et al., 2012; Seiler et al., 2014). Climate data for simulations of paleovegetation often originate from global climate models (GCMs), which have a rather coarse grid cell resolution. Hence, spatial downscaling is necessary to derive climatic drivers at an adequate scale.

This study is part of the German EarthShape priority research program (https://www.earthshape.net, last access: 15 September 2018), which investigates how biota shapes Earth surface processes along the climatic gradient of the Coastal

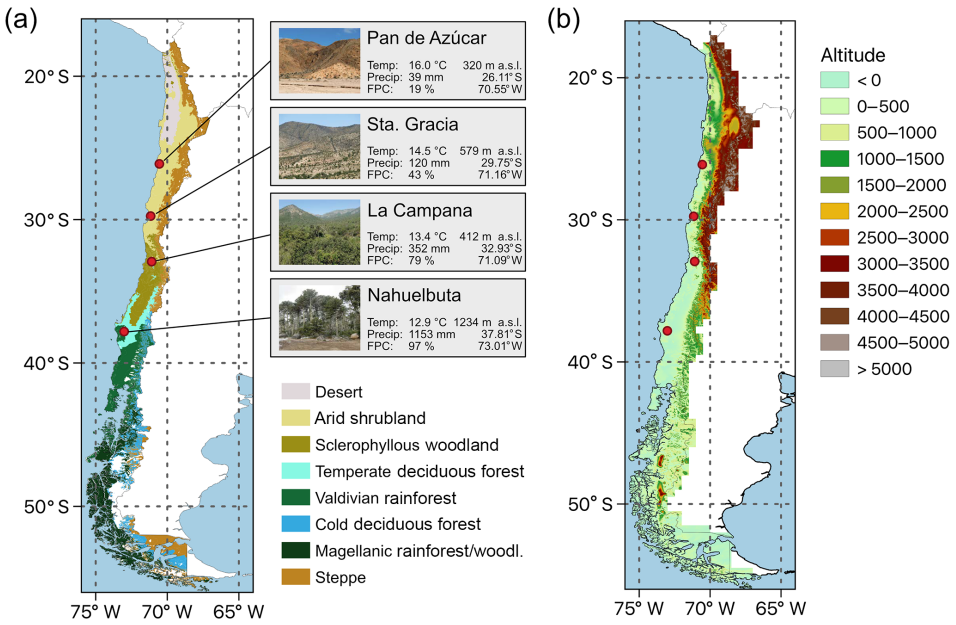

Figure 1. **(a)** Distribution of major vegetation zones in Chile the and location of the four EarthShape SPP focus sites: Pan de Azúcar, Sta. Gracia, La Campana, and Nahuelbuta ("Temp" represents average annual temperature, "Precip" represents average annual precipitation – data: ERA-Interim 1960–1989, and "FPC" represents foliage projected cover (MODIS VCF v6, total vegetation cover, 2001–2016 average, Dimiceli et al., 2015). Vegetation zones are based on Luebert and Pliscoff (2017). **(b)** Elevation of the model domain.

Cordillera of Chile. Here, we describe the climate data processing and vegetation modeling approach, and report results of simulations for the last 21 000 years. Specifically, we (a) develop a regionally adapted setup of LPJ-GUESS that also includes improvements in the sub-grid representation of vegetation (required for future coupling), (b) simulate potential natural vegetation (PNV) for Chile for present day (PD), MH, and LGM climate conditions, and (c) conduct transient simulations for four focus sites (Fig. 1a) at a monthly resolution spanning the full period from the LGM to the PD. Furthermore, we (d) investigat the effect of $[CO_2]$ and the use of different paleoclimate data for vegetation simulations of the LGM, and (e) explor the relationship between vegetation state, vegetation cover, and simulated surface runoff. A companion paper (part 2, Schmid et al., 2018) presents a sensitivity analysis of how transient climate and vegetation impact catchment denudation. This component is evaluated through the implementation of transient vegetation effects for hillslopes and rivers in a LEM. Although the approaches presented in these two companion papers are not fully coupled, the results of predicted vegetation cover change derived from our vegetation simulations provide the basis for the magnitudes of change in vegetation cover implemented in the companion paper. Together, these two papers provide a conceptual basis for understanding how transient climate and vegetation could impact catchment denudation. As a follow-up to these two studies we plan to couple the vegetation and LEMs.

2 Background

Climate and vegetation are key controls of the surface processes that shape landscapes. This is due to the fact that precipitation enables the transport of sediment down-slope, while vegetation cover has the ability to protect hillslopes from erosion due to root cohesion, obstruction of overland flow, and protection from splash erosion. Vegetation characteristics (i.e., composition and cover, which vary substantially by life-form, rooting, and phenological strategies) are not constant in space and time and vary with climate, topography, and soils. Furthermore, environmental forcing such as temperature, precipitation, radiation, and $[CO_2]$ change over longer timescales and lead to different vegetation assemblages, potentially differing vegetation cover, and thus protection from erosion.

2.1 Climate of Chile

Chile's location bordering the Pacific Ocean, its vast meridional extent of 4345 km, and its steep topographic longitudinal profile (Fig. 1b) result in highly variable climatic conditions. The large-scale subsidence of air masses over the southeast Pacific Ocean and other regional factors (e.g., rel-

ative cold coastal ocean currents) yield extremely arid desert conditions in northern Chile with as little as 2–20 mm of annual precipitation (Garreaud and Aceituno, 2007). In the south, a 1000 km long narrow band of Mediterranean-type climate exists on the western side of the Andes (Armesto et al., 2007). According to a general bioclimatic classification by Luebert and Pliscoff (2017), the tropical/Mediterranean boundary is located from 23° S (coast) to 27–28° S (inland) and the Mediterranean/temperate boundary is located at 36° S (in both the Chilean Coastal and Andes mountain ranges) to 39° S (the "Central Depression"), while the temperate/boreal boundary is found from 50.5 to 56° S. From a climatologic standpoint, the Mediterranean bioclimatic region has a warm temperate climate dominated by winter rain (the mean annual precipitation varies from 300 to 1500 mm from north to south, respectively) and hot, dry summers with dry periods varying from 7 months (north) to less than 4 months (south) in duration (Uribe et al, 2012). To the south, midlatitude westerly winds and orographic uplift by the coastal mountains and the Andes lead to an annual precipitation of up to 3000 and 5000 mm, respectively (Veblen et al., 1996). El Niño occurrences generally lead to above average precipitation rates in the austral winter and spring in the Mediterranean zone and reduced precipitation at 38–41° S in the following austral summer (Garreaud and Aceituno, 2007; Montecinos and Aceituno, 2003).

2.2 Vegetation of Chile

Considering the ecological divisions of South America (Young et al., 2007), Chile is represented by three noticeable areas: the Peruvian–Chilean desert, Mediterranean Chile, and the moist Pacific temperate area. These areas reflect the main floristic characteristics and vegetation types of the country; moreover, the distribution of vegetation within these areas is constrained by thermal and hydrological climatic factors that vary according to latitude and longitude (see Table 1 for an outline of the characteristic species, the biome classification, and modeled vegetation types). In the north, longitudinal variations in climate are the result of geomorphological and ombroclimatic changes. Between 17 and 28° S, the coastal zone is exposed to the influence of fog and orographic precipitation, allowing vegetation such as columnar cacti (*Eulychnia* genera) and a diverse group of shrubs (e.g., *Nolana*, *Heliotropium*, *Euphorbia*, *Tetragonia*) and succulents (e.g., *Deuterocohnia*, *Tillandsia*, *Puya*, *Neoporteria*) to develop (Luebert and Pliscoff, 2017). To the west, and between the Chilean Coastal and the Andes mountain ranges, a hyper-arid desert zone exists, which is characterized by the absence of rainfall or coastal-fog water inputs; therefore, no vascular plants are usually found in this area. However, with punctual water inputs due to local substrate conditions, such as the presence of a water table, some halophytic shrubs (e.g., *Prosopis* sp.) can develop (Luebert and Pliscoff, 2017). Vegetation in the Andes mountain range is constrained by altitude due to the decrease in temperature and the increase in precipitation. The major development regarding vegetation is observed at intermediate altitudes where shrubs tend to dominate (Luebert and Pliscoff, 2017).

Vegetation increases to the south with increasing winter precipitation (Rundel et al., 2007), allowing Mediterranean-type shrubland and woodland ecosystems to develop. In these ecosystems various plant species, commonly denominated sclerophyllous plants, have small, rigid, xeromorphic leaves adapted to hot, dry summers and wet, cool winters (Young et al., 2007). Sclerophyllous woodlands and forests extend from 30–31 to 37.5–38° S (Fig. 1a) and range from xeric thorn savanna elements to dense herbaceous cover in the Central Depression, whilst evergreen sclerophyllous trees and tall shrubs are found at higher elevations in which mesic conditions predominate. In these ecosystems, slope aspect can modify local moisture conditions, affecting the structure and composition of vegetation (Luebert and Pliscoff, 2017). To the south, these vegetation types transition into temperate deciduous *Nothofagus* forests (*Maule* or *Nothofagus* parklands. The dominant species in these areas being *Nothofagus obliqua*, *N. glauca*, and *N. alessandrii*) at the Coastal Cordillera and lower Andes ranges, before forming a broader vegetation zone (Donoso, 1982; Villagrán, 1995). The deciduous *Nothofagus* forests then grade into mixed deciduous–evergreen *Nothofagus* forests at 36° S (Young et al., 2007). With increasingly hydric conditions evergreen broad-leafed species begin to dominate forest stands at approximately 40° S and form the Valdivian rainforest (the northernmost rainforest type, ranging from 37°45′ to 43°20′ S) with high biomass and arboreal biodiversity and evergreen, deciduous, and needleleaf species (Veblen, 2007). Further south, the less diverse North Patagonian rainforest is mainly dominated by *Nothofagus betuloides* (Veblen, 2007) and transitions into the Magellanic rainforest at approx. 47.5° S and Magellanic moorland with waterlogged soils and a poor nutrition status at the coast (Arroyo et al., 2005). Cold deciduous forests stretch from 35 to 55° S along the Andes covering cooler and dryer sites as compared to the coastal rainforests. These forests occur at altitudes of approx. 1300 m and gradually descend to sea level in Tierra del Fuego (Pollmann, 2005). In Tierra del Fuego and east of the low Andes in southern Patagonia a gramineous steppe exists (Moreira-Muñoz, 2011), and a high-Andean steppe also extends north at higher altitudes.

3 Methods

3.1 Vegetation model

The Lund-Potsdam-Jena General Ecosystem Simulator (LPJ-GUESS; Smith et al., 2001, 2014) is a state-of-the-art dynamic vegetation model that also simulates detailed stand dynamics using a gap-model approach (Bugmann, 2001; Hickler et al., 2004). The model is developed by an international community of scientists and has been used in more

Table 1. Major vegetation zones, associated plant functional types (PFT), and representative species (modified after Escobar Avaria, 2013; Luebert and Pliscoff, 2017; the letters a–e are given to help the reader identify the PFT and the representative species).

Biome	Plant functional type	Species
Arid shrubland Matorral Sclerophyllous woodland	(a) Temperate evergreen shrubs (TeE_s). (b) Temperate raingreen shrubs (TeR_s). (c) Temperate broad-leaved evergreen sclerophyllous trees ($TeBE_{itscl}$).	(a) *Colliguaja odorifera, Porlieria chilensis, Fluorensia thurifera, Heliotropium stenohyllum.* (b) *Retanilla trinervia, Trevoa quinquinervia, Acacia caven, Prosopis sp.* (c) *Quillaja saponaria, Lithraea caustica, Peumus boldus, Cryptocarya alba.*
Temperate "Maule" forest	Temperate summergreen deciduous trees ($TeBS_{tm}$, $TeBS_{itm}$).	*Nothofagus alpine, N. glauca*, *N. obliqua, N. alessandrii.*
Valdivian rainforest (incl. North Patagonian rainforest)	(d) Temperate broad-leaved evergreen trees ($TeBE_{tm}$, $TeBE_{itm}$). (e) Temperate needle-leaved evergreen trees (TeNE).	(d) *Embothrium coccineum, Weinmannia trichosperma, Nothofagus dombeyi, N. nitida, Eucryphia cordifolia, Drimys winteri, Laureliopsis philippiana, Aextoxicon punctatum, Luma apiculata, Persea lingue, Amomyrtus luma, Lomatia hirsuta.* (e) *Fitzroya cuppressoides, Pilgerodendron uviferum, Saxegothaea conspicua, Podocarpus nubigena, Araucaria araucana.*
Magellanic rainforest/woodlands	Boreal broad-leaved evergreen trees (BBE).	*Nothofagus betuloides* (in hyper-humid areas).
Cold deciduous forest/woodlands	Boreal broad-leaved summergreen trees (BBS).	*Nothofagus pumilio, N. antarctica* (in humid areas).
No dominant biome	Boreal evergreen shrub (BE_s).	*Bolax gummifera, Azorella selago*.
(High-Andean) Steppe	Herbaceous vegetation (C3G).	Great floristic variability (from north to south): *Chaetanthera sphaeroidalis, Nastanthus spathulatus–Menonvillea spathulata, Oxalis adenophylla–Pozoa coriacea, Nassauvia dentata–Senecio portalesianus, Nassauvia pygmaea– Nassauvia lagascae.*

than 200 peer-reviewed international publications, including model evaluations against a large variety of benchmarks such as vegetation type distribution, vegetation structure and productivity, as well as carbon and water cycling at regional to global scales (https://www.nateko.lu.se/lpj-guess, last access: 15 September 2018). Vegetation development and functioning is based on the explicit simulation of photosynthesis rates, stomatal conductance, phenology, allometric calculations, and carbon and nutrient allocation. The model simulates the growth and competition of different plant functional types (PFT, see Bonan et al., 2002) based on their competition for space, water, nutrients, and light. Population dynamics are then simulated as stochastic processes that are influenced by current resource status, life history, and demography for each PFT. To enable a representative description of average site conditions within a landscape each grid cell is simulated as a number of replicate patches in order to allow different (stochastic) disturbance histories and development (successional) stages (see Hickler et al., 2004; Wramneby et al., 2008). Fire occurrence is determined by the model using temperature, fuel load, and soil moisture levels (Thonicke et al., 2001). Soil hydrology in LPJ-GUESS is represented by a simple two-layer bucket model with percolation between layers and deep drainage (see Gerten et al., 2004).

Vegetated surface area and runoff are affected by a range of model parameters in LPJ-GUESS. In "cohort" mode, an average individual from each PFT with a given age and development status is used to characterize vegetation state. Depending on PFT-specific parameters (i.e., maximum crown area, sapling density, allometric properties, leaf-to-sapwood area), age, and competition for light, water, space, nutrients, and demographic processes (establishment and mortality) individual cohorts can develop different states.

Using Eq. (1), we approximate the fraction A of the land surface covered by vegetation using the foliar projected cover (FPC) – the vertical projection of leaf area onto the ground (see Wramneby et al., 2010). In LPJ-GUESS the FPC is derived from daily leaf area index (LAI, the leaf area to ground

area ratio, $m^2\,m^{-2}$) summed for all simulated PFTs (n refers to the number of PFTs) using the Lambert–Beer extinction law (originally proposed by Monsi and Saeki in 1953 for the estimation of light extinction in plant canopies, see translation in Monsi and Saeki, 2005; Prentice et al., 1993):

$$A\,[\%] = \left(1.0 - \exp\left(-0.5 \times \sum_{i=0}^{n} \mathrm{PFT}_{\mathrm{LAI}}\right)\right) \times 100. \quad (1)$$

Thus, depending on the composition of PFTs and the disturbance regime, varying levels of ground cover can be simulated that not only reflect the environmental conditions but also vegetation diversity and development.

In addition, the hydrological cycle is also affected by PFT-specific interception and transpiration rates that are a function of PFT-specific parameters and the development stage. Thus, vegetation modulates infiltration via interception (that is a function of vegetation cover) and runoff (via plant uptake and transpiration of water) under the given environmental constraints. In LPJ-GUESS water enters the top soil layer as precipitation until this layer is fully saturated (excess water is lost as surface runoff, and evaporation removes water from a 20 cm sub-horizon of the top layer). During precipitation days, water can percolate from the top to the lower layer until the lower layer is saturated (excess water is lost as drainage). In addition, water from the lower layer can drain as baseflow with a fixed drainage rate (Gerten et al., 2004; Seiler et al., 2015). The model does not consider lateral water movement between grid cells nor does it take routing in a stream network into account (in this study we report the surface runoff component only).

3.2 Landform classification

To bridge the gap in spatial resolution between LPJ-GUESS (typical spatial resolution of $0.5° \times 0.5°$) and the LEM Landlab (Hobley et al., 2017; Schmid et al., 2018, typical spatial resolution ~ 100 m) and facilitate the future coupling of these models, we introduced the concept of landform disaggregation of grid cell conditions to smaller sub-pixel entities (Figs. 2, B1). The advantages of introducing sub-pixel entities as opposed to simply performing higher-resolution simulations are twofold. Firstly, higher-resolution simulations require climate forcing data of the desired output resolution that are not available for the intended simulation periods or region (and are not generally available for past time periods). Secondly, using sub-pixel entities incurs smaller additional computation costs than higher-resolution simulations.

Sub-pixel entities, hereafter termed "landforms", were derived for each grid cell using SRTM1-based elevation models (Kobrick and Crippen, 2017). Pixels from the elevation model (30 m spatial resolution) were classified based on their elevation (200 m bands) and their association with topographic features (ridges, mid-slope positions, valleys, and plains – based on slope and aspect), and similar pixels were grouped to form the landforms. The elevation of the landforms was used to modify the temperature at a given landform. Using the elevation difference between the average elevation of a landform as derived from the high-resolution elevation model and the reference elevation obtained from the $0.5° \times 0.5°$ grid, a temperature delta was calculated using the lapse rate from the International Standard Atmosphere model of $-6.5\,°C\,km^{-1}$ (e.g., Vaughan, 2015). However, it should be noted that this lapse rate is a global average rate that can substantially differ from local conditions and over multiple timescales (ranging from sub-daily to climatological), as it is controlled by various atmospheric thermodynamics and dynamics (i.e., radiative conditions, moisture content, large-scale circulation conditions). While a higher lapse rate would potentially be a better approximation for drier sites (e.g., Pan de Azúcar), this might not be the case for other sites or past time periods with different atmospheric conditions. Furthermore, the lack of defining environmental data and a mismatch of scales prohibits the use of more specific regional lapse rates in our simulations.

The slope and aspect were utilized to adjust the incoming radiation received by the landform (see Appendix B). The general topographic features were used to modify the depth of the lower soil layer (deeper soils in valleys and on plains,

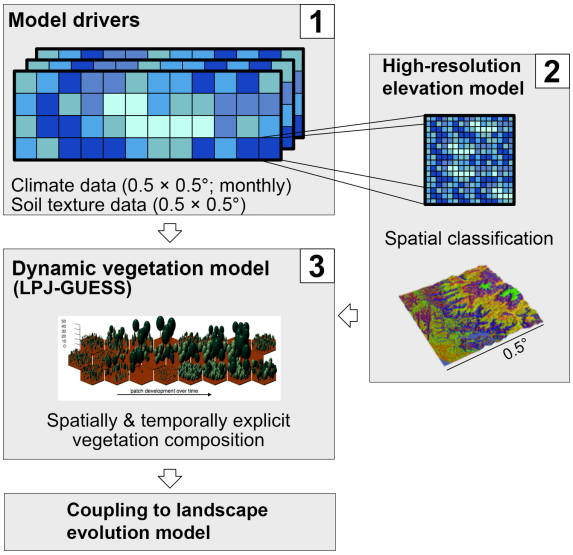

Figure 2. Schematic procedure of simulations. Coarse resolution model driving data (1) is disaggregated using a high-resolution elevation model and topographic landform classification (2), and the ecosystem model LPJ-GUESS then simulates vegetation state and dynamics using the landform classification to simulated topographic-adjusted patch composition (3). Vegetation cover and surface runoff results can then be passed on to a coupled landscape evolution model (LEM) (not implemented in this study, see Schmid et al. (2018) for a description of the LEM).

shallow soils on ridges) and to identify areas (valleys and plains) with a newly implemented time-buffered deep-water storage pool that is only accessible by tree PFTs. The classification resulted in 2 to 56 (the mean was 17) landforms for each grid cell depending on the topographic complexity.

In the proposed future coupled model, we envisage that the landform classification will be performed using elevation information from the LEM. The resulting per-landform (but non-spatially explicit) vegetation simulation results will be matched back to spatially explicit grid cells in the LEM, which will allow us to bridge the scale gap between the two models.

In the simulations presented here, all classified landforms with an area > 1 % of the total land area in a grid cell were simulated using 15 replicate patches each, and simulation results were aggregated by area-weighting the results to the grid cell level. For a summary of the implementation details see Fig. B1.

3.3 Parameterization of plant functional types and biome classification

In a previous study Escobar Avaria (2013) implemented the first regional simulation for Chilean ecosystems (also using LPJ-GUESS) for present day (PD) climate conditions using a region-specific parameterization, which the presented study adapts and builds upon. Eleven PFTs – three shrub types, seven tree types, and one herbaceous type – were defined in order to describe the major vegetation communities of Chile (Table C1). The definition of these PFTs are generally based on the proposed macro-units of Chilean vegetation (Luebert and Pliscoff, 2017) and follow the concept of representative/or dominant species for describing a physiognomic unit. Apart from growth habit and associated traits, PFTs were designed to differentiate between leaf morphology and strategy, shade-tolerant and shade-intolerant varieties, their adaption to water access (mesic, xeric type), and root distribution. An overview of major eco-zones, associated PFTs, and representative species is given in Table 1.

Using a biomization approach (see Prentice and Guiot, 1996 for the general concept), we classified the simulated PFTs into discrete vegetation types (referred to as biomes throughout the paper; see Fig. C1 for details of the classification procedure). Based on LAI thresholds and the ratio of certain key PFTs or PFT groups (i.e., boreal tree PFTs, xeric PFTs) to their peers, a cascading decision tree was implemented that led to 11 biomes resembling the general vegetation zones of Chile (Fig. 1a), but also included additional biome classes to capture the finer nuances of transitions between semi-arid and mesic vegetation communities and open woodlands. To keep the number of vegetation types reasonable we designed multiple decision paths for biomes that exist as dense forest ecosystems but also transition into lower canopy woodlands or transition into more open woodlands (i.e., Magellanic forest, cold deciduous forest; see Fig. C1). The classification was conducted at the landform level after the simulated 15 patches were averaged, and the grid cell classification was derived from picking the area-dominant class of the landforms of a grid cell.

3.4 Environmental driving data and modeling protocol

The climate forcing data for LPJ-GUESS is derived from TraCE-21ka (Liu et al., 2009), which is a transient coupled atmosphere–ocean simulation from LGM to PD using the Community Climate System Model version 3 (CCSM3; Collins et al., 2006). In this study we present time-slice simulations for the LGM, MH, and PD (1960–1989), using perpetual climate forcing data from 30-year monthly climatologies (Fig. 3). In addition, we show results from a transient model simulation that utilizes the full time-series data from the LGM to PD. All simulations were preceded by a 500-year spin-up period with de-trended climate data until vegetation and soils reached steady state. For time-slice simulations the last 30 years of the simulation were used.

Monthly temperature, precipitation, and downward shortwave radiation from the TraCE-21ka dataset (resolution T31; $\sim 3.7°$) were downscaled to a $0.5° \times 0.5°$ spatial resolution and bias-corrected using a monthly climatology from the ERA-Interim reanalysis (Dee et al., 2011, years 1979–2014). We used an additive bias correction for the temperature and multiplicative corrections for the precipitation and shortwave radiation (see Hempel et al., 2013; this technique was also used in, e.g., O'ishi and Abe-Ouchi, 2011). The multiplicative corrections for the precipitation and radiation are necessary because these fields can not have negative values. The resulting bias-corrected anomalies were subsequently downscaled to the ERA-Interim grid using a bilinear interpolation technique. The number of rain days within each month (used by LPJ-GUESS to distribute monthly precipitation totals to daily time steps internally) was derived from the monthly mean precipitation in the TraCE-21ka data and the day-to-day precipitation variability from ERA-Interim (see Appendix A). The $[CO_2]$ for each simulation year was obtained from Monnin et al. (2001) and Meinshausen et al. (2017). A comparison climate dataset for the LGM (referred to as ECHAM5 in this paper) was provided by Mutz et al. (2018). Soil texture data used for bare-ground initialization of the model was obtained from the ISRIC-WISE soil dataset (Batjes, 2012) and a default soil depth of 1.5 m (0.5 m topsoil, 1 m subsoil) was assumed.

We simulated vegetation dynamics using the process-based dynamic vegetation model LPJ-GUESS (Smith et al., 2001) version 3.1 (Smith et al., 2014) with the model additions outlined above. The model runs were carried out without nitrogen limitation, using the CENTURY carbon cycle model (see Smith et al., 2014). Patch destroying disturbance and establishment intervals were defined as 100 and 5 years, respectively, and fire dynamics were enabled. Further details of the PFT specific parameterizations are given in Table B1.

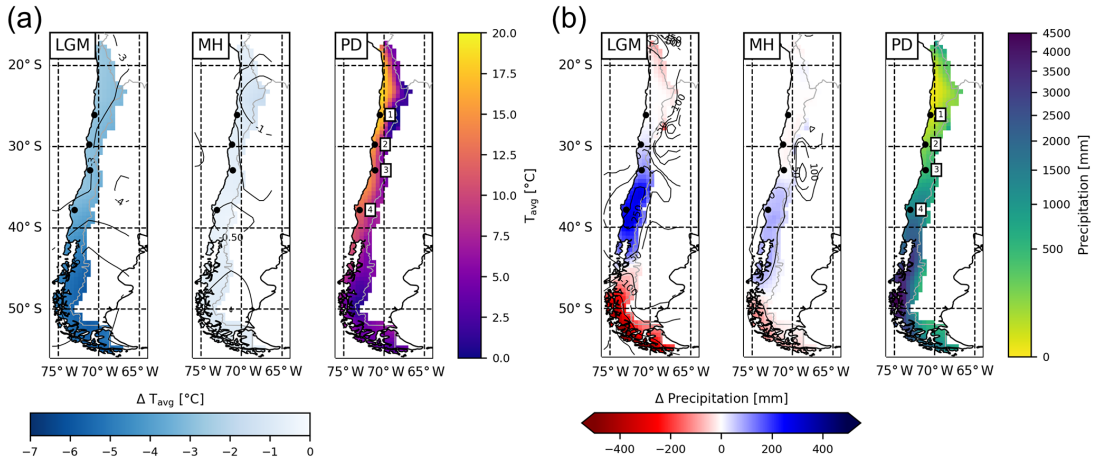

Figure 3. **(a)** Average annual temperature and **(b)** precipitation derived from the downscaled and bias-corrected TraCE-21ka transient paleoclimate data (Liu et al., 2009) for the Last Glacial Maximum (LGM), mid-Holocene (MH), and present day (PD) time slices (data is the average of 30 year monthly data; 1 represents Pan de Azúcar, 2 represents Sta. Gracia, 3 represents La Campana, and 4 represents Nahuelbuta).

The transient site-scale model runs were only conducted for the four focus sites of the EarthShape SPP due to (i) computing resource constraints, (ii) better comparability with other EarthShape SPP work (see Schmid et al., 2018), and (iii) better interpretability.

4 Results

In this study we present data from two types of simulations. First, we show results for time-slice (LGM, MH, PD) simulations. Direct model results (simulated LAI of individual PFTs) are presented first (Sect. 4.1) and then aggregated to a biome representation for easier visualization and comparison (Sect. 4.2). Next, foliar projected cover and surface runoff are investigated (Sect. 4.3). Then, we present results from the transient LGM-to-PD site simulations (Sect. 4.4), and finally a sensitivity analysis of the effect of $[CO_2]$ levels under LGM climate conditions on vegetation composition and cover is carried out (Sect. 4.5).

4.1 Distribution of simulated plant functional types

Vegetation communities (expressed as assemblages of PFTs in LPJ-GUESS) establish spatially depending on (a) environmental controls, (b) competition, and (c) stochastic events (i.e., fire incidents and mortality). An overview of the simulated vegetation distribution expressed as the simulated LAI for each PFT under PD climate conditions is given in Fig. 4 (for key PFT properties see Table C1; the PFT distribution maps for the MH and the LGM are given in the Supplement as Figs. S1 and S2 for completeness). Temperate broad-leaved evergreen trees ($TeBE_{tm}$, $TeBE_{itm}$; *t* represents shade-tolerant, it represents shade-intolerant, and *m* represents mesic) dominate the coastal and central areas from latitudes 40 to 46° S but also extend north into the Mediterranean zone. Further to the north, temperate broad-leaved summergreen PFTs ($TeBS_{tm}$, $TeBS_{itm}$) occur, with the shade-tolerant type dominating a relative small area between 37 and 40° S. Northward, and in coastal areas, the sclerophyllous temperate evergreen PFT ($TeBE_{itscl}$; scl represents sclerophyllous) starts to dominate, and with dryer conditions the total LAI (LAI_{tot}) is dominated by evergreen and raingreen shrubs (TeE_s, TeR_s; *s* represents shrub). South of 40° S, and in higher terrain as well as further north, boreal broad-leaved summergreen and evergreen tree PFTs (BBS_{itm}, BBE_{itm}) as well as boreal evergreen shrubs (BE_s) establish. In the Andean ranges and (to a lesser extent as secondary components) in the lowlands and coastal ranges from 35 to 50° S, temperate needle-leaved evergreen trees (TeNE) are simulated. Herbaceous vegetation (C3G) dominates LAI_{tot} at high altitudes along the Andean ranges and is also a substantial contributor to the total LAI in the Mediterranean zone (30 to 38° S). Herbaceous vegetation also contributes to a lesser extent in most other regions, except for in the hyper-arid desert areas. LAI_{tot} is highest in the zone from 36 to 50° S. While LAI decreases substantially at sea level towards the Atacama Desert, higher values of the LAI are found further north at higher altitudes (see inset in Fig. 4).

4.2 Distribution of simulated biomes at LGM, MH, and PD

The simulated biome distribution changes spatially (Fig. 5a), vertically (Fig. 5b), and over time. Under PD climate, the

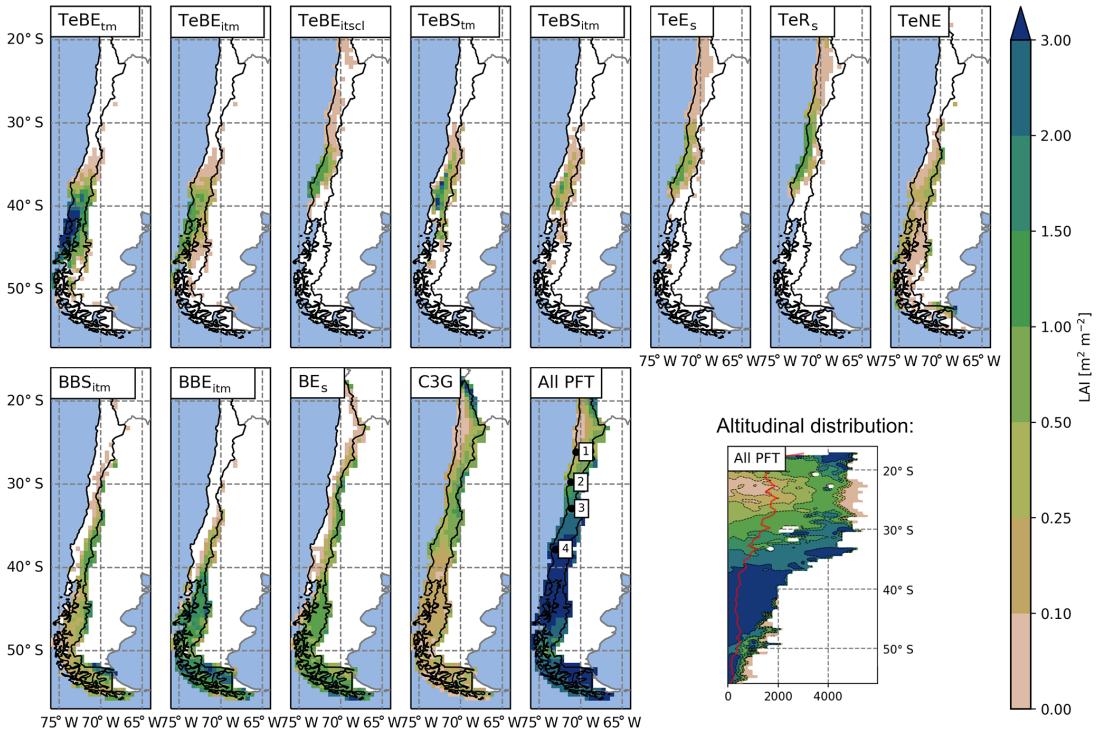

Figure 4. Spatial and altitudinal distribution of modeled plant functional types (PFT) for present-day climate conditions (LAI is the leaf area index – units $m^2\ m^{-2}$; the altitudinal subplot represents zonal mean LAI; the red line represents the average elevation). PFTs are as follows: TeBE$_{tm}$/TeBE$_{itm}$ (temperate broad-leaved evergreen trees; *t* is shade-tolerant, it is shade-intolerant, *m* is mesic), TeBE$_{itscl}$ (temperate broad-leaved evergreen trees; *scl* is sclerophyllous), TeBS$_{im}$/TeBS$_{itm}$ (temperate broad-leaved summergreen trees), TeE$_{s}$ (temperate evergreen shrubs; *s* is shrub), TeR$_{s}$ (temperate raingreen shrubs), TeNE (temperate needle-leaved evergreen trees), BBS$_{itm}$ (boreal broad-leaved summergreen trees), BBE$_{itm}$: (boreal broad-leaved evergreen trees), BE$_{s}$ (boreal evergreen shrubs), C3G (herbaceous vegetation). The number 1 represents Pan de Azúcar, 2 represents Sta. Gracia, 3 represents La Campana, and 4 represents Nahuelbuta.

simulated Valdivian temperate rainforests extend from 38 to 46° S at the coast and transition into the Magellanic forests/woodlands, that are dominated by the boreal PFTs. A small zone of deciduous "Maule" forest occurs to the north of the Valdivian rainforest at meso-temperate climates. With even dryer and warmer conditions the sclerophyllous woodland type establishes and (as the fraction of trees and LAI$_{tot}$ is reduced even further with increasing temperatures and even lower annual rainfall) eventually give way to shrub dominated matorral and finally the arid shrubland biome type. The cold deciduous forest type is classified for parts of Tierra del Fuego, and at higher elevations in the lower Andes in Patagonia. It also forms larger zones at altitude between 30 and 40° S. Mesic woodland occurs between 34 and 30° S at altitude (above the sclerophyllous woodland zone dominating the lowlands), and high-Andean steppe occurs between 18 and 30° S. A cold desert is present above the tree line in Patagonia and the highest Andean ranges, whereas hot desert (LAI$_{tot}$ < 0.2) is simulated for areas from 20 to 26° S. The model was able to simulate the general distribution of the biomes of Chile for most regions (Figs. 1a, 5), although accuracy for the occurrence of deciduous PFTs was low (deciduous "Maule" forest and cold deciduous forest, also previously reported by Escobar Avaria, 2013).

Owing to the similarity in climatic conditions (Fig. 3), the distribution simulated for the MH does not differ substantially from the PD (Table 2). The northern border of sclerophyllous woodland shifts to approx. 34° S, giving way to a matorral zone. In addition, the cold deciduous forest biome covers larger areas in Patagonia at the expense of Magellanic woodland (+27.5 % and −9.1 %, respectively; Table 2). However, the spatial and vertical distribution of biomes for the LGM is markedly different (Fig. 5a, b). The substantially lower temperatures (Fig. 3) lead to an expansion of cold deserts up to 45° S (coastal areas) and 40° S (higher altitudes), respectively. The boreal PFT dominated Magellanic woodland biome is substantially reduced in extent (16.5 % in the LGM versus 32.6 % in the PD of simulated area, Table 2) and is shifted further north (40 to 45° S at the coast, 43 to 35° S at higher altitudes inland). The area covered by tem-

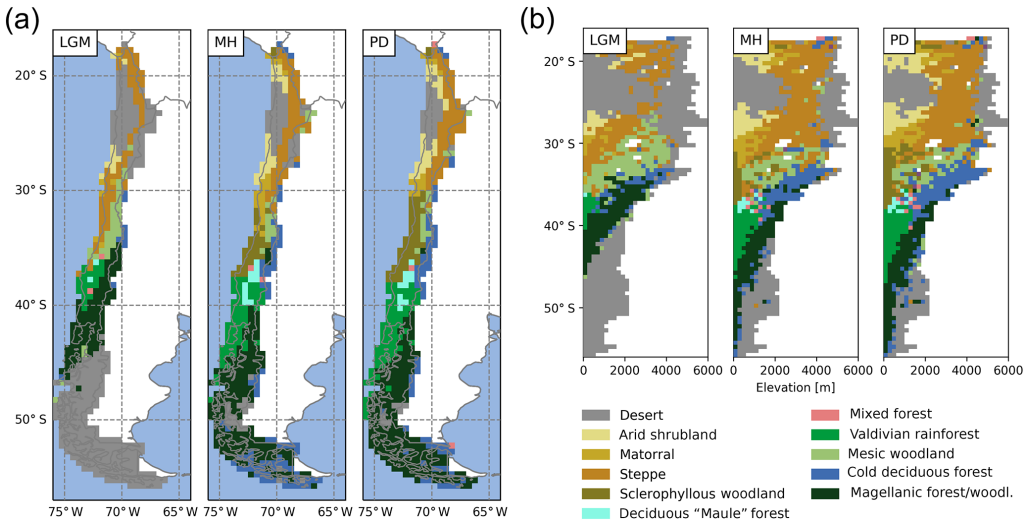

Figure 5. **(a)** Spatial and **(b)** altitudinal distribution of biomes for Last Glacial Maximum (LGM), the mid-Holocene (MH), and the present day (PD) (for the biome classification decision tree see Fig. C1).

Table 2. Areal extent of biomes in the simulation domain (units: percent of total area).

	LGM	MH	PD
Desert	53.7	12.6	7.6
Arid shrubland	1.9	4.5	5.6
Matorral	1.2	3.9	2.3
Steppe	13.6	11.6	12.4
Sclerophyllous woodland	–	5.6	8.7
Deciduous "Maule" forest	0.4	2.1	2.1
Mixed forest	0.4	0.4	0.6
Valdivian rainforest	4.1	11.2	13.4
Mesic woodland	6.6	2.9	2.7
Cold deciduous forest	1.7	15.3	12
Magellanic forest/woodland	16.5	29.8	32.6

perate rainforest is restricted to a small lowland area from 36 to 40° S, and the larger areas of cold deciduous forest at altitude are also substantially smaller (Fig. 5b; Table 2). Lowland steppe and mesic woodland biomes are simulated instead of matorral and sclerophyllous woodlands, and desert cover larger areas of the high-Andes to the north.

4.3 Foliar projected cover and surface runoff

The percentage of ground covered, and thus shielded from strong denudation, and surface runoff (as a major driver of erosion rates) are both influenced by the composition and state of vegetation communities. Therefore, we evaluate the regional and temporal changes of these important variables as simulated by LPJ-GUESS for the LGM, MH, and PD time slices. The simulated LAI of PFTs can be aggregated and converted to foliar projected cover (see Eq. 1); thus, this allows us to estimate the surface covered by vegetation. However, it should be noted that this is only an approximation of true ground cover, as small-scale vegetation variations are not simulated in a location-specific fashion (spatial lumping effects are not considered for instance). Nevertheless, the implementation of a sub-grid landform scale was, in part, motivated to improve the models' prediction of smaller scale differences, as it should allow for the differentiation of different sub-grid conditions for the major landforms within one simulation cell (see Sect. 5.1 and Appendix B for further information). Low FPC clearly coincides with the distribution of hyper- to semi-arid biomes (Figs. 5a, 6a). Under PD climate conditions, average FPC for the semi-arid and Mediterranean biome types, including arid shrubland, matorral, and sclerophyllous woodland are 16 %, 35 %, and 66 % (Table 3), respectively, and cover increases southward with increases in annual precipitation rates (Fig. 3b). South of 35° S, FPC values > 70 % are simulated for most grid cells except for high-altitude locations, the glacier fields of North Patagonia, and parts of the Magellanic moorland at the coast (see also Table 3).

Simulated FPC was lower than satellite-based estimates by the MODIS Vegetation Continuous Fields product (Dimiceli et al., 2015), likely due to methodological differences in foliar projected cover and total satellite-observed vegetation cover, but the general patterns were represented (Fig. 7). The most distinct regional discrepancy can be observed in coastal areas between 30 to 36° S and the Andean highlands in the north of the model domain. For the entire model domain the mean average error (MAE) of the FPC was 11.9 %.

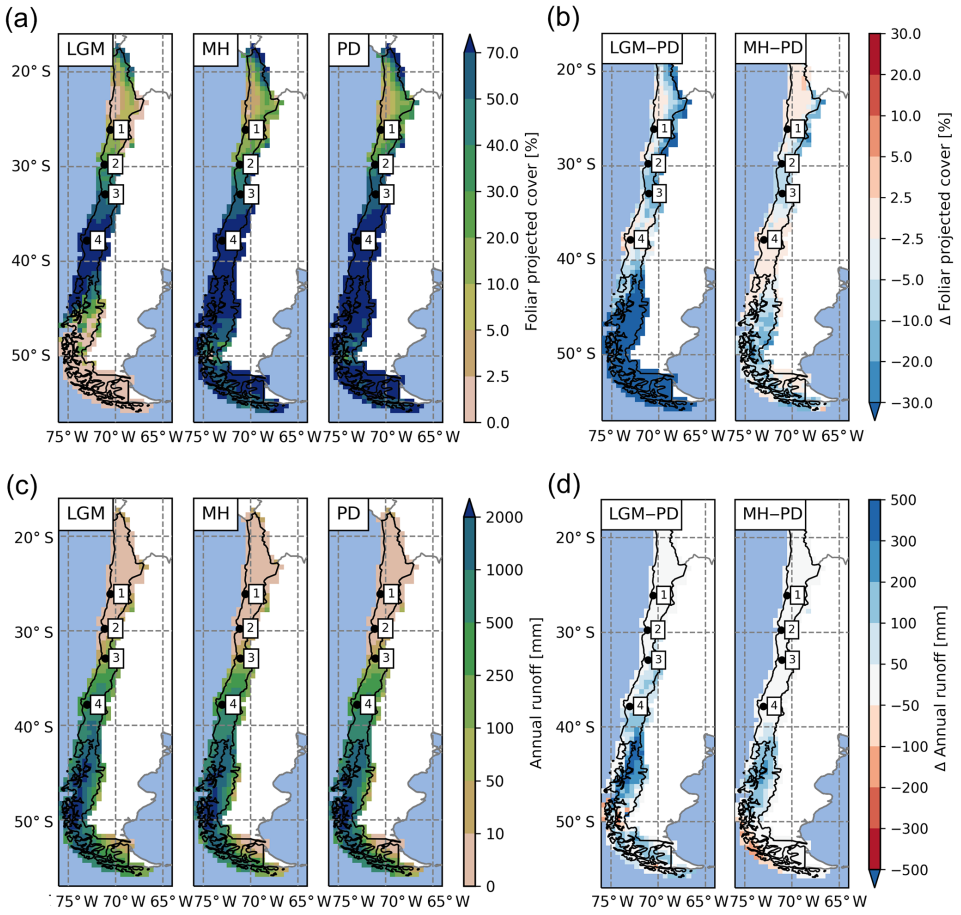

Figure 6. Spatial distribution of **(a)** foliar projected cover and **(c)** surface runoff simulated for the Last Glacial Maximum (LGM), the mid-Holocene (MH), and the present day (PD). Difference plots of LGM versus PD (left) and MH versus PD (right) for foliar projected cover **(b)** and runoff **(d)**, respectively (the number 1 represents Pan de Azúcar, 2 represents Sta. Gracia, 3 represents La Campana, and 4 represents Nahuelbuta).

The best agreements of 6.1 % and 6.3 % MAE were achieved for the arid shrubland and Valdivian rainforest biomes, while the discrepancies were greatest for mixed forest and cold deciduous forest biomes with 22.4 % and 22.1 % MAE, respectively (see Fig. 4a for biome locations; note that LPJ-GUESS often tends to underestimate the FPC of deciduous PFTs). A strong positive correlation between annual rainfall and FPC can be observed for all semi-arid, Mediterranean, and seasonally dry temperature eco-zones (Fig. 8a) and increases in annual rainfall lead to a strong rise of ground covered until 250–300 mm rainfall per year (arid shrubland: +14.5 %–16.3 % 100 mm^{-1}; matorral: +12.9 %–16.5 % 100 mm^{-1}; steppe: +13.5 %–17.8 % 100 mm^{-1}; Fig. 8a). At these levels, Mediterranean and temperate woodland biomes start to dominate but increases in precipitation only raise FPC by +2.7 %–3.3 % 100 mm^{-1} and +5.4 %–6.4 % 100 mm^{-1}, respectively (sclerophyllous woodland and mesic woodland).

A similar spatial pattern of FPC can be observed for the MH (Fig. 6a) and for the relationship to precipitation rates (Fig. 8a). No significant difference in FPC to PD conditions is apparent for the Atacama Desert or for most temperate forest areas from 36 to 42° S. FPC in high-Andes locations in the north and large parts of the Magellanic forest and cold deciduous forest biomes in the south is 10 %–20 % lower than under PD climate, whereas in the Mediterranean zone FPC is reduced by 5 %–10 % (Fig. 6b, Table 3). The reduction of MH FPC (47–54° S) coincides with a zone of lower temperature (> −0.5 °C, see Fig. 6b) and the areal extent of TeBE PFTs (Fig. S1). Lower [CO_2] at MH compared to PD might also be the reason for a general reduction of biomass productivity; however regional differences of the other climate

Table 3. Average foliar projected cover (FPC) and annual surface runoff for simulated biomes for present day (PD) and relative change within these PD areas for the Last Glacial Maximum (Δ LGM, LGM-PD) and the mid-Holocene (Δ MH, MH–PD).

	Foliar projected cover			Surface runoff		
	[%]	[% change]		[mm yr^{-1}]	[% change]	
	PD	Δ LGM	Δ MH	PD	Δ LGM	Δ MH
Arid shrubland	16	−5	−2	0	0	0
Matorral	35	−9	−5	0	0	0
Steppe	39	−23	−7	1	+4	+1
Sclerophyllous woodland	66	−6	−4	187	+35	+9
Deciduous "Maule" forest	85	−5	0	638	+114	+33
Mixed forest	85	−42	−1	193	+24	+5
Valdivian rainforest	88	−20	−1	910	+93	+63
Mesic woodland	56	−21	−10	81	+57	+10
Cold deciduous forest	78	−44	−6	200	+62	+13
Magellanic forest/woodland	77	−68	−7	966	+124	+35

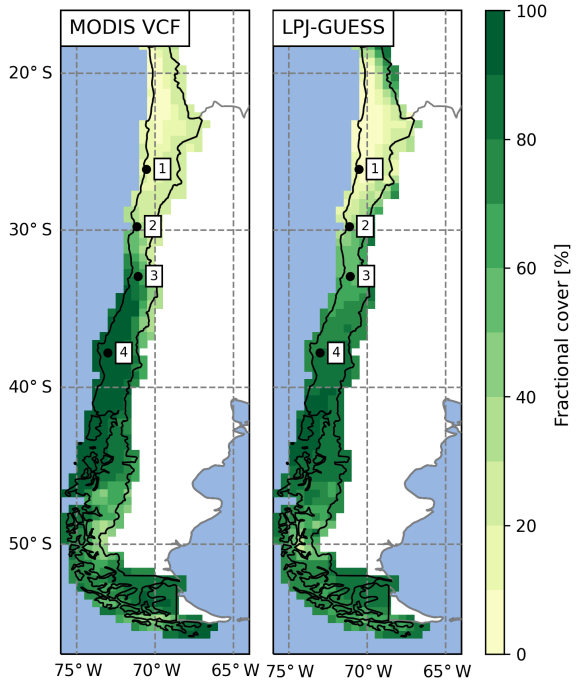

Figure 7. Comparison of satellite-derived vegetation cover and simulated average foliar projected cover of potential natural vegetation for present day (data: MODIS MOD44B VCF v6, total vegetation, 2001–2016 average; Dimiceli et al., 2017; 1 represents Pan de Azúcar, 2 represents Sta. Gracia, 3 represents La Campana, 4 represents Nahuelbuta).

drivers (i.e., temperature, precipitation) do alter this general trend.

Due to lower temperatures and reduced precipitation rates at high altitudes and in the southern part of the country (Fig. 3), FPC during the LGM in these areas is simulated to be strongly reduced (< −30 %, cold desert conditions for large areas south of 46° S); however, the FPC was lower for all areas of Chile (Fig. 6b, Table 3) which was likely also the effect of substantially lower [CO_2] (see Sect. 4.5 for a sensitivity analysis of the effect of the atmospheric CO_2 concentration). While the general correlation of FPC to precipitation can also be observed for the LGM (Fig. 8a), the variability in vegetation cover in mesic and xeric woodlands appears to be larger – indicating the potential for greater variability in erosion rates within the same biome. The strongest correlations between annual precipitation and FPC were observed for sclerophyllous woodland (adjusted r^2 values of 0.84, 0.91, and 0.9 for LGM, MD, and PD, respectively; $p < 0.001$).

Annual average runoff varies greatly from north to south (Fig. 6c) and coincides with annual precipitation (Figs. 3, 8b). For PD and MH climates, LPJ-GUESS simulated almost no surface runoff for arid and Mediterranean areas of Chile to approx. 32° S (see also Table 3). Thus, correlation between precipitation and runoff in the steppe and arid shrubland biomes was low (adjusted r^2: 0.16–0.27, 0.12–0.37, 0.11–0.35 for LGM, MH, and PD, respectively; $p < 0.01$). For all other systems (excluding matorral and mixed forests), correlation coefficients were generally >0.85 for all time slices; $p < 0.001$).

Runoff rates gradually increase southward and reach their peak (>2000 mm yr^{-1}) in areas of hyper-humid conditions along the Pacific coast. MH runoff rates are higher for areas of northern Patagonian and Magellanic rainforest (40–46° S), but lower for coastal areas of Magellanic moorlands (Fig. 6d). LGM runoff rates are higher for most areas (Table 3) and especially south of 34° S, with the strongest differences occurring from 40 to 46° S. However, we want to highlight that the low temporal variability of the TraCE-21ka precipitation data likely leads to a substantial underrepresentation of episodes of high hygric variability (see discussion).

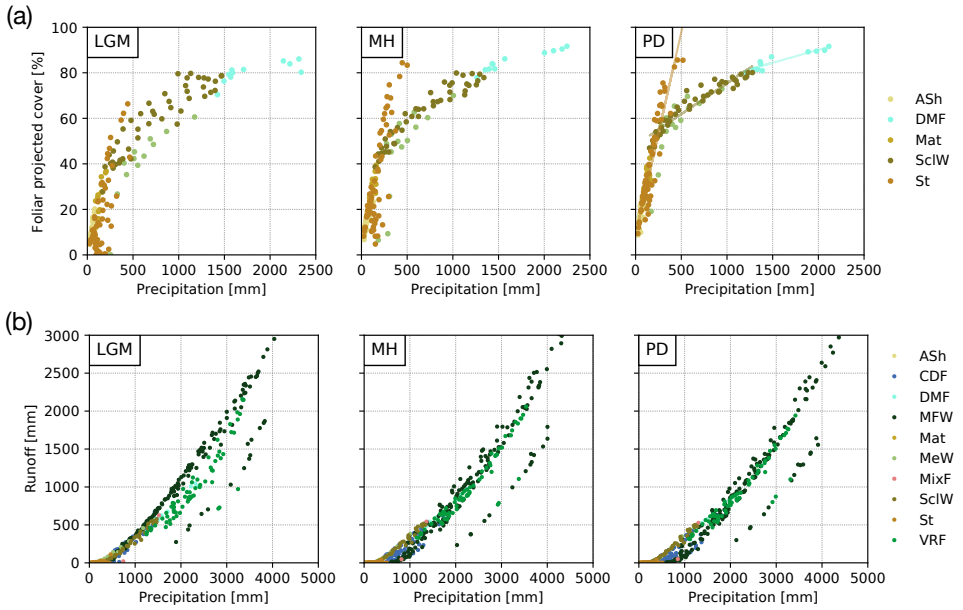

Figure 8. **(a)** Foliar projected cover (FPC) and **(b)** surface runoff as a function of annual average rainfall for the Last Glacial Maximum (LGM), the mid-Holocene (MH), and present day (PD) ("ASh" is arid shrubland, "CDF" is cold deciduous forest, "DMF" is deciduous "Maule" forest, "MFW" is Magellanic forest/woodland, "Mat" is matorral, "MeW" is mesic woodland, "MixF" is mixed forest, "SclW" is sclerophyllous woodland, "St" is steppe, "VRF" is Valdivian rainforest; temperate and boreal forest biomes (CDF, MixF, VRF, MFW) excluded from subplot **(a)** as they are also strongly dependent on temperature.

4.4 Transient changes of simulated vegetation from LGM to present

In this section we present transient simulation results for grid cells that contain the EarthShape focus sites (Fig. 9). The results are given for a single landform of the simulated grid cells in order to preserve successional transitions between PFTs that might otherwise be lost through averaging. The field site location and the represented area of the chosen landform within the grid cell are marked in the insets of Fig. 9a–d. The diversity of simulated vegetation cover for all landforms of the four EarthShape focus sites is illustrated in Fig. B2. The area-averaged mean of landform enabled LPJ-GUESS simulations closely matches the default model results at the Sta. Gracia and La Campana sites, but FPC at the Pan de Azúcar and Nahuelbuta sites is approx. 3 % greater than the default simulation result (Fig. B2a). However, results from all four sites show that the inter-landform variability of FPC varies by 10 %, 15 %, 25 %, and 18 % for the Pan de Azúcar, Sta. Gracia, La Campana, and Nahuelbuta sites, respectively.

Temperatures and [CO_2] start to increase at 18 000 BP and a marked pullback in temperatures during the Antarctic cold reversal ($\sim$ 14 500 BP) is present in the TraCE-21ka data for all four sites (Fig. 9a–d). Annual precipitation at the Pan de Azúcar site (21.11° S 70.55° W, 320 m a.s.l.) is extremely low (38–40 mm, hyper-arid) for the entire simulation period (Fig. 9a). The annual average temperature for the landform presented increases from 13.9 °C (LGM) to 16.8 °C (PD). As a result of these arid conditions only evergreen and raingreen shrubs and herbaceous vegetation can establish, and LAI, and consequently FPC, remains very low ($LAI_{tot} < 0.3$). For most episodes of the simulation this location is classified as desert according to the implemented biomization scheme, with only two periods switching to another state (arid shrubland, $LAI_{tot} > 0.2$) from approx. 17 000 to 15 000 BP, and more permanently, the late Holocene. Fire return intervals (expressed as the number of years between fire incidents) fluctuate greatly as fuel production is substantially limited by low vegetation growth. No surface runoff is simulated and FPC ranges from 8 % (LGM) to 13 % (PD).

Climatic conditions for the Sta. Gracia site (29.75° S 71.16° W, 579 m a.s.l.) show a similar temporal progression from the LGM to PD, but average temperatures are lower and range from 11.9 °C (LGM) to 14.9 °C (PD) (Fig. 9b). Annual precipitation does not change substantially from the LGM to PD (152 versus 122 mm). Vegetation from the LGM to approx. 18 000 BP is dominated by herbaceous vegetation, but (raingreen) shrubs increase with rising temperatures, leading to a biome shift from steppe to matorral. Fire return intervals decrease with increased (arboreal) litter production due to the encroachment of shrubs but FPC only increases by 7 %

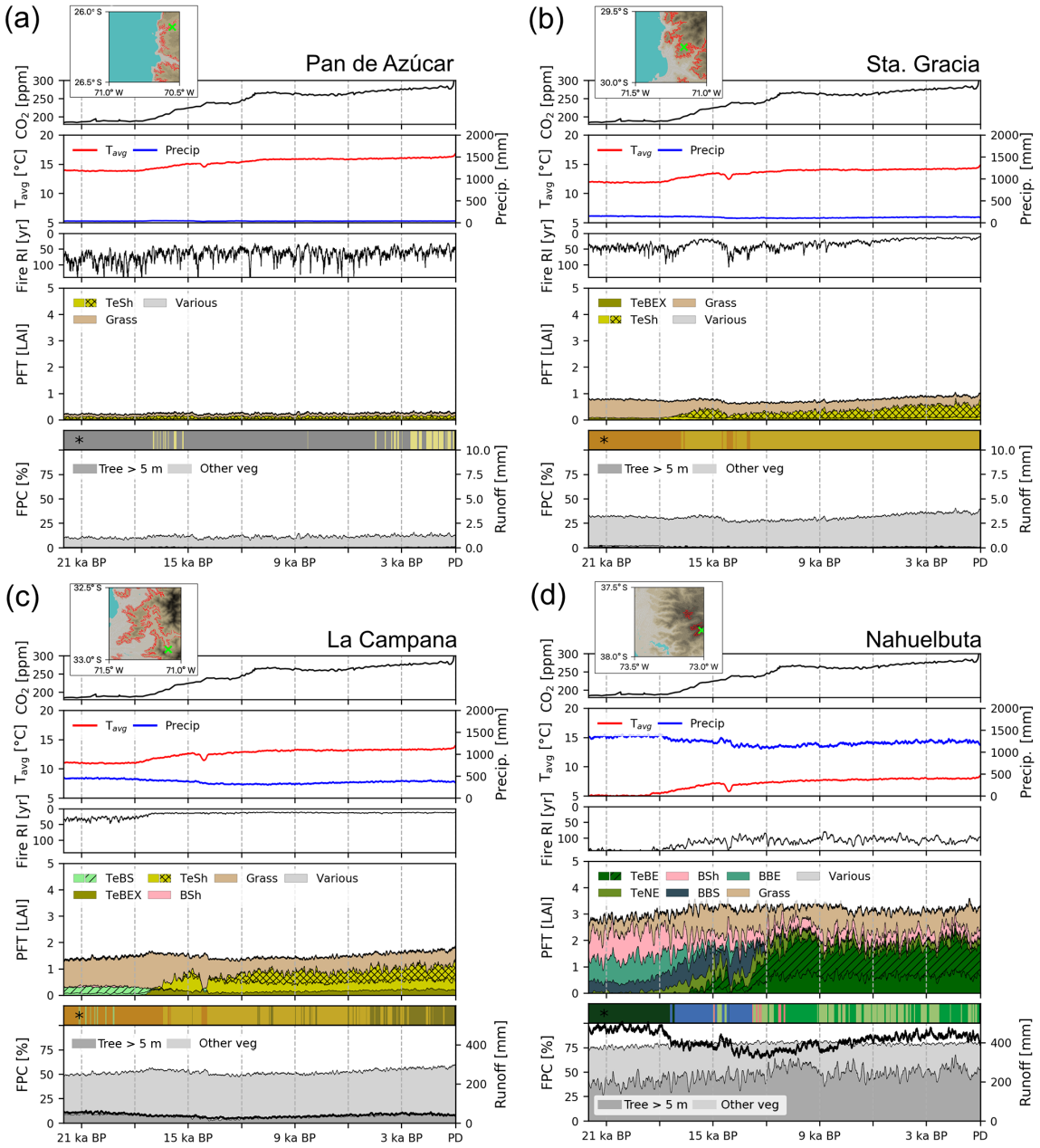

Figure 9. Transient simulations for the **(a)** Pan de Azúcar, **(b)** Sta. Gracia, **(c)** La Campana, and **(d)** Nahuelbuta sites. The insets show the location within the simulated $0.5° \times 0.5°$ grid cell and the area and location covered by the landform plotted in this figure (results given in other figures are an area-weighted aggregation of individual landform simulation results). Panels 1–3 (from top to bottom): "T_{avg}" is annual average temperature, "Precip" is annual precipitation, "Fire RI" is fire return interval. Panel 4: "PFT" is plant function type; (grouped) PFT abbreviations: "TeSh" is temperate shrubs, "Grass" is herbaceous vegetation, "TeBEX" is sclerophyllous temperate broad-leaved evergreen trees, "TeBS" is temperate broad-leaved summergreen trees (hashed represents shade-intolerant), "BSh" is boreal evergreen shrubs, "TeBE" is temperate broad-leaved evergreen trees, "TeNE" is temperate needle-leaved evergreen trees, "BBS" is boreal broad-leaved summergreen trees, "BBE" is boreal evergreen trees, "Various" refers to other PFTs (LAI<0.05); plain represents shade-intolerant, hatched represents shade-tolerant, cross-hatched represents raingreen. Panel 5: "FPC" is foliar projected cover; trees and shrubs > 5 m are denoted using dark gray, herbaceous vegetation and small trees and shrubs are denoted using light gray. "Runoff" is simulated surface runoff; * Biomization: for a legend on the applied classification see Figs. C1 and 4 for a color-coded legend. All data smoothed using 100-year averaging.

from 33 % (LGM) to 40 % (PD). Simulated surface runoff is insignificant for most simulation years.

Temperatures at the La Campana site (32.93° S 71.09° W, 412 m a.s.l.) increase from 11.0 °C (LGM) to 14.0 °C (PD), but annual precipitation amounts decrease from 446 mm (LGM) to approx. 320 mm before slightly increasing again to 355 mm at PD. The simulated LGM vegetation for the La Campana site is dominated by herbaceous plants and small fractions of temperate evergreen deciduous trees mixed with small fractions of boreal shrubs which leads to a steppe biome classification with short episodes of mesic woodlands (Fig. 9c). With the decrease of annual precipitation and increasing temperatures (approx. 17 500 BP) sclerophyllous woodlands displace the deciduous trees and evergreen and raingreen shrubs start to appear. The fire-return intervals shorten in this phase and reach values of less than 15 years for the remainder of the simulation. Raingreen shrubs expand at approx. 12 000 BP and push back on herbaceous vegetation and, in part, evergreen shrubs. The LAI of sclerophyllous broad-leaved evergreen trees and shrubs further increases during the last 5000 simulation years, which leads to a shift in our biome classification from matorral ($LAI_{tot} > 0.5$) to sclerophyllous woodland ($LAI_{woody} > 1$). Despite pronounced changes in vegetation composition, FPC only increases from approx. 51 % (LGM) to 59 % (PD), which translates to a relative stable vegetation cover for these regions over time; thus, there is likely only a low impact of biome shifts on erosive processes.

Climatic conditions at the Nahuelbuta site (37.81° S 73.01° W, 1234 m a.s.l.) are markedly different to the three previously mentioned sites, as this location receives substantially higher annual precipitation throughout the time series (> 1200 mm) and average temperatures at this latitude and elevation are substantially lower (5.1 °C for LGM and 8.6 °C for PD, Fig. 9d). However, it can be seen that the landform is only representative of a small fraction of the 0.5° × 0.5° grid cell as it is located on mountainous terrain, whereas most areas in the cell are covered by coastal lowlands with higher annual temperatures; thus, the site simulation results presented here differ from the total grid cell results presented in previous sections (see marked landform cover in inset; Figs. 9d and B2a, b). LPJ-GUESS simulates a diverse composition of PFTs and a transition from boreal, Magellanic woodland conditions at the LGM, to a period of cold deciduous forest (17 500–12 000 BP), followed by 12 000 years of Valdivian rainforest and mesic woodland alternations. During the LGM, boreal broad-leaved evergreen, deciduous tree, and shrub PFTs dominate and form a forest. Annual precipitation (> 1300 mm) and surface runoff (> 440 mm) is high during this period. With rising temperatures, the boreal shrubs and evergreen tree PFTs are displaced by temperate needle-leaved evergreen trees (TeNE) and increases in herbaceous vegetation. Temperate evergreen PFTs establish approx. 17 000 BP and, after another retreat at approx. 14 500 BP (coinciding with the Antarctic cold reversal), start to dominate the forest at this location. Fire frequency is low for the first 4000 simulation years and only rises to approx. 1 fire in 100 years afterwards. FPC remains at constantly high values (> 75 %) indicating a largely closed forest for the entire simulation period and thus low dynamics of erosive processes due to constant high vegetation cover in this area.

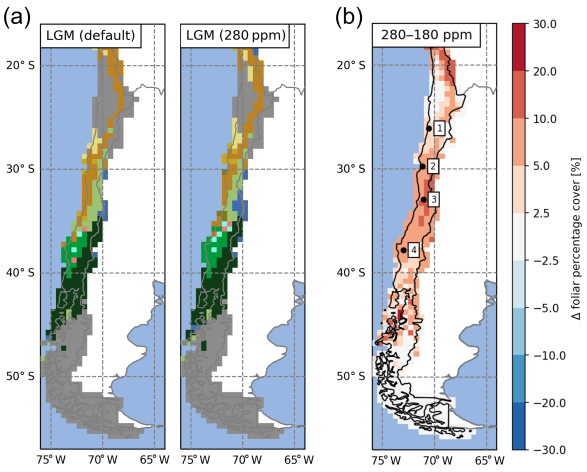

Figure 10. **(a)** Effect of atmospheric CO_2, represented as $[CO_2]$, concentrations on the simulated distribution of biomes for the Last Glacial Maximum (LGM) time-slice simulations (left panel: default LGM setup of this study with $[CO_2] = 180$ ppm; right panel: control run with preindustrial $[CO_2] = 280$ ppm). **(b)** Difference plot of resulting foliar projected cover (280–180 ppm). The number 1 represents Pan de Azúcar, 2 represents Sta. Gracia, 3 represents La Campana, and 4 represents Nahuelbuta.

4.5 Sensitivity of foliar projected cover to $[CO_2]$

The effectiveness of photosynthesis, and thus the plants ability to build up biomass, has a large dependence on $[CO_2]$ (Farquhar et al., 1980; Hickler et al., 2015). Increases in vegetation biomass (expressed in LAI) were observed in our simulations but coincide with a simultaneous rise in temperatures and $[CO_2]$ (Fig. 9b–d). To assess the direct effect of changes in $[CO_2]$, we conducted a sensitivity simulation under LGM climate conditions. We compared the default LGM simulations (TraCE-21ka, $[CO_2] =\sim 180$ ppm) with a preindustrial $[CO_2]$ level of 280 ppm (Fig. 10). This change led to an expansion of vegetated areas (high-Andean steppe), an increase of forest biomes at the expense of herbaceous vegetation (i.e., northward expansion of mesic woodland, cold deciduous forests, and Valdivian rainforest), and the establishment of small pockets of sclerophyllous woodland (Fig. 10a). In all vegetated areas FPC increased with higher $[CO_2]$, most notably between 30 and 40° S (+5–10 % FPC).

5 Discussion

The aim of this study was to demonstrate that a dynamic vegetation model with suitable modifications can simulate the state and transient changes of vegetation structure and composition at a temporal and spatial resolution that is suitable for coupling with LEMs which operate at higher spatial resolutions. To bridge the spatial scales and retain a high computational efficiency, we introduced sub-grid cell landform types in the DGVM LPJ-GUESS. Using this novel approach we are able to better reproduce observed spatial heterogeneity with existing DVMs. Furthermore, a regional parameterization of Chilean vegetation allowed us to simulated the present-day vegetation of Chile (Figs. 1a, 4, 5, 7; see also details in Sect. 5.1 below). In the PD simulations we found the largest regional discrepancy of observed and simulated vegetation cover to occur in coastal areas between 30 to 36° S, which might be attributed to the lack of fog precipitation in our model. Fog precipitation is strongly dependent on the distance to the coast, local topography, wind fields, and stratification of the troposphere (Lehnert et al., 2018) and can potentially contribute significant amounts of precipitation (Garreaud et al., 2008). However, a model representation of fog in LPJ-GUESS is difficult due to the scale mismatch and a lack of required input variables to determine the occurrence. Furthermore, precipitation amounts in the model drivers might be too low as the coarse spatial resolution of the original input data leads to an underrepresentation of orographic precipitation effects (i.e., Leung and Ghan, 1998). We also want to note that the MODIS VCF product was found to overestimate cover in sparsely vegetated areas (Sexton et al., 2013) and thus should rather be treated as a general guideline. Furthermore, LPJ-GUESS was applied to simulate the PNV, whereas MODIS VCF observes actual vegetation that includes anthropogenic land use (agricultural fields, degradation due to grazing, etc.).

Substantial changes in fire frequencies were observed in the transition simulations (Fig. 9b, c). LPJ-GUESS simulated these dynamics by considering available fuel which, in turn, is a function of present PFT composition and litter production. These rapid removals of vegetation cover have the potential to expose bare soil to erosion processes and could be critical in coupled simulations (a feature usually not considered in traditional landscape evolution modeling setups, i.e., Istanbulluoglu and Bras, 2005).

LPJ-GUESS explicitly simulates the soil moisture available for vegetation through a simple hydrological cycle (Gerten et al., 2004), and it is thus possible to calculate changes in runoff due to changes in transpiration, evaporation, and percolation at a site. Such information, in particular surface runoff, may also be provided to a LEM in a coupled model configuration. In this initial stage of our studies we did not use surface runoff in the LEM (see Schmid et al., 2018), but we envision that it will be incorporated in the planned coupled DVM–LEM model after proper evaluation. However, we caution the reader that the model used in this study uses a simple two-layer bucket model which cannot truly represent catchment scale hydrological features (i.e., no lateral flow, routing, or variable water table) but has been successfully coupled to mechanistic hydrological models in the past (Pappas et al., 2015).

5.1 Effects of landform simulation mode

As previously mentioned, the novel landform approach illustrated in this study (see Appendix B) was motivated by the fact that standard DVMs do not account for sub-grid heterogeneity controlled by topography and micro-climatic conditions. A common solution for this is to run these models at the same spatial resolution as a LEM, but this is generally computationally wasteful and often violates the scale assumptions of DVMs (i.e., patch size assumption in LPJ-GUESS; see Appendix B). The most striking advantage of landform implementation regarding the realism of simulated FPC is that it allows for the simulation of sub-grid topographic units (i.e., valleys, ridges, slopes) in a computationally efficient way as similar topographic locations are grouped to landforms and only simulated once (or rather n times for the patches of a given landform; see Fig. B1). North and south facing landforms receive a modified amount of solar radiation depending on their average slope and aspect orientation (which affects photosynthesis and transpiration in addition to water availability), and previous studies have showed that this can lead to distinct differences (i.e., Sternberg and Shoshany, 2001). Variable soil depth of landforms is associated with the topographic position (ridges are assumed to feature more shallow soils while valleys have deeper soils due to alluvial material). This results in a differing water storage potential which is especially relevant in dryer locations (Kosmas et al., 2000). Local temperature differences are also considered, as higher landforms are exposed to colder temperatures depending on the elevation difference to the reference elevation of the grid cell (see Appendix B). This leads to a more diverse PFT composition within a grid cell due to the fact that altitudinal zonation of vegetation within a grid cell can be represented (see Figs. 5b and B2b).

However, it has to be noted that we do not currently account for precipitation variations in the landform approach, as a good representation of these effects would require many additional model drivers (i.e., wind speed and direction, sea surface temperature for local fog precipitation; see Gerreaud et al., 2008, 2016; Lehnert et al., 2018) that are either not available at appropriate resolutions or for the time periods considered in this study. Future work may try to incorporate sophisticated statistical downscaling schemes (i.e., Karger et al., 2017) to address this shortcoming.

As can be observed (Fig. B2a), the implemented landform approach has differing effects for the four focus sites. The area-weighted average FPC at the Sta. Gracia site closely resembles the results from the default simulation mode (apart

from landform 810 – high altitudes – that only covers 1.7 % of the grid cell area, Fig. B2b). Average-landform and default results for the La Campana site also only differ marginally. However, here a set of landforms of higher altitudes has a substantially lower FPC than the average (~ -15 %). Variation at the hyper-arid Pan de Azúcar site is lower (as is the FPC), but it is generally higher than the default simulation. The larger vegetation cover simulated in the landform approach also better aligns with MODIS observations for the site, where the default model underestimates satellite-observed cover. The higher FPC in the new model setup is likely a result of the deeper soil profiles of flat and valley landforms that allow for longer water storage versus the default uniform 1.5m soil assumption of LPJ-GUESS. The larger variability of FPC at the Nahuelbuta site can be attributed to the relatively large altitudinal variation in this grid cell (coast to mountainous terrain) and is likely a temperature effect. From these results it can be postulated that the stronger heterogeneity of the simulated FPC using the landform approach will lead to more diverse denudation rates for the topographic units when linked to a LEM and should better resemble observed patterns of vegetation associations in the landscape (we will investigate this in detail in a future study using a coupled DVM–LEM setup).

In order to account for micro-site differences of temperature versus the average climate information per grid cell we stratified the landforms into elevation bins (Sect. 3.1 and Appendix B). Site temperature is an important environmental control for LPJ-GUESS as it impacts vegetation establishment (controlled for individual PFTs by their specific bioclimatic limits), photosynthesis rate, evapotranspiration, and soil decomposition (Smith et al., 2014). We selected 200 m as the bin width after a sensitivity analysis in order to keep the total number of landforms in complex terrain reasonable (potential temperature difference between 100 and 200 m bins < 0.3 °C; data not shown). Furthermore, using more topographic units (separating slopes into lower, mid, and upper slopes) also did not affect the simulation outcome and we therefore opted for a four-unit classification (see Appendix B). These configurations are subjective and should be tested before application under very different terrain or model scales.

5.2 Comparison to vegetation change proxy data

In general, regional vegetation cover of the past is difficult to quantify, as there are limited site-scale pollen, lake level, and midden proxy datasets available in Chile (Marchant et al., 2009). Pollen data from rodent midden (Quebrada del Chaco, 25.5° S, 2670–3550 m, Maldonado et al., 2005) suggest higher winter precipitation at the LGM, higher annual precipitation at 17–14 ka BP, and higher summer precipitation at 14–11 ka BP in northern Chile, but results from another study undertaken at lower elevations indicate absolute desert conditions throughout the Quaternary (Diaz et al., 2012) – which could be caused by regional fog-precipitation. TraCE-21ka precipitation for the Pan de Azúcar site (located at similar latitudes but in coastal lowlands) does not vary from PD conditions throughout the time series and as a result LPJ-GUESS simulates very little vegetation cover (Fig. 9a). Other studies also suggest that LGM conditions were extremely dry, but that the transition to modern climatic conditions in this area occurred as a nonlinear process of multiple moisture pulses over several centuries (Grosjean et al., 2001). Thus, this would imply that a coupled DVM–LEM model would underestimate episodes of high erosion potential due to poor model forcing data.

Pollen reconstructions from Laguna de Tagua Tagua 34.5° S 71.16° W (Heusser, 1990; Valero-Garcés et al., 2005) indicate the presence of extensive temperate woodlands at the LGM that match the simulated mesic woodland biome for this location in our simulations (Fig. 4a). Multiple lake sediment records of the region indicate dry and warm conditions in the MH and the onset of more humid, but strongly seasonal, conditions (winter rainfall) in the late Holocene (Heusser, 1990; Villa-Martínez et al., 2003; Valero-Garcés et al., 2005). While LPJ-GUESS simulates Mediterranean vegetation types (matorral and sclerophyllous woodland) for the MH and a shift to denser xeric woodlands in the late Holocene for this region, substantial variations in the precipitation regime as suggested by the lake records are not present in the TraCE-21ka data used.

Pollen records from the "Chilean Lake District" show a warming trend starting at 17 780 BP (Moreno and Videla, 2016), followed by a trend reversal with major cooling events (14 500 and 12 700 BP). In TraCE-21ka, a sharp cooling event is present at 14 500 BP (likely as an effect of the simulation setup of Meltwater Pulse 1A, Liu et al., 2009), but the second event is not. In our transient simulations this event is reflected in changes in the vegetation composition at three out of the four sites. This climatic change to colder and dryer conditions leads to a reduction of shrub PFTs at the Sta. Gracia (Fig. 9b) and La Campana sites (Fig. 9c) that established with rising temperature and [CO_2] starting at 18 000 BP. As a result, the site biome classification for Sta. Gracia briefly swings back to the initial steppe state and the reduced fuel accumulation leads to fewer fires. However, surface runoff is not affected due to the low precipitation rates. In contrast, the same event at the La Campana site does not result in changes of the fire frequency which is probably due to the presence of sufficient fuel owing to higher annual rainfall rates (> 350 mm). At the Nahuelbuta site this event briefly delays a transition from cold deciduous PFTs to a temperate evergreen/needle-leaved forest (Fig. 9d).

The early and mid-Holocene were the driest periods for central Chile (Heusser, 1990; Valero-Garcés et al., 2005; Maldonado and Villagrán, 2006). This is also visible in the TraCE-21ka dataset (La Campana and Nahuelbuta; Fig. 9c, d). However, the annual precipitation differences in the TraCE-21ka data from this period compared to the LGM and

PD are relatively minor; thus, we might not fully capture the true vegetation dynamics indicated by the proxy data of the region (centennial shifts from dry xeric to humid mesic vegetation).

Pollen proxy data from Villagrán (1988) indicate that coastal cool evergreen rainforests were shifted northwards by 5° during the LGM relative to their current position, and that these areas were covered by forest mosaics/parklands instead of the dense forest that is currently present. LPJ-GUESS simulations for the LGM reproduce this latitudinal biome shift (Fig. 5a). While we could not classify an open parkland vegetation type, the simulations show a 5 %–20 % lower FPC for this area at the LGM (Fig. 6b) which can be interpreted as more open conditions. For the MH, temperate Valdivian rainforests similar to PD conditions existed (Villagrán, 1988) and are also simulated by LPJ-GUESS (Fig. 5a)

LGM temperature reductions of up to 12 °C have been proposed for high altitudes in the tropics (Thompson et al., 1995), and LPJ-GUESS also simulates a more expansive belt of high-elevation cold desert for the LGM at the expense of high-Andean steppe (Fig. 5a, b). Furthermore, significantly lower tree lines and vegetation zones of up to 1500 m are reported for the LGM compared to PD (Marchant et al., 2009), which in our simulations is reflected in smaller areas of the cold deciduous forest biome and a shift to lower elevations (Fig. 5b).

In summary, the main forest transition in south-central Chile from the LGM to PD was the postglacial expansion of forests (∼ 15 ka BP). However, strong climate seasonality and forest clearing during early land utilization (as indicated by increased fire activities from 12 to 6 ka BP) and forest expansion into abandoned land after the Spanish colonial period (Lara et al., 2012) were other major, but anthropogenic, vegetation changes which were followed by intense land clearing for lumber extraction and farming (Armesto et al., 2010). Although significant for many areas, we opted to exclude anthropogenic land use in our analysis as spatial intensities and general utilization are not well understood and are hard to qualify; furthermore, we see this as beyond the scope of this particular study.

5.3 Sensitivity of simulation to paleoclimate input data

As demonstrated in this study, climatic forcing of the ecosystem model is crucial for the simulated vegetation composition, biome establishment, and associated vegetation cover and surface runoff, which are key controls of catchment denudation rates (Jeffery et al., 2014). The TraCE-21ka dataset was chosen since, to our knowledge, it is the only available dataset providing continuous transient monthly data. However, the low spatial resolution (T31/∼ 3.75°) is problematic in resolving regional-scale heterogeneity; therefore, we compare our LGM simulations with a regional paleoclimate model simulation (ECHAM5, resolution: T159/ 0.75° × 0.75°, Mutz et al., 2018). Although the general latitudinal patterns of temperature deviations from PD are similar to TraCE-21ka, precipitation gradients and regional anomalies during the LGM are stronger (see Fig. 3 for LGM anomaly plot of TraCE-21ka data and Fig. S1a, b for ECHAM5). While LGM precipitation anomalies in TraCE-21ka do not exceed 650 mm, precipitation rates in the ECHAM5 data vary by well over 1500 mm for the Andean highlands from 27 to 35° S and the coastal areas from 36 to 53° S but are markedly lower for the lower Andes and Tierra del Fuego (Fig. S1b). This leads to a different biome distribution pattern for the LGM (Fig. 11). Due to lower temperatures, the cold deserts extend further north and a small zone of temperate rainforest exists at latitudes from 40 to 42° S, whereas Magellanic woodlands are simulated with TraCE-21ka. A zone classified as Magellanic woodland stretches from 30 to 42° S along the Andean range which gives way to cold deciduous forest at 28 to 32° S at altitude. Temperate deciduous "Maule" forest exists north of 40° S and transitions into sclerophyllous woodland extending to 30° S, whereas TraCE-21ka results lead to steppe at the lowlands and mesic woodlands at higher altitudes. Higher precipitation levels north of 30° S also lead to higher vegetation cover, larger areas of matorral and arid shrubland, and a reduction of desert conditions. This results in substantial differences in simulated foliar projected cover (Fig. 11b). While cover of steppe and mesic woodlands simulated with TraCE-21ka is generally 10 %–20 % higher versus the ECHAM5 simulations, the cover from 35° S to the Atacama Desert is substantially lower than ECHAM5 (higher precipitation rates for this region). Cover south of 42° S is substantially higher for TraCE-21ka as the colder conditions in ECHAM5 simulations generally prohibit vegetation establishment.

The results show that the choice of paleoclimate data clearly has an influence on the simulated vegetation composition, but the impact on vegetation cover depends on the type and location of change. For instance, forest-to-forest transitions due to changes in temperature can have little effect on FPC, while a different annual precipitation rate in Mediterranean to semi-arid conditions can lead to substantial changes in FPC (Sta. Gracia: +200–500 mm precipitation in ECHAM5 LGM data results in > +20 % FPC; Fig. 8a). Given the results from our study we might severely underestimate episodes of elevated erosion in future coupled model exercises – thus, thorough sensitivity studies will be required.

5.4 Impact of atmospheric CO_2 on vegetation cover

The effectiveness of photosynthesis, and the related ability of plants to build up biomass, has a large dependence on [CO_2] (Farquhar et al., 1980; Hickler et al., 2015). Increases in vegetation biomass (expressed in LAI) were observed in our simulations but coincide with simultaneous rises in temperature and [CO_2] (Fig. 9b–d). As observed in the CO_2 sensitivity runs for LGM climate conditions, higher [CO_2] concentrations lead to an expansion of vegetated areas at higher el-

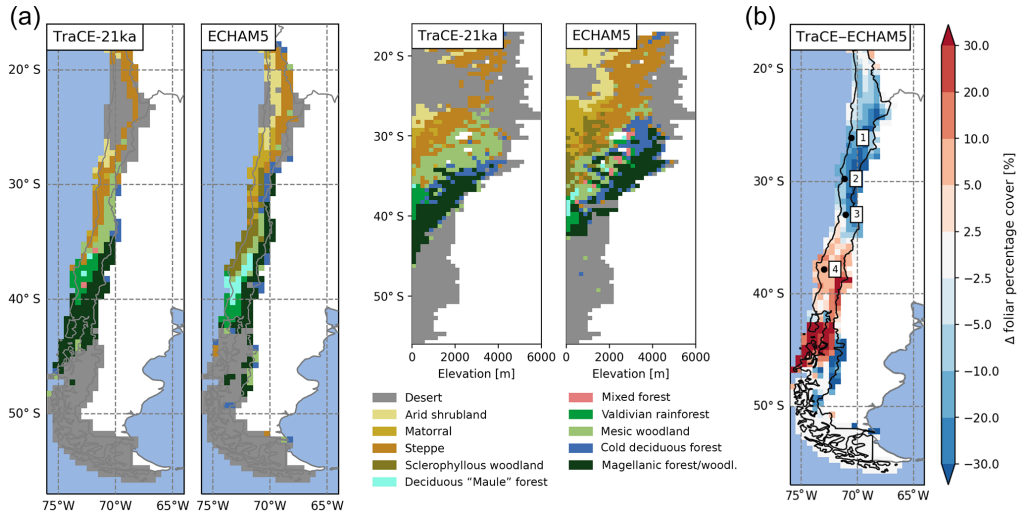

Figure 11. **(a)** The effect of paleoclimate input data used for LPJ-GUESS simulations on the spatial and altitudinal biome distribution and **(b)** the effect on simulated foliage projected cover (given as the difference between TraCE-21ka simulation and ECHAM5 simulation results, Mutz et al., 2018). For a comparison of the differences between average temperatures and precipitation between the two climate datasets see Figs. 3 and S3. The number 1 represents Pan de Azúcar, 2 represents Sta. Gracia, 3 represents La Campana, and 4 represents Nahuelbuta.

evations and an expansion of forest biomes at the expense of herbaceous vegetation. Such changes and the magnitude of the CO_2 effect are consistent with earlier LGM simulations (Harrison and Prentice, 2003; Bragg et al., 2013). These changes suggest that [CO_2] could play crucial role in understanding landscape evolution over longer timescales – a factor that again is not considered in previous studies of landscape evolution (i.e., Istanbulluoglu and Bras, 2005; Collins et al., 2004).

The strong limiting role of [CO_2] during the LGM is generally accepted, but the extent to which substantial CO_2 fertilization effects still occur as concentrations increase and rise beyond the current stage is highly debated (Hickler et al., 2015). However, the LPJ-GUESS model with the enabled nitrogen cycle, and nitrogen limiting CO_2 effects, has been shown to generally reproduce experimental observations from "Free Air Carbon Dioxide Enrichment" (FACE) experiments (e.g., Zaehle et al., 2014; Medlyn et at al., 2015; De Kauwe et al., 2017). Enabling the nitrogen cycle in LPJ-GUESS is crucial if one aims to understand vegetation response and landscape evolution at [CO_2] levels above those of the present day, as have occurred in various episodes of Earths' history (i.e., the Miocene).

In general, we were able to show a temporal compatibility of paleovegetation state, vegetation transitions, and simulated vegetation composition using our model (Sect. 5.2). Our results also indicate that the simulated vegetation is strongly influenced by climatic model drivers (see Sect. 5.3) and [CO_2], and by feedback mechanisms occurring within the model (i.e., fire return intervals as controlled by climate and the production of fuel). Given the sensitivity of the vegetation cover to the climate forcing, careful consideration must be made regarding paleoclimate data and its characteristics and uncertainties. The TraCE-21ka data does not show high levels of variability, instead exhibiting only gradual changes over time (temperature, atmospheric CO_2 concentration); furthermore, the TraCE-21ka data does not display strong, centennial to millennial scale trends (precipitation). In contrast, available proxy data suggest stronger variability, at least locally, although this is difficult to generalize for larger areas (see Sect. 5.2). Regional paleoclimate simulations with a higher spatial resolution might be required to obtain better landscape-scale model forcing. Another approach may be to modify the climate model derived forcing based on proxy data, such as increasing inter- and intra-annual variability within reasonable ranges (e.g., Giesecke et al., 2010).

6 Conclusions

In this study, we demonstrated how a DGVM can be applied to estimate vegetation features through time. These features can play an important role in the evolution of landforms, and at a spatial and temporal resolution adequate for coupling with LEMs. The simulation also captures vegetation change drivers that are not explicitly represented in simplified vegetation representations used in LEMs to date, such as plant-physiological effects of changing [CO_2], fire dynamics that vary greatly with PFT composition, and interaction with soil water resources via different rooting strategies. The sensitiv-

ity of landscape evolution to vegetation and climate changes is evaluated in the companion paper by Schmid et al. (2018). Although our two studies stop short of presenting results from a fully coupled (dynamic vegetation and surface process) model, the results we present highlight (a) how much vegetation likely changed in the Coastal Cordillera of Chile since the LGM (this study), and (b) the general sensitivity of topography and erosion rates to the magnitudes of change identified here (Schmid et al., 2018). In future work we will implement a two-way coupling of LPJ-GUESS to Landlab. LPJ-GUESS will be driven by climate data and will produce a continuous dataset of vegetation cover and surface hydrology that is passed to Landlab. Landlab will use this vegetation cover and simulated denudation rates and will provide updated topography (and after a landform classification, updated areal cover of landforms) and the associated soil depth information to LPJ-GUESS. The novel approach of representing sub-grid diversity in vegetation by landforms allows for efficient computation with existing coarse-scale climate data in addition to coupling to LEMs with higher spatial representations of topography.

From the experiments presented here, our main conclusions are as follows:

1. The regionally adapted version of LPJ-GUESS was able to simulate the latitudinal and altitudinal distribution of potential natural vegetation and the satellite-observed vegetation cover for present-day conditions in most areas of Chile.

2. While simulated MH vegetation did not differ substantially compared to PD PNV, simulated vegetation of the LGM indicates a marked northward shift of biome distribution, a reduction of the tree line, and a downward shift of vegetation zones at altitude. Vegetation cover was generally reduced compared to PD conditions and cold and hot desert covered substantially larger areas of the simulation domain.

3. An analysis of the results from a transient site simulation indicate that temperature and [CO_2] caused most of the observed shifts in vegetation composition and (in some cases) transitions between biomes over time. A sensitivity study highlighted the impact of "CO_2 fertilization" on vegetation cover under LGM climate conditions.

4. Comparisons with proxy data suggest that coarse-scale climatic forcing underestimates centennial to millennial climate variability. A combination of proxy-derived estimates and climate model results or higher-resolution climate models might be necessary to capture such variability.

5. Our results show that vegetation cover in semi-arid to Mediterranean ecosystems responds strongly to changes in precipitation, while changes in climatic conditions for temperate to boreal forest ecosystems also causes a change in vegetation cover, although to a lesser extent.

6. We consider the implementation of a landform classification a feasible tool to (a) mediate between coarse DVM model resolutions and generally higher-resolution LEMs with little computational expense, and (b) to account for sub-grid variability of micro-climate conditions that are otherwise absent from DVM simulations at larger scales. We envision that it will also allow new applications of LPJ-GUESS to research questions where a better representation of vegetation composition and state, especially the heterogeneity of the simulated sub-pixel vegetation, is important.

In summary, we suggest that coupling state-of-the-art dynamic vegetation modeling with LEMs has great potential for improving our understanding of the evolution of landforms. This is due to the fact that DVMs using the landform approach can approximate the spatial heterogeneity observed in the field which is otherwise not represented by standard DVM implementations. The FPC linked to topography structure will likely result in varying denudation rates in the landscape and will thus have the potential to influence landscape evolution. The regional model adaptation and illustrated model improvements are an important step towards applying a coupled model such as this to the EarthShape study area.

Data availability. Model setup and results are available upon request from the authors.

Appendix A: Calculation of monthly wet days

It is a well-documented problem that climate models, such as CCSM3, have a tendency to overestimate the precipitation frequency in dry regions (e.g., Dai, 2006). Therefore, we parameterize the number of "wet days" (number of days in a month with rainfall greater than 0.1 mm day^{-1}) based on ERA-Interim daily climatology. It is assumed that the daily precipitation in a month follows a gamma distribution, which is determined by the shape and scale parameters (α and β, respectively) as follows:

$$\alpha = (x_{\text{mean}}/x_{\text{std}})^2$$
$$\beta = x_{\text{std}}^2/x_{\text{mean}},$$

where x_{mean} is the monthly mean precipitation, and x_{std} is its standard deviation (day-to-day variability). A characteristic feature of the gamma distribution is its ability to attain two completely different shapes depending on the value of α. If $\alpha < 1$ (typical for dry regions), the probability density attains maximum value at zero precipitation and decreases exponentially towards higher precipitation values, and if $\alpha > 1$ (typical for wet regions), the probability density function has a shape more reminiscent of a Gaussian distribution.

The number of wet days is estimated from the cumulative gamma distribution:

$$F(x\alpha\beta) = \frac{1}{\beta^{\alpha}\Gamma(\alpha)} \int_0^x t^{\alpha-1}\exp(-t/b)\mathrm{d}t,$$

where Γ is the gamma function. The result of this equation is the probability that an observation will fall in the interval $[0x]$. Hence for our purposes, the number of wet days (n_{wet}) is determined by

$$n_{\text{wet}} = n_{\text{day}}(1 - F(x_t\alpha\beta)), \tag{A1}$$

where n_{day} is the number of days in a month, and x_t is the threshold value for a wet day (0.1 mm day^{-1}).

In our experiments the TraCE-21k climatology influences monthly n_{wet} by modifying x_{mean} at each grid cell. However, due to the poor representation of precipitation frequencies in the TraCE-21ka data, we use a monthly climatology of x_{std} calculated from ERA-Interim.

Appendix B: Implementation of landforms in LPJ-GUESS

LPJ-GUESS, by default, acknowledges within grid cell variability of vegetation using the concept of patches (Smith et al., 2014). A patch represents a subset of the grid cell that is usually 0.5° × 0.5° in size. Patches are not spatially registered to any particular location within this cell. By definition, they represent an area of 0.1 ha – the assumed maximum area a mature tree might cover. The replication of these patches ensures that stochastic events (i.e., vegetation establishment and mortality, fire) effect only subsets of a grid cell and allow the model to simulate gap-dynamics and succession. Studies usually are configured with $n >= 100$ patch replications to prevent the stochastic events from dominating simulated average grid cell results. In this study we introduce "landforms" into LPJ-GUESS. The aim is to address two problems. First, the default grid cell size (0.5 × 0.5) does not allow observed landscape heterogeneity to be addressed (i.e., local site conditions, topographic structure of a catchment). While LPJ-GUESS has been applied at higher resolutions, the lack of high-quality environmental forcing for these resolutions often makes this approach impractical. Second, this new approach allows us to link two models of different model resolutions (LPJ-GUESS and climate drivers 0.5° × 0.5°, LEM Landlab 100 × 100 m) to approximate the true DEM characteristics into homogeneous landform units that aim to characterize the dominant topographic units within this 0.5° × 0.5° grid cell. Thus, the landform concept can be used to mediate the information exchange between these two models. In the implemented landform concept we define a set of patch groups for each landform (i.e., a subset of the grid that shares the same topographic features and similar elevation, slope and aspect). The classification is based on a high-resolution elevation model of the grid cell (SRTM1 data, 30 m), but in a future coupled model the high-resolution DEM will be provided and continuously updated by the landscape evolution model coupled to LPJ-GUESS. The model forcing (0.5° × 0.5° climate and soil texture) is modified for the defined landforms of a given grid cell (see also Fig. B1).

B1 Classification of landforms and modification of environmental drivers

In order to classify landforms, we use the elevation and computed slope and aspect of the grid cells of the high-resolution DEM. Furthermore, aspect and slope are used to compute a topographic position index (TPI) – the difference between elevation and the elevation of surrounding positions (focal radius 300 m; see Weiss, 2001). The TPI and slope values are then used to classify positions into discrete topographic classes (here: ridges – TPI > 1 SD, mid-slopes – TPI > −1 SD and TPI < 1 SD and slope >= 6°, valleys – TPI <= −1 SD and flats – TPI > −1 SD and TPI < 1 SD and slope < 6°). These classes are then stratified by elevation intervals to finally form the landforms (the number of landforms per grid cell depends on complexity of the terrain: mean is 17, 25 % quantile is 11, and 75 % quantile is 23). The average elevation, slope, and aspect are then used to adapt the environmental forcing for this landform.

In this study, we adapt the landform surface temperature via the elevation difference of the 0.5° × 0.5° grid cell elevation E_{GC} and the average elevation of the high-resolution DEM occupied by a landform (E_{LF}). We also adjust the tem-

perature with the global lapse rate γ of $-6.5\,^{\circ}\mathrm{C\,km^{-1}}$.

$$T_{\mathrm{LF}} = T_{\mathrm{GC}} + \gamma\,(E_{\mathrm{LF}} - E_{\mathrm{GC}}).$$

Furthermore, we adapt the amount of absorbed radiation based on the landform slope, aspect, and the time of the year. The solar declination (δ) at any given day of the year (doy: day of year) is calculated in LPJ-GUESS as follows (Prentice et al., 1993, all angles in radians):

$$\delta = -23.4 \times \cos\left(2\pi \times \frac{\mathrm{doy} + 10.5}{365}\right). \quad \text{(B1)}$$

The solar angle at noon is calculated from the latitude (lat) and δ as follows:

$$A_Z = \mathrm{lat} - \delta.$$

The corrected radiation at the landform (R_{LF}) for north or south facing slopes depending on their aspect (ψ) and slope angle (β) is then calculated from the grid cell radiation in LPJ-GUESS (R_{GC}):

$$R_{\mathrm{LF}} = R_{\mathrm{GC}} \times \left(\frac{1}{\cos A_Z}\right) \times \cos(|A_Z| \pm \beta \times \cos(\beta \times |\psi|)). \quad \text{(B2)}$$

Finally, the soil depth of the landform is adjusted based on the TPI of the landform. The default soil depth (DSD) of 1.5 m is scaled by multiplying the height of the lower soil layer (default: 1 m) with fixed values for ridges (0.25), mid-slope positions (0.5), and valleys (1.5) resulting in a total soil depth of 0.75, 1, and 2 m, respectively.

In the future coupled model actual soil depth will be provided by the landscape evolution model.

B2 Model setup with landforms

Instead of running LPJ-GUESS with one environmental condition for all n patches ($n >= 100$) of a grid cell, the model is now executed for each landform and its adjusted environmental conditions n times ($n = 15$). In both model setups the grid cell results are reported as the average results over all n patches (Fig. C1). However, in the landform setup the results are reported as area-weighted averages (the area fraction equals landform fraction within the grid cell). Patches within a landform are averaged in the same way as they are in the default model setup. In a model-coupling setup the model results per landform will be disaggregated back onto the high-resolution DEM of the landscape evolution model to provide a spatially explicit vegetation cover.

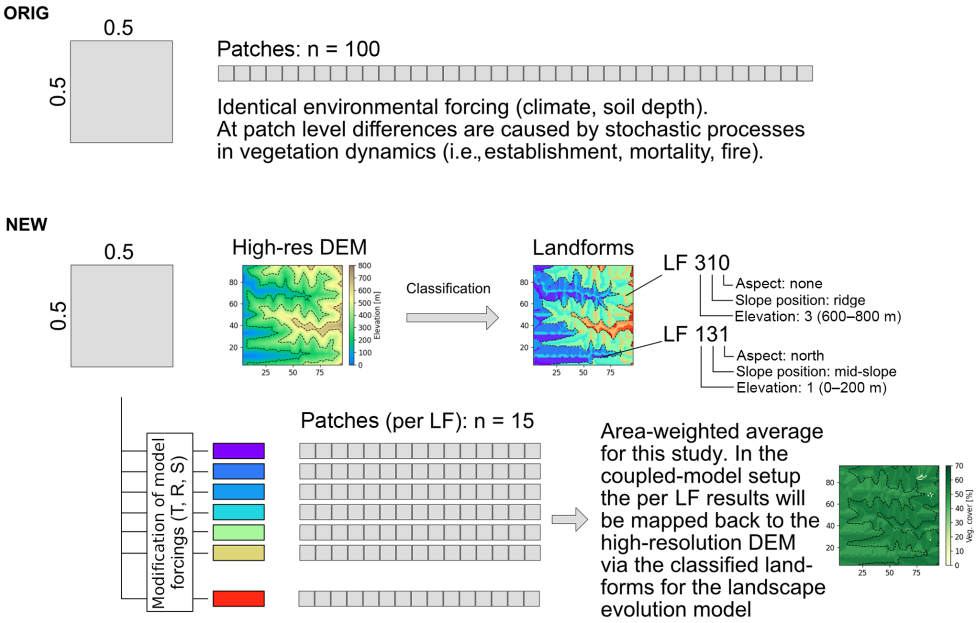

Figure B1. Conceptual difference between original LPJ-GUESS patch setup and the new landform addition (T is temperature, R is radiation, S is soil depth, and LF is landform).

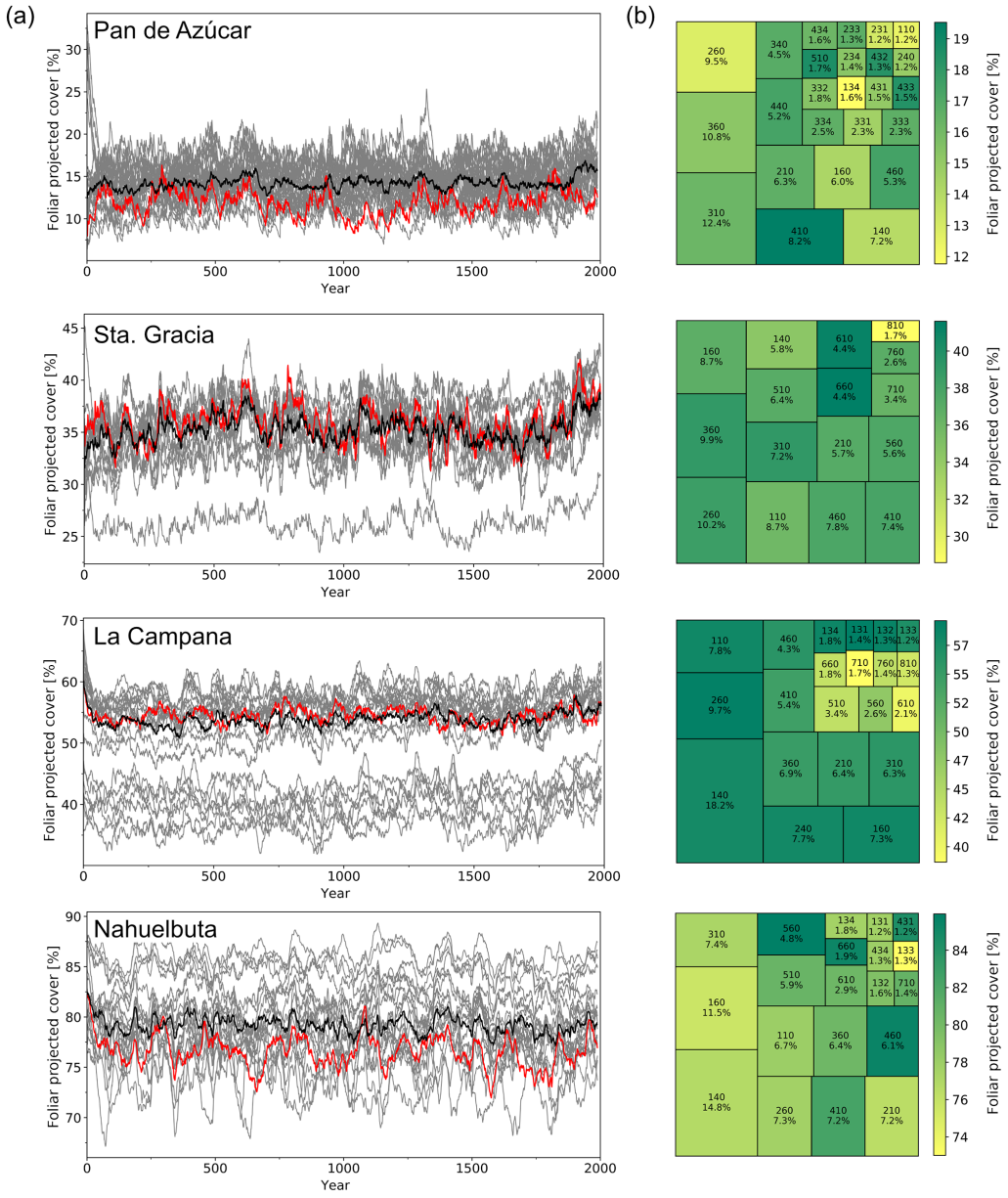

Figure B2. **(a)** Change of foliar projected cover for the individual landforms (gray), the area-weighted mean of all landforms (black), and the default LPJ-GUESS setup with no landforms (red) for the last 2000 years of the transient simulations. **(b)** Areal extent and foliar projected cover of the individual landforms in the four simulated grid cells (averaged for the last 100 years of the time series; text: landform ID code and percentage of the total grid cell covered by this landform.

Appendix C: Plant functional type setup and biomization scheme

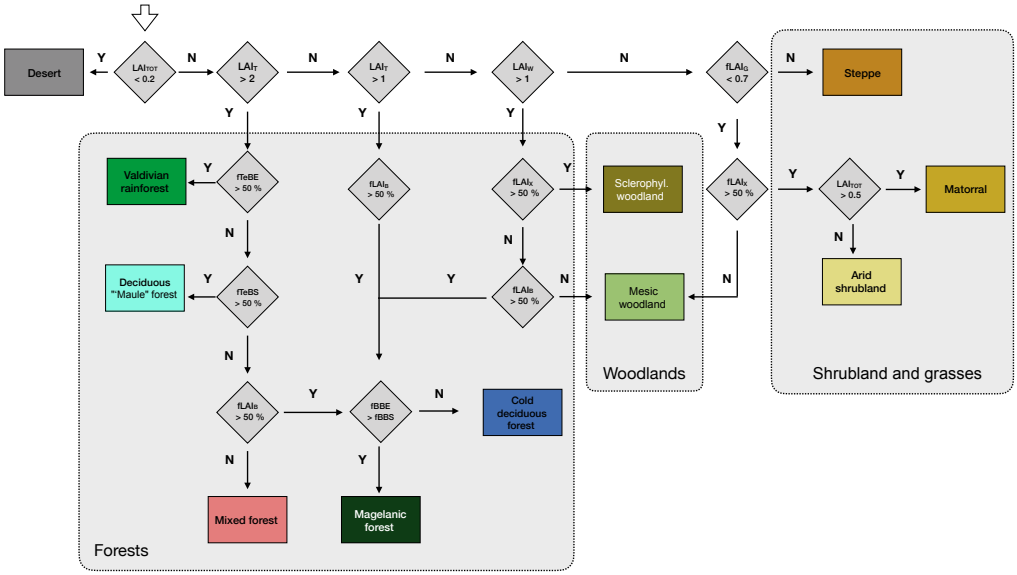

Figure C1. Flowchart of the decision tree used to classify plant functional types (PFTs) into biomes. LAI_{TOT} is the LAI of all PFTs; LAI_T is the LAI of tree PFTs; LAI_W is the LAI of trees + shrubs; LAI_G is the LAI of herbaceous PFTs; LAI_X is the LAI of xeric PFTs; LAI_B is the LAI of boreal PFTs; $fLAI_n$ is the fraction of the LAI PFT_n versus its peers (all tree PFTs, boreal PFTs, etc.); TeBE is temperate broad-leaved evergreen trees; TeBS is temperate broad-leaved summergreen trees; BBE is boreal broad-leaved evergreen trees; and BBS is boreal broad-leaved summergreen trees.

Table C1. Plant functional type (PFT) characteristics used in this study. Climate classes are associated with differing photosynthesis optimum temperatures and base respiration rates (see Smith et al., 2001; Te is temperate, B is boreal; M is Mediterranean was newly introduced with PS temperatures min: 0, low: 17, high: 27, max: 40; resp. coefficient: 1.0). k_{allom1} is a constant in allometry equations (Smith et al., 2001; higher values equal wider crowns); $T_{\mathrm{c,min}}$ is the minimum coldest-month temperature for survival; $T_{\mathrm{c,max}}$ is the maximum coldest-month temperature for establishment; GDD_5 is the minimum degree-day sum above 5 °C for establishment; fAWC is the minimum growing-season (daily temperature > 5 °C) fraction of available soil water holding capacity in the first soil layer; r_{fire} is the fraction of individuals that survive fire; $k_{\mathrm{la:sa}}$ is the leaf area to sapwood cross-sectional area ratio; z_1 is the fraction of roots in first soil layer (the reminder being allocated to second soil layer); a_{leaf} is the leaf longevity; a_{ind} is the maximum, non-stressed longevity; $\mathrm{CA}_{\mathrm{max}}$ is the maximum woody crown area. r is the base respiration rate (modified after Hickler et al., 2012).

PFT	Climate	r ($\mathrm{g\,C\,g\,N^{-1}\,d^{-1}}$)	Life form	k_{allom1}	$T_{\mathrm{c,min,s}}$ (°C)	$T_{\mathrm{c,min}}$ (°C)	$T_{\mathrm{c,max}}$ (°C)	T_{wmin}	GDD_5 (°C d)	fAWC	Shade tol.	r_{fire}	$k_{\mathrm{la:sa}}$	z_1	a_{leaf} (yr)	a_{ind} (yr)	$\mathrm{CA}_{\mathrm{max}}$ (m^2)
$\mathrm{TeBE_{tm}}$	Te	0.055	Tree	250	−1	0	15		900	0.3	Tolerant	0.1	6000	0.7	2.0	500	30
$\mathrm{TeBE_{itm}}$	Te	0.055	Tree	250	−1	0	15		900	0.3	Intolerant	0.1	6000	0.7	2.0	400	30
$\mathrm{TeBE_{itscl}}$	Te/M	0.055	Tree	250	1	4	18.8		2400	0.01	Intolerant	0.5	4000	0.5	2.0	250	30
$\mathrm{TeBS_{tm}}$	Te	0.055	Tree	250	−14	−13	6	5	1800	0.3	Tolerant	0.2	6000	0.6	0.5	500	30
$\mathrm{TeBS_{itm}}$	Te	0.055	Tree	250	−14	−13	6	5	1800	0.3	Intolerant	0.2	6000	0.6	0.5	400	30
$\mathrm{TeE_s}$	Te/M	0.055	Shrub	100	1	1	–		2600	0.001	Intolerant	0.5	3000	0.5	2.0	100	10
$\mathrm{TeR_s}$	Te/M	0.055	Shrub	100	1	1	–		2800	0.001	Intolerant	0.5	3000	0.5	1.0	50	10
TeNE	Te	0.055	Tree	150	−7	−7	22		600	0.3	Intolerant	0.5	5000	0.7	2.0	400	30
$\mathrm{BBS_{itm}}$	B	0.11	Tree	250	−30	−30	3		150	0.1	Intolerant	0.1	6000	0.6	0.5	300	30
$\mathrm{BBE_{itm}}$	B	0.11	Tree	250	−30	−30	5		250	0.5	Intolerant	0.1	6000	0.8	2.0	400	30
$\mathrm{BE_s}$	B	0.11	Shrub	100		–	4.5		150	0.3	Intolerant	0.1	2000	0.8	2.0	50	10
C3G	–	0.055	Herbac.	–		–	–		–	0.1	–	0.5	–	0.9	0.75	–	–

Supplement. The supplement related to this article is available online at: https://doi.org/10.5194/esurf-6-829-2018-supplement.

Author contributions. Model development, setup, simulations and analysis were conducted by CW. The preparation of the paper was carried out by CW in coordination with TH, MS and TAE, with contributions from all coauthors.

Competing interests. The authors declare that they have no conflict of interest.

Acknowledgements. This study was funded as part of the German science foundation priority research program Earth-Shape: Earth surface shaping by biota (grant no. EH329-14-1 to Todd A. Ehlers and HI1538/5-1 to Thomas Hickler). We also thank the national park service of Chile (CONAF) for access to the study areas during field excursions.

Edited by: Rebecca Hodge
Reviewed by: two anonymous referees

References

Acosta, V. T., Schildgen, T. F., Clarke, B. A., Scherler, D., Bookhagen, B., Wittmann, H., von Blanckenburg, F., and Strecker, M. R.: Effect of vegetation cover on millennial-scale landscape denudation rates in East Africa, Lithosphere, 7, 408–420, https://doi.org/10.1130/L402.1, 2015.

Allen, J. R. M., Hickler, T., Singarayer, J. S., Sykes, M. T., Valdes, P. J., and Huntley, B.: Last glacial vegetation of northern Eurasia, Quaternary Sci. Rev., 29, 2604–2618, https://doi.org/10.1016/j.quascirev.2010.05.031, 2010.

Armesto, J. J., Arroyo, M. T. K., and Hinojosa, L. F.: The Mediterranean environment of central Chile, in: The Physical Geography of South America, edited by: Veblen, T. T., Young, K. R., and Orme, A. R., Oxford University Press, 184-199, 2007.

Armesto, J. J., Manuschevich, D., Mora, A., Smith-Ramirez, C., Rozzi, R., Abarzua, A. M., and Marquet, P. A.: From the Holocene to the Anthropocene: A historical framework for land cover change in southwestern South America in the past 15 000 years, Land Use Policy, 27, 148–160, https://doi.org/10.1016/j.landusepol.2009.07.006, 2010.

Arroyo, M. T. K., Pliscoff, P., Mihoc, M., and Arroyo-Karlin, M.: The Magellanic moorland, in: The World's Largest Wetlands, edited by: Fraser, L. H. and Keddy, P. A., Cambridge University Press 424–445, 2005.

Batjes, N. H.: ISRIC-WISE Derived soil properties on a 5 by 5 arcminutes grid (version 1.2), ISRIC Report 2012/01, 2012.

Bonan, G. B.: Forests and climate change: Forcings, feedbacks, and the climate benefits of forests, Science, 320, 1444–1449, https://doi.org/10.1126/science.1155121, 2008.

Bonan, G. B., Levis, S., Kergoat, L., and Oleson, K. W.: Landscapes as patches of plant functional types: An integrating concept for climate and ecosystem models, Global Biogeochem. Cy., 16, 1021–1025, https://doi.org/10.1029/2000GB001360, 2002.

Bragg, F. J., Prentice, I. C., Harrison, S. P., Eglinton, G., Foster, P. N., Rommerskirchen, F., and Rullkötter, J.: Stable isotope and modelling evidence for CO_2 as a driver of glacial-interglacial vegetation shifts in southern Africa, Biogeosciences, 10, 2001–2010, https://doi.org/10.5194/bg-10-2001-2013, 2013.

Brook, E.: Windows on the greenhouse, Nature, 453, 291–292, 2008.

Brovkin, V., Raddatz, T., Reick, C. H., Claussen, M., and Gayler, V.: Global biogeophysical interactions between forest and climate, Geophys. Res. Lett., 36, L07405, https://doi.org/10.1029/2009GL037543, 2009.

Bugmann, H.: A review of forest gap models, Climatic Change, 51, 259–305, 2001.

Collins, D. B. G., Bras, R. L., and Tucker, G. E.: Modeling the effects of vegetation-erosion coupling on landscape evolution, J. Geophys. Res.-Earth, 109, F03004, https://doi.org/10.1029/2003JF000028, 2004.

Collins, W. D., Bitz, C. M., Blackmon, M. L., Bonan, G. B., Bretherton, C. S., Carton, J. A., Chang, P., Doney, S. C., Hack, J., James, Henderson, T. B., Kiehl, J. T., Large, W. G., McKenna, D. S., Santer, B. D., and Smith, R. D.: The Community Climate System Model Version 3 (CCSM3), J. Climate, 19, 2122–2143, https://doi.org/10.1175/JCLI3761.1, 2006.

Cramer, W., Bondeau, A., Woodward, F., Prentice, I., Betts, R., Brovkin, V. and, Cox, P., Fisher, V., Foley, J., Friend, A., Kucharik, C., Lomas, M., Ramankutty, N., Sitch, S., Smith, B, White, A., and Young-Molling, C.: Global response of terrestrial ecosystem structure and function to CO_2 and climate change: results from six dynamic global vegetation models, Glob. Change Biol., 7, 357–373, https://doi.org/10.1046/j.1365-2486.2001.00383.x, 2001.

Dai, A.: Precipitation characteristics in eighteen coupled climate models, J. Climate, 19, 4605–4630, Precipitation Characteristics in Eighteen Coupled Climate Models, 2006.

Dee, D. P., Uppala, S. M., Simmons, A. J., Berrisford, P., Poli, P., Kobayashi, S., Andrae, U., Balmaseda, M. A., Balsamo, G., Bauer, P., Bechtold, P., Beljaars, A. C. M., Berg, L. van de, Bidlot, J., Bormann, N., Delsol, C., Dragani, R., Fuentes, M., Geer, A. J., Haimberger, L., Healy, S. B., Hersbach, H., Hólm, E. V., Isaksen, L., Kållberg, P., Köhler, M., Matricardi, M., McNally, A. P., Monge-Sanz, B. M., Morcrette, J. J., Park, B. K., Peubey, C., Rosnay, P. de, Tavolato, C., Thépaut, J. N., and Vitart, F.: The ERA-Interim reanalysis: configuration and performance of the data assimilation system, Q. J. Roy. Meteor. Soc., 137, 553–597, https://doi.org/10.1002/qj.828, 2011.

De Kauwe, M. G., Medlyn, B. E., Walker, A. P., Zaehle, S., Asao, S., Guenet, B., Harper, A. B., Hickler, T., Jain, A. K., Luo, Y., Lu, X., Luus, K., Parton, W. J., Shu, S., Wang, Y.-P., Werner, C., Xia, J., Pendall, E., Morgan, J. A., Ryan, E. M., Carrillo, Y., Dijkstra, F. A., Zelikova, T. J., and Norby, R. J.: Challenging terrestrial biosphere models with data from the long-term multifactor Prairie Heating and CO_2 Enrichment experiment, Glob. Change Biol., 23, 3623–3645, https://doi.org/10.1111/gcb.13643, 2017.

Diaz, F. P., Latorre, C., Maldonado, A., Quade, J., and Betancourt, J. L.: Rodent middens reveal episodic, long-distance plant colonizations across the hyperarid Atacama Desert over the last 34 000 years, J. Biogeogr., 39, 510–525, https://doi.org/10.1111/j.1365-2699.2011.02617.x, 2012.

Dimiceli, C., Carroll, M., Sohlberg, R., Kim, D. H., Kelly, M., and Townshend, J. R. G.: MOD44B MODIS/Terra Vegetation Continuous Fields Yearly L3 Global 250m SIN Grid V006. 2015, distributed by NASA EOSDIS Land Processes DAAC, doi.org/10.5067/MODIS/MOD44B.006, 2015.

Donoso, C. D. O.: Reseña ecologica de los bosques mediterraneos de Chile, Bosque (Valdivia), 4, 117–146, 1982.

Escobar Avaria, C. A.: Simulating current regional pattern and composition of Chilean native forests using a dynamic ecosystem model, Student thesis series INES, available at: http://lup.lub.lu.se/student-papers/record/3877156 (last access: 15 September 2018), 2013.

Farquhar, G. D., von Caemmerer, S, and Berry, J. A.: A biochemical model of photosynthetic CO_2 assimilation in leaves of C3 species, Planta, 149, 78–90, https://doi.org/10.1007/BF00386231, 1980.

Forrest, M., Eronen, J. T., Utescher, T., Knorr, G., Stepanek, C., Lohmann, G., and Hickler, T.: Climate-vegetation modelling and fossil plant data suggest low atmospheric CO_2 in the late Miocene, Clim. Past, 11, 1701–1732, https://doi.org/10.5194/cp-11-1701-2015, 2015.

Garreaud, R. and Aceituno, P.: Atmospheric circulation and climatic variability, in: The Physical Geography of South America, edited by: Veblen, T. T., Young, K. R., and Orme, A. R., Oxford University Press, 45–59, 2007.

Garreaud, R., Barichivich, J., Christie, D. A., and Maldonado, A.: Interannual variability of the coastal fog at Fray Jorge relict forests in semiarid Chile, J. Geophys. Res., 113, G04011, https://doi.org/10.1029/2008JG000709, 2008.

Garreaud, R., Falvey, M., and Montecinos, A.: Orographic Precipitation in Coastal Southern Chile: Mean Distribution, Temporal Variability, and Linear Contribution, J. Hydrometeorol., 17, 1185–1202, https://doi.org/10.1175/JHM-D-15-0170.1, 2016.

Gerten, D., Schaphoff, S., Haberlandt, U., Lucht, W., and Sitch, S.: Terrestrial vegetation and water balance – hydrological evaluation of a dynamic global vegetation model, J. Hydrol., 286, 249–270, https://doi.org/10.1016/j.jhydrol.2003.09.029, 2004.

Gerten, D., Lucht, W., Schaphoff, S., Cramer, W., Hickler, T., and Wagner, W.: Hydrologic resilience of the terrestrial biosphere, Geophys. Res. Lett., 32, L21408, https://doi.org/10.1029/2005GL024247, 2005.

Giesecke, T., Miller, P. A., Sykes M. T., Ojala, A. E. K., Seppä, H., and Bradshaw, R. H. W.: The effect of past changes in inter-annual temperature variability on tree distribution limits, J. Biogeogr., 37, 1394–1405, https://doi.org/10.1111/j.1365-2699.2010.02296.x, 2010.

Grosjean, M., Van Leeuwen, J. F. N., Van Der Knaap, W. O., Geyh, M. A., Ammann, B., Tanner, W., Messerli, B., Núñez, L. A., Valero-Garcés, B. L., and Veit, H.: A 22 000 14C year BP sediment and pollen record of climate change from Laguna Miscanti (23° S), northern Chile, Global Planet. Change, 28, 35–51, https://doi.org/10.1016/S0921-8181(00)00063-1, 2001.

Gyssels, G., Poesen, J., Bochet, E., and Li, Y.: Impact of plant roots on the resistance of soils to erosion by water: a review, Prog. Phys. Geogr., 29, 189–217, https://doi.org/10.1191/0309133305pp443ra, 2005.

Harrison, S. P. and Prentice, C. I.: Climate and CO_2 controls on global vegetation distribution at the last glacial maximum: analysis based on palaeovegetation data, biome modelling and palaeoclimate simulations, Glob. Change Biol., 9, 983–1004, https://doi.org/10.1046/j.1365-2486.2003.00640.x, 2003.

Hempel, S., Frieler, K., Warszawski, L., Schewe, J., and Piontek, F.: A trend-preserving bias correction – the ISI-MIP approach, Earth Syst. Dynam., 4, 219–236, https://doi.org/10.5194/esd-4-219-2013, 2013.

Heusser, C. J.: Ice age vegetation and climate of subtropical Chile, Palaeogeogr. Palaeocl., 80, 107–127, 1990.

Hickler, T., Smith, B., Sykes, M. T., Davis, M. B., Sugita, S., and Walker, K.: Using a generalized vegetation model to simulate vegetation dynamics in northeastern USA, Ecology, 85, 519–530, https://doi.org/10.1890/02-0344, 2004.

Hickler, T., Vohland, K., Feehan, J., Miller, P. A., Smith, B., Costa, L., Giesecke, T., Fronzek, S., Carter, T. R., Cramer, W., Kühn, I., and Sykes, M. T.: Projecting the future distribution of European potential natural vegetation zones with a generalized, tree species-based dynamic vegetation model, Global Ecol. Biogeogr., 21, 50–63, https://doi.org/10.1111/j.1466-8238.2010.00613.x, 2012.

Hickler, T., Rammig, A., and Werner, C.: Modelling CO_2 impacts on forest productivity, Curr. Forestry Rep., 1, 1–12, https://doi.org/10.1007/s40725-015-0014-8, 2015.

Hobley, D. E. J., Adams, J. M., Nudurupati, S. S., Hutton, E. W. H., Gasparini, N. M., Istanbulluoglu, E., and Tucker, G. E.: Creative computing with Landlab: an open-source toolkit for building, coupling, and exploring two-dimensional numerical models of Earth-surface dynamics, Earth Surf. Dynam., 5, 21–46, https://doi.org/10.5194/esurf-5-21-2017, 2017.

Hopcroft, P. O., Valdes, P. J., Harper, A. B., and Beerling, D. J.: Multi vegetation model evaluation of the Green Sahara climate regime, Geophys. Res. Lett., 44, 6804–6813, https://doi.org/10.1002/2017GL073740, 2017.

Huntley, B., Allen, J. R. M., Collingham, Y. C., Hickler, T., Lister, A. M., Singarayer, J., Stuart, A. J., Sykes, M. T., and Valdes, P. J.: Millennial climatic fluctuations are key to the structure of Last Glacial ecosystems, PLOS One, 8, e61963, https://doi.org/10.1371/journal.pone.0061963, 2013.

Istanbulluoglu, E. and Bras, R. L.: Vegetation-modulated landscape evolution: Effects of vegetation on landscape processes, drainage density, and topography, J. Geophys. Res.-Earth, 110, F02012, https://doi.org/10.1029/2004JF000249, 2005.

Jeffery, M. L., Yanites, B. J., Poulsen, C. J., and Ehlers, T. A.: Vegetation-precipitation controls on Central Andean topography, J. Geophys. Res.-Earth, 119, 1354–1375, https://doi.org/10.1002/2013JF002919, 2014.

Karger, D. N., Conrad, O., Böhner, J., Kawohl, T., Kreft, H., Soria-Auza, R. W., Zimmermann, N. E., Linder, H. P., and Kessler, M.: Climatologies at high resolution for the earth's land surface areas, Scientific Data, 4, 170122, 2017.

Kobrick, M. and Crippen, R.: SRTMGL1: NASA Shuttle Radar Topography Mission Global 1 arc second V003, https://doi.org/10.5067/MEaSUREs/SRTM/SRTMGL1.003, 2017.

Kosmas, C., Danalatos, N. G., and Gerontidis, S.: The effect of land parameters on vegetation performance and degree of erosion under Mediterranean conditions, Catena, 40, 3–17, 2000.

Langbein, W. B. and Schumm, S. A.: Yield of sediment in relation to mean annual precipitation, EOS T. Am. Geophys. Un., 39, 1076–1084, https://doi.org/10.1029/TR039i006p01076, 1958.

Lehnert, L., Thies, B., Trachte, K., Achilles, S., Osses, P., Baumann, K., Schmidt, J., Samolov, E., Jung, P., Leinweber, P., Büdel, B., and Bendix, J.: A case study on fog/low stratus occurrence at Las Lomitas, Atacama Desert (Chile) as a water source for biological soil crusts, Aerosol Air Qual. Res., 18, 254–269, 2018.

Leung, L. R. and Ghan, J., S.: Parameterizing subgrid orographic precipitation and surface cover in climate models, Mon. Weather Rev., 126, 3271–3291, https://doi.org/10.1175/1520-0493(1998)126<3271:PSOPAS>2.0.CO;2, 1998.

Lara, A., Solari, M. E., Del Rosario Prieto, and Peña, M. P.: Reconstrucción de la cobertura de la vegetación y uso del suelo hacia 1550 y sus cambios a 2007 en la ecorregión de los bosques valdivianos lluviosos de Chile (35°– 43°30'S). Bosque (Valdivia), 33, 03–04, https://doi.org/10.4067/S0717-92002012000100002, 2012.

Liakka, J., Colleoni, F., Ahrens, B., and Hickler, T.: The impact of climate-vegetation interactions on the onset of the Antarctic ice sheet, Geophys. Res. Lett., 41, 1269–1276, https://doi.org/10.1002/2013GL058994, 2014.

Liu, Z., Otto-Bliesner, B. L., He, F., Brady, E. C., Tomas, R., Clark, P. U., Carlson, A. E., Lynch-Stieglitz, J., Curry, W., Brook, E., Erickson, D., Jacob, R., Kutzbach, J., and Cheng, J.: Transient simulation of last deglaciation with a new mechanism for Bølling-Allerød warming, Science, 325, 310–314, https://doi.org/10.1126/science.1171041, 2009.

Luebert, F. and Pliscoff, P.: Sinopsis bioclimática y vegetacional de Chile, 2Nd Edition, Editorial Universitaria, Santiago, Chile, 384 pp., 2017.

Lovelock, J. E. and Whitfield, M.: Life span of the biosphere, Nature, 296, 561–563, https://doi.org/10.1038/296561a0, 1982.

Maldonado, A. and Villagrán, C.: Climate variability over the last 9900 cal yr BP from a swamp forest pollen record along the semiarid coast of Chile, Quaternary Res., 66, 246–258, https://doi.org/10.1016/j.yqres.2006.04.003, 2006.

Maldonado, A., Betancourt, J. L., Latorre, C., and Villagran, C.: Pollen analyses from a 50 000-yr rodent midden series in the southern Atacama Desert (25° 30' S), J. Quaternary Sci., 20, 493–507, https://doi.org/10.1002/jqs.936, 2005.

Marchant, R., Cleef, A., Harrison, S. P., Hooghiemstra, H., Markgraf, V., van Boxel, J., Ager, T., Almeida, L., Anderson, R., Baied, C., Behling, H., Berrio, J. C., Burbridge, R., Björck, S., Byrne, R., Bush, M., Duivenvoorden, J., Flenley, J., De Oliveira, P., van Geel, B., Graf, K., Gosling, W. D., Harbele, S., van der Hammen, T., Hansen, B., Horn, S., Kuhry, P., Ledru, M.-P., Mayle, F., Leyden, B., Lozano-García, S., Melief, A. M., Moreno, P., Moar, N. T., Prieto, A., van Reenen, G., Salgado-Labouriau, M., Schäbitz, F., Schreve-Brinkman, E. J., and Wille, M.: Pollen-based biome reconstructions for Latin America at 0, 6000 and 18 000 radiocarbon years ago, Clim. Past, 5, 725–767, https://doi.org/10.5194/cp-5-725-2009, 2009.

Medlyn, B. E., Zaehle, S., De Kauwe, M. G., Walker, A. P., Dietze, M. C., Hanson, P. J., Hickler, T., Jain, A. K., Luo, Y., Parton, W., Prentice, I. C., Thornton, P. E., Wang, S., Wang, Y.-P., Weng, E., Iversen, C. M., McCarthy, H. R., Warren, J. M., Oren, R., and Norby, R. J.: Using ecosystem experiments to improve vegetation models, Nat. Clim. Change 5, 528–534, https://doi.org/10.1038/nclimate2621, 2015.

Meinshausen, M., Vogel, E., Nauels, A., Lorbacher, K., Meinshausen, N., Etheridge, D. M., Fraser, P. J., Montzka, S. A., Rayner, P. J., Trudinger, C. M., Krummel, P. B., Beyerle, U., Canadell, J. G., Daniel, J. S., Enting, I. G., Law, R. M., Lunder, C. R., O'Doherty, S., Prinn, R. G., Reimann, S., Rubino, M., Velders, G. J. M., Vollmer, M. K., Wang, R. H. J., and Weiss, R.: Historical greenhouse gas concentrations for climate modelling (CMIP6), Geosci. Model Dev., 10, 2057–2116, https://doi.org/10.5194/gmd-10-2057-2017, 2017.

Monnin, E., Indermuhle, A., Dallenbach, A., Fluckiger, J., Stauffer, B., Stocker, T. F., Raynaud, D., and Barnola, J. M.: Atmospheric CO_2 concentrations over the last glacial termination, Science, 291, 112–114, https://doi.org/10.1126/science.291.5501.112, 2001.

Monsi, M. and Saeki, T.: On the factor light in plant communities and its importance for matter production, Ann. Bot., 95, 549–567, https://doi.org/10.1093/aob/mci052, 2005.

Montecinos, A. and Aceituno, P.: Seasonality of the ENSO-related rainfall variability in central Chile and associated circulation anomalies, J. Climate, 16, 281–296, https://doi.org/10.1175/1520-0442(2003)016<0281:SOTERR>2.0.CO;2, 2003.

Morales, P., Hickler, T., Rowell, D. P., Smith, B., and Sykes, M. T.: Changes in European ecosystem productivity and carbon balance driven by regional climate model output, Glob. Change Biol., 13, 108–122, https://doi.org/10.1111/j.1365-2486.2006.01289.x, 2007.

Moreira-Muñoz, A.: Plant Geography of Chile, Springer Netherlands, Dordrecht, 2011.

Moreno, P. I. and Videla, J.: Centennial and millennial-scale hydroclimate changes in northwestern Patagonia since 16,000 yr BP, Quaternary. Sci. Rev., 149, 326–337, https://doi.org/10.1016/j.quascirev.2016.08.008, 2016.

Mutz, S. G., Ehlers, T. A., Werner, M., Lohmann, G., Stepanek, C., and Li, J.: Estimates of late Cenozoic climate change relevant to Earth surface processes in tectonically active orogens, Earth Surf. Dynam., 6, 271–301, https://doi.org/10.5194/esurf-6-271-2018, 2018.

O'ishi, R. and Abe-Ouchi, A.: Polar amplification in the mid-Holocene derived from dynamical vegetation change with a GCM, Geophys. Res. Lett., 38, L14702, https://doi.org/10.1029/2011GL048001, 2011.

Pappas, C., Fatichi, S., Rimkus, S., Burlando, P., and Huber, M. O.: The role of local-scale heterogeneities in terrestrial ecosystem modeling, J. Geophys. Res.-Biogeosci., 120, 341–360, https://doi.org/10.1002/2014JG002735, 2015.

Pollmann, W.: A long-term record of *Nothofagus* dominance in the southern Andes, Chile, Aust. Ecol., 30, 91–102, https://doi.org/10.1046/j.1442-9993.2004.01427.x 2005.

Prentice, I. C. and Guiot, J.: Reconstructing biomes from palaeoecological data: a general method and its application to European pollen data at 0 and 6 ka, Clim. Dynam., 12, 185–194, https://doi.org/10.1007/BF00211617, 1996.

Prentice, I. C., Sykes, M. T., and Cramer, W.: A simulation model for the transient effects of climate change on forest landscapes, Ecol. Modell., 65, 51–70, https://doi.org/10.1016/0304-3800(93)90126-D, 1993.

Prentice, I. C., Bondeau, A., Cramer, W., Harrison, S. P., Hickler, T., Lucht, W., Sitch, S., Smith, B., and Sykes, M. T.: Dynamic global vegetation modeling: Quantifying terrestrial ecosystem responses to large-scale environmental change Terres-

trial Ecosystems in a Changing World, in: Terrestrial Ecosystems in a Changing World, edited by: Canadell, J. G., Pataki, D. E., Pitelka, L. F., Springer, 175–192, 2007.

Prentice, I. C., Harrison, S. P., and Bartlein, P. J.: Global vegetation and terrestrial carbon cycle changes after the last ice age, New Phytol., 189, 988–998, https://doi.org/10.1111/j.1469-8137.2010.03620.x, 2011.

Raddatz, T. J., Reick, C. H., Knorr, W., Kattge, J., Roeckner, E., Schnur, R., Schnitzler, K.-G., Wetzel, P., and Jungclaus, J.: Will the tropical land biosphere dominate the climate–carbon cycle feedback during the twenty-first century?, Clim. Dynam., 29, 565–574, https://doi.org/10.1007/s00382-007-0247-8, 2007.

Reick, C. H., Raddatz, T., Brovkin, V., and Gayler, V.: Representation of natural and anthropogenic land cover change in MPI-ESM, J. Adv. Model. Earth Syst., 5, 459–482, https://doi.org/10.1002/jame.20022, 2013.

Riebe, C. S., Kirchner, J. W., Granger, D. E., and Finkel, R. C.: Minimal climatic control on erosion rates in the Sierra Nevada, California, Geology, 29, 447–450, https://doi.org/10.1130/0091-7613(2001)029<0447:MCCOER>2.0.CO;2, 2001.

Rundel, P. W., Villagra, P. E., Dillon, M. O., Roig-Juñent, S., and Debandi, G.: Arid and semi-arid ecosystems, in: The Physical Geography of South America, edited by: Veblen, T. T., Young, K. R., and Orme, A. R., Oxford University Press, 158–183, 2007.

Schmid, M., Ehlers, T. A., Werner, C., Hickler, T., and Fuentes-Espoz, J.-P.: Effect of changing vegetation and precipitation on denudation – Part 2: Predicted landscape response to transient climate and vegetation cover over millennial to million-year timescales, Earth Surf. Dynam. Discuss., 6, 859–881, https://doi.org/10.5194/esurf-6-859-2018, 2018.

Seiler, C., Hutjes, R. W. A., Kruijt, B., Quispe, J., Añez, S., Arora, V. K., Melton, J. R., Hickler, T., and Kabat, P.: Modeling forest dynamics along climate gradients in Bolivia, J. Geophys. Res.-Biogeosci., 119, 758–775, https://doi.org/10.1002/2013JG002509, 2014.

Seiler, C. R., Hutjes, W. A., Kruijt, B., and Hickler, T.: The sensitivity of wet and dry tropical forests to climate change in Bolivia, J. Geophys. Res.-Biogeosci., 120, 399–413, https://doi.org/10.1002/2014JG002749, 2015.

Sexton, J. O., Song, X.-P., Feng, M., Noojipady, P., Anand, A., Huang, C., Kim, D.-H., Collins, K. M., Channan, S., DiMiceli, C., and Townshend, J. R.: Global, 30-m resolution continuous fields of tree cover: Landsat-based rescaling of MODIS vegetation continuous fields with lidar-based estimates of error, Int. J. Digit. Earth, 6, 427–448, https://doi.org/10.1080/17538947.2013.786146, 2013.

Shellito, C. J. and Sloan, L. C.: Reconstructing a lost Eocene Paradise, Part II: On the utility of dynamic global vegetation models in pre-Quaternary climate studies, Glob. Planet. Change, 50, 18–32, https://doi.org/10.1016/j.gloplacha.2005.08.002, 2006.

Smith, B., Prentice, I. C., and Sykes, M. T.: Representation of vegetation dynamics in the modelling of terrestrial ecosystems comparing two contrasting approaches within European climate space, Global Ecol. Biogeogr., 10, 621–637, https://doi.org/10.1046/j.1466-822X.2001.t01-1-00256.x, 2001.

Smith, B., Wårlind, D., Arneth, A., Hickler, T., Leadley, P., Siltberg, J., and Zaehle, S.: Implications of incorporating N cycling and N limitations on primary production in an individual-based dynamic vegetation model, Biogeosciences, 11, 2027–2054, https://doi.org/10.5194/bg-11-2027-2014, 2014.

Snell, R. S., Huth, A., Nabel, J. E., Bocedi, G., Travis, J. M., Gravel, D., Bugmann, H., Gutiérrez, A. G., Hickler, T., Higgins, S. I., Reineking, B., Scherstjanoi, M., Zurbriggen, N., and Lischke, H.: Using dynamic vegetation models to simulate plant range shifts, Ecography, 37, 1184–1197, https://doi.org/10.1111/ecog.00580, 2014.

Sternberg, M. and Shoshany, M.: Influence of slope aspect on Mediterranean woody formations: Comparison of a semi-arid and an arid site in Israel, Ecol. Res., 16, 335–345, https://doi.org/10.1046/j.1440-1703.2001.00393.x, 2001.

Thompson, L. G., Mosley-Thompson, E., Davis, M. E., Lin, P. N., Henderson, K. A., Cole-Dai, J., Bolzan, J. F., and Liu, K.-B.: Late Glacial Stage and Holocene tropical ice core records from Huascarán, Peru, Science, 269, 46–50, https://doi.org/10.1126/science.269.5220.46, 1995.

Thonicke, K., Venevsky, S., Sitch, S., and Cramer, W.: The role of fire disturbance for global vegetation dynamics: coupling fire into a Dynamic Global Vegetation Model, Glob. Ecol. Biogeogr., 10, 661–677, https://doi.org/10.1046/j.1466-822X.2001.00175.x, 2001.

Uribe, J. M., Cabrera, R., de la Fuente, A., and Paneque M: Atlas Bioclimático De Chile, Santiago, Universidad de Chile, 2012.

Valero-Garcés, B. L., Jenny, B., Rondanelli, M., Delgado-Huertas, A., Burns, S. J., Veit, H., and Moreno, A.: Palaeohydrology of Laguna de Tagua Tagua (34° 30′ S) and moisture fluctuations in Central Chile for the last 46 000 yr, J. Quaternary Sci., 20, 625–641, https://doi.org/10.1002/jqs.988, 2005.

Vanacker, V., von Blanckenburg, F., Govers, G., Molina, A., Poesen, J., Deckers, J., and Kubik, P: Restoring dense vegetation can slow mountain erosion to near natural benchmark levels, Geology, 35, 303–306, https://doi.org/10.1130/G23109A.1, 2007.

Vaughan, W. W.: Basic atmospheric structure and concepts, Standard Atmosphere, 12–16, 2015.

Veblen, T. T.: Temperate forests of the Southern Andean region, in: The Physical Geography of South America, edited by: Veblen, T. T., Young, K. R., and Orme, A. R., Oxford University Press, 217–231, 2007.

Veblen, T. T., Donoso, C., Kitzberger, T., and Rebertus, A. J.: Ecology of southern Chilean and Argentinean *Nothofagus* forests, in: The ecology and biogeography of *Nothofagus* forests, edited by: Veblen, T. T., Hill, R. S., and Read, J., Yale University Press, 293–253, 1996.

Villa-Martínez, R., Villagran, C., and Jenny, B.: The last 7500 cal yr B.P. of westerly rainfall in Central Chile inferred from a high-resolution pollen record from Laguna Aculeo (34° S), Quaternary Res., 60, 284–293, https://doi.org/10.1016/j.yqres.2003.07.007, 2003.

Villagrán, C. M.: Expansion of Magellanic Moorland during the late Pleistocene: Palynological evidence from northern Isla de Chiloé, Chile, Quaternary Res., 30, 304–314, https://doi.org/10.1016/0033-5894(88)90006-3, 1988.

Villagrán, C. M.: Quaternary history of the Mediterranean vegetation of Chile, in: Ecology and biogeography of Mediterranean ecosystems in Chile, California, and Australia, edited by: Arroyo, M. T. K., Zedler, P. H., and Fox, M. D., Springer New York, 1995.

Weiss, A.: Topographic position and landforms analysis, Poster presentation, ESRI User Conference, San Diego, CA, Vol. 200, 2001.

Wramneby, A., Smith, B., Zaehle, S., and Sykes, M. T.: Parameter uncertainties in the modelling of vegetation dynamics – Effects on tree community structure and ecosystem functioning in European forest biomes, Ecol. Modell., 216, 277–290, https://doi.org/10.1016/j.ecolmodel.2008.04.013, 2008.

Wramneby, A., Smith, B., and Samuelsson, P.: Hot spots of vegetation-climate feedbacks under future greenhouse forcing in Europe, J. Geophys. Res., 115, D21119, https://doi.org/10.1029/2010JD014307, 2010.

Young, K. R., Berry, P. E., and Veblen, T. T.: Flora and vegetation, in: The Physical Geography of South America, edited by: Veblen, T. T., Young, K. R., and Orme, A. R., Oxford University Press, 91–100, 2007.

Yu, M., Wang, G., and Chen, H.: Quantifying the impacts of land surface schemes and dynamic vegetation on the model dependency of projected changes in surface energy and water budgets, J. Adv. Model. Earth Syst., 8, 370–386, https://doi.org/10.1002/2015MS000492, 2016.

Zaehle, S., Medlyn, B. E., De Kauwe, M. G., Walker, A. P., Dietze, M. C., Hickler, T., Luo, Y., Wang, Y.-P., El-Masri, B., Thornton, P., Jain, A., Wang, S., Wårlind, D., Weng, E., Parton, W., Iversen, C. M., Gallet-Budynek, A., McCarthy, H., Finzi, A., Hanson, P. J., Prentice, I. C., Oren, R., and Norby, R. J.,: Evaluation of 11 terrestrial carbon-nitrogen cycle models against observations from two temperate Free-Air CO_2 Enrichment studies, New Phytol., 202, 803–822, https://doi.org/10.1111/nph.12697, 2014.

3.1.3 Paper : Part 2 - Predicted landscape response to transient climate and vegetation cover over millennial to million-year timescales

Earth Surf. Dynam., 6, 859–881, 2018
https://doi.org/10.5194/esurf-6-859-2018

Earth Surface Dynamics Open Access EGU

Effect of changing vegetation and precipitation on denudation – Part 2: Predicted landscape response to transient climate and vegetation cover over millennial to million-year timescales

Manuel Schmid[1], Todd A. Ehlers[1], Christian Werner[2], Thomas Hickler[2,3], and Juan-Pablo Fuentes-Espoz[4]

[1]Department of Geosciences, University of Tuebingen, Wilhelmstrasse 56, 72074 Tuebingen, Germany
[2]Senckenberg Biodiversity and Climate Research Center (BiK-F),
Senckenberganlage 25, 60325 Frankfurt, Germany
[3]Department of Physical Geography, Geosciences, Goethe University,
Altenhoeferallee 1, 60438 Frankfurt, Germany
[4]Department of Silviculture and Nature Conservation, University of Chile,
Av. Santa Rosa 11315, La Pintana, Santiago RM, Chile

Correspondence: Todd A. Ehlers (todd.ehlers@uni-tuebingen.de)

Received: 6 February 2018 – Discussion started: 21 February 2018
Revised: 3 July 2018 – Accepted: 17 July 2018 – Published: 8 October 2018

Abstract. We present a numerical modeling investigation into the interactions between transient climate and vegetation cover with hillslope and detachment limited fluvial processes. Model simulations were designed to investigate topographic patterns and behavior resulting from changing climate and the associated changes in surface vegetation cover. The Landlab surface process model was modified to evaluate the effects of temporal variations in vegetation cover on hillslope diffusion and fluvial erosion. A suite of simulations were conducted to represent present-day climatic conditions and satellite derived vegetation cover at four different research areas in the Chilean Coastal Cordillera. These simulations included steady-state simulations as well as transient simulations with forcings in either climate or vegetation cover over millennial to million-year timescales. Two different transient variations in climate and vegetation cover including a step change in climate or vegetation were used, as well as 100 kyr oscillations over 5 Myr. We conducted eight different step-change simulations for positive and negative perturbations in either vegetation cover or climate and six simulations with oscillating transient forcings for either vegetation cover, climate, or oscillations in both vegetation cover and climate. Results indicate that the coupled influence of surface vegetation cover and mean annual precipitation shifts basin landforms towards a new steady state, with the magnitude of the change being highly sensitive to the initial vegetation and climate conditions of the basin. Dry, non-vegetated basins show higher magnitudes of adjustment than basins that are situated in wetter conditions with higher vegetation cover. For coupled conditions when surface vegetation cover and mean annual precipitation change simultaneously, the landscape response tends to be weaker. When vegetation cover and mean annual precipitation change independently from one another, higher magnitude shifts in topographic metrics are predicted. Changes in vegetation cover show a higher impact on topography for low initial surface cover values; however, for areas with high initial surface cover, the effect of changes in precipitation dominate the formation of landscapes. This study demonstrates the sensitivity of catchment characteristics to different transient forcings in vegetation cover and mean annual precipitation, with initial vegetation and climate conditions playing a crucial role.

Published by Copernicus Publications on behalf of the European Geosciences Union.

1 Introduction

Plants cover most of the Earth's surface and interact chemically and physically with the atmosphere, lithosphere, and hydrosphere. The abundance and distribution of plants throughout Earth's history is a function, amongst other things, of changing climate conditions that can impact the temporal distribution of plant functional types and the vegetation cover present in an area (Hughes, 2000; Muhs et al., 2001; Walther et al., 2002). The physical feedbacks of vegetation on the Earth's near surface mainly manifest themselves through the influence of plants on weathering, erosion, transport, and the deposition of sediments (Marston, 2010; Amundson et al., 2015). Although the effects of biota on surface processes has been recognized for over a 100 years (e.g., Gilbert, 1877; Langbein and Schumm, 1958), early studies mainly focused on qualitative descriptions of the underlying processes. With the rise of new techniques to quantify mass transport from the plot-scale to the catchment-scale, and the emergence of improved computing techniques and landscape evolution models, research has shifted more towards building a quantitative understanding of how biota influence both hillslope and fluvial processes (Stephan and Gutknecht, 2002; Roering et al., 2002; Marston, 2010; Curran and Hession, 2013). These previous studies motivate the companion papers presented here. In part 1 (Werner et al., 2018) a dynamic vegetation model is used to evaluate the magnitude of past (last glacial maximum to present) vegetation change along the climate and ecological gradient in the Coastal Cordillera of Chile. Part 2 (this study) presents a sensitivity analysis of how transient climate and vegetation impact catchment denudation. This component is evaluated through the implementation of transient vegetation effects for hillslopes and detachment limited rivers in a landscape evolution model.

Previous research in agricultural engineering has focused on plot-scale models to predict total soil loss in response to land use change (Zhou et al., 2006; Feng et al., 2010) or general changes in plant surface cover (Gyssels et al., 2005); however, previous studies do not draw conclusions about large-scale geomorphic feedbacks active over longer (millennial) timescales and larger spatial scales. Nevertheless, a better understanding of how vegetation influences the large-scale topographic features (e.g., relief, hillslope angles, and catchment denudation) is crucial to understanding the evolution of modern landscapes. At the catchment scale, observational studies have found a correlation between higher values of mean vegetation cover and basin wide denudation rates or topographic metrics (Jeffery et al., 2014; Sangireddy et al., 2016; Acosta et al., 2015). Parallel to the previous observational studies, numerical modeling experiments of the interactions between landscape erosion and surface vegetation cover have also made progress. For example, Collins et al. (2004) was one of the first studies that attempted to couple vegetation dynamics with a landscape evolution model; they found that the introduction of plants to their model resulted in steeper equilibrium landscapes with a higher variability in the magnitude of erosional events. Following this, subsequent modeling studies built upon the previous findings with more sophisticated formulations of vegetation–erosion interactions (Istanbulluoglu and Bras, 2005), including the influence of root strength on hillslopes (Vergani et al., 2017). These studies found that not only is there a positive relationship between vegetation cover and mean catchment slope and elevation, but an inverse relationship also exists between vegetation cover and drainage density due to plants' abilities to hinder fluvial erosion and channel initiation.

The advances of the previous studies are mainly limited by their consideration of static vegetation cover or very simple formulations of dynamic vegetation cover. The exceptions to this are Istanbulluoglu and Bras (2005) who also considered the lag time for vegetation regrowth on hillslopes after a mass wasting event and Yetemen et al. (2015) who considered more complex hydrology in their models, but on a smaller spatial scale. However, numerous studies (Ledru et al., 1997; Allen and Breshears, 1998; Bachelet et al., 2003) document that vegetation cover changes in tandem with climate change over a range of timescales (decadal to million year). Missing from previous landscape evolution studies, is consideration of not only how transient vegetation cover influences catchment denudation, but also how coeval changes in precipitation influence catchment-wide mean denudation. While the effects of climate change over geologic timescales on denudation rates and sediment transport dynamics have been investigated by others (e.g., Schaller et al., 2002; Dosetto et al., 2010; McPhillips et al., 2013), the combined effects of vegetation and climate change on catchment denudation have not. Thus, over longer (geologic) timescales, we are left with a complicated situation of both vegetation and climate changes, and the individual contributions of these changes to catchment-scale denudation are difficult to disentangle.

In this study, we build upon previous research by investigating both the temporal and spatial sensitivities of landscapes to the coupled vegetation–climate system. By focusing on simplified transient forcings such as a step change, or 100 kyr oscillations in climate and vegetation cover we present a sensitivity analysis of the landscape response to each of these changes, including a better understanding of the direction, magnitude, and rates of landscape change. Our model setup is motivated by four study areas along the climate and vegetation gradient in Chile (Fig. 1a), and illuminates the transient catchment response to biotic vs. climate changes. These study areas are part of the recently initiated German priority research program EarthShape: Earth surface shaping by biota (https://www.earthshape.net, last access: 7 August 2018). This region is used to provide a basis for our model setup regarding covariation in precipitation

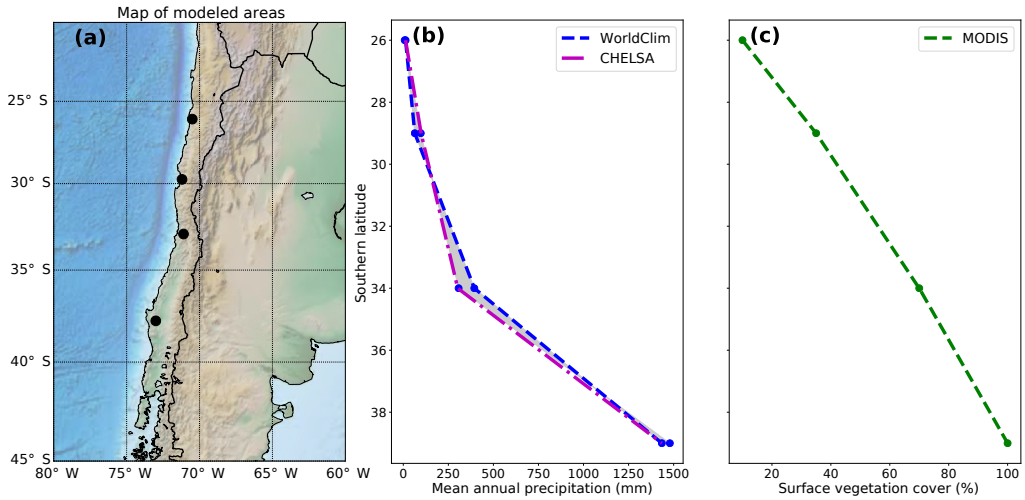

Figure 1. Overview of the geographic location, precipitation, and vegetation cover of the Chilean Coastal Cordillera study areas used for the model setup. **(a)** Digital topography of the areas considered in this study, which correspond to the EarthShape (https://www.earthshape.net) focus areas where ongoing related research is located. **(b)** Observed present-day mean annual precipitation from the WorldClim and CHELSA datasets used as model input. **(b)** Present-day maximum surface vegetation cover from MODIS data.

and vegetation present in a natural setting. While we present results representative of the Chilean Coastal Cordillera, it is beyond the scope of this study to provide a detailed calibration for this area. Hence, our main objective is identifying the sensitivity and emergent behavior of catchment denudation to changing precipitation and vegetation cover over millennial timescales. This study also builds upon results from the companion paper (Werner et al., 2018) by imposing temporal variations in vegetation cover identified in that study.

2 Background for the model setup

The model setup and the range of initial conditions chosen for the models were based on four study areas located in the Chilean Coastal Cordillera (26 to 38° S). The focus areas shown in Fig. 1a were chosen due to their similar granitic lithology and geologic and tectonic history (Andriessen and Reutter, 1994; McInnes et al., 1999; Juez-Larré et al., 2010; Maksaev and Zentilli, 1999; Avdievitch et al., 2018), in addition to the large gradient in climate and vegetation cover over the region (Fig. 1b, c). These study areas include (from north to south): Pan de Azúcar National Park, Santa Gracia Natural Reserve, La Campana National Park, and Nahuelbuta National Park. Although this study does not explicitly present landscape evolution model results "calibrated" to these specific areas, we have chosen the model input (e.g., precipitation, initial vegetation cover, rate of tectonic rock uplift) to represent these areas. This has been done in order to provide simulation results that represent the nonlinear relationship between precipitation and vegetation cover (e.g., Fig. 1b, c) over a large climate gradient.

Topographic metrics such as mean basin slope, total basin relief, mean basin channel steepness, mean surface vegetation cover, and mean annual precipitation were extracted for the main catchments and a subset of adjacent catchments (Figs. 1, 2). Topographic metrics were extracted from a 30 m resolution digital elevation model from the NASA shuttle radar topography mission (SRTM), and vegetation related datasets from the Moderate Resolution Imaging Spectroradiometer (MODIS) satellite data (https://landcover.usgs.gov/green_veg.php, last access: 7 August 2018) (Broxton et al., 2014).

Landscape evolution modeling approach and the applicability of these results

Landscape evolution model studies can be assigned to different general approaches, which were conceptually defined by Dietrich et al. (2013). The different approaches presented in the Dietrich et al. (2013) study mostly differ in the complexity of the input parameters and in the resulting claim for reproducing realistic complexity in modeled landscapes. For this study we have chosen the approach of essential realism, which acknowledges a system-inherent indeterminacy in the evolving topography but focuses on predicting the first-order trends within a system and the differences between landscapes, based on different external conditions, incorporated in the model (Howard, 1997).

While we do not claim to reproduce the topographic metrics of the four different focus areas in Chile on a realistic level, our approach determines the general first-order effects of millennial timescale changes in precipitation and vege-

tation cover that can impact topography. Superimposed on the effects documented in this study would be the effects of seasonal changes in precipitation and vegetation cover, subcatchment variations in vegetation cover, transport limited fluvial and vegetation interactions, and stochastic variations in precipitation in different climate zones. This being said, more detailed aspects of the effects of precipitation–vegetation interactions on erosion could be independent studies of their own and can not be covered in a single study. Thus, the modeling approach and results of this study should be considered as documenting the longer (millennial) timescale climate and vegetation forcings on fluvial and surface processes.

3 Methods

3.1 Model description and governing equations

For this study, we use the open-source model framework Landlab (Hobley et al., 2017). We chose a model domain with an area of 100 km^2 that is implemented as a rectangular grid divided into 0.01 km^2 spaced grid cells. For simplification in the presentation of results, we present our results for the driest, northern most area (Pan de Azucar National Park) and for La Campana National Park. La Campana National Park is situated at 32° S latitude (Fig. 1) and shows the highest values in analyzed basin metrics (Fig. 2), although the general behavior and results presented here are also representative of the other two areas (not shown). The topographic evolution of the landscape is a result of tectonic uplift and surface processes, incorporating detachment limited fluvial erosion and linear diffusive transport of sediment across hillslopes (Fig. 3). These processes are linked to, and vary in their effectiveness due to, surface vegetation density. Details of the implementation of these processes in Landlab are explained in the following subsections.

This model setup is simplified with regards to hydrological parameters such as soil moisture and groundwater and unsaturated zone flow. Furthermore, the erosion and transport of material due to mass-wasting processes such as rockfalls and landslides are not considered. We argue that these processes do not play a major role in the basins we used for model calibration, and that the processes acting continuously along hillslopes and channels have the largest impact on shaping our reference landscapes. The detachment-limited approach was chosen because the focus areas represent small, bedrock dominated headwater catchments. Additional caveats and limitations of the modeling approach used are discussed in Sect. 5.4. Main model parameters used in the model (and described below) are provided in Table 1.

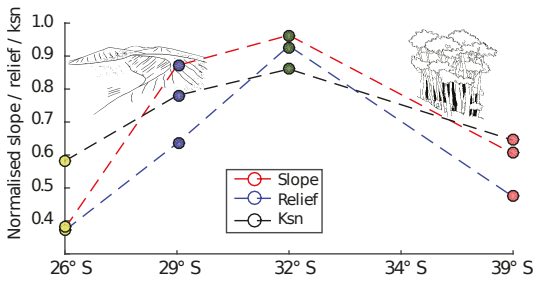

Figure 2. Normalized basin metrics for study areas derived from 30 m SRTM digital topography (from the study areas shown in Fig. 1a). Colored dots represent cumulative mean values of normalized slope, relief, and channel steepness calculated for all locations using five to eight representative catchments in each area. Dotted lines represent linear interpolation between values. Note the gradual increase, then decrease in all metrics around study area at ∼ 32° S.

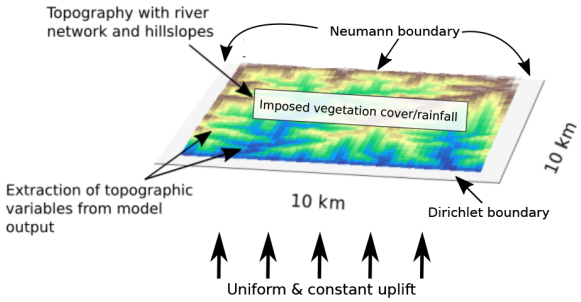

Figure 3. An example of the model setup used in the simulations in this study, showing model predicted topography with a set drainage network, draining to the south. Boundary conditions and parameterizations used in the models are labeled. Blue represents low elevations and brown represents higher elevations. Additional details of parameters used are specified in Table 1.

3.2 Boundary and initial conditions and model free parameters

In an effort to keep simulations comparable, we minimized the differences in parameters between simulations. The exceptions to this include the surface vegetation cover and the mean annual precipitation, which were varied between simulations. One of the main controls on topography is the rock uplift rate. We kept the rock uplift rate temporally and spatially uniform across the domain at 0.2 mm yr^{-1} (Table 1). Studies of the exhumation and rock uplift history of the Chilean Coastal Cordillera are sparse at the latitudes investigated here; however, existing and in progress studies further to the north are broadly consistent with the rock uplift rate used here (Juez-Larré et al., 2010; Avdievitch et al., 2018).

The EarthShape focus sites are situated in similar granitic lithologies (Oeser et al., 2018), which allows for the assump-

Table 1. Model parameters used for the Landlab model setup.

Model parameter	Unit	Value
Uplift (U)	$\mathrm{mm\,yr^{-1}}$	0.2
Fluvial erodibility (k_e)	$\mathrm{m\,yr^{-1}\ (kg\,m^{-1}\,s^{-2})^{-1}}$	7.00×10^{-6}
Critical shear stress (τ_c)	Pa	58
m, n	–	0.6/0.7
Base diffusivity (K_b)	$\mathrm{m^2\,yr^{-1}}$	0.02
Manning number (fully vegetated, n_vr)	–	0.6
Manning number (bare soil, n_s)	–	0.01
Reference vegetation cover (V_r)	%	100
w	–	1
Alpha	–	0.3
p	–	1
Transient vegetation cover amplitude (±dV)	%	10

tion that the same critical shear stress, baseline diffusivity, and fluvial erodibility can be used.

Vegetation cover was chosen to be spatially uniform across model domains. While vegetation can change in high-relief catchments due to precipitation and temperature changes with elevation, this simplifying assumption was made based on the low to moderate relief (500–1500 m, mean $\sim$ 750 m) of the Coastal Cordillera areas investigated, in addition to the minimal field and MODIS observed changes in type and cover with elevation. The exception to this was the La Campana study area ($\sim$ 1500 m relief), which had an observed change in vegetation type and cover in the upper 500 m of the catchment. Furthermore, dynamic vegetation modeling results presented in the companion paper "part 1" (Fig. 5b in Werner et al., 2018) indicate that although elevation gradients in plant functional types have occurred in the region since the last glacial maximum, the elevation range of the catchments in the Coastal Cordillera ($<$ 1500 m) exhibits only minor changes with elevation. Vegetation cover near trunk streams within catchments is observed (via field observations) to increase, most likely due to local-scale hydrology and more abundant water in these areas. However, these regions are often restricted to with tens of meters of the trunk stream, well below the 100 m grid resolution of the model; therefore, they are difficult to accurately resolve within the simulations presented.

The initial topography used in our simulations was a random white-noise topography with $<$ 1 m relief. To avoid unwanted transients related to the formation of this initial topography we conducted simulations to produce an equilibrium topography for each set of the different climate and vegetation scenarios (see below). These equilibrium topographies were produced by running the model for 15 Myr until a topographic steady state was reached. The equilibrium topography after 15 Myr was used as the input topography for subsequent experiments that imposed transient forcings in climate, vegetation, or both (Fig. 4). The model simulation time shown in subsequent plots is the time since the completion of this initial 15 Myr steady-state topography development. In the results section, we present these results starting with differences in the initial steady-state topographies (prior to imposing transient forcings) and then add different levels of complexity by imposing either (1) a single transient step change for the vegetation cover (Fig. 4b), (2) a step change in the mean annual precipitation (Fig. 4d), (3) 100 kyr oscillations in the vegetation cover (Fig. 4a), (4) 100 kyr oscillations in the mean annual precipitation (Fig. 4c), or (5) 100 kyr oscillation in both the vegetation cover and mean annual precipitation (both Fig. 4a and c). This approach was used to produce a stepwise increase in model complexity for evaluating the individual, and then the combined, effects of fluvial and hillslope processes to different forcings.

The magnitude of induced rainfall transient forcings were based upon the present-day conditions along the Coastal Cordillera study areas (Fig. 1b, c). The step change and oscillations in vegetation cover and mean annual precipitation imposed on the experiments were designed to investigate vegetation and precipitation change effects on topography over the last $\sim$ 0.9 Ma – the period during which a 100 kyr orbital forcing is dominant in Earth's climate (Broecker and van Donk, 1970; Muller and MacDonald, 1997). Given this timescale of interest, we impose a 10 % magnitude change in the step-increase or decrease, or the amplitude change in oscillations for the vegetation cover. This magnitude of vegetation cover change is supported by dynamic vegetation modeling of vegetation changes over glacial–interglacial cycles in Chile (see companion paper by Werner et al., 2018), and to some degree elsewhere in the world (Allen et al., 2010; Prentice et al., 2011; Huntley et al., 2013); however, for the sake of simplicity we use a fixed forcing of ±10 % for all simulations instead of a spatially variable forcing, which would be dependent on ecosystem behavior for each separate area. We assume that the present-day conditions of combined vegetation cover and mean annual precipitation along the north–south gradient of the Coastal Cordillera are directly linked (Fig. 1b, c); therefore, we follow an empirical ap-

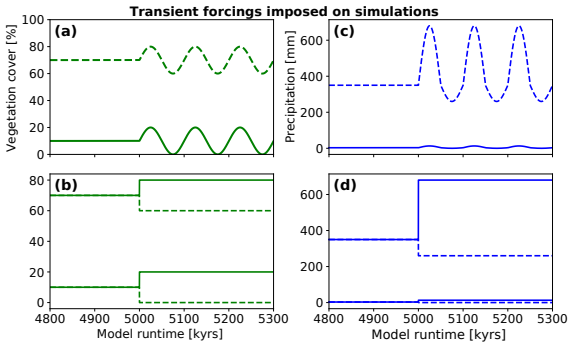

Figure 4. Transient forcings in vegetation and precipitation considered in model experiments. Simulations were run for 15 Myr prior to the runtime shown in the figure. All transients imposed started at a runtime of 5 Myr. **(a)** Variations in vegetation cover imposed in the oscillating experiment conditions for an initial vegetation cover of 10 and 70 %. Oscillations have a 10 % amplitude and a 100 kyr periodicity. **(b)** 10 % positive and negative step changes in vegetation cover imposed on simulations with 10 % and 70 % initial vegetation cover. **(c)** Oscillating mean annual precipitation. Positive and negative amplitudes of oscillation resemble the magnitude of precipitation change extracted from the vegetation cover–rainfall relationship from satellite data (Fig. 5). **(d)** Positive and negative step changes in mean annual precipitation. The initial precipitation was based on values extracted from the WorldClim climate dataset for respective focus areas.

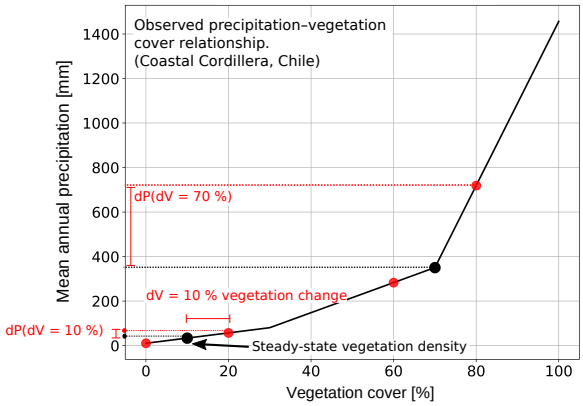

Figure 5. Graphical representation of the observed precipitation – vegetation relationship in the Chilean focus areas (shown in Fig. 1), and how precipitation amounts were selected when perturbations in vegetation cover were imposed. Black dots represent vegetation–precipitation values used in the steady-state model conditions and prior to any transients. Red dots show how vegetation cover perturbations of ±10 % in the model simulations were used to select corresponding mean annual precipitation amounts. Note that the observed relationship between observed precipitation and vegetation cover in the Chilean Coastal Cordillera is nonlinear, and is a source of the nonlinear behavior in the model forcing (e.g., Fig. 4) and results (Fig. 17) presented here.

proach based on the present-day mean annual precipitation, which directly links to the present-day vegetation cover in Chile (Fig. 5). We do this by associating each 10 % change in vegetation cover (dV) with a corresponding change in mean annual precipitation (dP, Fig. 5) present in the study areas considered. We impose a predefined, fixed amplitude change in surface vegetation cover as a transient forcing for simulations. For our prescribed changes in vegetation cover we then choose corresponding values of mean annual precipitation based on the relationship shown in Figs. 1 and 5. The simulations were parameterized in terms of changes in vegetation cover (instead of precipitation) for two reasons. First, the emphasis of this study is on advancing our knowledge of how vegetation changes impact surface processes. Given this, we wanted to present results based on reasonable changes in vegetation cover change. Second, results from the companion paper and this paper (Werner et al., 2018) suggest that the Chilean Coastal Cordillera has experienced ±10 % changes in vegetation cover over the last 21 kyr. We adopt this result in this study as the current best estimate for the changes in the study areas considered. Thus, the changes in precipitation and vegetation imposed in this study are empirically based on observations from the climate and ecological gradient in the Coastal Cordillera.

The boundary conditions used in the model were the same for all of the simulations explained above (Fig. 3). One boundary was held at a fixed elevation and open to flow outside the domain. The other three were allowed to increase in elevation and had a zero-flux condition. This design for boundary conditions is similar to previous landscape evolution modeling studies (Istanbulluoglu and Bras, 2005), and provides a means for analyzing the effects of different vegetation cover and precipitation forcings on the individual catchment and subcatchment scale.

3.3 Vegetation cover dependent geomorphic transport laws

The governing equation used for simulating topographic change in our experiments follows the continuity of mass. Changes in elevation at different points of the model domain over time $\delta z(x, y, t)$ depend on the following:

$$\frac{\delta z(x,y)}{\delta t} = U - \frac{\delta z}{\delta t}|_{\text{hillslope}} - \frac{\delta z}{\delta t}|_{\text{fluvial}}, \quad (1)$$

where z is elevation; x, y are lateral distance; t is time; U is the rock uplift rate; $\frac{\delta z}{\delta t}|_{\text{hillslope}}$ is the change in elevation due to hillslope processes; and $\frac{\delta z}{\delta t}|_{\text{fluvial}}$ is the change in elevation due to fluvial processes (Tucker et al., 2001).

3.3.1 Vegetation cover influenced diffusive hillslope transport

The change in topography in a landscape over time caused by hillslope-dependent diffusion can be characterized as follows:

$$\frac{\delta z}{\delta t}|_{\text{hillslope}} = -\nabla q_{\text{sd}}. \tag{2}$$

Landscape evolution models characterize the flux of sediment (q_{sd}) as either a linear or nonlinear function of surface slope (S) (Culling, 1960; Fernandez and Dietrich, 1997). In order to keep the number of free parameters for the simulation to a minimum, we used the linear description of hillslope diffusion:

$$q_{\text{sd}} = K_{\text{d}} S. \tag{3}$$

Following the approach of Alberts et al. (1995), Dunne et al. (1995), Istanbulluoglu and Bras (2005) and Dunne et al. (2010), we assign the linear diffusion coefficient K_{d} as a function of the surface vegetation density V, an exponential coefficient α, and a baseline diffusivity K_{b}, such that

$$K_{\text{d}} = K_{\text{b}} e^{-(\alpha V)}. \tag{4}$$

3.3.2 Vegetation cover influence on overland flow and fluvial erosion

Fluvial detachment-limited erosion of material due to water is calculated in this study by the widely used "stream power equation" (Howard and Kerby, 1983; Howard et al., 1994; Whipple and Tucker, 1999; Braun and Willet, 2013):

$$\frac{\delta z}{\delta t}|_{\text{fluvial}} = k_{\text{e}}(\tau - \tau_{\text{c}})^{p} \quad \text{for} \quad \tau > \tau_{\text{c}}, \tag{5}$$

where k_{e} represents the erodibility of the bed; τ represents the bed shear stress, which acts on the surface at each node; τ_{c} is the critical shear stress that needs to be overcome to erode the bed material; and p is a constant.

By following the approach of Istanbulluoglu and Bras (2005) and Istanbulluoglu et al. (2004), we reformulate the standard equation of shear stress: $\tau_{\text{b}} = \rho_{\text{w}} g R S$, where ρ_{w} is the density of water, g is the acceleration of gravity, R is the hydraulic radius, and S is the local slope, to a form which incorporates Manning roughness. This is undertaken in order to quantify the effect of vegetation cover on bed shear stress (Willgoose et al., 1991; Istanbulluoglu et al., 2004) and takes the following form:

$$\tau_{\text{v}} = \rho_{\text{w}} g (n_{\text{s}} + n_{\text{v}})^{\frac{6}{10}} q^{m} S^{n} F_t, \tag{6}$$

where n_{s} and n_{v} represent Manning numbers for bare soil and vegetated ground,respectively, q is the water discharge per node that is approximated with the steady-state uniform precipitation per time step P and the surface area per node A ($q = A \times P$), S is the local slope per node, and m and n are constants. n_{v} for each node is calculated as a function of the local surface vegetation cover

$$n_{\text{v}} = n_{\text{vr}} \left(\frac{V}{V_{\text{r}}} \right)^{w}, \tag{7}$$

with n_{vr} being the Manning number for a defined reference vegetation cover, V and V_{r} being the vegetation cover at each node and the reference vegetation cover, respectively, and w being an empirical scaling parameter.

The last variable in Eq. (6) represents the shear-stress partitioning ratio F_t (after Foster, 1982; Istanbulluoglu and Bras, 2005), which is used to scale the shear stress at each node to the vegetation cover present as follows:

$$F_t = \left(\frac{n_{\text{s}}}{n_{\text{s}} + n_{\text{v}}} \right)^{\frac{3}{2}}. \tag{8}$$

By combining the formulation for shear stress from Eq. (6) with the general stream power from Eq. (5), we formulate a new factor K_{v} that represents the bed erodibility per node as a function of surface vegetation cover. This leads to a new expression of fluvial erosion:

$$K_{\text{v}} = k_{\text{e}} \rho_{\text{w}} g (n_{\text{s}} + n_{\text{v}})^{\frac{6}{10}} F_t \tag{9}$$

$$\frac{\delta z}{\delta t}|_{\text{fluvial}} = K_{\text{v}} q^{m} S^{n}. \tag{10}$$

An illustration of the effect of vegetation cover on K_{d} and K_{v} is presented in Fig. 6.

3.4 Model evaluation

Model performance was evaluated using the above equations and different initial vegetation covers and mean annual precipitation. Our focus in this study is on the general surface process response to different transient vegetation and climate conditions. Given this, topographic metrics of relief, mean slope, and normalized steepness index (K_{sn}) were computed from the model results and compared to observed values from the 30 m SRTM DEM for each of the four areas (Fig. 2). This was done to evaluate if our implementation of the governing equations in Sect. 3.4 produced topographies within reason of present-day topographies in the four Chilean areas. A more detailed model calibration is beyond the scope of this study, and not meaningful without additional observational constraints on key parameters such latitudinal variations in the rock uplift rate and erosivity. Our aim is not to reproduce the present-day topography of the Coastal Cordillera study areas, but rather to identify the sensitivity and emergent behavior of vegetation-dependent surface processes to gradients of vegetation cover and precipitation in Chile.

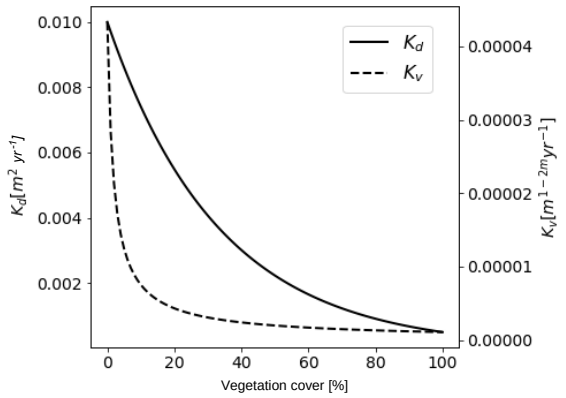

Figure 6. Predicted values of hillslope diffusivity (K_d) (solid line) and fluvial erodibility (K_v) (dashed line) as a function of vegetation surface cover. Although absolute values can not be compared due to different units, the shape of the curves representing the different parameters show different sensitivities to changes in vegetation cover. Major sources of the nonlinearities are discussed in the text. Fluvial erodibility shows the highest magnitude of change for vegetation cover values $< 25\,\%$, whereas hillslope diffusivity reacts in a more linearly fashion with the highest change observed below $< 65\,\%$ vegetation cover.

4 Results

Our presentation of results is structured around three groups of simulations. These groups of simulations include the following:

1. Steady-state simulations where equilibrium topographies are calculated for different magnitudes of vegetation cover and identical precipitation forcing. This includes a second set of steady-state simulations with the same magnitudes of vegetation cover as the first, but with different precipitation forcings corresponding to each vegetation cover (Fig. 5, Sect. 4.1).

2. Simulations with a transient step change in either the surface vegetation density or precipitation (Sect. 4.2) that is initiated after the landscape has reached steady state.

3. Simulations with a transient 100 kyr oscillating time series of changing vegetation or precipitation that occurs after the landscape has reached steady state (Sect. 4.3).

For each group of transient simulations, we show the topographic evolution with help of standard topographic metrics and the corresponding erosion rates after the induced change.

4.1 Equilibrium topographic metrics

Topographic metrics from each of the four Chilean focus areas (Fig. 1a) were extracted for comparison to equilibrium topographies predicted after 15 Myr of model simulation time. This comparison was undertaken to document the model response to changing vegetation cover (with the climate held constant) and changing vegetation cover and precipitation, but also to demonstrate the fact that the modeling approach employed throughout the rest of this study captures the general characteristics of different topographic metrics along the Chilean Coastal Cordillera.

Analysis of the digital elevation model for each of our four Chilean focus areas illustrates observed changes in catchment relief, slope, and channel steepness (K_{sn}) in relation to the surface vegetation (Fig. 7, red points) and latitude (Fig. 2). The general trend in the observed metrics shows a nonlinear increase in each metric until a maximum is reached for regions with 70 % vegetation cover. Following this, all observed metrics show a decline towards the area with 100 % vegetation cover.

The model predicted equilibrium topographies (Fig. 7a, b, c) from four different steady-state simulations, with different vegetation cover in each simulation and a constant mean annual precipitation ($900\,mm\,yr^{-1}$), show a nearly linear increase in all observed basin metrics with increasing vegetation cover; therefore, they do not reflect the overall trend observed from the study areas (red line/symbols). For example, basin relief and slope are both underpredicted for simulations with $V < 100\,\%$ (Fig. 7a, b), and only the predicted maximum relief for a fully vegetated simulation resembles the DEM maximum value. For the normalized channel steepness, only two observed mean values (for $V = 10\,\%$ and 70 %) lie within the range of the mean to maximum predicted K_{sn} values (Fig. 7c).

The resulting equilibrium topographies from simulations with different mean annual precipitation and vegetation cover in each simulation (Fig. 7d, e, f) show an improved representation of the general trend of the DEM data. The vegetation cover and precipitation values used in these simulations come from the Chilean study areas (Figs. 1b, c, 5). In these simulations, the maximum in the observed basin metrics is situated at values of $V = 30\,\%$ with a subsequent slight decrease in the metric for $V = 30\,\%$ to $V = 70\,\%$, followed by a steeper decrease in metrics from $V = 70\,\%$ to $V = 100\,\%$. Generally the model-based results tend to underestimate the basin relief and overestimate the basin channel steepness (Fig. 7d, f). Variations in basin slope are captured for all but the non-vegetated state (Fig. 7e).

Although the above comparison between the models and the observations demonstrates a range of misfits between the two, there are several key points worth noting. First, the model results shown are simplified in their setup (e.g., assuming similar rock uplift rate and identical lithology and constants), and assume the present-day topography is in steady state for the comparison. Second, despite the previous simplifying assumptions, the degree of misfit between the observations and the model is surprisingly small when both vegetation and precipitation are considered (Fig. 7d,

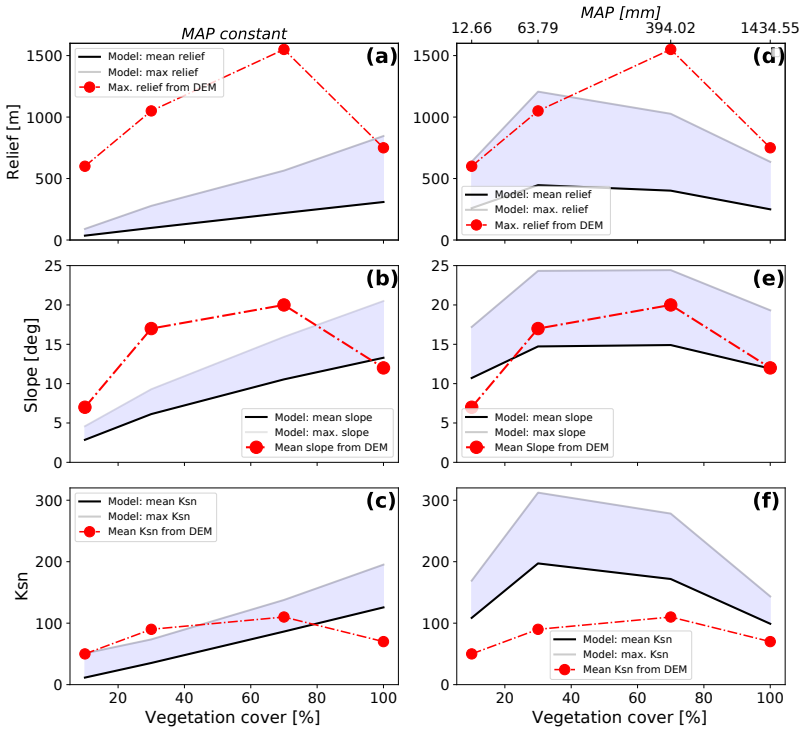

Figure 7. The steady-state model predicted (shaded regions) and observed (red dots) topographic metrics from the study areas shown in Fig. 1 for different vegetation cover amounts. Observed topographic metrics were extracted from SRTM 90 m DEM. Model predicted values are shown for the cases of constant mean annual precipitation **(a, b, c)** or variable precipitation **(d, e, f)**. Variable precipitation rates and vegetation covers were selected for these simulations using the observed values from the focus areas (Fig. 5). Note that for variable precipitation and vegetation cover simulations **(d, e, f)** the predicted values (similar to the observations) develop a hump-shaped pattern of an increase in each parameter followed by a decrease. This suggests that changes in both precipitation and vegetation cover are needed to reproduce the general trend seen in observations. The sources of misfit between the predicted and observed values are due to the simplified (and untuned) setup of the simulations, and are discussed in the text.

e, f). Finally (third), the general "hump-shaped" curve observed in the Chilean areas is captured in the model predictions (Fig. 7d, e, f), with the notable exception that the maximum in observed values occurs at a higher vegetation cover ($V = 70\,\%$) than the model predictions ($V = 30\,\%$). Explanations for the possible source of these differences are revisited in the discussion section of this paper.

4.2 Transient topography from a step change in vegetation or precipitation

The evolution of topographic metrics after an induced instantaneous disturbance (Fig. 4) of either only the surface vegetation cover (Fig. 8, green lines) or only the mean annual precipitation (Fig. 8, blue lines) is analyzed for changes in the topographic metrics for either a positive disturbance (Fig. 8a, b, c) or a negative disturbance (Fig. 8d, e, f). This scenario was chosen to analyze and isolate the effects of these specific transient forcings, and are useful for understanding the more complex changes in vegetation and precipitation presented later. Mean catchment erosion rates are also analyzed for their evolution after the disturbance (Fig. 9). For simplicity in presentation, results are shown for only two of the four Chilean study areas with initial vegetation (V) and precipitation (P) values for vegetation covers of 10 and 70 %, and precipitation rates that correspond to these vegetation covers (i.e., $P(V = 10\,\%)$ or $P(V = 70\,\%)$) (Fig. 5). The results described below show a general positive correlation between all observed topographic metrics and surface vegetation cover, and a negative correlation between observed topographic metrics and mean annual precipitation.

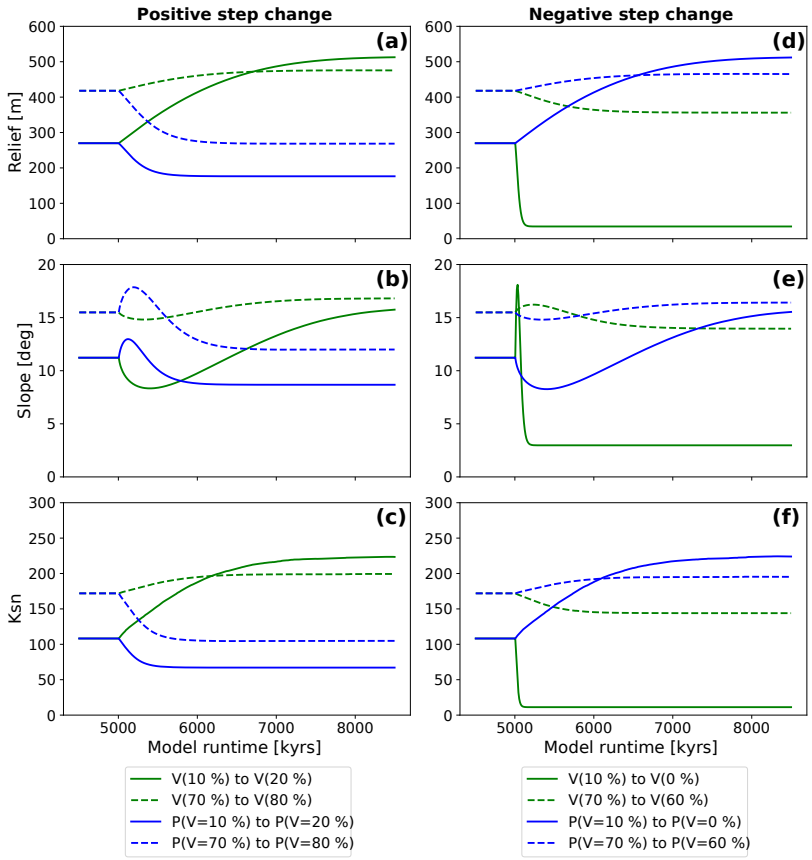

Figure 8. Observed evolution of topographic metrics after a step change in either vegetation (green lines) or mean annual precipitation (blue lines). Results are shown for two different initial vegetation cover amounts of $V = 10$ and 70 %. Imposed mean annual precipitation changes were undertaken by selecting the precipitation amount corresponding to the initial and final vegetation amounts used in the simulations for vegetation cover "only" change. Panels **(a)**, **(b)**, and **(c)** show the reaction of model topographies to positive changes in boundary conditions. Panels **(d)**, **(e)**, and **(f)** show the reaction to negative changes in boundary conditions.

4.2.1 Positive step change in vegetation cover or precipitation

Topographic analysis

A positive step change in vegetation cover (V) from $V = 10\,\%$ to $V = 20\,\%$ (solid green line Fig. 8a, b, c) leads to a factor of 1.9, 1.42, and 2.1 change in mean basin relief (from 270 to 520 m), mean basin slope (11.2 to 15.9°), and mean basin channel steepness (108 to 222 $m^{-0.9}$), respectively. The adjustment time until a new steady state in each metric is reached is 3.1 Ma. The corresponding positive change in mean annual precipitation (solid blue lines, Fig. 8a, b, c) leads to a decrease of the mean basin relief to 176 m, the mean basin slope to 8.6° and the mean basin channel steepness to 67 $m^{-0.9}$. This corresponds to a decrease by factors of 1.5, 1.2, and 1.6, respectively. The adjustment time to new steady-state conditions in this case is shorter and was found to be 1.1 Ma (Fig. 8a, b, c). A second feature of these results is the brief increase and then decrease in basin average slope angles following the step change (Fig. 8b).

For simulations with $V = 70\,\%$ initial surface vegetation cover, a positive increase to $V = 80\,\%$ leads to an increase of the mean basin relief from 418 to 474 m, the mean basin slope from 15.5 to 16.8°, and the mean basin channel steepness from 172 to 199 $m^{-0.9}$. This causes an increase in each metric by a factor of 1.1, 1.1, and 1.2, respectively. The adjustment time to steady-state conditions is 1.9 Ma (dotted green lines, Fig. 8a, b, c). The corresponding positive change in mean annual precipitation leads to a decrease of relief to 268 m, a decrease in slope to 11.9°, and a decrease of channel steepness to 105 $m^{-0.9}$. This resembles a decrease by factors of 1.5, 1.3, and 1.6, respectively. Adjustment time in this case is 1.7 Ma (dotted blue lines, Fig. 8a, b, c). The basin slope data show similar behavior as the $V_{ini} = 10\,\%$ simula-

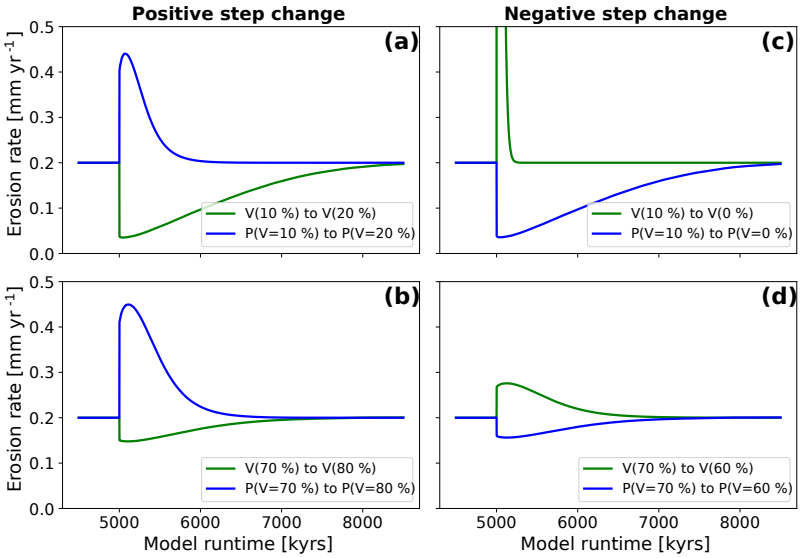

Figure 9. Mean catchment-wide erosion rates after a step-change disturbance in model boundary conditions. Blue lines represent erosion rates for models with changes in precipitation only; green lines represent erosion rates for models with changes in vegetation cover only. Panels **(a)** and **(b)** show the evolution after positive step change. Panels **(c)** and **(d)** show the evolution for models with negative step change. Note that the direction of change (positive or negative) from the initial state is in the opposite directions for precipitation and vegetation cover changes. This effect is manifested in the subsequent plots.

tions with an initial decrease and subsequent increase for a vegetation cover step change, and an initial increase and subsequent decrease for a step change in mean annual precipitation. A comparison of the change in the topographic metrics for the low ($V = 10\,\%$) and high ($V = 70\,\%$) initial vegetation covers, shows that the magnitude of change in each metric is larger when the step change occurs on a low, rather than a higher, initial vegetation cover topography.

Erosion rate changes

The model results show a negative relationship between increases in vegetation cover and erosion and a positive relationship between increases in precipitation and erosion (Fig. 9). Although the response between the disturbances and changes in erosion rates are instantaneous, the maximum or minimum in the change is reached after some lag time, and the magnitude and duration of nonequilibrium erosion rates varies between different simulation setups.

For an initial vegetation cover of $V = 10\,\%$, a change in vegetation cover (dV) of $+10\,\%$ leads to a decrease in erosion rates from 0.2 to 0.03 mm yr^{-1} (a factor of 5.7 decrease, Fig. 9a green line). The minimum erosion rate is reached 43.5 kyr after the step change occurs. Following this minimum in erosion rates, the rates increase until the steady-state erosion rate is reached after the adjustment time. An increase in mean annual precipitation, corresponding to a vegetation cover of $10\,\%$ (i.e., $P(V = 10\,\%)$ to $P(V = 20\,\%)$; Fig. 5), leads to an increase in erosion rates to a maximum of 0.44 mm yr^{-1} after 74.8 kyr (a factor of 2.2 increase, Fig. 9a, blue line). For an initial vegetation cover of $V = 70\,\%$, a vegetation increase of dV $= +10\,\%$ results in minimum erosion rates of 0.14 mm yr^{-1} after 117.7 kyr (a factor of 1.4 decrease, Fig. 9b, green line). A corresponding increase in precipitation for these same vegetation conditions leads to maximum erosion rates of 0.44 mm yr^{-1} after 107.5 kyr, which is an increase by a factor of 2.2 (Fig. 9b, blue line). The previous results for a positive step change in vegetation or precipitation demonstrate that the magnitude of the change in erosion rates is larger for changes in precipitation rate than for vegetation cover changes; furthermore, in low initial vegetation cover settings ($V = 10\,\%$) the magnitude of the change in erosion rates for changing vegetation is larger (compare green lines Fig. 9a with b).

4.2.2 Negative step change in vegetation cover or precipitation

Topographic analysis

For negative step changes in vegetation (green curves, Fig. 8d, e, f), the results show a sharp decrease in the topographic metrics associated with shorter adjustment times compared to the positive step change experiments (compare Fig. 8d, e, f with a, b, c). For step changes in pre-

cipitation (blue curves, Fig. 8d, e, f), the increase of topographic metrics happens slower, which equates to longer adjustment times. A negative step change in vegetation cover from $V = 10\,\%$ by $\mathrm{dV} = -10\,\%$ leads to a decrease of the mean basin relief from 269 to 35 m, the mean basin slope from 11.2 to 2.3°, and the mean basin channel steepness from 108 to 11 $\mathrm{m}^{-0.9}$, which resembles decreases by factors of 7.8, 3.8, and 9.6, respectively. The adjustment time until a new steady state is reached is 0.26 Ma (solid green lines, Fig. 8d, e, f). The corresponding negative change in precipitation leads to an increase in the mean basin relief to 512 m, the mean basin slope to 15.8°, and the mean basin channel steepness to 223 $\mathrm{m}^{-0.9}$. These increases reflect changes by factors of 1.9, 1.4, and 2.1, respectively, with an adjustment time of 4.9 Ma (dotted green lines, Fig. 8d, e, f). Mean basin slope results (Fig. 8e) for a step change in vegetation illustrate a pulse-like feature of initially increasing slope values, followed by a decrease to lower slope values. In contrast, a negative step change in precipitation induces an initial decrease in slope, followed by a gradual increase in slope to a value higher than was initially observed before the change.

Simulations with initial vegetation cover of $V = 70\,\%$ and $\mathrm{dV} = -10\,\%$ show a decrease in the mean basin relief from 418 to 356 m, the mean basin slope from 15.5 to 13.6°, and the mean basin channel steepness from 172 to 144 $\mathrm{m}^{-0.9}$, which resembles changes by respective factors of 1.2, 1.1, and 1.2 and an adjustment time of 2.1 Ma (dotted green lines, Fig. 8d, e, f). Corresponding negative changes in precipitation lead to increase of the basin relief of 465 m, the basin slope to 16.4°, and the channel steepness to 195 $\mathrm{m}^{-0.9}$, which resembles changes by factors of 1.1 for all three values. Adjustment time in this case is 2.2 Ma (dotted blue lines, Fig. 8d, e, f). Behavior of mean basin slope after the step change follows the $V = 10\,\%$ simulations, but shows lower amplitudes of basin slope for both step changes in vegetation and precipitation.

Erosion rates

The positive step-change results (Fig. 9a, b) indicated that erosion rates reach their minimum or maximum with a lag time. The results also show significant differences in the magnitude and duration of nonequilibrium conditions depending on if vegetation or precipitation were changing. Simulations with a decrease from $V = 10\,\%$ to $V = 0\,\%$ (Fig. 9c) show a sudden increase in erosion rates to a maximum value of 3.5 mm yr^{-1}, which is an increase from steady-state conditions by a factor of 17.7. This value is reached after 19.5 kyr (green line, Fig. 9c). A step decrease in precipitation for this corresponding vegetation difference (i.e., $P(V = 10\,\%)$ to $P(V = 0\,\%)$ leads to a smaller, and protracted (longer adjustment time) decrease in erosion rates to 0.03 mm yr^{-1} after 50.1 kyr. These conditions cause a factor of 5.6 decrease (blue line, Fig. 9c). Simulations of $V = 70\,\%$ with a vegetation change of $\mathrm{dV} = -10\,\%$ show an increase in erosion rates to 0.27 mm yr^{-1}, which is a factor of 1.4 increase after 126.3 kyr (Fig. 9d). For the corresponding decrease in precipitation the data show a decrease in erosion rates to 0.15 mm yr^{-1} after 124.5 kyr. This resembles change by factor of 1.2 (blue line, Fig. 9d).

4.3 Transient topography – oscillating

4.3.1 Oscillating surface vegetation cover and constant precipitation

Topographic analysis

The topographic evolution in simulations with a constant precipitation (10 and 360 mm yr^{-1} for $V = 10\,\%$ and $V = 70\,\%$, respectively) and oscillating vegetation cover show a different response than the previous step change experiments. The differences depend on the initial steady-state vegetation cover prior to the onset of 100 kyr oscillations. All observed basin metrics (Fig. 10) show an initial oscillating decrease in values until a new dynamic steady state is reached where the amplitude in oscillations is less than in the preceding initial adjustment period. Simulations with $V = 10\,\%$ (Fig. 10a) show a factor of 2.5 decline in the basin relief (from 269 to 107 m). For simulations with $V = 70\,\%$ the reaction and adjustment to the new dynamic steady state is less pronounced with a factor of 1.01 decline in relief (from 410 to 407 m), and positive and negative amplitudes in the dynamic steady state of 1.6 m. While these changes are unmeasurable in reality, they highlight that changes in vegetation cover alone would be difficult to detect for high initial vegetation cover settings. The analysis of the mean basin slope for the model topographies with low ($V = 10\,\%$) vegetation shows a similar behavior with a factor of 1.6 decrease of the mean slope (from 11.2° prior to the onset of oscillations, to 6.0°, Fig. 10b). However, before this new equilibrium is reached, the slopes show an increase in the mean slope for the first two periods of vegetation oscillation, which then declines towards the new long-term stable dynamic equilibrium. This equilibrium is reached after approximately 500 kyr. Local maxima of the mean basin slope coincide with local minima in basin relief. For the $V = 70\,\%$ simulations, the reaction is significantly smaller with no change in mean slope for the new dynamic equilibrium and both positive and negative amplitudes of 0.16°. Mean basin channel steepness (Fig. 10c) reflects the behavior of mean basin elevation. For $V = 10\,\%$ simulations the mean channel steepness decreases by a factor of 2.7 (from 108 to 40 $\mathrm{m}^{-0.9}$) with a positive amplitude of 3.7 $\mathrm{m}^{-0.9}$ and a negative amplitude of 6.1 $\mathrm{m}^{-0.9}$. For $V = 70\,\%$ simulations the response is again only minor, compared to the lower initial vegetation cover simulations with a change of mean channel steepness from 186 to 167 $\mathrm{m}^{-0.9}$, positive amplitudes of 1.1 $\mathrm{m}^{-0.9}$, and negative amplitudes of 0.9 $\mathrm{m}^{-0.9}$. Like the elevation data, the steepness data show a distinct oscillating pattern with a slow increase to local maxima and rapid decrease to local minima, which coincide with

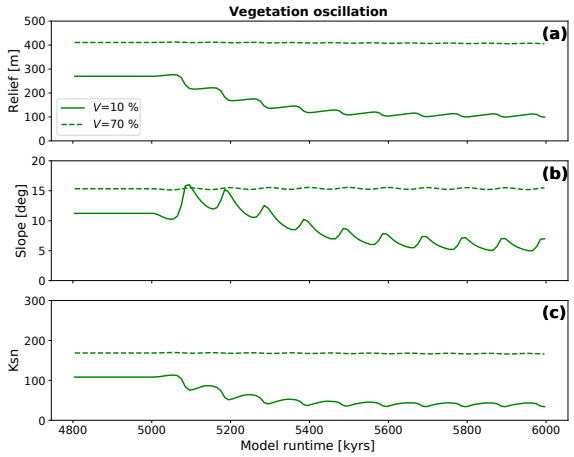

Figure 10. Evolution of topographic metrics for simulations with oscillating surface vegetation cover and constant precipitation corresponding to the initial vegetation cover prior to the transient in vegetation cover. Panels a, b, and c show the mean basin relief, the mean basin slope, and the mean basin channel steepness (K_{sn}), respectively.

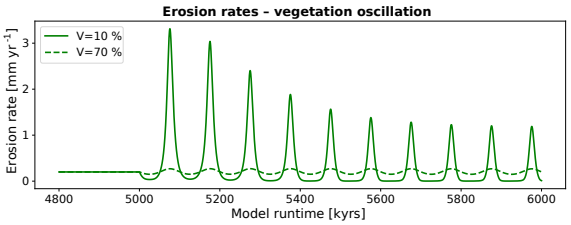

Figure 11. Predicted mean catchment erosion rates for simulations with oscillating surface vegetation cover and constant precipitation. Note that the magnitude of change in erosion rates for a ±10 % change in vegetation cover differs depending on the initial (or background) vegetation cover. This nonlinear response is due, in part, to the vegetation cover effects on rock erodibility and diffusivity shown in Fig. 6.

maxima/minima of elevation data. Taken together, the previous observations demonstrate a larger change in topography for oscillations in poorly vegetated areas compared to those with higher vegetation cover. Furthermore, the magnitude of topographic change that oscillations in vegetation impose on topography are largest in the first ∼ 500 kyr after the onset of an oscillation, and diminish thereafter.

Erosion rates

The erosion history for simulations with oscillating vegetation cover (Fig. 11) demonstrate large variations in the erosion rate that depend on the average vegetation cover of the oscillation. Furthermore, pronounced differences in the amplitude of erosion occur if the vegetation cover is above or below the mean of the oscillation (Fig. 4a). More specifically, simulations with $V = 10\,\%$ show a pattern of a small decrease in erosion rates (from 0.2 to 0.03 mm yr^{-1}) when vegetation cover increases above the mean cover, in contrast to a large increase in erosion rates (up to 3.3 mm yr^{-1}) when vegetation cover decreases below the mean of the oscillation (Figs. 2, 11). Maximum erosion rates decline over multiple periods of oscillation until they reach a dynamic steady state with maximum rates (1.2 mm yr^{-1}) at 760 kyr after the onset. Time periods of higher erosion rates ($>$ 0.2 mm yr^{-1}) have a mean duration of 28 kyr, whereas periods of lower erosion rates ($<$ 0.2 mm yr^{-1}) have a mean duration of 72 kyr. For simulations with high vegetation cover ($V = 70\,\%$) the maximum and minimum erosion rates are 0.28 and 0.15 mm yr^{-1}, respectively. The magnitude of maximum and minimum erosion rates are not significantly time-dependent, meaning that they are constant over the simulation. The mean duration of periods with higher erosion rates ($>$ 0.2 mm yr^{-1}) is 55 kyr, whereas the duration for periods with lower rates ($<$ 0.2 mm yr^{-1}) is 45 kyr. These results demonstrate that areas with low vegetation cover experience not only larger amplitudes of change in erosion rates, but also an asymmetric change whereby decreases in erosion rates are of a lower magnitude than the increases in erosion rates.

4.3.2 Oscillating precipitation and constant vegetation

Topographic analysis

The evolution of topographic parameters for simulations with oscillating mean annual precipitation and two different constant surface vegetation covers ($V = 10$ or $70\,\%$, Fig. 12) shows a less extreme and smaller temporal change in erosion rate to variations in precipitation compared to the previously discussed effects of oscillating vegetation cover (Fig. 11). In Fig. 12a, the mean basin relief results for $V = 10\,\%$ and oscillating precipitation show small variations (+4.9 to −3.8 m) in relief around a mean of 269 m, which is similar to the mean relief prior to the onset of oscillations at 5000 kyr. For simulations with $V = 70\,\%$ the change in relief is slightly more pronounced with factor of 1.1 adjustment to a new mean (380 from 418 m) in steady-state conditions. The evolution of the topographic slope (Fig. 12b) for $V = 10\,\%$ simulations shows a factor of 1.05 adjustment to a new dynamic equilibrium (from 11.2 to 10.6°). For $V = 70\,\%$ the mean slope values do not significantly change from steady-state to transient conditions. Mean channel steepness (Fig. 12c) for $V = 10\,\%$ shows a factor of 1.01 adjustment (from 108 to 110 m$^{-0.9}$), and would be difficult to measure in reality. The amplitude of oscillation is 4 m$^{-0.9}$ for both negative and positive amplitudes. For $V_{ini} = 70\,\%$ simulations, a factor 1.1 change in channel steepness occurs (from 171 to 152 m$^{-0.9}$) with amplitudes of 4.5 m$^{-0.9}$ for both positive and negative

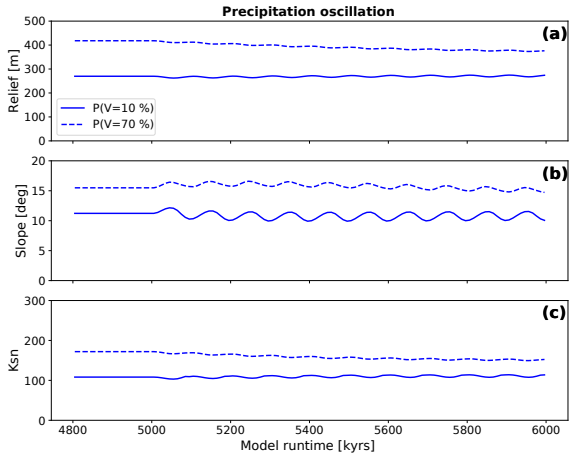

Figure 12. Evolution of topographic metrics for simulations with oscillating mean annual precipitation and constant vegetation cover. The vegetation cover was held constant at the value corresponding to the precipitation rate prior to the onset of the transient at 5000 kyr. Panels **(a)**, **(b)**, and **(c)** show the mean basin relief, the mean basin slope, and the mean basin channel steepness (K_{sn}), respectively.

changes. Figure 12 illustrates changes in topographic metrics that result from oscillations in precipitation occurring around vegetation covers of 10 and 70 %. These changes are significantly smaller than those predicted for constant precipitation with oscillating vegetation conditions (Fig. 10).

Erosion rates

Predicted erosion rates from simulations with constant surface vegetation cover and oscillating mean annual precipitation indicate different amplitudes of change around the mean erosion rate depending on the vegetation cover. For simulations with $V = 10\,\%$ (Fig. 13, blue solid line) erosion rates oscillate symmetrically around the steady-state erosion rate ($0.2\,\mathrm{mm\,yr^{-1}}$). The maximum and minimum erosion rates of 0.42 and $0.01\,\mathrm{mm\,yr^{-1}}$, respectively, do not lead to a shift in the mean value of erosion rates over time. In contrast, predicted rates with a higher vegetation cover of $V = 70\,\%$ (Fig. 13, blue dotted line) demonstrate an asymmetric oscillation in rates around the mean, whereby the maximum rates ($0.43\,\mathrm{mm\,yr^{-1}}$) have a larger difference above the mean rate than the minimums in the oscillation do ($0.12\,\mathrm{mm\,yr^{-1}}$). For this higher vegetation cover scenario, a gradual decrease in the mean erosion rate occurs as time progresses. Furthermore, the maximum and minimum erosion rates decline over several oscillation periods. Taken together, these results indicate that oscillations in precipitation impact erosion, with the magnitude of the effect depending on the amount of vegetation cover. Areas with low vegetation cover demonstrate the highest and most symmetric oscillation of erosion rates due

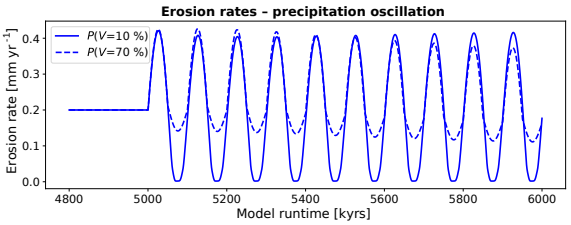

Figure 13. Mean catchment erosion rates for simulations with oscillating mean annual precipitation and constant surface vegetation cover. The amplitude of change in the erosion rates varies with the initial vegetation cover, in part due to the nonlinear relationship between precipitation and vegetation cover (Figs. 4, 5).

to changes in precipitation, whereas in areas with high vegetation cover the effect of negative changes in precipitation is dampened by vegetation.

5 Discussion

The previous results highlight different sensitivities to changes in either surface vegetation cover or mean annual precipitation. In the following, we synthesize the previous results and then build upon them to discuss the scenario of synchronous variation in both precipitation and vegetation cover.

5.1 Interpretation of steady-state simulations

Landscapes in a topographic steady state show distinct features in topographic metrics that are widely used to estimate catchment-averaged erosion rates and the related leading processes of erosion within a landscape (DiBiase et al., 2010). The steady-state simulations presented here can reproduce (Fig. 7) variations in topographic metrics over different climate and vegetation states than those seen in other studies (Langbein and Schumm, 1958; Walling and Webb, 1983). The comparison of simulations with homogeneous precipitation and changing values of vegetation cover (Fig. 7a, b, c) to simulations with both changing precipitation and vegetation cover values (Fig. 7d, e, f), indicates that we can only reproduce a similar trend with a distinct peak in topographic metrics when both precipitation and vegetation cover variables are considered. From this, we conclude that modern model-based landscape evolution studies, which aim to compare areas with different climates, should incorporate vegetation dynamics in their simulations. Misfits between the predicted and Chilean observed topographic metrics (Fig. 7d, e, f), present when the vegetation and precipitation both vary, likely stem from the simplicity of the model setup used and the likelihood of differences in the rock uplift rate and lithologies present in these areas.

5.2 Interpretation of step change experiments

Our analysis shows that changes in vegetation cover typically have a higher magnitude of impact on topographies for lower values of initial vegetation cover, compared to simulations with high initial vegetation cover (Figs. 8, 9). In these settings the influence of vegetation cover outweighs the influence of precipitation regarding cases of negative and positive directions of the step change. The reason for this is the higher impact of changes in vegetation than the impact of changes in precipitation on erosivity and diffusivity (parameter K_v, K_d; Eqs. 4, 10).

Furthermore, a negative step change in vegetation cover impacts the topographic metrics by a factor of 2 more than positive step change changes do (Fig. 8d, e, f). This response is interpreted to be due to the nonlinear reaction of diffusivity and fluvial erodibility to changes in vegetation cover (See Fig. 6). Negative changes in vegetation cover lead to a higher overall change in diffusivity and erodibility compared to positive step changes.

Model results for the topographic metrics and erosion rates also indicate a difference in the adjustment times of the system until a new steady state is reached when either precipitation or vegetation cover changes (Figs. 8, 9). For simulations with positive step changes (Fig. 8a, b, c) the adjustment time for changes in vegetation cover to reach a new equilibrium in topographic metrics or erosion rates is 3 times longer than the adjustment time for changes in precipitation. Simulations with negative step changes in vegetation cover show an adjustment time that is shorter by a factor of 18 compared to negative changes in precipitation. This difference in adjustment time is again a result of the nonlinear behavior of erosion parameters K_d and K_v, which influence how effectively a signal of increasing or decreasing erosion can travel through a river basin (Perron et al., 2012). High values of K_d and K_v are associated with lower adjustment times and are a result of negative changes in vegetation cover. The influence of changing precipitation on adjustment time behaves in a more linear fashion; therefore, it mostly depends on the overall magnitude of change. Thus, positive step changes in vegetation cover decrease K_d and K_v, which leads to higher adjustment times than the corresponding changes in precipitation.

An increase and subsequent decrease, or decrease and subsequent increase, in predicted slope and erosion rates is observed for both the positive and negative step change experiments (Figs. 8b, e and 9). This nonlinear response in both positive and negative step changes in precipitation and vegetation cover is also manifested in the subsequent oscillation experiments, although it is most clearly identifiable in the step change experiments. The explanation for this behavior is as follows. A positive step change in vegetation cover (Fig. 8b) leads to a decrease in fluvial capacity, as increased vegetation cover increases the Manning roughness (parameter n_v, Eq. 8). The effect of changing the Manning roughness varies with the location within the catchment, and influences which processes (fluvial or hillslope) most strongly impact slopes and erosion rates. In the upper part of catchments, where contributing areas (and discharge) are low, this increase in Manning roughness causes many areas to be below threshold conditions; therefore, fluvial erosion is less efficient, and hillslope diffusion increases in importance and reduces slopes. In the lower part of catchments, where contributing area and discharge are higher, changes in the Manning roughness are not large enough to impact fluvial erosion because these areas remain at, or above, threshold conditions for erosion. With time, the lower regions of the catchments that are at or above threshold conditions propagate a wave of erosion up to the higher regions that are below threshold conditions. This propagating wave of erosion eventually leads to an increase in slope angles, which is essential due to the response time of the fluvial network to adjust to the new Manning roughness conditions.

In contrast, a positive step change in mean annual precipitation leads to an initial increase in fluvial shear stress, which initially causes headward incision of river channels and leads to a wave of erosion that propagates upstream and increases channel slope values (Fig. 8b, see also e.g., Bonnet and Crave, 2003). The increase in channel slopes leads to an increase in the hillslope diffusive flux adjacent to the channels that then propagates upslope. Eventually, this increase in the hillslope flux leads to a decrease in hillslope angles, and an overall reduction in mean catchment slopes after the systems reaches equilibrium.

Negative step changes in vegetation cover or precipitation (Fig. 8e, green curves) show the opposite behavior to the previous positive step change description. A negative step change in vegetation cover leads to an initial increase of fluvial erosion throughout the catchment, as the Manning roughness decreases everywhere. This catchment-wide decrease in Manning roughness leads to fluvial incision throughout the catchment and an increase in mean slope. However, eventually hillslope processes catch up with increased slopes near the channels, and with time an overall reduction of slope occurs. Negative changes in precipitation (Fig. 8e, blue curves) lead to an initial decrease in fluvial erosion, thereby leading to an increase in the significance of hillslope processes such that slope angles between channels and ridges decrease as hillslope processes fill in channels. With time, the fluvial network equilibrates to lower precipitation conditions by increasing slopes to maintain equilibrium between erosion and rock uplift rates.

Thus, the contrasting behavior of either initially increasing or decreasing slopes and erosion rates, followed by a change in the opposite direction of this initial change, highlight a complicated vegetation–climate induced response to changes in either parameter. This nonlinear behavior, and the millennial timescales over which these changes occur, suggest that modern systems that have experienced past changes in climate and vegetation will likely be in a state of transience;

therefore, the concept of a dynamic equilibrium in hillslope angles and erosion rates may be difficult to achieve in these natural systems.

Previous studies have inferred relationships between mean catchment erosion rates derived from cosmogenic radionuclides and topographic metrics (e.g., DiBiase et al., 2010; DiBiase and Whipple, 2011). However, the previous discussion of how topographic metrics change in response to variable precipitation and vegetation suggests that empirical relationships between erosion rates and topographic metrics contain a signal of climate and vegetation cover in the catchment. We illustrate the effect of step changes in climate and vegetation on the new steady state of topographic metrics in Fig. 14. In this example, the new steady-state conditions in basin relief and mean slope after a modest (±10 %) change in vegetation or precipitation (triangles) differ from the initial steady-state condition (circles). These changes in topographic metrics when the new steady state is achieved occur despite the rock uplift rate remaining constant.

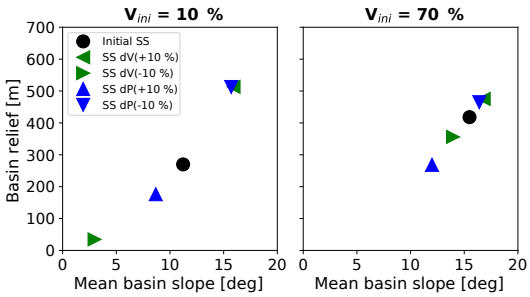

Figure 14. Shifts in the mean basin slope–mean basin relief relationship for simulations with positive and negative step changes in either vegetation cover (green triangles) or mean annual precipitation (blue triangles). Black dots represent initial steady-state conditions prior to any imposed transient in vegetation cover or mean annual precipitation. Note that the sensitivity of topographic relief to perturbations in precipitation or vegetation cover is highest for low vegetation cover (10 %) settings.

5.3 Interpretation of oscillation experiments

The results from the 100 kyr oscillating vegetation and precipitation conditions show that oscillating vegetation cover without the corresponding oscillations in precipitation leads to adjustments of topographic features, which results in a new dynamic equilibrium after approximately 1.5 Ma (Figs. 10, 11). The previously described response of topographic metrics and erosion rates to oscillating vegetation (see results section) are due to processes described in the previous step change experiments. For example, the asymmetric oscillations in topographic metrics for $V = 10\,\%$ (Fig. 10) are due to the superposition of the positive, and subsequent negative, changes described in Sect. 5.2. Variations in the imposed Manning roughness, and the relative strengths of fluvial vs. hillslope processes in different parts of the catchments at different times cause the topographic metrics and erosion rates to have variable amplitudes and shapes of response due to the symmetric oscillations imposed on the topography (Fig. 4a).

Simulations with oscillating precipitation and constant vegetation cover show a less pronounced shift to new equilibrium conditions and lower amplitudes of oscillation in both topographic metrics and erosion (Figs. 12, 13). This difference in the response of the topographic metrics and erosion rates shown in Figs. 12 and 13, compared to the oscillating vegetation cover experiments (Figs. 10, 11), is due to the higher impact of changes in vegetation cover on parameters that guide erosion rates and the related adjustment to topographic metrics compared to the corresponding changes in precipitation in our model domains (Fig. 5). Especially for simulations with low initial vegetation cover, the effect of changing vegetation has a larger magnitude of effects due to the nonlinear response of diffusivity and fluvial erodibility to changes in vegetation cover compared to the linear response to changes in precipitation.

5.4 Coupled oscillations in both vegetation and precipitation

The previous sections present a sensitivity analysis of how step changes or oscillations in either vegetation cover or precipitation influence topography. Here we present a step-wise increase towards reality by investigating the topographic response to changes in both precipitation and climate at the same time. The amplitude of change prescribed for both precipitation and vegetation is based upon the present empirical relationship observed in the Chilean study areas for initial vegetation covers of 10 and 70 %, and mean annual precipitations of 10 and 360 mm yr^{-1} (Fig. 5). As with the previous experiments, oscillations in parameters were imposed upon steady-state topography that was developed with the previous values, and a rock uplift rate of 0.2 mm yr^{-1}.

Figure 15 shows the evolution of topographic metrics for simulations with combined oscillations in precipitation and vegetation. The variation in topographic metrics resembles those described for simulations with constant vegetation cover and oscillating climate by showing little to no significant adjustment towards new dynamic steady-state conditions. The amplitudes of oscillation are dampened from those of previous results because of the opposing effects of changes in precipitation and vegetation cover (e.g., compare blue and green curves in Figs. 8 and 9).

However, inspection of the predicted erosion rates (Fig. 16) for the combined oscillations indicates a significant (~ 0.1 – ~ 0.15 mm yr^{-1}), and highly nonlinear, response. The response between the 70 % and 10 % vegetation cover scenarios are very different. For heavily vegetated ar-

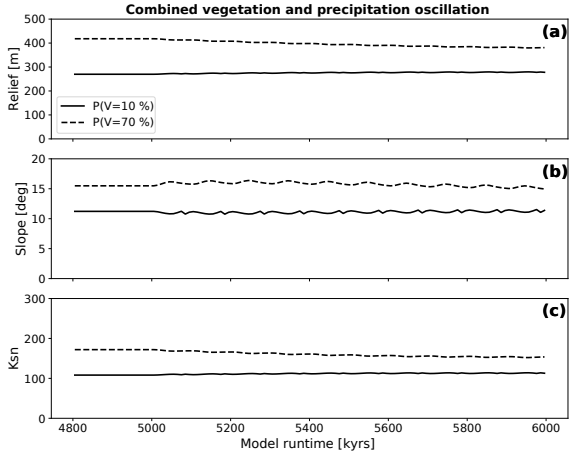

Figure 15. Evolution of topographic metrics for coupled simulations where both changes in surface vegetation cover and a corresponding change in mean annual precipitation (Fig. 5) are simultaneously imposed. The amplitudes and frequency of the forcings that were imposed on the simulations are the same as those used for the simulations with isolated transient forcings. Panels **(a)**, **(b)**, and **(c)** show the evolution of the mean basin relief, the mean basin slope, and the mean basin channel steepness (K_{sn}) after the start of the oscillation at 5 Ma. Note the muted/damped response relative to previous simulations of oscillating vegetation cover or precipitation conditions.

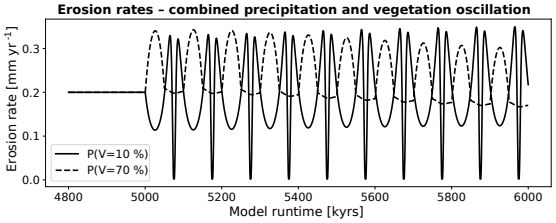

Figure 16. Mean catchment erosion rates for coupled simulations with changes in surface vegetation cover and mean annual precipitation. The first cycle in the time series is expanded in Fig. 17. The variable amplitude and nonlinear response shown here is due to the combined nonlinear forcings in precipitation (Figs. 4, 5) and rock erodibility and diffusivity (Fig. 6) for different initial vegetation cover amounts.

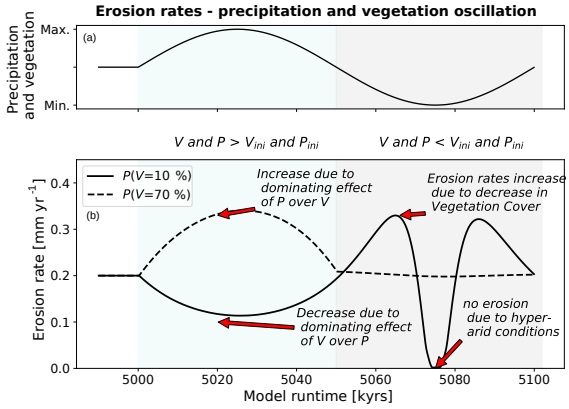

Figure 17. Mean catchment erosion rates for coupled simulations for one period of oscillation after the start of transient conditions (see also Fig. 15). Panel **(a)** shows conceptualized transient forcing in vegetation cover and mean annual precipitation. Panel **(b)** shows the erosion rates for simulations with low (black line) and high (dotted line) initial vegetation cover and precipitation values.

eas ($P(V = 70\,\%)$) erosion rates typically increase during an oscillation, whereas for the low vegetation cover conditions ($P(V = 10\,\%)$) erosion rates initially show a decrease and then increase and decrease at a higher frequency.

To better understand this contrast in the response to combined precipitation and vegetation changes, the first 100 kyr cycle is shown in Fig. 17. After an oscillation starts, the 10 % initial vegetation cover simulations show a decline in erosion rates with the minimum erosion rate correlated with the highest values of both vegetation cover and mean annual precipitation (compare top and bottom panels). This part of the response is interpreted as resulting from the hindering effect of increased vegetation on erosion rates outweighing the impact of higher precipitation on erosion rates because vegetation decreases the effectiveness of erosion and transport of surface material (Fig. 17). After values of vegetation cover and precipitation start to decline, erosion rates show a very rapid increase to values of $\sim 0.3\,\mathrm{mm\,yr^{-1}}$. This increase in erosion rates is due to an increase in both K_v and K_d (Fig. 3b, Eqs. 4, 5), which outcompetes the effect of precipitation decrease.

Following this, a sudden drop in erosion rates occurs (to $0\,\mathrm{mm\,yr^{-1}}$) and lasts for 3 kyr due to the onset of hyper-arid conditions at minimum precipitation. After this low in erosion rates, they once again increase (to $0.3\,\mathrm{mm\,yr^{-1}}$) as precipitation and vegetation cover increase, while the effect of increased precipitation outweighs the effect of the nonlinear decrease in K_v and K_d (Fig. 3b, c; Eqs. 4, 5). Finally, at the end of this complex cycle a decrease in erosion rates occurs (Fig. 17b), while vegetation and precipitation are increasing (upper panel) because the effect of vegetation increases K_v/K_d and outweighs the effect of increasing precipitation.

Lastly, a clearly different erosion rate behavior occurs for settings with higher vegetation cover (e.g., $P(V = 70\,\%)$, Fig. 17) compared to the previous lower vegetation cover scenarios. As the vegetation cover and precipitation increase (Fig. 17a) in the first half of the 100 kyr cycle, the erosion rates increase (to $0.35\,\mathrm{mm\,yr^{-1}}$). This is due to the increase in precipitation, which outcompetes the decline in vegetation influenced erosivity/diffusivity parameters, K_d and K_v. Following this, when vegetation cover and precipitation decrease in the second half of the cycle, little to no change oc-

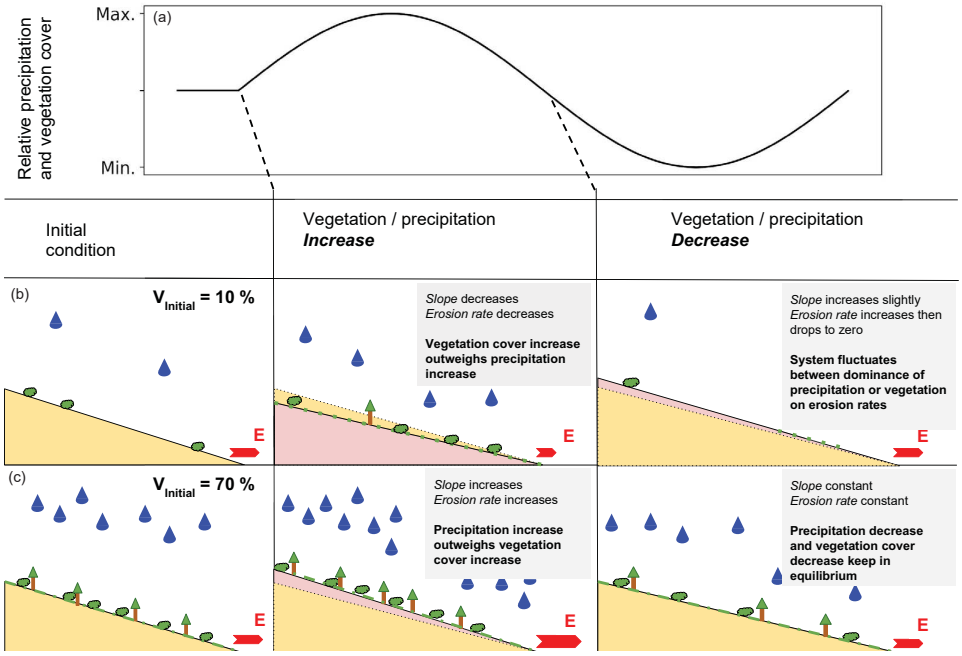

Figure 18. Conceptual figure showing the topographic response from simulations with coupled oscillation of mean annual precipitation and vegetation cover (see Fig. 17 for erosion rates). Panel **(a)** illustrates transient forcings, panels **(b)** and **(c)** show the initial topography (yellow) and the resulting transient topography (pink). Changes in topography are not to scale. Vegetation and rainfall amounts are shown qualitatively on the hillslopes.

curs in the erosion rates. This near static behavior in erosion rates while precipitation and vegetation cover decrease is due to an equilibrium between the negative effect on erosion rates for decreasing precipitation and the positive effect on erosion rates for decreasing vegetation cover.

In summary, the nonlinear shape of the vegetation dependent erosivity (K_v) and hillslope diffusivity (K_d) in combination with the linear effects of mean annual precipitation on erosion rates, exert a primary control on the direction and magnitude of change in catchment average erosion rates. Despite the simple oscillating behavior in precipitation and vegetation cover, a complex and nonlinear response in erosion rates occurs. In Fig. 18 we depicted the conceptual endmembers of landscape behavior for the different scenarios of increasing or decreasing vegetation cover and mean annual precipitation for different initial landscapes. The implications of this are large for observational studies of catchment average erosion rates and suggest that the direction and magnitude of the response observed in a setting is highly dependent on the mean vegetation and precipitation conditions of the catchment, as well as when the observations are made within the cycle of varying vegetation and precipitation. Furthermore, these results highlight the need for future modeling studies (and motivation for our ongoing work) to investigate the response of catchment topography and erosion rates to more realistic climate and vegetation change scenarios. A broader range of initial vegetation covers and precipitation rates than those explored here would also be beneficial, such that the threshold in behavior between the two curves shown in Fig. 17b can be understood.

5.5 Potential observational approaches to test model predictions

The behavior discussed in the previous section matches field data reported by Owen et al. (2010) who analyzed soil production rates from bedrock in different climate regimes. This data, under the assumption of steady-state soil thickness, can be translated into denudation rates. The data show that for low values of mean annual precipitation, soil production rates vary between 0 and $2\,\mathrm{m\,Ma^{-1}}$ due to the abiotic processes controlling soil production rates. These observations resemble the effect of our simulations with a 10 % initial vegetation cover, which shows the same variations in erosion rates with intervals of a zero erosion rate for hyper-arid conditions (Fig. 17). Areas with higher values of mean annual precipitation show higher values for the soil production rate. These data points were not corrected for different uplift rates in the sample areas, so it is not possible to isolate the effect of vegetation/precipitation and tectonic uplift. In general, the ob-

servations show no clear isolated trend but more of a cluster of soil production rates among a common mean, situated in a zone controlled by biotic conditions. Compared to our model data for simulations with 70 % initial vegetation cover, this resembles the nonintuitive behavior of an increase in erosion rate for increasing values of vegetation cover and precipitation compared to a constant erosion rate for decreasing values of vegetation cover and precipitation.

Schaller et al. (2018) and Oeser et al. (2018) present millennial timescale (cosmogenic radionuclide derived) hillslope denudation, and soil production, rates from the Chilean (EarthShape) study areas (Fig. 1a) considered in this paper. They find the lowest hillslope denudation rates in the arid and poorly vegetated north. Moving south towards higher precipitation and vegetation cover the denudation rates increase until the southernmost location, with highest rainfall and vegetation cover, where denudation rates decrease again. This nonlinear relationship of hillslope denudation rates with vegetation cover and precipitation is not directly comparable to the results presented here, but is consistent with (a) the notion emphasized here that interactions between precipitation and vegetation cover on denudation are nonlinear, and (b) that the study areas considered here, although tectonically quiescent for tens of millions of years, have varying denudation rates that suggest either variable rock uplift rates, and/or a persistent state of transience in hillslope denudation induced by millennial timescale oscillations in climate and vegetation.

Beyond the previous studies, limited observations are available for comparison to the predictions shown here. The millennial to million-year timescales investigated here can best be evaluated from observations of catchment-wide denudation over similar timescales. Cosmogenic radionuclide measurements from modern river sediments offer one means to evaluate these results. Work by Acosta et al. (2015) in east Africa and Olen et al. (2016) in the Himalayas, are also consistent with the results presented here for the range of vegetation cover available in each of these areas. However, the integration timescales that these studies are sensitive to are shorter than what is presented here and prohibit a detailed comparison. A final approach that future studies could pursue is to calculate paleo-denudation rates for catchments from a time series of sediment deposits preserved in either lakes (e.g., Marshall et al., 2015) or fluvial river terraces (e.g., Schaller and Ehlers, 2006; Schaller et al., 2016). However, to be most effective, these studies need to target multiple study areas with terrace or lake deposits that span a range of vegetation covers in the upstream catchments.

5.6 Model restrictions and caveats

Similar to previous work on this topic (Collins et al., 2004; Istanbulluoglu and Bras, 2005), the model setup used in this study was simplified to document how different vegetation and climate related factors impact topography over long (geologically relevant) timescales. We acknowledge that future model studies should address some of the restrictions imposed by our approach to evaluate their significance for the results presented here. Future work should consider a transport-limited fluvial model or a fully coupled alluvial sedimentation and transport model. These additions could bring new understanding regarding how vegetation not only influences detachment limited systems, but also influences sedimentation and entrainment of material. However, this added level of complexity could limit (due to computational concerns) the temporal scales over which an investigation like this could be conducted. Future studies could improve upon this work by considering a more in-depth parameterization of how vegetation related processes (e.g., changes in root depth and density, plant functional type) influence topographic metrics and erosion rates. Also, although supported by various publications (Dunne et al., 1995, 2010), the assumption of a nonlinear response of the effectiveness of diffusional and fluvial processes to increases in vegetation cover has a major impact on the results of this study. A better field-based understanding of these processes, and the relationships involved, could improve the accuracy of model studies like this.

Furthermore, due to the long timescales considered here, mean annual precipitation rather than a stochastic distribution of precipitation was implemented. Future work should evaluate how stochastic distributions in precipitation and extreme events in arid, poorly vegetated settings, impact these results. However, the long timescale forcings in precipitation and vegetation imposed in this study will likely persist as the background template upon which high-frequency changes are active.

Regarding the vegetation and water budget, a more sophisticated model of evapotranspiration and infiltration as a function of surface plant cover and plant functional traits, such as rooting depth, would improve model predictions and is a priority for our future work. Improvements will come from the planned coupling of the surface process model with the dynamic vegetation model LPJ-GUESS (Werner et al., 2018; Smith et al., 2014).

Our assumption that an increase in surface vegetation cover directly translates to an increase in Manning roughness is an additional simplification. The real value of the Manning roughness of a surface will be a function of the fractional densities of different plant communities per model patch. However, we argue that this simplification is necessary because it is not possible to know the composition of the plant community for specific areas at our modeled timescales. This could be resolved by fully coupling a landscape evolution model to a dynamic vegetation model to resolve inter-patch differences of surface vegetation cover and intra-patch plant functional types.

We also acknowledge that the transient forcings we have chosen for driving our model are simplistic and could be improved by a higher-fidelity time series of climate over the last millennia. We choose a 100 kyr, eccentricity driven, pe-

riodicity because it is widely recognized that the eccentricity cycles have been a main control driving Earth's glacial cycle over the last 0.9 Ma. While this approach is reasonable for a sensitivity analysis such as the one we have conducted, it prohibits a detailed comparison to observations in specific study areas without additional refinement. Our results suggest that a shorter periodicity, which would resemble other periodicities in the Milankovitch cycle (e.g., 41, 23 kyr) or shorter timescale climate variations such as Heinrich events (see Huntley et al., 2013), would lead to smaller magnitudes of adjustment to new dynamic equilibria, because of short time spans in highly erosive or only slightly erosive climate conditions within one period. Regarding the long timeperiods considered, we chose to have a steady-state climate driver in the model without frequency driven modulation of rainfall events. We argue that over large timescales the occurrence of these events can be integrated into a meaningful mean value but acknowledge that the incorporation of those events could alter the results on a short cycle basis. However, because there is no meaningful way to test these frequency distributions against past climates, this would add additional unknowns and assumptions into our model parameterization.

Finally, we emphasize that a subset of our results, which resemble small magnitude changes of topographic relief (e.g., factor of change 1.01, Sect. 4.3.1, 4.3.2), are valid results for the predicted synthetic landscapes in our model framework and not a numerical artefact. However, we acknowledge that these predicted changes are too small to be measured in a real-world setting.

6 Conclusions

The results from our experiments show that the interaction of vegetation cover and mean annual precipitation on the evolution of landscapes is a complex system with competing effects. The main conclusions that emerge from this study are as follows:

i. Vegetation cover has a hindering effect on hillslope and fluvial erosion, but the magnitude at which changes in vegetation cover affect these processes is a function of the initial state of the system. Changes in systems with higher initial values of vegetation cover have a less pronounced effect than changes in systems with lower initial vegetation cover.

ii. The relationship between precipitation and surface vegetation cover in the Chilean Coastal Cordilleras, shows a distinct shape: for a 10 % increase in surface vegetation cover, the corresponding increase in the mean annual precipitation is smaller in areas of lower vegetation cover and increases for areas with higher vegetation cover. This has an effect on transient topographies by shifting the equilibrium of vegetation and precipitation effects on erosion rates.

iii. Following our step-change simulations, model results show different behaviors for changes in vegetation cover and mean annual precipitation. While increases in mean annual precipitation have an increasing effect on erosion rates and a related long-term negative effect on topographic metrics, an increase in vegetation cover hinders erosion and leads to higher topographic metrics. The magnitude of these changes is again dependent on the initial vegetation cover and precipitation before the step change.

iv. Simulations with either oscillating vegetation cover or oscillating precipitation show adjustments to new dynamic mean values around which the basin metrics oscillate. The magnitude of the adjustment is highly sensitive to initial vegetation cover, where simulations with 10 % initial cover show higher magnitudes than simulations with 70 % cover, for oscillating vegetation. Oscillating precipitation leads to lower/no adjustments and an oscillation of basin metrics around the initial mean values with generally lower amplitudes compared to simulations with oscillating vegetation cover.

v. Simulations with coupled oscillations of both vegetation cover and precipitation show only small magnitudes of adjustments in topography metrics to new dynamic equilibrium, similar to simulations with a oscillation in only precipitation. However, corresponding erosion rates show a complex pattern of rapid increases and decreases, which results from an interplay of competing effects such as the hindering of erosion by vegetation and the aiding of erosion by precipitation.

Interpreted together, the above findings from this study highlight a highly variable behavior regarding how variations in vegetation cover impact erosion and topographic properties. The complexity of how vegetation cover and precipitation changes influence topography demonstrates the need for future work to consider both of these factors in tandem, rather than singling either parameter out (vegetation cover or precipitation), in order to understand potential transients in topography.

Code and data availability. The source code used in this study is freely available upon request.

Author contributions. Project design and funding were done by TAE and TH. Model setup, programming, simulations, and analysis were conducted by MS and TAE. All authors contributed to the application of the results to the Chilean study areas. Paper preparation was done by MS, TAE, and CW, with editing from all coauthors.

Competing interests. The authors declare that they have no conflict of interest.

Acknowledgements. This study was funded as part of the German science foundation priority research program Earth-Shape: Earth surface shaping by biota (grant EH329-14-1 to Todd A. Ehlers and Thomas Hickler). We thank Erkan Istanbulluoglu, Taylor Schildgen, and two anonymous reviewers for constructive reviews that improved the manuscript. We also thank associate editor Rebecca Hodge for thoughtful handling of the manuscript. We thank the national park service in Chile (CONAF) for providing access to, and guidance through, the study areas during field trips. Daniel Hobley and the Landlab "slack" community are thanked for constructive suggestions during the Landlab program modifications implemented for this study.

Edited by: Rebecca Hodge
Reviewed by: two anonymous referees

References

Acosta, V. T., Schildgen, T. F., Clarke, B. A., Scherler, D., Bookhagen, B., Wittmann, H., von Blanckenburg, F., and Strecker, M. R.: Effect of vegetation cover on millennial-scale landscape denudation rates in East Africa, Lithosphere, 7, 408–420, https://doi.org/10.1130/L402.1, 2015.

Alberts, E. E., Nearing, M. A., Weltz, M. A., Risse, L. M., Pierson, F. B., Zhang, X. C., Laflen, J. M., and Simanton, J. R.: Soil component, chap. 7, in: USDA Water Erosion Prediction Project Hillslope Profile and Watershed Model Documentation, edited by: Flanagan D. C. and Nearing M. A., NSERL Report No. 10. USDA-ARS National Soil Erosion Research Laboratory, West Lafayette, Ind., USA, 47 pp., 1995.

Allen, C. D. and Breshears, D. D.: Drought-induced shift of a forest–woodland ecotone: rapid landscape response to climate variation, P. Natl. Acad. Sci. USA, 95, 14839–14842, 1998.

Allen, C. D., Macalady, A. K., Chenchouni, H., Bachelet, D., McDowell, N., Vennetier, M., Kitzberger, T., Rigling, A., Breshears, D. D., Hogg, E. H. (Ted), Gonzalez, P., Fensham, R., Zhang, Z., Castro, J., Demidova, N., Lim, J.-H., Allard, G., Running, S. W., Semerci, A., and Cobb, N.: A global overview of drought and heat-induced tree mortality reveals emerging climate change risks for forests, Forest Ecol. Manag., 259, 660–684, https://doi.org/10.1016/j.foreco.2009.09.001, 2010.

Amundson, R., Heimsath, A., Owen, J., Yoo, K., and Dietrich, W. E.: Hillslope soils and vegetation, Geomorphology, 234, 122–132, https://doi.org/10.1016/j.geomorph.2014.12.031, 2015.

Andriessen, P. A. and Reutter, K.-J.: K-Ar and fission track mineral age determination of igneous rocks related to multiple magmatic arc systems along the 23° S latitude of Chile and NW Argentina, in: Tectonics of the southern central Andes, edited by: Reutter, K. J., Scheuber, E., and Wigger, P. J., Springer, Berlin, Heidelberg, 141–154, https://doi.org/10.1007/978-3-642-77353-2_10, 1994.

Avdievitch, N. N., Ehlers, T. A., and Glotzbach, C.: Slow long-term exhumation of the West Central Andean Plate Boundary, Chile, Tectonics, https://doi.org/10.1029/2017TC004944, 2018.

Bachelet, D., Neilson, R. P., Hickler, T., Drapek, R. J., Lenihan, J. M., Sykes, M. T., Smith, B., Sitch, S., and Thonicke, K.: Simulating past and future dynamics of natural ecosystems in the United States, Global Biogeochem. Cy., 17, 1045, https://doi.org/10.1029/2001GB001508, 2003.

Bonnet, S. and Crave, A.: Landscape response to climate change: Insights from experimental modeling and implications for tectonic versus climatic uplift of topography, Geology, 31, 123–126, 2003.

Braun, J. and Willett, S. D.: A very efficient O(n), implicit and parallel method to solve the stream power equation governing fluvial incision and landscape evolution, Geomorphology, 180–181, 170–179, https://doi.org/10.1016/j.geomorph.2012.10.008, 2013.

Broecker, W. S. and van Donk, J.: Insolation changes, ice volumes, and the O^{18} record in deep-sea cores, Rev. Geophys., 8, 169–198, https://doi.org/10.1029/RG008i001p00169, 1970.

Broxton, P. D., Zeng, X., Scheftic, W., and Troch, P. A.: A MODIS-Based Global 1-km Maximum Green Vegetation Fraction Dataset, J. Appl. Meteorol. Clim., 53, 1996–2004, https://doi.org/10.1175/JAMC-D-13-0356.1, 2014.

Collins, B. D., Bras, R. L., and Tucker, G. E.: Modeling the effects of vegetation-erosion coupling on landscape evolution, J. Geophys. Res., 109, F03004, https://doi.org/10.1029/2003JF000028, 2004.

Culling, W. E.: Analytical Theory of Erosion, J. Geol., 68, 336–344, 1960.

Curran, J. C. and Hession, W. C.: Vegetative impacts on hydraulics and sediment processes across the fluvial system, J. Hydrol., 505, 364–376, https://doi.org/10.1016/j.jhydrol.2013.10.013, 2013.

DiBiase, R. A. and Whipple, K. X.: The influence of erosion thresholds and runoff variability on the relationships among topography, climate, and erosion rate, J. Geophys. Res., 116, F04036, https://doi.org/10.1029/2011JF002095, 2011.

DiBiase, R. A., Whipple, K. X., Heimsath, A. M., and Ouimet, W. B.: Landscape form and millennial erosion rates in the San Gabriel Mountains, CA, Earth Planet. Sc. Lett., 289, 134–144, https://doi.org/10.1016/j.epsl.2009.10.036, 2010.

Dietrich, W. E., Bellugi, D. G., Sklar, L. S., Stock, J. D., Heimsath, A. M., and Roering, J. J.: Geomorphic Transport Laws for Predicting Landscape form and Dynamics, in: Geophysical Monograph Series, edited by: Wilcock, P. R. and Iverson, R. M., American Geophysical Union, Washington, D.C., USA, 103–132, 2013.

Dosseto, A., Hesse, P. P., Maher, K., Fryirs, K., and Turner, S.: Climatic and vegetation control on sediment dynamics during the last glacial cycle, Geology, 38, 395–398, https://doi.org/10.1130/G30708.1, 2010.

Dunne, T., Whipple, K. X., and Aubry, B. F.: Microtopography of hillslopes and initiation of channels by horton overland flow, in Geophysical Monograph Series, vol. 89, edited by: Costa, J. E., Miller, A. J., Potter, K. W., and Wilcock, P. R., American Geophysical Union, Washington, D.C., USA, 27–44, 1995.

Dunne, T., Malmon, D. V., and Mudd, S. M.: A rain splash transport equation assimilating field and laboratory measurements, J. Geophys. Res., 115, F01001, https://doi.org/10.1029/2009JF001302, 2010.

Feng, X., Wang, Y., Chen, L., Fu, B., and Bai, G.: Modeling soil erosion and its response to land-use change in hilly catchments of the Chinese Loess Plateau, Geomorphology, 118, 239–248, https://doi.org/10.1016/j.geomorph.2010.01.004, 2010.

Fernandez, N. F. and Dietrich, W.: Hillslope evolution by diffusive processes: The timescale for equilibrium adjustments, Water Resour. Res., 33, 1307–1318, 1997.

Foster, G. R.: Modeling the erosion process, in Hydrologic Modeling of Small Watersheds, ASAE Monogr., edited by: Haan, C. T., vol. 5, 295–380, Am. Soc. Agric. Eng., St. Joseph, Mo, USA, 1982.

Gilbert, G. K.: Report on the Geology of the Henry Mountains, Dept. of the Interior, US Govt Printing Office, Washington, D.C., USA, 1877.

Gyssels, G., Poesen, J., Bochet, E., and Li, Y.: Impact of plant roots on the resistance of soils to erosion by water: a review, Prog. Phys. Geog., 29, 189–217, https://doi.org/10.1191/0309133305pp443ra, 2005.

Hobley, D. E. J., Adams, J. M., Nudurupati, S. S., Hutton, E. W. H., Gasparini, N. M., Istanbulluoglu, E., and Tucker, G. E.: Creative computing with Landlab: an open-source toolkit for building, coupling, and exploring two-dimensional numerical models of Earth-surface dynamics, Earth Surf. Dynam., 5, 21–46, https://doi.org/10.5194/esurf-5-21-2017, 2017.

Howard, A. D.: Badland Morphology and Evolution: Interpretation Using a Simulation Model, Earth Surf. Proc. Land., 22, 211–227, https://doi.org/10.1002/(SICI)1096-9837(199703)22:3<211::AID-ESP749>3.0.CO;2-E, 1997.

Howard, A. D. and Kerby, G.: Channel changes in badlands, Geol. Soc. Am. Bull., 94, 739–752, 1983.

Howard, A. D., Dietrich, W. E., and Seidl, M. A.: Modeling fluvial erosion on regional to continental scales, J. Geophys. Res.-Sol. Ea., 99, 13971–13986, https://doi.org/10.1029/94JB00744, 1994.

Hughes, L.: Biological consequences of global warming: is the signal already, Trends Ecol. Evol., 15, 56–61, https://doi.org/10.1016/S0169-5347(99)01764-4, 2000.

Huntley, B., Allen, J. R. M., Collingham, Y. C., Hickler, T., Lister, A. M., Singarayer, J., Stuart, A. J., Sykes, M. T., and Valdes, P. J.: Millennial Climatic Fluctuations Are Key to the Structure of Last Glacial Ecosystems, PLoS ONE, 8, e61963, https://doi.org/10.1371/journal.pone.0061963, 2013.

Istanbulluoglu, E. and Bras, R.: Vegetation-modulated landscape evolution: Effects of vegetation on landscape processes, drainage density, and topography, J. Geophys. Res., 110, F02012, https://doi.org/10.1029/2004JF000249, 2005.

Istanbulluoglu, E., Tarboton, D. G., Pack, R. T., and Luce, C. H.: Modeling of the interactions between forest vegetation, disturbances, and sediment yields, J. Geophys. Res.-Earth, 109, F01009, https://doi.org/10.1029/2003JF000041, 2004.

Jeffery, M. L., Yanites, B. J., Poulsen, C. J., and Ehlers, T. A.: Vegetation-precipitation controls on Central Andean topography, J. Geophys. Res.-Earth, 119, 1354–1375, https://doi.org/10.1002/2013JF002919, 2014.

Juez-Larré, J., Kukowski, N., Dunai, T. J., Hartley, A. J., and Andriessen, P. A. M.: Thermal and exhumation history of the Coastal Cordillera arc of northern Chile revealed by thermochronological dating, Tectonophysics, 495, 48–66, https://doi.org/10.1016/j.tecto.2010.06.018, 2010.

Langbein, W. B. and Schumm, S. A.: Yield of sediment in relation to mean annual precipitation, Eos, Transactions American Geophysical Union, 39, 1076–1084, https://doi.org/10.1029/TR039i006p01076, 1958.

Ledru, M.-P., Labouriau, M. L. S., and Lorscheitter, M. L.: Vegetation dynamics in southern and central Brazil during the last 10,000 yr B.P., Review of Palaeobotany and Palynology, 99, 131–142, 1997.

Maksaev, V. and Zentilli, M.: Fission Track Thermochronology of the Domeyko Cordillera, Northern Chile: Implications for Andean Tectonics and Porphyry Copper Metallogenesis, Explor. Min. Geol., 8, 65–89, 1999.

Marshall, J. A., Roering, J. J., Bartlein, P. J., Gavin, D. G., Granger, D. E., Rempel, A. W., Praskievicz, S. J., and Hales, T. C.: Frost for the trees: Did climate increase erosion in unglaciated landscapes during the late Pleistocene?, Science Advances, 1, e1500715, https://doi.org/10.1126/sciadv.1500715, 2015.

Marston, R. A.: Geomorphology and vegetation on hillslopes: Interactions, dependencies, and feedback loops, Geomorphology, 116, 206–217, https://doi.org/10.1016/j.geomorph.2009.09.028, 2010.

McInnes, B. I. A., Farley, K. A., Sillitoe, R., and Kohn, B. P.: Application of Apatite (U-th)/He Thermochronometry to the determination of the sense and amount of vertical fault displacement at the Chuquicamata Porphyry Copper Deposit, Chile, Econ. Geol., 94, 937–948, 1999.

McPhillips, D., Bierman, P. R., Crocker, T., and Rood, D. H.: Landscape response to Pleistocene-Holocene precipitation change in the Western Cordillera, Peru: 10Be concentrations in modern sediments and terrace fills, J. Geophys. Res.-Earth, 118, 2488–2499, https://doi.org/10.1002/2013JF002837, 2013.

Muhs, D. R., Ager, T. A., and Beget, J. E.: Vegetation and paleoclimate of the last interglacial period, central Alaska, Quaternary Sci. Rev., 20, 41–61, 2001.

Muller, R. A. and MacDonald, G. J.: Spectrum of 100-kyr glacial cycle: Orbital inclination, not eccentricity, P. Natl. Acad. Sci. USA, 94, 8329–8334, https://doi.org/10.1073/pnas.94.16.8329, 1997.

Oeser, R., Stroncik, N., Moskwa, L.-M., Bernhard, N., Schaller, M., Canessa, R., Brink, L. van den, Köster, M., Brucker, E., Stock, S., Fuentes-Espoz, J. P., Godoy, R., Matus, F., Oses Pedraza, R., Osses McIntyre, P., Paulino, L., Seguel, O., Bader, M. Y., Boy, J., Dippold, M., Ehlers, T. A., Kühn, P., Kuzyakov, Y., Leinweber, P., Scholten, T., Spielvogel, S., Spohn, M., Übernickel, K., Tielbörger, K., Wagner, D., and von Blanckenburg, F.: Chemistry and microbiology of the critical zone along a steep climate and vegetation gradient in the Chilean Coastal Cordillera, CATENA, 170, 183–203, https://doi.org/10.1016/j.catena.2018.06.002, 2018.

Olen, S. M., Bookhagen, B., and Strecker, M. R.: Role of climate and vegetation density in modulating denudation rates in the Himalaya, Earth Planet. Sc. Lett., 445, 57–67, https://doi.org/10.1016/j.epsl.2016.03.047, 2016.

Owen, J. J., Amundson, R., Dietrich, W. E., Nishiizumi, K., Sutter, B., and Chong, G.: The sensitivity of hillslope bedrock erosion to precipitation, Earth Surf. Proc. Land., 36, 117–135, https://doi.org/10.1002/esp.2083, 2010.

Perron, J. T., Richardson, P. W., Ferrier, K. L., and Lapôtre, M.: The root of branching river networks, Nature, 492, 100–103, https://doi.org/10.1038/nature11672, 2012.

Prentice, I. C., Harrison, S. P., and Bartlein, P. J.: Global vegetation and terrestrial carbon cycle changes after the last ice age, New Phytol., 189, 988–998, https://doi.org/10.1111/j.1469-8137.2010.03620.x, 2011.

Roering, J. J., Almond, P., Tonkin, P., and McKean, J.: Soil transport driven by biological processes over millennial time scales, Geology, 30, 1115–1118, 2002.

Sangireddy, H., Carothers, R. A., Stark, C. P., and Passalacqua, P.: Controls of climate, topography, vegetation, and lithology on drainage density extracted from high resolution topography data, J. Hydrol., 537, 271–282, https://doi.org/10.1016/j.jhydrol.2016.02.051, 2016.

Schaller, M. and Ehlers, T. A.: Limits to quantifying climate driven changes in denudation rates with cosmogenic radionuclides, Earth Planet. Sc. Lett., 248, 153–167, https://doi.org/10.1016/j.epsl.2006.05.027, 2006.

Schaller, M., von Blanckenburg, F., Veldkamp, A., Tebbens, L. A., Hovius, N., and Kubik, P. W.: A 30 000 yr record of erosion rates from cosmogenic ^{10}Be in Middle European river terraces, Earth Planet. Sc. Lett., 204, 307–320, https://doi.org/10.1016/S0012-821X(02)00951-2, 2002.

Schaller, M., Ehlers, T. A., Stor, T., Torrent, J., Lobato, L., Christl, M., and Vockenhuber, C.: Spatial and temporal variations in denudation rates derived from cosmogenic nuclides in four European fluvial terrace sequences, Geomorphology, 274, 180–192, https://doi.org/10.1016/j.geomorph.2016.08.018, 2016.

Schaller, M., Ehlers, T. A., Lang, K. A. H., Schmid, M., and Fuentes-Espoz, J. P.: Addressing the contribution of climate and vegetation cover on hillslope denudation, Chilean Coastal Cordillera (26°–38° S), Earth Planet. Sc. Lett., 489, 111–122, https://doi.org/10.1016/j.epsl.2018.02.026, 2018.

Smith, B., Wårlind, D., Arneth, A., Hickler, T., Leadley, P., Siltberg, J., and Zaehle, S.: Implications of incorporating N cycling and N limitations on primary production in an individual-based dynamic vegetation model, Biogeosciences, 11, 2027–2054, https://doi.org/10.5194/bg-11-2027-2014, 2014.

Stephan, U. and Gutknecht, D.: Hydraulic resistance of submerged flexible vegetation, J. Hydrol., 269, 27–43, 2002.

Tucker, G., Lancaster, S., Gasparini, N. and Bras, R.: The channel-hillslope integrated landscape development model (CHILD), in: Landscape erosion and evolution modeling, Springer, Boston, MA, USA, 349–388, 2001.

Vergani, C., Giadrossich, F., Buckley, P., Conedera, M., Pividori, M., Salbitano, F., Rauch, H., Lovreglio, R., and Schwarz, M.: Root reinforcement dynamics of European coppice woodlands and their effect on shallow landslides: A review, Earth-Sci. Rev., 167, 88–102, https://doi.org/10.1016/j.earscirev.2017.02.002, 2017.

Walling, D. and Webb, B.: Patterns of sediment yield, in: Background to Palaehydrology, edited by: Gregory, K. J., Wiley, Chichester, UK, 69–100, 1983.

Walther, G.-R., Post, E., Convey, P., Menzel, A., Parmesan, C., Beebee, T. J., Fromentin, J.-M., Hoegh-Guldberg, O., and Bairlein, F.: Ecological responses to recent climate change, Nature, 416, 389–395, 2002.

Werner, C., Schmid, M., Ehlers, T. A., Fuentes-Espoz, J. P., Steinkamp, J., Forrest, M., Liakka, J., Maldonado, A., and Hickler, T.: Effect of changing vegetation and precipitation on denudation – Part 1: Predicted vegetation composition and cover over the last 21 thousand years along the Coastal Cordillera of Chile, Earth Surf. Dynam. Discuss., 6, 829–858, https://doi.org/10.5194/esurf-6-829-2018, 2018.

Whipple, K. X. and Tucker, G. E.: Dynamics of the stream-power river incision model: Implications for height limits of mountain ranges, landscape response timescales, and research needs, J. Geophys. Res., 104, 17661–17674, https://doi.org/10.1029/1999JB900120, 1999.

Willgoose, G., Bras, R. L., and Rodriguez-Iturbe, I.: Results from a new model of river basin evolution, Earth Surf. Proc. Land., 16, 237–254, 1991.

Yetemen, O., Istanbulluoglu, E., Flores-Cervantes, J. H., Vivoni, E. R., and Bras, R. L.: Ecohydrologic role of solar radiation on landscape evolution, Water Resour. Res., 51, 1127–1157, https://doi.org/10.1002/2014WR016169, 2015.

Zhou, Z. C., Shangguan, Z. P., and Zhao, D.: Modeling vegetation coverage and soil erosion in the Loess Plateau Area of China, Ecol. Model., 198, 263–268, https://doi.org/10.1016/j.ecolmodel.2006.04.019, 2006.

3.2 LGM - PD climatic differences control catchment erosion rates

3.2.1 Declaration of contributions to joint publication

Table 4: Author contribution (in %) of manuscript *LGM to PD climatic and vegetational modulation of catchment-wide erosion rates in the Chilean Coastal Cordillera.*

Author	Author position	Scientific ideas [%]	Data generation [%]	Analysis & Interpretation [%]	Paper writing [%]
MS	1	40	90	70	60
TE	2	40	0	20	30
CW	3	10	10	10	10
TH	4	10	0	0	0

This subsection of the dissertation is currently in preparation at late manuscript stage. Probable title of the manuscript will be "LGM to PD climatic and vegetational modulation of catchment-wide erosion rates in the Chilean Coastal Cordillera". Most recent version of the manuscript is provided in section 3.2.1.

Four authors contributed to the manuscript as follows: Manuel Schmid (MS), Christian Werner (CW), Todd Ehlers (TE) and Thomas Hickler (TH). Todd Ehlers and Thomas Hickler developed the initial idea of coupling a dynamic vegetation model to a landscape evolution model. Manuel Schmid, with help of Todd Ehlers and Christian Werner, developed the coupling algorithm for mapping and handling of LPJ-GUESS output to a Landlabnative model object. Manuel Schmid and Christian Werner developed the input/output handling code structure. Manuscript preparation was done by Manuel Schmid with help from Todd Ehlers and Christian Werner. Detailed contributions are provided in table 4

3.2.2 Manuscript Draft : LGM to PD climatic and vegetational modulation of catchment-wide erosion rates in the Chilean Coastal Cordillera

LGM to PD climatic and vegetational modulation of catchment-wide erosion rates in the Chilean Coastal Cordillera.

Manuel Schmid[1], Todd Ehlers[1],
Christian Werner[2], Thomas Hickler[3,4]

(1): University of Tuebingen
(2): Karlsruhe Institute of Technology
(3): Goethe-University Frankfurt
(4): Senckenberg Research Center

Abstract

We utilized a novel coupled numerical modelling approach between a dynamic vegetation model (LPJ-GUESS) and landscape evolution model (Landlab), both driven by paleoclimate climates since the Last Glacial Maximum (LGM) to Present Day (PD) . We present results for mean catchment erosion rates, for four study areas in the Chilean Coastal Cordilleras as a function of changing precipitation and grass, shrub, and tree cover. Three sets of simulations are presented to evaluate the sensitivity of erosion rates to changes in precipitation and vegetation cover. These simulations include: (1) LPJ-GUESS derived transient LGM-PD variations in catchment vegetation cover with constant LGM-level values of precipitation. 2. Constant LPJ-GUESS derived LGM-levels of vegetation cover with transient LGM-PD variations in precipitation. 3. Fully coupled simulations with fully transient variations in vegetation cover and precipitation for the LGM-PD time series. We present mean catchment erosion rates per timestep for all simulations and erosion rates for specific topographic conditions for fully coupled simulation. Results indicate that precipitation, and vegetation cover and composition, changes from LGM to PD lead to a high variability in erosion rates primarily for the very arid and very humid study areas, but with no long-term significant adjustment of mean erosion rates from steady-state rock uplift rates. Areas that are situated in semi-arid to mediterranean climatic conditions show more minor short-term variability but a more pronounced decrease in mean erosion rates compared to rock uplift rates. Changes of erosion rates due to vegetation change are due to shifts in the intra area vegetation composition and the controlling vegetation type is identified for each study area. This study demonstrates that there exists a difference in sensitivity of individual study areas to changes in precipitation and vegetation and that changes in vegetation composition (e.g. from grasses to shrubs or trees) can cause significant adjustments of erosion rates without large, associated changes in total vegetation cover.

1 Introduction

Climatic change from the last glacial maximum (LGM) at 21 ka before present (BP) to present day conditions (PD) introduces a high transient factor in catchment wide erosion rate, due to changes in precipitation, temperature, radiation and atmospheric CO_2 concentrations [Kirchner et al., 2001, Schaller et al., 2002, Mutz et al., 2018]

These climatic changes influence topographic evolution either directly, by increasing river runoff and thus capacity for erosion and transportation of sediment [Hooke, 1979, Mohamadi and Kavian, 2015] or indirectly through various feedback loops, e.g an increase in mean annual precipitation/temperature increases the mean vegetation cover within a drainage area and therefore decreases the erosional capacity of surface processes [Kosmas et al., 1997].

This highly non-linear system of competing processes has been shown to have complex effects on topographic evolution and the transient reactions to climatic changes [Collins and Bras, 2004, Schmid et al., 2018]. The effect of changes in precipitation and vegetation cover on landscape evolution and the sensitivity of catchments to changes in these parameters is a field of active research since the inherent coupled nature of these systems makes it troublesome to attribute transient effects to specific changes in either climatic conditions or biotic conditions.

It is a challenge in modern geomorphology to decompose the signal that these ecologic and climatic drivers of topographic change exert on landscapes and the evolution of catchment-wide erosion rates. Previous work on this subject laid the foundation for a numerical quantification of the effect of vegetation cover on erosion rates as well as a better understanding of the changes in plant functional type composition within catchments, based on climatic changes.

For example Molina et al. [2007] measured a distinct hillslope runoff response which is dependent on the vegetation cover in the landscape, where lower values of vegetation cover lead to a rapid, hortonian-like runoff generation while higher vegetation covers lead to lower and more steady runoff. Bautista et al. [2007] and Mohammad and Adam [2010], found that the surface runoff generated on a hillslope is a function not only of vegetation cover, but also of plant functional type distribution, because of a shift in unvegetated areas between plant patches which modulate the effectiveness of rain interception and root infiltration. Dunjó et al. [2004] showed that there is not only a difference in runoff generation for different plant types but also for associated sediment yield. Vanacker et al. [2007] analyzed catchment average denudation rates in mountainous environments and found that vegetation cover exerts a first-order control on the erosion-rates in tropical mountain areas and that areas with a high natural vegetation cover tend to show mean erosion rates that are near to the natural benchmark. Yetemen et al. [2015a] showed in numerical model experiments, that the changes in plant density between north and south

oriented slopes at the catchment level can lead to strong hillslope asymmetry driven by differences in erosional efficiency for hillslopes with heterogenous values of vegetation cover.

Missing from previous studies in this field is the feedback between climatic changes, associated changes in plant distribution and effects on erosion rates on different topographic positions within a catchment. For example while multiple model studies [Collins and Bras, 2004, Yetemen et al., 2015a, Schmid et al., 2018] incorporate a simple cumulative total vegetation cover metric in respect to the modulation of surface processes, they lack the incorporation of the effects of shifts in plant functional type composition within a grid cell or use simple ecohydraulic growth equations [Collins and Bras, 2010] which underrepresented the complexity of the system. Also missing from previous modelling studies is the use of realistic climatic input over larger timescales. Collins and Bras [2010] and Yetemen et al. [2015b] used a Poisson rectangular pulse rainfall model, developed by Eagleson [1978] to simulate rainfall dynamics over a time series. While this a very valuable approach to analyze the effect of coupled rainfall/vegetation dynamics on landscapes for storm/inter-storm periods, its missing the information of realistic climatic and biotic dynamics over a climate gradient. This study expands previous work by a showing the results of a new fully coupled model framework which combines the process based dynamic vegetation model "LPJ-GUESS" [Smith et al., 2001] and the landscape evolution model "Landlab" [Hobley et al., 2017].

We incorporate a full-cycle-feedback between erosional processes and associated topographic metrics (elevation, slope, aspect, soil depth) and inter-area plant functional type distribution and percentage cover. Feedback between plant cover and surface processes where calculated from LGM to PD, driven by a fully-transient climatic time series (TraCE-21ka) and calculated on a 100yr timestep for 4 different study areas in different climatic conditions in the Chilean Coastal Cordillera (Fig. 1).

We show that there is a shift in importance of different phenological plant types which are able to dampen the increase in erosion rates by increases in MAP going from North to South and that only in the southermost area of Nahuelbuta, the erosion rates are mainly controlled by vegetation changes, while other areas still show precipitation dominated transient erosion rates.

Figure 1: Map of central Chile. Black dots represent location of Earthshape Study Areas.

2 Methods

The four Earthshape study areas are located in the Chilean Coastal Cordillera (26 to 38°S) and show a distinct N-S trend of increasing mean annual precipitation (MAP) and decreasing mean annual temperature (MAT). We assume that the areas do not show significant differences in tectonic history and anthropogenic overprint of topographies, so that the topographic signal within and between the areas are a function of only the differences in climatic setting and resulting changes in biota [Maksaev and Zentilli, 2000, Avdievitch et al., 2018, Schmid et al., 2018]. The study areas consist of (from north to south): Pan de Azucar, Santa Gracia Natural Reserve, La Campana National Park and Nahuelbuta National Park. The main input for the coupled model regarding these study areas is the TraCE-21ka climatic dataseries from the last glacial maximum to present, the weathering rates and the topographic base elevation to constrain elevation dependent temperature distributions (see section 2.1).

2.1 General Model Input

The main input drivers for the coupled model framework between Landlab and LPJ-GUESS are the MAP, MAT and incoming solar radiation (Fig. 2). These were downscaled and bias-corrected from TraCE-21ka data [Liu et al., 2009] for half-degree grid cells containing the individual study areas using a monthly climatology from the ERA-Interim reanalysis dataset [Dee et al., 2011]. While the MAT and radiation data is only used within LPJ-GUESS to calculate plant functional type (PFT) distribution within the model domain, MAP-values are also used in LandLab to calculate river discharge. Soil production rates for the focus areas were constrained by using Be 10 - derived denudation rates [Schaller et al., 2018] in soil pits within the areas. These point measurements of denudation rates where transformed to maximum soil production rates for each focus area using a global soil production rate compilation [Stockmann et al., 2014]. Atmospheric CO2 concentration was derived from Monnin [2001] and Meinshausen et al. [2017] and is assumed to be equal for all four study areas.

2.2 Despriction of LPJ-GUESS Vegetation Model

LPJ-GUESS (Lund-Potsdam-Jena General Ecosystem Simulator) [Smith et al., 2001,0] is a state-of-the art dynamic vegetation model which has been tested in numerous studies to achieve realistic results for the modelling of vegetation structure, vegetation type distribution and nutrient cycling (for a comprehensive list of papers see http://iis4.nateko.lu.se/lpj-guess/ last access: 03 June, 2019). LPJ-GUESS simulates the vegetation type composition of a landscape as a function of the competition of growing plant functional types (PFT's, see Bonan et al. [2002]) for space, nutrients, light and water. Stochastic effects

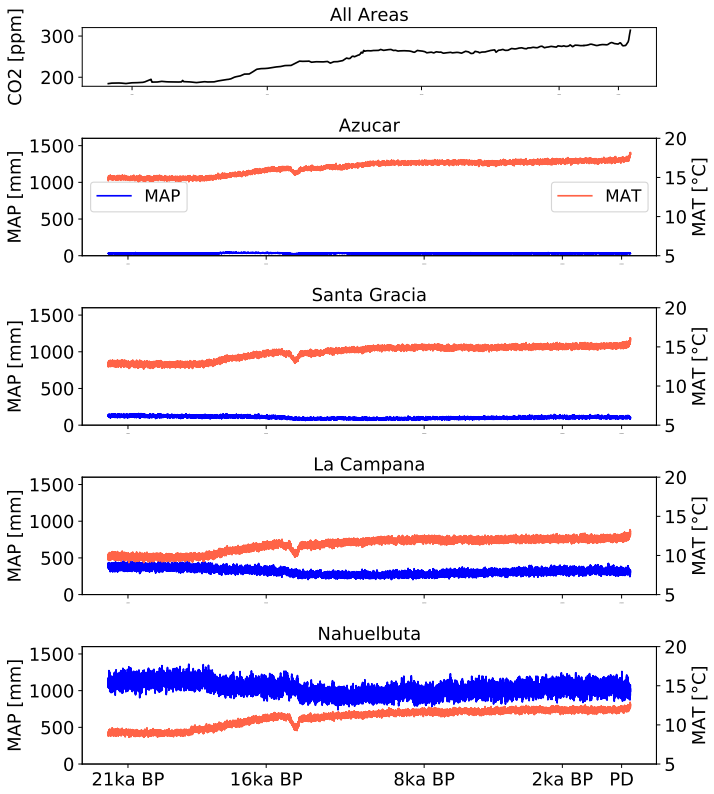

Figure 2: Climatic input drivers for coupled simulations between LPJ-GUESS and Landlab. Red and blue lines represent MAT/MAP values over 100yr running mean for 21ka TraCE dataset. CO2 data (top panel) is assumed to not change between focus areas.

like tree-throw, wildfire and patch disturbance are incorporated by patch replication and allow the simulation of vegetation successions and disturbances [Hickler et al., 2004]. The model has recently been extended to account for sub-pixel resolution effects of topographic variations within the larger scale simulation cells and adapted to the major vegetation compositions of Chile [Werner et al., 2018]. In this paper we use the model and simulation setup as described by Werner et al. [2018] and refer the reader to this paper for a detailed description of the configuration. Within the coupled model framework, the main output parameter of LPJ-GUESS is the leaf area index (LAI) on PFT level which is categorized in three main phenological classes, representive of geomorphic valuable plant types ("Trees", "Shrubs", "Grass"). For further information about the coupling algorithm, we refer the reader to section 2.4.

2.3 Vegetation Cover implementation in Geomorphic Laws

Topographic change within the model domain is constrained by three governing principles: 1. erosion and transport of material due to overland waterflow, 2. transport of material

due to hillslope erosion, 3. weathering of material from bedrock to sediment. Elevation changes at each node in the model domain over time are therefore a function of:

$$\frac{\delta z(x,y)}{\delta t} = U - \frac{\delta z}{\delta t_{hillslope}} - \frac{\delta z}{\delta t_{fluvial}} \tag{1}$$

where z is the topographic elevation per node; x,y are the lateral coordinates within the model domain; t is the model runtime; U is the tectonic uplift rate; $\frac{\delta z}{\delta t_{hillslope}}$ is the change in elevation due to transport of soils by diffusive processes and $\frac{\delta z}{\delta t_{fluvial}}$ is the change in elevation due to fluvial processes [Tucker et al., 2001]

Vegetation influence on diffusive hillslope transport

Building up on Schmid et al. [2018] we use the approach laid out by Alberts et al. [1995], Dunne et al. [1995], Istanbulluoglu and Bras [2005], Dunne et al. [2010] and incorporate it in a depth-dependent soil diffusion case, following Johnstone and Hilley [2015] as follows:

$$\frac{\delta z}{\delta t_{hillslope}} = -\nabla q_{sq} \tag{2}$$

The flux of sediment (q_{sd}) is characterized as a linear function of the hillslope diffusivity (K_d), the surface slope (S) at each node, the sediment depth at each node (H) and the characteristic sediment transport depth (H^*):

$$q_{sd} = K_d S(1 - e^{\frac{H}{H^*}}) \tag{3}$$

The hillslope diffusivity K_d is a function of cumulative vegetation cover in each cell (V), a baseline diffusivity K_b and an exponential coefficient α

Vegetation influence on overland flow and fluvial erosion

For fluvial erosion by overland flow within our model domain we implemented the SPACE model [Shobe et al., 2017] where the sediment entrainment rate E s is formulated as

$$E_s = (K_s Q S^n - \omega_{cs})(1 - e^{-H/H^*}) \tag{4}$$

where K_s is the sediment erodibility parameter, Q is water discharge per unit channel width, S is the channel slope, ω_{cs} is the threshold stream power for sediment entrainment, H is the sediment thickness at each cell and H^* is the bedrock roughness length scale.

The bedrock erosion rate E_r is formulated as

$$E_r = (K_s Q S^n - \omega_{cs}) e^{-H/H^*}) \tag{5}$$

Table 1: Parameters used for coupled simulations.

Parameter	Unit	Value
U	mm/yr	0.1
K_b	$s/m^{1/3}$	0.01
α	-	0.3
n_s	$s/m^{1/3}$	0.01
n_S	$s/m^{1/3}$	0.6
n_G	$s/m^{1/3}$	0.3
n_T	$s/m^{1/3}$	0.5
w	-	1
m/n	-	0.6/1
K_es	$m/yr(kgm^{-1}s^{-2})^{-1}$	1e-7
K_er	$m/yr(kgm^{-1}s^{-2})^{-1}$	1e-8

where K_r is the bedrock erodibility parameter for bedrock and ω_{cr} is the threshold stream power for bedrock detachment.

By implementing the approach of Istanbulluoglu et al. [2004], Istanbulluoglu and Bras [2005], Schmid et al. [2018] we modify the values K_s and K_r accordingly:

$$K_s = K_{es}\rho_w g(n_s + n_T + n_S + n_G)^{6/10}(n_s/(n_s + n_T + n_S + n_G))^{3/2} \tag{6}$$

$$K_r = K_{er}\rho_w g(n_s + n_T + n_S + n_G)^{6/10}(n_s/(n_s + n_T + n_S + n_G))^{3/2} \tag{7}$$

where K_{es} and K_{er} are the baseline erodibility factors for sediment and bedrock, ρ_w is the density of water, g is the acceleration of gravity, n_s , n_T , n_S , n_G are the manning's roughness coefficients for soil, trees, shrubs and grass (see Table 1).

Sediment production rates within areas

The maximum sediment production rates through weathering of bedrock within the areas were implemented as a exponential weathering rate following Ahnert [1976] and [Amundson et al., 2015]

$$PR = PR_{max}e^{H/Hs^*} \tag{8}$$

where PR is the sediment production rate at each node, PR_{max} is the maximum sediment production rate for zero soil thickness, H is the sediment depth at each node and Hs^* is the characteristic weathering depth.

The maximum sediment production rate per area was constrained by using denudation rates (Pr) from Schaller et al. [2018] which were measured in soil-pits within the study

areas at the bedrock/saprolith interface (hd) and a global compilation of characteristic rate constants (b) from Stockmann et al. [2014]:

$$PR_{max} = Pr/e^{hd/b} \tag{9}$$

2.4 Model coupling between LPJ-GUESS and Landlab

To numerically incorporate spatial intra-area differences in vegetation cover on surface processes we implemented the concept of landforms in Landlab. We define 3 primary factors of topographic metrics which are controlling the vegetation cover within a node: 1. Topographic elevation, 2. Slope position, 3. Aspect. We classify topographic elevation in 100m steps and assert a continuous, positive integer value to each nodes, based on the node elevation. For the slope position, we follow the approach of Weiss [2001] and Werner et al. [2018] by classifying the node into four different categories ('Hilltop', 'Mid Slope', 'Flat' and 'Valley'), based on their elevation and slope angle in respect to surrounding nodes within a 300m classification window (Fig. 3).

The aspect for each node is classified with the underlying assumption that the top-boundary for our model-domains represents north. This classification scheme results in a landform ID for each node within our model domain, consisting of three different integers which represent one distinct biome which can be represented in a separate LPJ-GUESS simulation. The main input for the respective LPJ-GUESS model runs consists of the landform-mean topographic slope, elevation, aspect and soil depth which are parsed to the LPJ-GUESS model during runtime for each timestep.

The resulting LPJ-GUESS output, consisting of PFT composition per landform, is then classified into three different phenological types ('Trees', 'Shrubs', 'Grass) and mapped to each node within the Landlab grid with the respective node landform ID. Based on the vegetation type covers in each cell, Landlab calculates topographic changes per grid-cell by hillslope diffusion and erosion through overland flow modulated by percentage vegetation cover (see chapter 2.3). The resulting landscape is again classified in the respective landforms and this concludes one timestep of the fully-coupled transient model (see Fig. 4).

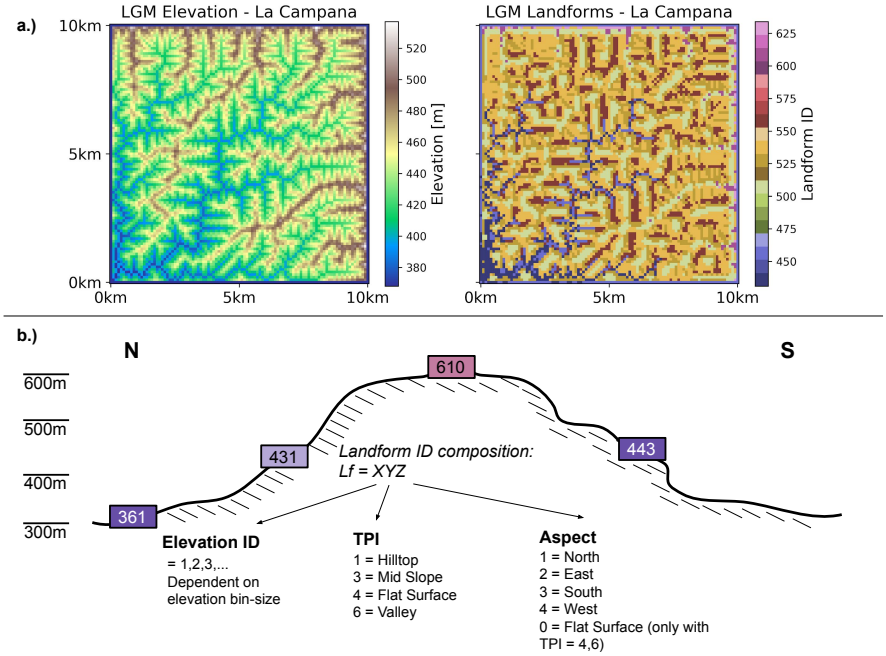

Figure 3: Example of landform classifier landlab component. Top panel shows a standart Landlab DEM grid (left side) and the resulting landform ID grid (right side). Bottom Panel depicts classification scheme and four different examplatory classification results, based on elevation, slope ID and aspect.

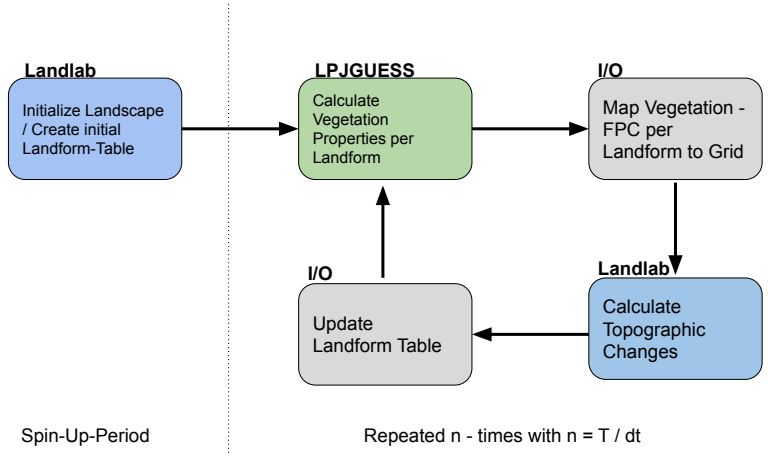

Figure 4: Description of coupling algorithm between LPJ-GUESS and Landlab. Spin-up Period is only executed once at the beginning of each run, main coupling loop is then repeated until total model runtime is reached. Number of iterations therefore depends on total runtime T and timestep dt.

3 Results

We present the results of 3 different sets of simulations:

1. LGM to PD simulations for all 4 study areas with a constant value of MAP which was derived from LGM conditions and a fully-transient time series of vegetation cover changes derived from TraCE-21ka climate data within LPJ-GUESS as input for Landlab.

2. LGM to PD simulations for all 4 study areas with constant values for individual plant types derived from LGM conditions and TraCE-21ka precipitation data as input for Landlab.

3. Fully coupled LGM to PD simulations with transient feedback between LPJ-GUESS and Landlab, with complete TraCE-21ka dataset as climate driver and resulting shifts in plant distribution within Landlab grid.

For each group of simulations we show MAP values from LGM to PD, resulting mean plant cover densities within model domain and mean catchment-wide erosion rates. We show additional data and analysis for the fully coupled simulation to separate the effects of precipitation/temperature and plant types on erosion rates.

3.1 Constant LGM Precipitation in Landlab, Variable TraCE-21ka Precipitation and resulting vegetation cover in LPJ-GUESS

Mean catchment-wide erosion rates were calculated Earthshape study areas from LGM to PD conditions with a timestep of 100 yrs. For this set of simulations we used the TraCE-21ka climate data as input for LPJ-GUESS to derive a fully transient evolution of vegetation cover for each timestep which were used as input for Landlab. Precipitation was kept constant on LGM level over timespan of simulation. This was done to single out the transient effect of LGM to PD changes in vegetation cover on erosion rates. Fig. 5 shows the MAP and vegetation cover data and the according mean catchment erosion rates and the mean value for whole LGM-PD time series.

For northern area Pan de Azucar it shows a constant MAP value of 38mm, a mean grass cover of 3.9%, with minimum of 2.8% at 19.4ka BP and maximum 4.9% at 3.1ka BP, a mean shrub cover 5.4% with a minimum of 3.4% at 14.4 ka BP and a maximum of 7.9% 3.5 ka BP and a mean tree cover of 0.2% with maximum 0.5% at 15.7 ka BP and minimum of 0.1% at 17.6 ka BP (Fig. 5(A)). Erosion rates range from a minimum of 0.08 mm/yr at 17 ka BP to a maximum of 0.12 mm/yr at 14.3 ka BP with a over-time average of 0.09 mm/yr (Fig. 5(B)).

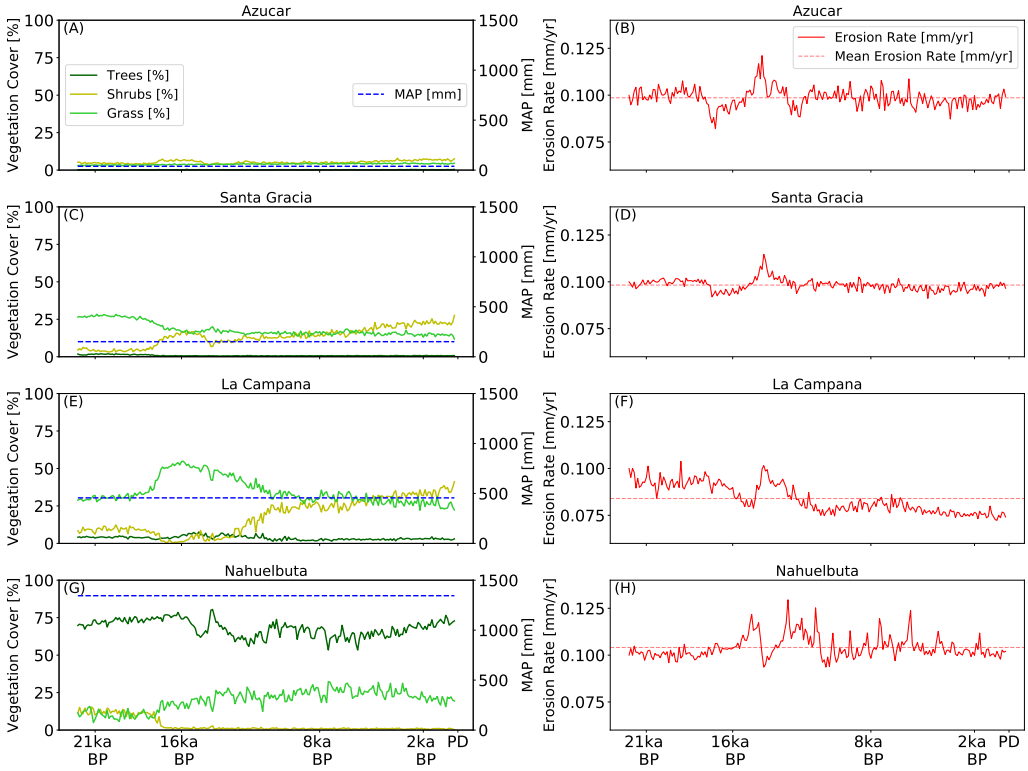

Figure 5: Simulation results for model experiments with constant MAP values over timeseries and transient LPJ-GUESS derived timeseries of vegetation change (left panel). Right side shows resulting mean catchment-wide erosion rates and mean value over timeseries.

For Santa Gracia the data shows a MAP values of 150 mm, mean grass cover of 17% with minimum/maximum values of 11% at PD conditions and 28% 20.9 ka BP, mean shrub cover of 14% with minimum/maximum values of 3% at 19.8 ka BP and 27% at 0.2 ka BP and mean tree cover of 0.8% with minimum/maximum values of 0.3% at PD conditions and 2.0% at 19.8ka BP (Fig. 5(C)). Erosion rates for this study area show a time average of 0.09 mm/yr with minimum values of 0.09 mm/yr at 4.7 ka BP and maximum values of 0.11 mm/yr at 14.2 ka BP (Fig. 5(D)).

La Campana study area shows MAP values of 455 mm, mean grass cover of 34% with minimum/maximum values of 22% at 2.2 ka BP and 54% at 15.9 ka BP, mean shrub cover of 18% with minimum/maximum values of 0.3% at 16.5 ka BP and 42% at 0.1 ka BP, mean tree cover of 3.5% with minimum and maximum values of 1.3% at 10.7 ka BP and 7.6% at 15.0 ka BP (Fig. 5(E)). Mean catchment erosion rates show mean values of 0.083 mm/yr, minimum values of 0.069 mm/yr at PD conditions and maximum values of 0.103 mm/yr at at 19 ka BP (Fig. 5(F)).

Nahuelbuta study area shows MAP values of 1344 mm, mean grass cover of 20% with minimum/maximum values of 4.9% at 21.1 ka BP and 32.3% at 7.5 ka BP, mean shrub

cover of 3.2% with minimum/maximum values of 0.2% at 9.7 ka BP and 15.3% at 21.2 ka BP, mean tree cover of 68.4% with minimum and maximum values of 53.4% at 5.8 ka BP and 80.5% at 14.2 ka BP (Fig. 5(G)). Mean catchment erosion rates show mean values of 0.103 mm/yr with minimum values of 0.094 mm/yr at 10.6 ka BP and maximum values of 0.129 mm/yr (Fig. 5(H)).

This shows a modulation of mean catchment erosion rates through LGM to PD changes in transient vegetation cover leads to a shift of mean catchment erosion rates from steady-state conditions mainly for La Campana focus area with a drop of mean erosion rates by 17%, whereas for Azucar and Santa Gracia the negative shift of meanerosion rates is only 2%. Nahuelbuta witnesses a vegetation-dynamics induced increase in mean catchment erosion rates by 3%.

3.2 Constant LGM Vegetation and complete TraCE21ka MAP values in Landlab

Fig. 6 shows results for LGM to PD simulations were Landlab input consists of constant LGM level vegetation covers and a fully transient MAP timeseries for LGM to PD conditions. These simulations were run as a means to separate the effect of transient LGM to PD MAP data on catchment wide erosion rates. For Pan de Azucar, the data shows mean values of tree, shrub, grass cover (Fig. 6(A)) of 0.3%, 4.6% and 2.9%. MAP time series shows a mean of 38mm with minimum values of 29mm at 14.3ka BP and maximum values of 48mm 17.1ka BP. Resulting erosion rates (Fig. 6(B)) fluctuate between a minimum of 0.067 mm/yr at 14 ka BP and maximum of 0.136 mm/yr at 17.0 ka BP with a mean of 0.101 mm/y.

Santa Gracia study area shows values of vegetation cover (Fig. 6(C)) of trees, shrubs and grass of 2.2%, 3.6% and 26.5% with MAP values of mean, min. and max. of 124mm, 98mm at 10.5 ka BP and 156mm at 20.9ka BP. The erosion rates (Fig. 6(D)) show a new mean over LGM to PD time series of 0.085 mm/yr with a minimum value of 0.662 mm/yr at 13.7ka BP and a maximum value of 0.104 mm/yr at 20.8ka BP. From there on, mean catchment erosion rates increase again to a value of 0.082 mm/yr at PD timeslice.

The La Campana simulation shows vegetation cover values of trees, shrubs and grass of 5.3%, 7.4% and 25.7% LGM vegetation cover (Fig. 6(E)). MAP values start at 443mm for LGM conditions, decline to PD conditions with time-series means, min. and max. values of 373mm, 302mm at 10.7ka BP and 469mm at 20.9 ka BP. According erosion rates (Fig. 6(F)) show mean values for LGM - PD time series of 0.092 mm/yr with maximum of 0.102 mm/yr at 20.8 ka BP and maximum of 0.078 mm/yr at 13.9 ka BP.

Nahuelbuta model runs show vegetation covers (Fig. 6(G)) of 77.9% for tree PFTs, 9.59% for shrub PFTs and 5.0% for grass PFTs. MAP shows LGM value of 1302mm and PD value of 1157 mm. Mean, min. und max. values are 1227 mm, 1083 mm at

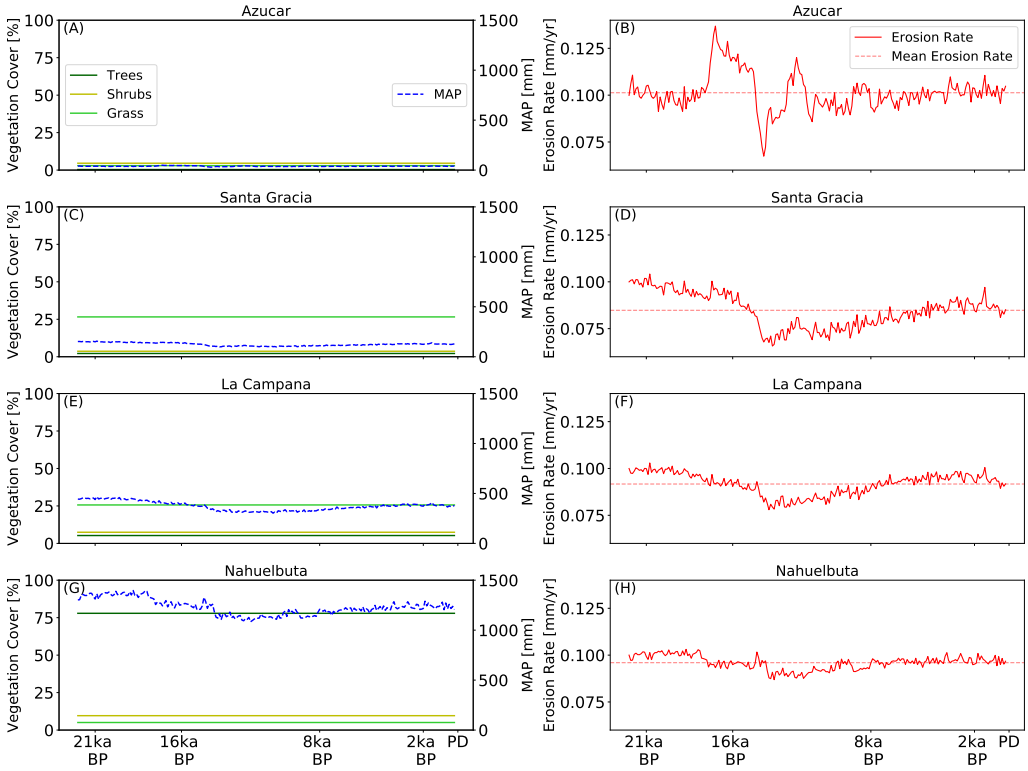

Figure 6: Simulation results for model experiments with constant LGM values for vegetation cover and fully transient TraCE derived mean annual precipitation values (left panel). Right side shows resulting timeseries of mean catchment erosion rates and mean value over LGM to PD conditions.

12 ka PB and 1397 mm at 18.8 ka BP. Erosion rates for these simulations (Fig. 6(H)) show LGM values of 0.100 mm/yr and PD values of 0.091 mm/yr with maximum value of 0.103 mm/yr at 18.7 ka BP and minimum value of 0.086 mm/yr at 13.6 ka BP and a overall LGM to PD mean value of 0.095 mm/yr.

3.3 Fully coupled model with TraCE-21ka precipitation values and TraCE-21ka derived LPJ-GUESS vegetation cover values

Fully coupled simulations for four focus areas with continuous updates between topographic metrics, determined in the Landlab landscape evolution model and associated landform vegetation cover, determined in LPJ-GUESS dynamic vegetation model were done to determine how coupled dynamics between climate change and changes in the vegetation cover within catchments control the catchment-wide erosion rates. Fig. 7 shows the MAP time series from LGM to PD, related LPJ-GUESS derived vegetation cover in the left panels and the according mean catchment erosion rate and mean values

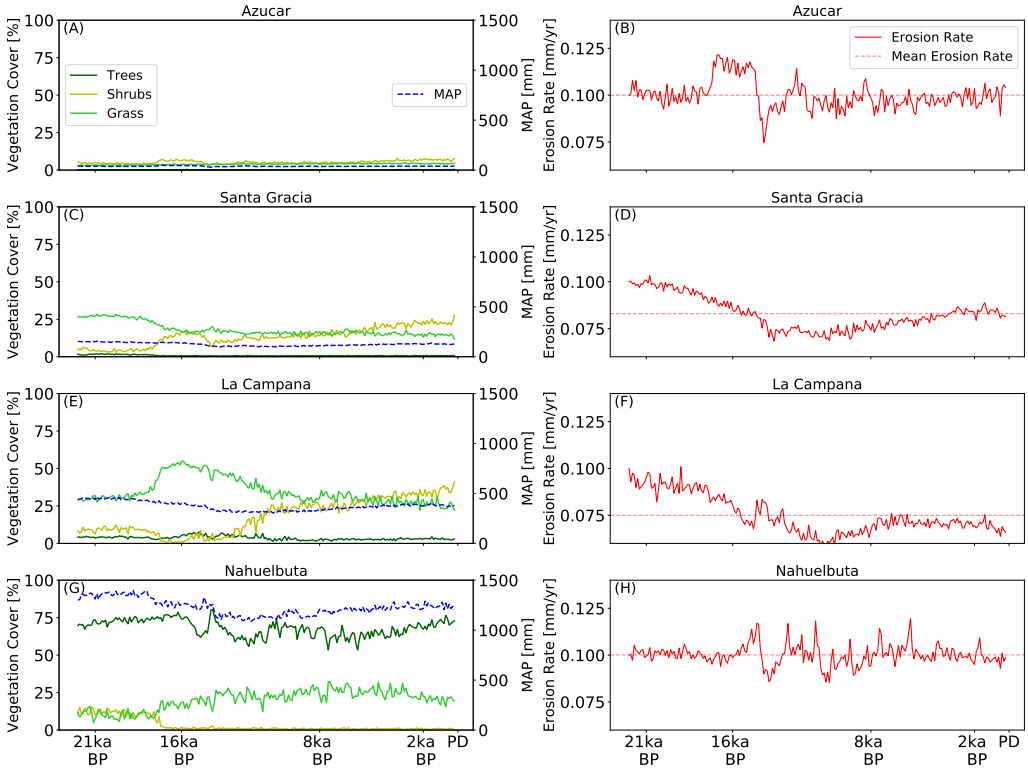

Figure 7: Simulation results for the fully-coupled model runs with continous feedback between LPJ-GUESS and Landlab and fully transient timeseries for vegetation cover and precipitation (left side). Right side shows resulting catchment-wide erosion rates and mean erosion rates over LGM to PD timeseries.

for time series LGM to PD in the right panels. The MAP values are equal to the values described in section 3.2 for the respective areas.

For Pan de Azucar simulation the coupled model predicts values for catchment-wide LGM to PD mean vegetation cover (Fig 7(A)) for trees, shrubs and grass of 0.3%, 5.3% and 3.9%. Maximum and minimum tree cover for the modeled time series were 0.5% at 15.7ka BP and 0.2% at 17.6ka BP, for shrubs cover the model predicts maximum and minimum values of 7.9% at 3.5ka BP and 3.4% at 14.4ka BP and for grass cover a maximum value of 4.9% at 3.1ka BP and a minimum value of 2.9% at 14.4 ka BP. The corresponding catchment-wide erosion rates (Fig 7(B)) show a LGM - PD mean value of 0.09 mm/yr with maximum values of 0.123mm/yr at 16.9ka BP and minimum values of 0.075 at 14.2ka BP.

Coupled simulation for Santa Gracia shows catchment-wide mean LGM - PD vegetation cover values (Fig 7(C)) for 0.8% tree vegetation, 13.6% shrub vegetation and 18.2% grass vegetation with maximum and minimum values for trees of 2.0% at 19.8ka BP and 0.4% at 10.4ka BP, 27.6% at 0.2ka BP and 3.1% at 19.8ka BP for shrub vegetation and

for grass vegetation cover a maximum of 28.4% at 20.8ka BP and 11.8% at 0.2ka BP. Erosion rates (Fig 7(D)) show a maximum of 0.103 mm/yr at 20.8ka BP and a minimum of 0.068 mm/yr at 13.6ka BP with a LGM - PD mean value of 0.083 mm/yr.

La Campana coupled simulations show mean vegetation cover values for catchment-wide LGM-PD covers (Fig 7(E)) for trees, shrubs and grasses of 3.6%, 17.9% and 34.7%. Maximum and minimum vegetation covers for tree vegetation are 7.7% at 15ka BP and 1.4% at 10.7ka BP. For shrub vegetation maximum and minimum covers are 41.2% at 0.2ka BP and 0.4% at 16.5 ka BP and grass vegetation reaches maximum of 54.9% ar 15.9ka BP and minimum of 22.1% at 2.2ka BP. Mean catchment erosion rates (Fig 7(F)) show a maximum at 0.100mm/yr at 19ka BP and minimum of 0.058ka BP with a LGM to PD mean of 0.07mm/yr.

Simulations for Nahuelbuta study area predict mean vegetation covers (Fig 7(G)) for trees, shrubs and grass vegetation covers of 68.2%, 3.3% and 20.0% with a maximum tree cover of 80.7% at 14.2ka BP, minimum tree cover of 53.4% at 5.8ka BP, maximum shrub cover of 15.3% at 21.2ka B, minimum shrub cover of 0.2% at 9.7ka BP, maximum grass cover of 32.3% at 7.5ka BP and minimum grass cover of 4.9% at 21.1ka BP. Related catchment-wide erosion rates (Fig 7(H)) show a maximum of 0.119mm/yr at 5.7ka BP and minimum of 0.085mm/yr at 10.4ka BP which results in a LGM to PD mean of 0.100mm/yr.

These results show that for northernmost and southernmost areas Pan de Azucar and Nahuelbuta, the predicted catchment-wide mean erosion from LGM to PD conditions shows strong fluctuations within the modeled time series of up to 20% difference of erosion rate from steady-state uplift rate but the mean value over time series does not show large shifts from uplift rate of 0.1mm/yr. For areas Santa Gracia and La Campana the catchment-wide mean erosion rates show lower short-term fluctuations but a large-scale trend of declining erosion rates with lowest values between 13ka BP and 10ka BP and a LGM-PD mean value which is 18% lower than uplift rate for Santa Gracia and 25% lower for La Campana. In the next subsections we show inter-area specific results for different landform positions and the according correlation coefficients for each study area.

3.3.1 Pan de Azucar

In Fig. 8 we show mean erosion rates from LGM to PD time series for fully coupled simulations and the imposed changes in vegetation cover for different topographic positions within the Pan de Azucar model domain. The data shows distinct differences in how the erosion rates at landform level reacts to changes in vegetation cover with highest variations of erosion rates for flat and valley positions. Hilltop positions show variations in erosion rates between a maximum of 0.128 mm/yr and a minimum of 0.076 mm/yr with

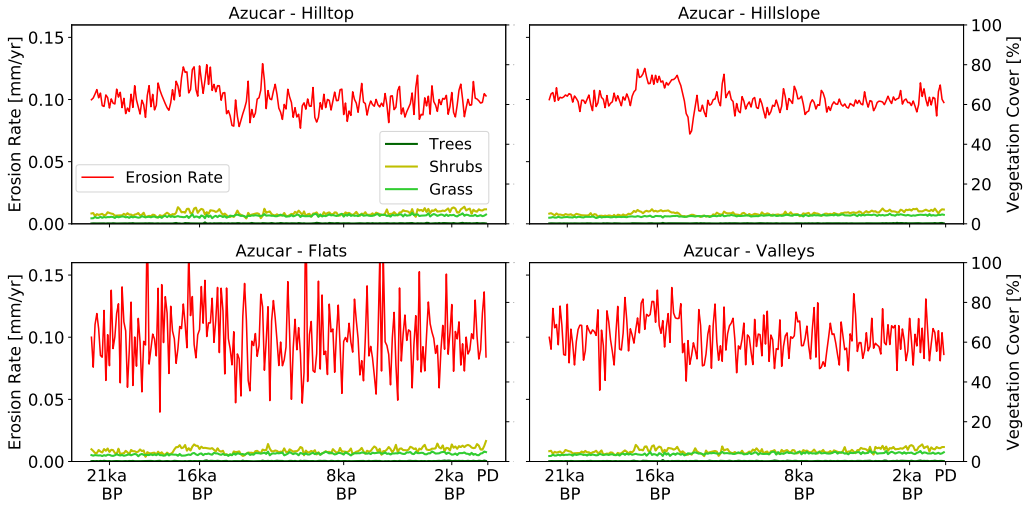

Figure 8: Vegetation cover values and erosion rates of Pan de Azucar simulation for the four different topographic position indices within model-framework.

mean over time series of 0.099 mm/yr. Hillslope positions show maximum and minimum erosion rates values of 0.125 mm/yr and 0.072 mm/yr with a LGM to PD mean of 0.100 mm/yr. Topographic flats show maximum erosion rates of 0.215 mm/yr and minimum rates of 0.039 mm/yr with time series mean of 0.098 mm/yr. Valley positions show an erosion rate maximum of 0.139 mm/yr, minimum of 0.058 mm/yr with time series mean of 0.099 mm/yr. The coefficients of variation for cumulative vegetation cover and erosion rates are 0.16 and 0.09 for on hilltop landforms, 0.14 and 0.08 on hillslope landforms, 0.2 and 0.26 on flat landforms and 0.17 and 0.15 for valley landforms so the higher variability of erosion rates follows higher variability in vegetation cover for flat and valley landform positions.

The correlation coefficients between erosion rates and selected parameters of our coupled model, which are depicted in Fig. 8 show that erosion rates for arid Pan de Azucar study area show highest positive correlation with MAP values (r = 0.8) while MAT shows slight negative correlation (r = -0.3). The grass vegetation type is the only vegetation class that shows a negative, albeit small, correlation with erosion rate (r = -0.2), while shrub and tree vegetation class shows slight to medium positive correlation with erosion rates (r = 0.1, r = 0.4).

Therefore, for Pan de Azucar simulation, the only vegetation type that is able to dampen the positive effect that an increase of MAP has on catchment-wide erosion rates is the grass type, while shrub and tree vegetation do not grow effective enough to have an hindering effect on erosion rates by increase in vegetation cover.

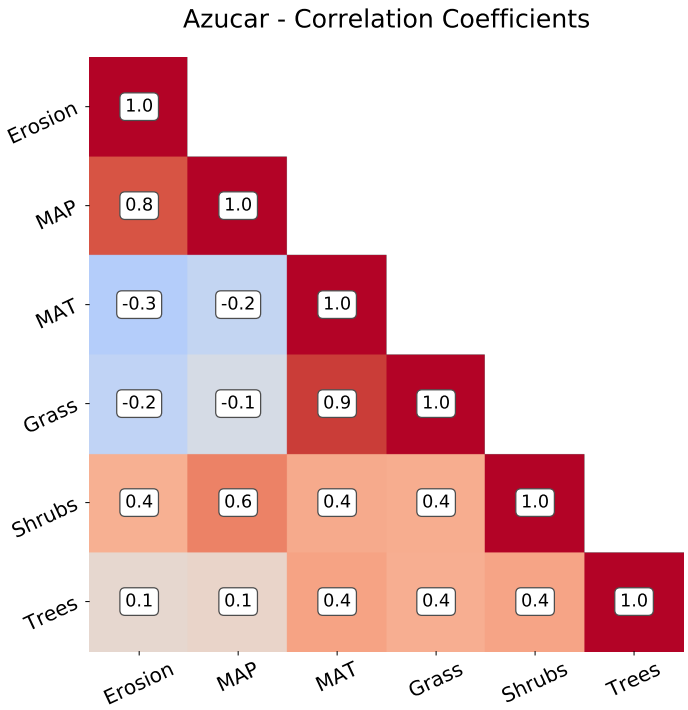

Figure 9: Pearson Correlation Coefficients for selected model parameters for Pan de Azucar simulation.

3.3.2 Santa Gracia

Fig. 10 depicts the erosion rate and vegetation cover time series for different topographic positions for Santa Gracia study area. Data shows a slightly higher variation of erosion rates for flat and valley landforms than for hilltop and hillslope landforms. All four topographic positions show a decline in erosion rate at ca. 12ka BP and then a slow increase towards PD conditions.

Hilltop landforms show erosion rates with a time series mean from LGM to PD of 0.008 mm/yr with maximum of 0.101 mm/yr and minimum of 0.066 mm/yr. Hillslope positions show maximum and minimum value of 0.103 mm/yr and 0.068 mm/yr and a LGM to PD mean of 0.083 mm/yr. Flat landforms show maximum values of 0.104 mm/yr, minimum values of 0.061 mm/yr and mean value over time series of 0.082 mm/yr. Maximum and minimum erosion rates for valley landforms are 0.105 mm/yr and 0.062 mm/yr with time series mean of 0.082 mm/yr. Coefficients of variation of vegetationn cover and erosion rates are 0.10 and 0.11 for hilltop positions, 0.11 and 0.11 for hillslope positions, 0.09 and 0.11 for flat positions and 0.10 and 0.11 for valley positions.

This data suggests that the variability in erosion rates can be in a first-order approximation explained by a corresponding variability in vegetation cover within the focus area. In Fig. 11 we show correlation coefficients between different selected parameters

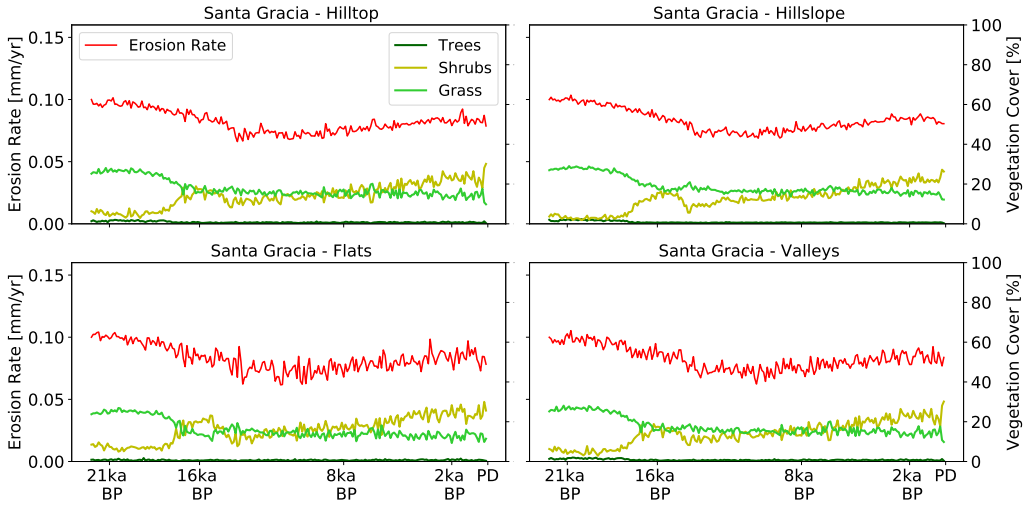

Figure 10: Vegetation cover values and erosion rates of Santa Gracia simulation for the four different topographic position indices within model-framework.

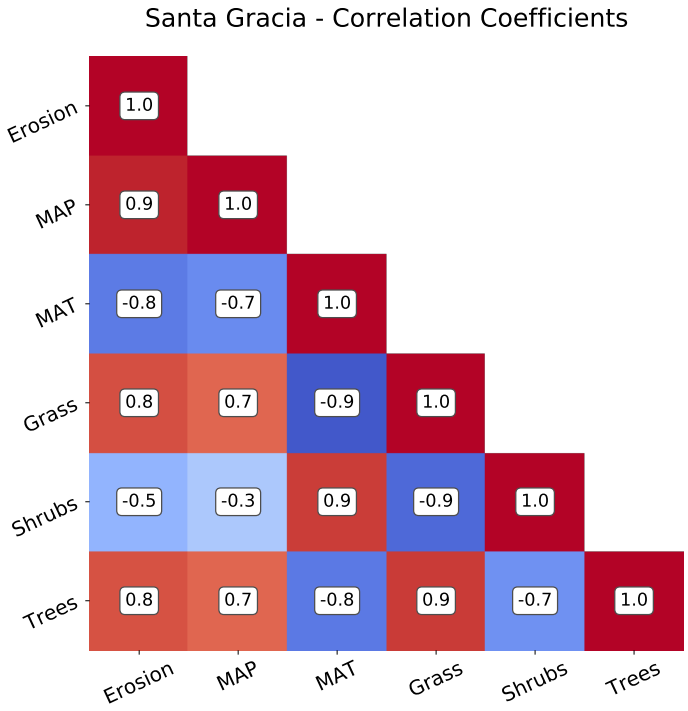

Figure 11: Pearson Correlation Coefficients for selected model parameters for Santa Gracia simulation.

of the coupled model. MAP shows highest positive correlation with erosion rate (r = 0.9) whereas MAT has a strong negative correlation with erosion rate (r = -0.8). The three different vegetation type classes show high positive correlation with erosion rates

for grasses and trees (r = 0.8, r = 0.8) and a medium negative correlation for the shrub vegetation type (r = -0.5) which suggests that for Santa Gracia model area the shrub vegetation cover is the only one able to hinder increases of erosion rates by increases of MAP.

3.3.3 La Campana

In Fig. 12, we show the same vegetation cover and erosion rates values as in the previous plots for La Campana study area. Data shows a strong increase in shrub vegetation cover for all four different topographic positions (10% to 50%) over time series, starting at 16ka BP, while grass cover peaks at 18ka BP and then reduces again to approximately 20% for different slope positions. Tree cover shows no large increases over model runs and stays <10% continuously. Erosion rates show a decline from steady-state conditions of 0.1 mmy/r to modeled PD values of approximately 0.075 mm/yr for all four topographic positions.

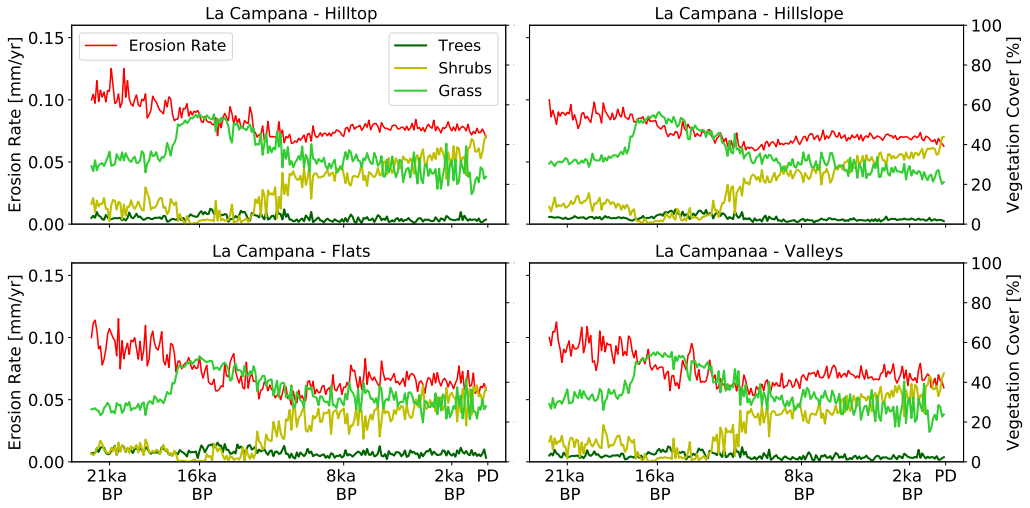

Figure 12: Vegetation cover values and erosion rates of La Campana simulation for the four different topographic position indices within model-framework.

Hilltop positions show minimum erosion rates of 0.062 mm/yr and maximum erosion rates of 0.125 mm/yr with a mean value over the modeled LGM to PD time series of 0.082 mm/yr. Hillslope positions show minimum and maximum erosion rates values of 0.058 mm/yr and 0.099 mm/yr which leads to LGM to PD mean value of 0.073 mm/yr. Topographic flat positions show minimum and maximum values of erosion rates of 0.045 mm/yr and maximum values of 0.115 mm/yr with a LGM to PD mean of 0.069mm/yr and the valley topographic positions show minimum and maximum erosion rates of 0.053 mm/yr and 0.112 mm/yr with a LGM to PD mean of 0.073 mm/mr. The calculated coefficients of variations show values for cumulative vegetation cover and erosion rates

of0.12 and 0.14 for hilltop positions, 0.11 and 0.13 for slope positions, 0.15 and 0.20 for flat positions and 0.15 and 0.17 for topographic valley positions. This shows that the highest variability in erosion rates for flat and valley landforms follows the highest variability of vegetation cover for these respective topographic positions.

Fig. 13 depicts the correlation coefficients between model parameters. While there is a strong positive correlation between MAP and erosion rates (r = 0.8)there exists a stronger negative correlation between MAT and erosion rates (r = -0.9). Positive correlations between vegetation cover and erosion rates show smaller values than in previous model areas with correlation between grass and erosion rate being r= 0.1 and correlation between tree vegetation and erosion being r = 0.3. Shrub vegetation and erosion rate show a medium to large negative correlation with erosion rates (r = -0.6).

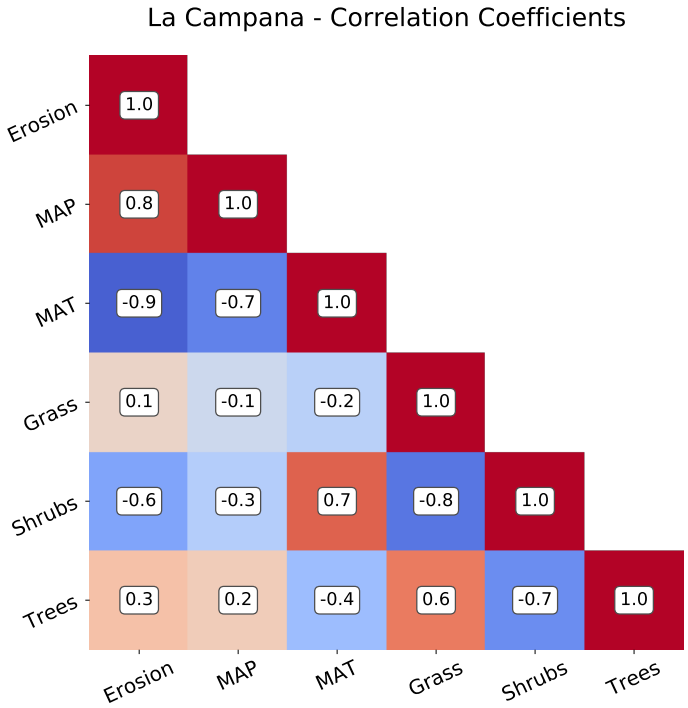

Figure 13: Pearson Correlation Coefficients for selected model parameters for La Campana simulation.

3.3.4 Nahuelbuta

Fig. 14 shows the mean vegetation cover values for the three different vegetation classes and the mean erosion rate for the different topographic positions within the model domain for fully coupled Nahuelbuta simulation. The data shows a drop in shrub vegetation from a initial LGM value of 10% - 20% for the different topographic positions to nearly 0% at approximately 17.5ka BP, while grass vegetation cover starts to increase at the same time from initial values of 10% to 25%, with the highest increase of grassy vegetation cover for hillslope positions.

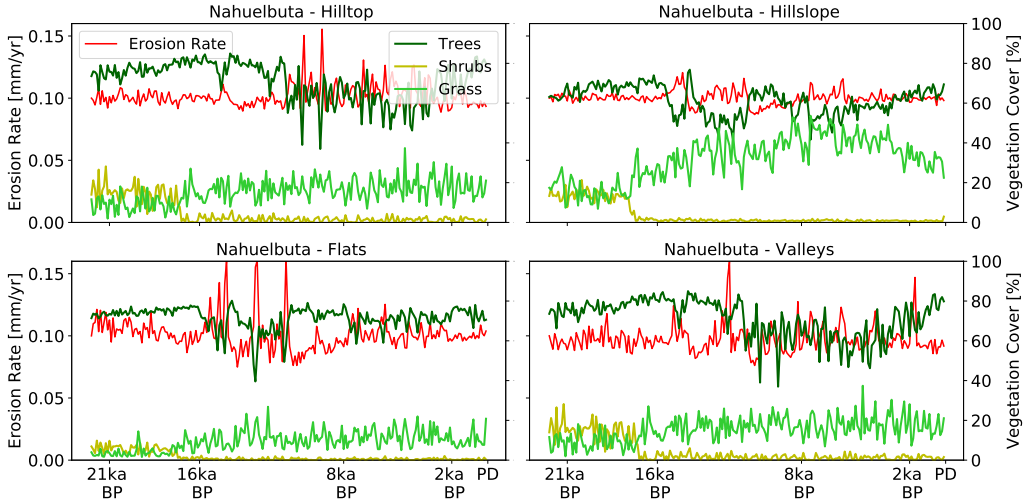

Figure 14: Vegetation cover values and erosion rates of Nahuelbuta simulation for the four different topographic position indices within model-framework.

Tree vegetation cover shows initial values of 75% for different topographic positions at depicts variation of tree cover in the time between 16ka BP and 2 ka BP with values of vegetation cover decreasing to values of up to 40% for hilltop, flat and valley landforms for short periods of time before increasing towards PD values of 75%. Erosion rates do not show large variations going from LGM to 16ka BP. From 16ka BP to 4ka BP the data indicateslarge variations with short periods of increases in erosion rates up to 0.155 mm/yr. For hilltop positions, erosion rates show minimum values of 0.088 mm/yr and maximum values of 0.156 mm/yr which leads to a LGM to PD mean of 0.101 mm/yr. Hillslope positions show minimum erosion rate values of 0.086 mm/yr and maximum rates of 0.121 mm/yr with a time series mean of 0.099 mm/yr. The topographic flats within the model domain show largest variation in erosion rates with minimum values of 0.75 mm/yr and maximum values of 0.163 mm/yr. The mean of 0.100 mm/yr however does not show a shift from steady-state conditions. Valley positions in our model domain show minimum values of 0.076 mm/yr and maximum values of 0.158 mm/yr with a mean value of 0.097 mm/yr for LGM to PD conditions. This indicates that there is no significant

shift of LGM to PD mean erosion rates for any of the 4 observed topographic positions from steady-state conditions of 0.1 mm/yr. Coefficients of variation for the different topographic positions for vegetation cover and erosion rates are 0.12 and 0.09 for hilltop positions, 0.06 and 0.05 for hillslope positions, 0.07 and 0.12 for flat positions and 0.07 and 0.11 for topographic valley positions. This suggests that for Nahuelbuta simulations the higher variation for erosion rates for flat and valley positions can not be explained by a higher variation cumulative vegetation cover.

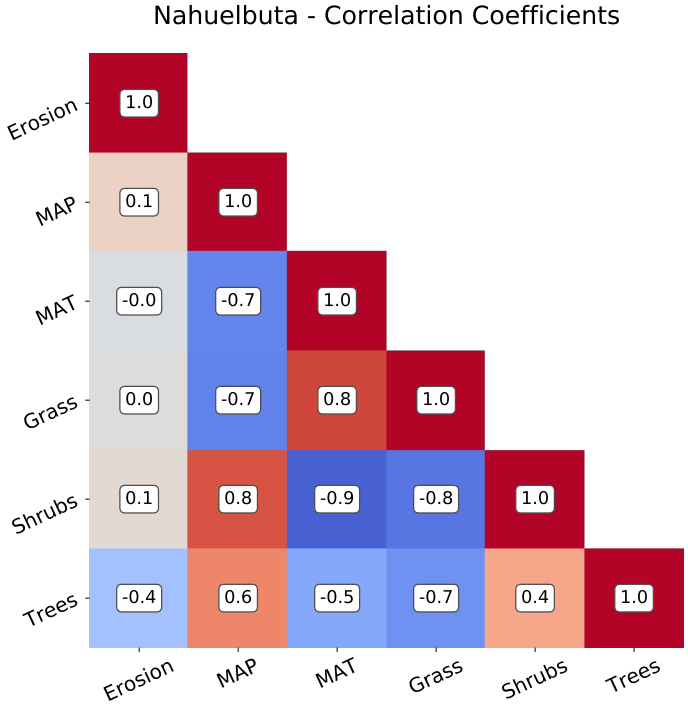

Figure 15: Pearson Correlation Coefficients for selected model parameters for Nahuelbuta simulation

Fig. 15 shows the associated pearson correlation coefficients for the Nahuelbuta coupled simulation. While MAP, MAT and grass and shrub vegetation cover shows no real correlation with erosion rate (r = 0.1, 0.0, 0.0, 0.1), the only parameters which shows a medium negative correlation with erosion rate is tree vegetation cover (r = -0.4). This suggests that catchment wide erosion rates for Nahuelbuta study area are mainly controlled by the change of vegetation cover for tree vegetation class, in comparison to simulations for other study areas which were mainly controlled by MAP.

4 Discussion

The results from the individual simulation experiments with a.) constant LGM precipitation values and a transient LGM to PD time series of vegetation cover change,b.) constant LGM vegetation cover values and a transient LGM to PD time series of precipitation values and c.) fully coupled simulations with transient LGM to PD vegetation cover and precipitation values suggest that there exists differences between the analyzed study areas in the main controlling factors for catchment wide erosion rates and between the different topographic positions within the catchment. In the following we summarize the results, described in section 3 and discuss how changes in climate from LGM to PD for 4 different areas located in different climatic zones along the Chilean Coastal Cordillera react to transient changes.

4.1 Interpretation of simulations with constant LGM precipitation and transient LGM to PD vegetation cover

Changes in vegetation cover are known to be a primary control on catchment wide erosion rates by modulation of surface characteristics (e.g infiltration rate, soil cohesion, flow resistance) [Prosser and Dietrich, 1995, Loch, 2000, Dosseto et al., 2010, Schmid et al., 2018]. The results of simulations with constant MAP values and changing vegetation covers for three different vegetation classes (Fig. 5) show variations of transient erosion rates from steady-state value of 0.1mm/yr. We make a distinction between two different end-member cases: 1.) Erosion rate time series with high frequency of events of increasing or decreasing erosion rates up to approximately 30% from steady-state value but with no significant deviation of long-term mean erosion rates from LGM to PD. 2.) time series of erosion rates with lower frequency of high amplitude changes in erosion rates but an overall long-term adjustment of mean LGM to PD erosion rate. While simulations for Pan de Azucar, Santa Gracia and Nahuelbuta show a series of short, burst-like events of increases and decreases in mean catchment erosion rates (up to 0.130 mm/yr, which resembles a 30% deviation fromsteady-state) for Nahuelbuta simulation, they show no large adjustment for LGM to PD mean from the 0.1 mm/yr steady-state uplift rate. Data from La Campana simulation shows one larger event of increasing erosion rates at 16ka BP, which coincides with similar events in other simulated areas, but shows a drop of mean erosion rates from LGM to PD by approximately 17%. This shows that with no changes in precipitation, isolated transient changes in LGM to PD vegetation cover lead to short bursts of large magnitude changes in erosion rate and a general trend of erosion rate lowering for La Campana study area.

4.2 Interpretation of simulations with constant LGM vegetation cover and transient LGM to PD precipitation values

The positive linkage between MAP and erosion rates is a well-known and researched subject in the field of geomorphology, where increases in MAP values are commonly associated with increases in catchment-wide erosion rates [Langbein and Schumm, 1958, Reiners et al., 2003, Owen et al., 2011] and vice versa. In Fig. 6 we show the effect of the TraCE-21ka precipitation time series on our model domains with constant, time independent LGM vegetation covers, to single out the effect of the transient changes in MAP values on catchment erosion rates from LGM to present. Data shows that arid area of Pan de Azucar shows highest short-term variability of erosion rates with changes of approximately 40% magnitude in positive as well as negative directions with the biggest increase of erosion rates at 18.5ka and the biggest decrease at 16ka BP. From 16ka BP to present, the variability decreases, and we see no large general shift of LGM to PD mean erosion rates. Simulations for Santa Gracia, La Campana and Nahuelbuta areas however show smaller short-term changes in erosion rates with no large burst-like events of increases or decreases buta long-term trend of declining erosion rates, with lowest values reached at 16ka BP, followed by a slight increase of erosion rates and an overall LGM to PD mean which is 17% lower than steady-state conditions for Santa Gracia area and 8 lower than steady-state conditions for La Campana area. Nahuelbuta study area shows a lesser pronounced change in erosion rates both for short-term changes and also for long-term LGM to PD mean with a decline by only 4% magnitude. These changes in erosion rates follow the variation of TraCE-21ka MAP value which show a decrease in precipitation from LGM conditions to 16ka BP, followed by a mild increase to PD conditions.

4.3 Interpretation of fully coupled simulations with transient TraCE-21ka precipitation values and associated changes in catchment vegetation cover

While the previous simulation experiments with either constant vegetation cover or constant mean annual precipitation were conducted in order to isolate the unique effects of either the TraCE-21ka derived time series of climatic conditions or associated changes in vegetation cover on catchment wide erosion rates, this fully coupled model run shows the effect of simultaneous changes of precipitation and the corresponding changes in vegetation as well as possible changes in vegetation distribution through adjustment of landform positions within a catchment.

Fig. 7 shows the evolution of catchment-wide erosion rates for fully coupled simulations. The variations of catchment mean erosion rates, with high amplitude changes

for Pan de Azucar and Nahuelbuta and low amplitude changes for Santa Gracia and La Campana, suggests different sensitives of catchment topography to climatic and biotic changes. Fig. 16 shows the normalized values for MAP, MAT, cumulative vegetation cover and the absolute difference between the catchment-wide erosion rate and the uplift rate for Pan de Azucar study area. While the cumulative vegetation cover generally follows the values of MAP, with increases in precipitation leading to increases in vegetation cover, the main controlling factor over erosion rates is the evolution of MAP, with higher values of MAP leading to higher values of erosion rates, despite the associated increase in vegetation cover. This is supported by the strong correlation between erosion rate and MAP for Pan de Azucar (Fig. 9, r = 0.8) and the weak correlation between erosion rates and different vegetation types (r = -0.2 – 0.4).

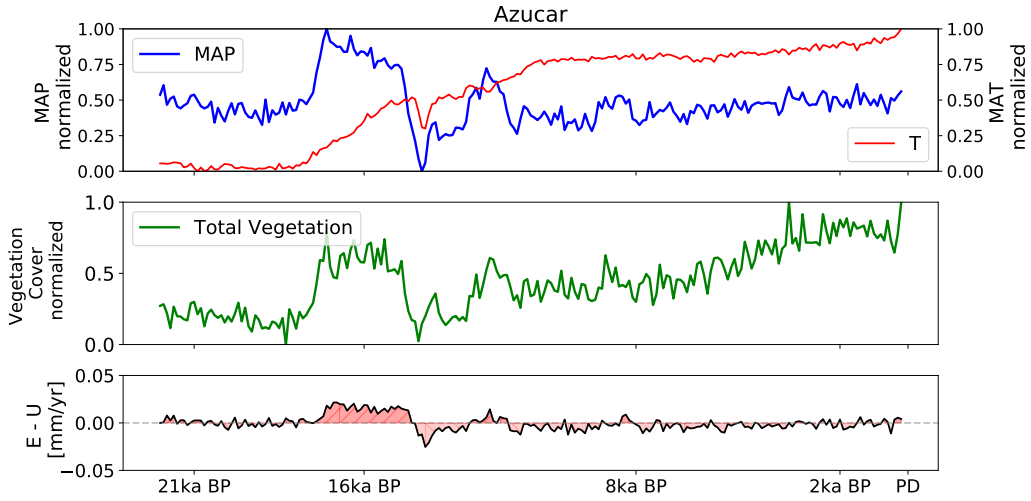

Figure 16: Normalized timeseries values for MAP and MAT (top panel), cumulative vegetation cover (middel panel) and the difference between erosion rate and uplift rate (bottom panel) for Pan de Azucar Simulation.

For Santa Gracia model domain we see that the highest values of precipitation are associated with lowest values of temperature and intermediate values of vegetation cover (see Fig. 17). Erosion rates decrease from LGM conditions to a minimum between 16ka and 10ka BP and follow the decrease of MAP values. However after 10ka BP, values for MAP show increase over time series until PD conditions with associated increase in vegetation cover values within catchment which leads to maximum vegetation cover at PD conditions with only 50% of initial, maximum precipitation values for Santa Gracia Study area, which we attribute to the controlling factor that an increase in temperature has on vegetation cover. Erosion rates show no significant increase after 10ka BP which suggests that the hindering effect of vegetation cover which is controlled by the increase in MAP but also MAT outweighs the direct positive effect of MAP on erosion rates.

This is supported by the correlation coefficients (Fig. 11) which show a strong positive correlation between MAP and erosion rates (r = 0.9) but a nearly equally strong negative correlation between MAT and erosion rates (r = -0.8).

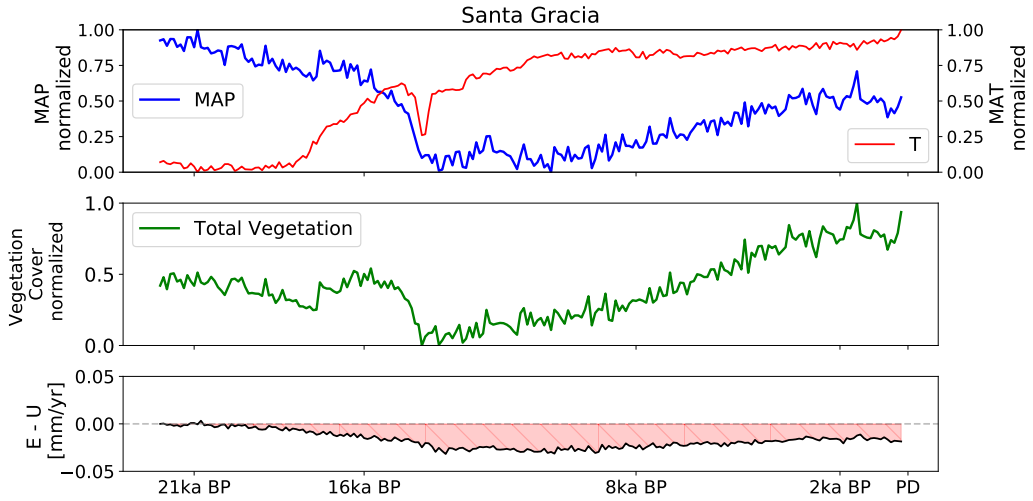

Figure 17: Normalized timeseries values for MAP and MAT (top panel), cumulative vegetation cover (middel panel) and the difference between erosion rate and uplift rate (bottom panel) for Santa Gracia Simulation.

La Campana study area shows similar behavior than Santa Gracia, highest values of MAP and lowest values of MAT for LGM conditions with a decline of MAP to minimum values at 11 ka BP and a steady increase of MAT towards PD conditions with a short period of decrease a 16ka BP (Fig. 18). Vegetation cover shows continuous increase from LGM to PD conditions which suggests that the vegetation does not react much to declining MAP values because of a general enough abundance of water for the PFT composition within the area but reacts to the increases in MAT. This leads to erosion rates which show a decrease from LGM conditions with lowest values at 11ka BP, which coincide with the lowest values for MAP but then show no significant increase as MAP increases again which we attribute to the dampening effect of the steadily increasing vegetation cover. The correlation coefficients (Fig. 13) support this argument with a higher negative correlation between erosion rates and MAT (r = -0.9) than positive correlation between erosion rate and MAP (r = 0.8) and a medium negative correlation between shrub vegetation class and erosion rates (r = -0.6).

The simulations for Nahuelbuta study area shows similar trend regarding MAP and MAT value as Santa Gracia and La Campana but show no significant increase in vegetation cover over LGM to PD time series, rather the mean cumulative vegetation cover tends to stay the same but with short periods of either increased or decreased values (Fig. 19). However the erosion rates show a reversed behaviour regarding changes in

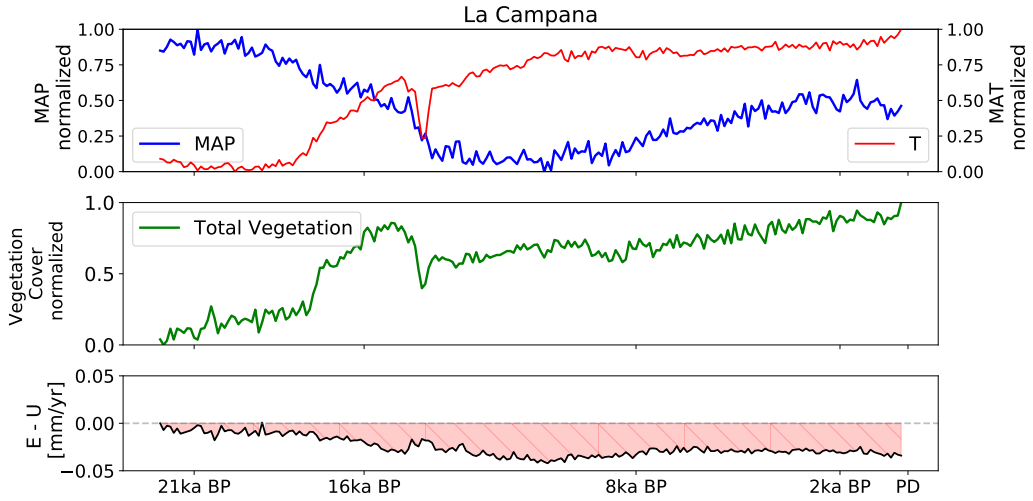

Figure 18: Normalized timeseries values for MAP and MAT (top panel), cumulative vegetation cover (middel panel) and the difference between erosion rate and uplift rate (bottom panel) for La Campana Simulation.

MAP and vegetation cover, so that for periods of declining MAP and vegetation cover, the erosion rates show increases (Fig. 19). We argue that the erosion rates in Nahuelbuta area mainly controlled by the changes in surface vegetation cover and not precipitation, which is also shown in the correlation coefficients (Fig. 15) with no significant correlation between erosion rates and MAP (r = 0.1) and a medium negative correlation between erosion rates and tree vegetation cover (r = -0.4).

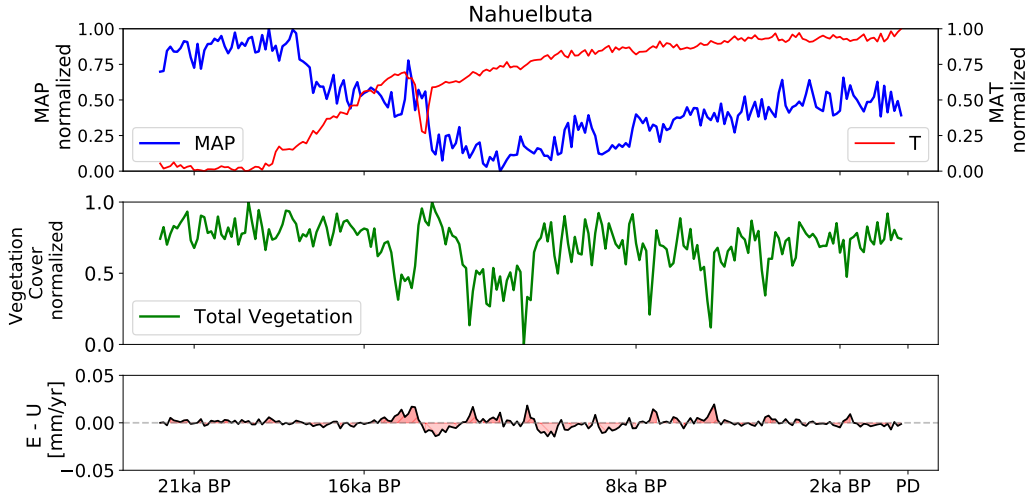

Figure 19: Normalized timeseries values for MAP and MAT (top panel), cumulative vegetation cover (middel panel) and the difference between erosion rate and uplift rate (bottom panel) for Nahuelbuta Simulation.

In summary this suggests that the modification of overland flow resistance and soil diffusion by vegetation cover modifies the erosion rates for the four observed study areas in different magnitudes. While the erosion rates for northernmost area Pan de Azucar follow the evolution of MAP with no real observable modification by vegetation cover, the two following areas to the south, Santa Gracia and La Campana, show a first-order control of MAP on erosion rates but with the effect of a steady increase of vegetation cover from LGM to PD hindering the erosion rates to follow the increase of MAP after 16ka BP. Southernmost area Nahuelbuta shows erosion rates that are mainly controlled by changes in vegetation cover, with short periods of smaller vegetation cover having simultaneously higher erosion rates, despite of smaller values of MAP. The control of vegetation cover on erosion rates also shows intra-area effects by modulating erosion rates with highest values of variance for flat and valley positions within the model domain, which also show highest values of variance for vegetation cover. Furthermore the data suggests that there exists a shift in the vegetation class which has the highest dampening effect on erosion rates going from north to south.

In Pan de Azucar, grass vegetation type shows highest negative correlation with erosion rates (r = -0.2), for Santa Gracia and La Campana the shrub-type vegetation class shows highest negative correlations (r = -0.5 and r = -0.6) and for Nahuelbuta area the tree vegetation cover is the only parameter with a negative correlation with erosion rates with medium significance (r = -0.4). This suggests that there exists a shift of the main controlling factor on erosion rates between the different climatic zones from MAP for Pan de Azucar, Santa Gracia and La Campana and vegetation for Nahuelbuta but also a shift in the main vegetation type that has a effect in the respective basins.

5 Conclusion

Results from our presented simulations indicate that the reaction of the investigated study areas Pan de Azucar (very arid), Santa Gracia (arid), La Campana (humid) and Nahuelbuta (very humid), to changes in climate and vegetation cover for LGM to PD conditions varies in magnitude and frequency and shows a complex pattern of transient erosion rates. Main findings from the conducted model experiments are:

1. Climatic changes since LGM to PD cause only small changes in total cumulative vegetation cover in study areas. However there are large shifts in the composition of vegetation cover due to a shift in climatic limits and adjustment of PFT stability.

2. Changes in mean annual precipitation since LGM conditions result in highly variable short-term reactions of mean catchment erosion rates for Pan de Azucar and Santa Gracia Area. La Campana and Nahuelbuta don't show large variations in erosion rates, due to precipitation changes. Santa Gracia and La Campana also show significant lowering of erosion rates under steady-state uplift rate.

3. Changes in vegetation (cumulative and composition) lead to high short-term variability in erosion rates for Pan de Azucar and Nahuelbuta area around the steady-state mean and therefore show no significant adjustment to a new dynamic mean value. Santa Gracia and La Campana show lower variability in short-term erosion rates. The La Campana area shows large decrease of mean values below the steady-state uplift rate.

4. Coupled simulations (with varying precipitation and vegetation cover) show large short-term variations in erosion rates for Pan de Azucar and Nahuelbuta. Santa Gracia and La Campana areas show a decrease of the long-term mean erosion rates but lesser short-term variations. This suggests that climate change since LGM conditions has lead to an significant decrease in catchment wide erosion rates for study areas in semi-arid to mediterranean conditions.

5. Correlation coefficients between erosion rates and different model parameters show that the influence of precipitation changes on erosion rates decreases going from N to S. Southern area of Nahuelbuta shows dominant effects of tree vegetation cover on erosion rates, compared to precipitation values. In general the data suggests that for the arid to semi-arid areas, grass and shrub vegetation has most impact on erosion rates while for mediterranean and humid areas, tree vegetation is the dominant class for reduction of erosion values.

Taken together, these results suggest a high sensitivity of investigated focus areas to LGM to PD climatic changes. Comparison of three sets of simulations also show that

coupled simulations predict different reactions than simulations with single input forcing and show the need for landscape evolution models to incorporate a better representation of erosion/vegetation feedbacks if the goal is to predict testable, realistic results

References

F. Ahnert. Brief description of a comprehensive three-dimensional process-response model for landform development. *Zeitschrift fur Geomorphologie*, 25:29 – 49, 1976.

E. E. Alberts, M. A. Nearing, M. A. Weltz, L. M. Risse, F. B. Pierson, X. C. Zhang, J. M. Laflen, and J. R. Simanton. Soil component, in USDA—Water Erosion Prediction Project. 1995.

R. Amundson, A. Heimsath, J. Owen, K. Yoo, and W. E. Dietrich. Hillslope soils and vegetation. *Geomorphology*, 234:122–132, 2015. 10.1016/j.geomorph.2014.12.031.

N. N. Avdievitch, T. A. Ehlers, and C. Glotzbach. Slow long-term exhumation of the West Central Andean Plate Boundary, Chile. *Tectonics*, 2018. 10/gdwrpk.

S. Bautista, Á. G. Mayor, J. Bourakhouadar, and J. Bellot. Plant Spatial Pattern Predicts Hillslope Runoff and Erosion in a Semiarid Mediterranean Landscape. *Ecosystems*, 10: 987–998, 2007. 10.1007/s10021-007-9074-3.

G. B. Bonan, S. Levis, L. Kergoat, and K. W. Oleson. Landscapes as patches of plant functional types: An integrating concept for climate and ecosystem models. *Global Biogeochemical Cycles*, 16:1 – 23, 2002. 10.1029/2000GB001360.

D. B. G. Collins and R. L. Bras. Modeling the effects of vegetation-erosion coupling on landscape evolution. *Journal of Geophysical Research*, 109, 2004. 10.1029/2003JF000028.

D. B. G. Collins and R. L. Bras. Climatic and ecological controls of equilibrium drainage density, relief, and channel concavity in dry lands. *Water Resources Research*, 46, 2010. 10.1029/2009WR008615.

D. P. Dee, S. M. Uppala, A. J. Simmons, P. Berrisford, P. Poli, S. Kobayashi, U. Andrae, M. A. Balmaseda, G. Balsamo, P. Bauer, P. Bechtold, A. C. M. Beljaars, L. van de Berg, J. Bidlot, N. Bormann, C. Delsol, R. Dragani, M. Fuentes, A. J. Geer, L. Haimberger, S. B. Healy, H. Hersbach, E. V. Hólm, L. Isaksen, P. Kållberg, M. Köhler, M. Matricardi, A. P. McNally, B. M. Monge-Sanz, J.-J. Morcrette, B.-K. Park, C. Peubey, P. de Rosnay, C. Tavolato, J.-N. Thépaut, and F. Vitart. The ERA-Interim reanalysis: Configuration and performance of the data assimilation system. *Quarterly Journal of the Royal Meteorological Society*, 137:553–597, 2011. 10.1002/qj.828.

A. Dosseto, P. Hesse, K. Maher, K. Fryirs, and S. Turner. Climatic and vegetation control on sediment dynamics during the last glacial cycle. *Geology*, 38:395–398, 2010. 10.1130/G30708.1.

G. Dunjó, G. Pardini, and M. Gispert. The role of land use–land cover on runoff generation and sediment yield at a microplot scale, in a small Mediterranean catchment. *Journal of Arid Environments*, 57:239–256, 2004. 10.1016/S0140-1963(03)00097-1.

T. Dunne, K. X. Whipple, and B. F. Aubry. Microtopography of hillslopes and initiation of channels by horton overland flow. *Geophysical Monograph Series*, 89:27–44, 1995. 10.1029/GM089p0027.

T. Dunne, D. V. Malmon, and S. M. Mudd. A rain splash transport equation assimilating field and laboratory measurements. *Journal of Geophysical Research*, 115, 2010. 10 .1029/2009JF001302.

P. S. Eagleson. Climate, soil, and vegetation: 2. The distribution of annual precipitation derived from observed storm sequences. *Water Resources Research*, 14:713–721, 1978. 10.1029/WR014i005p00713.

T. Hickler, B. Smith, M. T. Sykes, M. B. Davis, S. Sugita, and K. Walker. Using a generalized vegetation model to simulate vegetation dynamics in northeastern USA. *Ecology*, 85:519–530, 2004. 10.1890/02-0344.

D. E. J. Hobley, J. M. Adams, S. S. Nudurupati, E. W. H. Hutton, N. M. Gasparini, E. Istanbulluoglu, and G. E. Tucker. Creative computing with Landlab: An open-source toolkit for building, coupling, and exploring two-dimensional numerical models of Earth-surface dynamics. *Earth Surface Dynamics*, 5:21–46, 2017. 10.5194/esurf-5 -21-2017.

J. Hooke. An analysis of the processes of river bank erosion. *Journal of Hydrology*, 42: 39–62, 1979. 10.1016/0022-1694(79)90005-2.

E. Istanbulluoglu and R. Bras. Vegetation-modulated landscape evolution: Effects of vegetation on landscape processes, drainage density, and topography. *Journal of Geophysical Research*, 110, 2005. 10.1029/2004JF000249.

E. Istanbulluoglu, D. G. Tarboton, R. T. Pack, and C. H. Luce. Modeling of the interactions between forest vegetation, disturbances, and sediment yields. *Journal of Geophysical Research: Earth Surface*, 109, 2004. 10.1029/2003JF000041.

S. A. Johnstone and G. E. Hilley. Lithologic control on the form of soil-mantled hillslopes. *Geology*, 43:83–86, 2015. 10.1130/G36052.1.

J. W. Kirchner, R. C. Finkel, C. S. Riebe, D. E. Granger, J. L. Clayton, J. G. King, and W. F. Megahan. Mountain erosion over 10 yr, 10 k.y., and 10 m.y. time scales. pages 591 – 594, 2001. 10.1130/0091-7613(2001)029<0591:MEOYKY>2.0.CO;2.

C. Kosmas, N. Danalatos, L. Cammeraat, M. Chabart, J. Diamantopoulos, R. Farand, L. Gutierrez, A. Jacob, H. Marques, J. Martinez-Fernandez, A. Mizara, N. Moustakas, J. Nicolau, C. Oliveros, G. Pinna, R. Puddu, J. Puigdefabregas, M. Roxo, A. Simao, G. Stamou, N. Tomasi, D. Usai, and A. Vacca. The effect of land use on runoff and soil erosion rates under Mediterranean conditions. *CATENA*, 29:45–59, 1997. 10.1016/S0341-8162(96)00062-8.

W. B. Langbein and S. A. Schumm. Yield of sediment in relation to mean annual precipitation. *Transactions, American Geophysical Union*, 39:1076 – 1084, 1958. 10.1029/TR039i006p01076.

Z. Liu, M. Pagani, D. Zinniker, R. DeConto, M. Huber, H. Brinkhuis, S. R. Shah, R. M. Leckie, and A. Pearson. Global Cooling During the Eocene-Oligocene Climate Transition. *Science*, 323:1187–1190, 2009. 10.1126/science.1166368.

R. J. Loch. Effects of vegetation cover on runoff and erosion under simulated rain and overland flow on a rehabilitated site on the Meandu Mine, Tarong, Queensland. *Soil Research*, 38:299 – 312, 2000. 10.1071/SR99030.

V. Maksaev and M. Zentilli. Fission Track Thermochronology of the Domeyko Cordillera, Northern Chile: Implications for Andean Tectonics and Porphyry Copper Metallogenesis. 8:56 – 89, 2000.

M. Meinshausen, E. Vogel, A. Nauels, K. Lorbacher, N. Meinshausen, D. M. Etheridge, P. J. Fraser, S. A. Montzka, P. J. Rayner, C. M. Trudinger, P. B. Krummel, U. Beyerle, J. G. Canadell, J. S. Daniel, I. G. Enting, R. M. Law, C. R. Lunder, S. O'Doherty, R. G. Prinn, S. Reimann, M. Rubino, G. J. M. Velders, M. K. Vollmer, R. H. J. Wang, and R. Weiss. Historical greenhouse gas concentrations for climate modelling (CMIP6). *Geoscientific Model Development*, 10:2057–2116, 2017. 10.5194/gmd-10-2057-2017.

M. A. Mohamadi and A. Kavian. Effects of rainfall patterns on runoff and soil erosion in field plots. *International Soil and Water Conservation Research*, 3:273–281, 2015. 10.1016/j.iswcr.2015.10.001.

A. G. Mohammad and M. A. Adam. The impact of vegetative cover type on runoff and soil erosion under different land uses. *CATENA*, 81:97–103, 2010. 10.1016/j.catena .2010.01.008.

A. Molina, G. Govers, V. Vanacker, J. Poesen, E. Zeelmaekers, and F. Cisneros. Runoff generation in a degraded Andean ecosystem: Interaction of vegetation cover and land use. *CATENA*, 71:357–370, 2007. 10.1016/j.catena.2007.04.002.

E. Monnin. Atmospheric CO2 Concentrations over the Last Glacial Termination. *Science*, 291:112–114, 2001. 10.1126/science.291.5501.112.

S. G. Mutz, T. A. Ehlers, M. Werner, G. Lohmann, C. Stepanek, and J. Li. Estimates of late Cenozoic climate change relevant to Earth surface processes in tectonically active orogens. *Earth Surface Dynamics*, 6:271–301, 2018. 10.5194/esurf-6-271-2018.

J. J. Owen, R. Amundson, W. E. Dietrich, K. Nishiizumi, B. Sutter, and G. Chong. The sensitivity of hillslope bedrock erosion to precipitation. *Earth Surface Processes and Landforms*, 36:117–135, 2011. 10.1002/esp.2083.

I. P. Prosser and W. E. Dietrich. Field Experiments on Erosion by Overland Flow and Their Implication for a Digital Terrain Model of Channel Initiation. *Water Resources Research*, 31:2867–2876, 1995. 10.1029/95WR02218.

P. W. Reiners, T. A. Ehlers, S. G. Mitchell, and D. R. Montgomery. Coupled spatial variations in precipitation and long-term erosion rates across the Washington Cascades. *Nature*, 426:645–647, 2003. 10.1038/nature02111.

M. Schaller, F. von Blanckenburg, A. Veldkamp, L. Tebbens, N. Hovius, and P. Kubik. A 30 000 yr record of erosion rates from cosmogenic 10Be in Middle European river terraces. *Earth and Planetary Science Letters*, 204:307–320, 2002. 10.1016/S0012 -821X(02)00951-2.

M. Schaller, T. Ehlers, K. Lang, M. Schmid, and J. Fuentes-Espoz. Addressing the contribution of climate and vegetation cover on hillslope denudation, Chilean Coastal Cordillera (26°–38°S). *Earth and Planetary Science Letters*, 489:111–122, 2018. 10 .1016/j.epsl.2018.02.026.

M. Schmid, T. A. Ehlers, C. Werner, T. Hickler, and J.-P. Fuentes-Espoz. Effect of changing vegetation and precipitation on denudation – Part 2: Predicted landscape response to transient climate and vegetation cover over millennial to million-year timescales. *Earth Surface Dynamics*, 6:859–881, 2018. 10.5194/esurf-6-859-2018.

C. M. Shobe, G. E. Tucker, and K. R. Barnhart. The SPACE 1.0 model: A Landlab component for 2-D calculation of sediment transport, bedrock erosion, and landscape evolution. *Geoscientific Model Development*, 10:4577–4604, 2017. 10.5194/gmd-10-4577 -2017.

B. Smith, I. C. Prentice, and M. T. Sykes. Representation of vegetation dynamics in the modelling of terrestrial ecosystems: Comparing two contrasting approaches within European climate space: Vegetation dynamics in ecosystem models. *Global Ecology and Biogeography*, 10:621–637, 2001. 10.1046/j.1466-822X.2001.t01-1-00256.x.

B. Smith, D. Wårlind, A. Arneth, T. Hickler, P. Leadley, J. Siltberg, and S. Zaehle. Implications of incorporating N cycling and N limitations on primary production in an individual-based dynamic vegetation model. *Biogeosciences*, 11:2027–2054, 2014. 10.5194/bg-11-2027-2014.

U. Stockmann, B. Minasny, and A. B. McBratney. How fast does soil grow? *Geoderma*, 216:48–61, 2014. 10.1016/j.geoderma.2013.10.007.

G. Tucker, S. Lancaster, N. Gasparini, and R. Bras. The channel-hillslope integrated landscape development model (CHILD). In *Landscape Erosion and Evolution Modeling*, pages 349–388. Springer, Boston, MA, 2001.

V. Vanacker, F. von Blanckenburg, G. Govers, A. Molina, J. Poesen, J. Deckers, and P. Kubik. Restoring dense vegetation can slow mountain erosion to near natural benchmark levels. *Geology*, 35:303 – 306, 2007. 10.1130/G23109A.1.

A. D. Weiss. Topographic Position and Landforms Analysis. In *The Nature Conservancy*, Seattle, 2001.

C. Werner, M. Schmid, T. A. Ehlers, J. P. Fuentes-Espoz, J. Steinkamp, M. Forrest, J. Liakka, A. Maldonado, and T. Hickler. Effect of changing vegetation and precipitation on denudation – Part 1: Predicted vegetation composition and cover over the last 21 thousand years along the Coastal Cordillera of Chile. *Earth Surface Dynamics*, 6: 829–858, 2018. 10.5194/esurf-6-829-2018.

O. Yetemen, E. Istanbulluoglu, and A. R. Duvall. Solar radiation as a global driver of hillslope asymmetry: Insights from an ecogeomorphic landscape evolution model. *Water Resources Research*, 51:9843–9861, 2015a. 10.1002/2015WR017103.

O. Yetemen, E. Istanbulluoglu, J. H. Flores-Cervantes, E. R. Vivoni, and R. L. Bras. Ecohydrologic role of solar radiation on landscape evolution. *Water Resources Research*, 51:1127–1157, 2015b. 10/f6574c.

4 Conclusions

Despite the fact that nearly all physical processes on the Earth's surface are modified by the presence of biota, due to the lack of completely abiotic environments on Earth, only little data exists to exactly constrain the controlling parameters of vegetation cover and composition on the erosion and deposition of material on a large scale. Since the early, ground breaking studies which incorporate an empirical approach for the determination of the influence of vegetation cover and climate on erosion and sediment flux [Kramer and Weaver, 1936, Langbein and Schumm, 1958], our current knowledge about vegetation-erosion interactions was expanded by a number of experimental, theoretical and numerical studies [Collins and Bras, 2004, Dietrich and Perron, 2006, Collins and Bras, 2010, Yetemen et al., 2010].

This thesis aims to advance the knowledge in the field of large-scale interactions between climate, vegetation and landscape evolution by developing a numerical model framework which incorporates the hindering effect of vegetation on surface processes as well as precipitation-erosion interactions and a new, innovative, coupled model-scheme which allows for a more precise description of the feedbacks of climate to the plant biosphere and topographic changes.

The investigated hypothesis were:

(I) The effects of vegetation cover on surface processes occur over temporal and spatial scales shorter than geologic processes (e.g. rock uplift, climate change). However, short term vegetation effects on topography are recorded over geologic timescales in the form of variations in different topographic metrics (e.g relief, slope, channel steepness)

(II) Climatic change since the last glacial maximum has lead to an increase in the density and changes in the composition of vegetation cover and has a measurable stabilizing effect on catchment properties such as mean erosion rates, relief or slope in the Chilean Coastal Cordillera.

The following sections gives a brief overview and interpretation about the main findings of the three research packages that belong to this thesis and proposes a scientific outlook about the main problems that need to be addressed in the future to gain more valuable knowledge about vegetation - landscape interactions.

4.1 Summary of results

4.1.1 Evaluation of Hypothesis (I)

The qualitative effect of vegetation cover as a geomorphic agent which slows the erosion of landscapes has been well established by previous works. However, the functional relationships in which these processes work and their quantitative total effect on equilibrium topographies and the transient reactions to changes was so far only insufficiently constrained. Especially the threshold behaviour of erosional processes, which governs if the catchment system is dominated by the erosion-enhancing effect of precipitation or the erosion-dampening effect of vegetation cover still is subject to active research. These problems were approached in this thesis by the development of a numerical model framework, which incorporates vegetation cover into surface process equations, that was calibrated to reproduce the topographic gradient for four areas in the Chilean Coastal Cordillera. These areas were chosen because their lithologic and tectonic similarities allow for better constrainment of free parameters of the landscape evolution model and are situated in four different climate zones with associated differences in vegetation cover which were used as initial parameters for model setup.

The results for these respective model experiments [Schmid et al., 2018] show that it is possible to reproduce the topographic gradient (relief, slope, channel steepness) between the four Earthshape focus areas in steady-state simulations, with only precipitation and vegetation cover as free parameters which were derived from available remote sensing data for individual study areas.

Factual, this gives evidence for the fact that the decreasing effect of vegetation on the efficiency of surface processes poses a large enough magnitude to modify topographies to build up a large equilibrium gradient without differences in tectonic uplift or lithological parameters. Although in previous studies, the effect of vegetation cover on the shape of landscapes was recognized [Istanbulluoglu and Bras, 2005, Dietrich and Perron, 2006] and connections between sediment yield and vegetation covers were drawn [Langbein and Schumm, 1958, Jansson, 1988] but vegetation was mostly described as a second-order control on topographies and erosion rates, behind the thought-of first order control of relief and slope which results from differences in tectonics, lithology or climate [Montgomery and Brandon, 2002, Roering et al., 2007, van Dongen et al., 2019]. This thesis shows that vegetation cover should be taken into account as a first-order control on topographic catchment metrics since it directly affects the mean basin slope angle and the topographic relief.

This is also supported by the findings of the transient experiments, also conducted in Schmid et al. [2018]. The results of the conducted experiments, which include transient shifts either by a instantaneous step-change or a homogeneous oscillation of vegetation cover and mean annual precipitation, both separately and coeval, show that a separate transient change in vegetation cover leads to a reaction of topographic metrics and erosion rates which outweighs the opposed effects of a transient change in associated precipitation values, for arid areas. In humid areas, the difference between the magnitudes of topographic adjustment by either changing vegetation cover or precipitation decreases but still, the effect of vegetation cover is able to compensate the effect of changes in precipitation. This suggests that there exists a fundamental difference in the reaction of areas, situated in different climate zones to changes in their surface vegetation cover and gives hints about a controlling threshold where the main sensitivity of catchment topographies is either dominated by the hindering effect of vegetation or the erosion increasing effect of precipitation. This proposed behaviour is supported by the findings of a study by Moglen et al. [1998] which found a difference in sensitivity of catchment drainage density between arid and humid landscapes, where the reaction of landscapes was mostly controlled by the initial values of precipitation or vegetation.

Regarding the the initial proposed hypothesis that **although the processes that lead to an establishment or change in vegetation cover act on shorter timescales than geologic processes, their net effect on topographies can be of a magnitude that is recorded in topographic metrics**, these results prove that landscapes show distinguished reactions to changes in vegetation cover which act as a first-order control on catchment topography. Arid landscapes generally show a stronger topographic reaction to changes in vegetation cover than humid landscapes, which results from the higher sensitivity of the hillslope diffusion coefficient and the fluvial erodibility to changes in vegetation cover for arid regimes and that the amount of precipitation needed to increase surface vegetation cover increases in more humid areas.

Since it proves difficult in a real-world setting to determine the exact triggers of a topographic reaction because changes in climate and topography mostly happen coeval, numerical modelling, as conducted in this thesis, proves as a valuable tool which may be of help to disentangle the complex erosional history of catchments.

4.1.2 Evaluation of Hypothesis (II)

To build up upon this hypothesis, which shows that while changes in vegetation cover represent a main control in the evolution of catchments but the absolute magnitude is highly dependent on the climatic regime, a more in-depth view about realistic climatic histories and associated changes in vegetation composition and density for individual study areas was developed. The climatic histories and resulting vegetation composition for each individual Earthshape study area are presented in Werner et al. [2018].

The vegetation history, produced by LPJ-GUESS, for the study areas suggests that cumulative catchment vegetation cover for LGM conditions was generally lower than PD cover for all four study areas. However, the increase in vegetation cover over LGM to PD conditions shows different sensitivities to external forcings between the focus areas. While arid to semi-arid focus areas of Pan de Azucar and Santa Gracia show a more pronounced reaction of vegetation cover to changes in precipitation, the more temperate and humid areas of La Campana and Nahuelbuta exhibit a higher sensitivity to changes in temperature. This is also supported by the direct correlation between precipitation and FPC values for individual PFT's: While PFT's which are adjusted and situated in arid climates show a steep, linear increase for FPC values with increasing precipitation whereas the PFT's which are situated in more humid conditions tend to show a less pronounced increase in FPC value for increasing precipitation.

This effect is in agreement with the current, empirical derived relationship between cumulative vegetation cover and mean annual precipitation for the Eartshape focus areas [Schmid et al., 2018] and other studies [Yu et al., 2003, Kong et al., 2017] which suggests that the amount of increase in precipitation, which is needed to increase the vegetation cover, gets higher for more humid conditions.

While the cumulative vegetation cover of the focus areas shows no large shifts as a result of LGM to PD climate forcing, the PFT composition of individual areas shows large adjustments: while desertic environments (cold and hot) dominate LGM conditions, with vegetation mostly composed of grass and shrubs, there is a development towards a higher variety in occuring PFT's , with an increase in tree PFT classes, and therefore development towards forest-like vegetation for PD conditions for La Campana and Nahuelbuta while Santa Gracia area develops vegetation cover from grass to mostly temperate shrubs.

To quantify these findings in terms of the influence of vegetation cover changes on catchment evolution, a coupled model framework was developed which gives a direct feedback between LPJ-GUESS derived vegetation cover values and physical surface processes.

The results from the experiments conducted with this newly developed model framework, presented in [Schmid et al., in prep.] suggest that there exists significant difference in the reaction of the individual Earthshape areas to the climatic history since LGM conditions.

While the very arid and very humid areas of Pan de Azucar and Nahuelbuta show no long-term deviation of mean catchment erosion rate from the steady-state value but only short shifts of mean erosion rates to either smaller or larger values, areas located in more intermediate, mediterranean conditions like Santa Gracia and La Campana show lesser short-term variation in mean erosion rates but a long-term decrease, with mean erosion rates being constantly less than the steady-state uplift value. Compared to other studies [Schaller et al., 2018, van Dongen et al., 2019], which postulate higher values of denudation and catchment-wide erosion for these areas, these results give evidence for an, possibly tectonically triggered, topographic in-equilibrium which results in higher erosion rates than the climate and vegetation history does predict.

Correlation coefficients between erosion rates and either vegetation types or precipitation, show that the effect that vegetation cover exerts on the mean catchment erosion rates increases from North to South, with Nahuelbuta study area showing highest correlation between erosion rates and tree vegetation cover compared to other areas.

Correlation between mean temperature and erosion rates is strongly negative for Pan de Azucar, Santa Gracia and La Campana study area but shows no significant correlation for Nahuelbuta. This leads to an argument, supported by the initial findings in Werner et al. [2018], that vegetation cover is highly sensitive to changes in temperature, in humid environments where the ecosystem is not water-limited but more temperature-limited. Therefore changes in mean annual temperature can indirectly affect the mean catchment-wide erosion rates by modifying catchment vegetation cover.

These results show that the second examined hypothesis, that the **climatic change since the last glacial maximum has lead to an increase in the density and changes in the composition of vegetation cover and has a measurable stabilizing effect on catchment properties in the study areas**, can be accepted with some restrictions: the transient decrease of mean LGM-PD erosion rates for Santa Gracia and La Campana area due to climatic and associated vegetation changes, lead to an increase in topographic elevation, relief and slope in these areas, since the erosion rates are smaller than the proposed tectonic uplift rates, which leads to a positive net mass balance.

However, for Pan de Azucar and Nahuelbuta, the constant LGM to PD mean erosion rates would lead to no long-term adjustment of topographic metrics as a result of short-

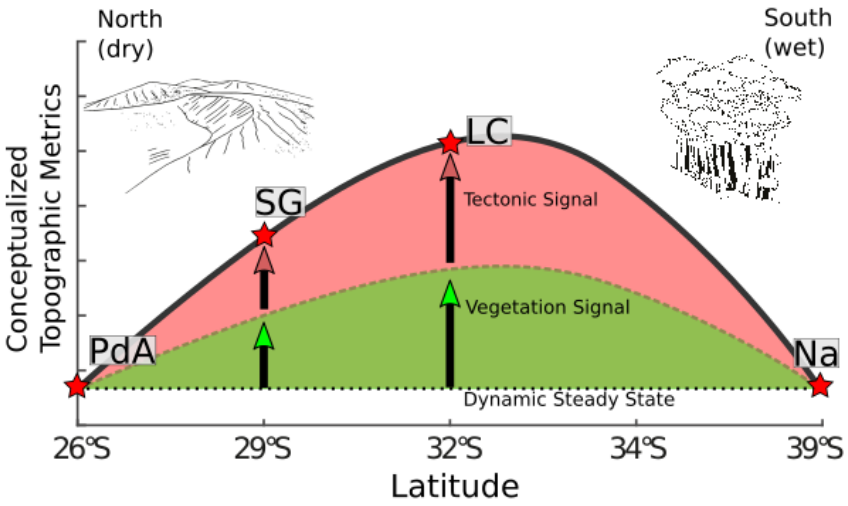

Figure 9: Conceptualized sketch of the topographic gradient along the Earthshape Study areas in the Chilean Coastal Cordilleras (position along the gradient depicted with red stars). This shows the proposed qualitative composition of the topographic signal which is observed between Earthshape study areas of Pan de Azucar in the North and La Campana in the South. Overall change in topographic metrics is proposed to be a composite effect of lowered long-term erosion rates and higher tectonic uplift rates for Santa Gracia and La Campana area.

term variations in erosion rates. This acts as evidence of a climatic and biotic signal within the topographic gradient along the Coastal Cordilleras which modulates the topographic metrics of the Santa Gracia and Nahuelbuta study areas. However, the LGM to PD shifts in mean erosion rates for these areas are not large enough to explain the absolute differences in elevation by their own, so, a second, tectonic signal which modulates the topographic evolution of the study areas is most likely. This proposed combination of the tectonic and biotic influence on the topographic gradient between the focus areas is shown in Fig. 9 in a conceptualized sketch, where the black dotted line depicts the dynamic equilibrium that acts as a baseline topographic state that areas of Pan de Azucar and Nahuelbuta have adjusted to. Green dotted line and green shaded area depict the amount of increase in topographic metrics (e.g relief, slope, channel steepness; compare Fig. 6) that are due to precipitation/vegetation interactions. The black solid line, with the red shaded area depicts the proposed tectonic signal that acts independent from the precipitation/vegetation interactions but magnifies differences between focus areas.

4.2 Scientific Outlook

While the work that was done in this thesis provides new insights about the interaction between climate, vegetation and physical surface processes, there still remains a lot of knowledge to be gained. With more concise empirical work, both in the field or in the laboratory, the parameters than govern the evolution of landscapes within a numerical framework can be more precisely constrained. This would lead to a better numerical approximation of the absolute behaviour of topographies, regarding changes in climate and associated vegetation changes.

The equations that govern the rate of erosion and sediment transport through a landscape are well-tested in the 'classic' use-cases, which focus mainly on the interaction between tectonics and precipitation on topographic dynamics, but there exists little knowledge about the laws of bedrock weathering and material transport on hillslopes, which take into account the coupled effect of precipitation and biota.

This could be resolved by the combination of flume-studies which focus on the effect of submerged vegetation on flow dynamics within a river channel (e.g Järvelä [2002, 2005]) and small-scale experiments on hillslope plots to determine the rate of transport of sediment due to diffusive hillslope processes as a function of precipitation and vegetation (e.g Marston [2010]).

Compared to the strict negative relationship between vegetation cover and the hillslope diffusion coefficient [Istanbulluoglu and Bras, 2005] there are studies that suggest a positive relationship between the efficiency of soil diffusion and an increase in mean annual precipitation cover [Owen et al., 2011, Perron, 2017] or a decoupling of climate and hillslope sediment flux for short timescales due to buffering of sediment in the fluvial network until large flood events occur [Lavé and Burbank, 2004]. This shows the need to explore the processes in which physical external forcings erode and transport sediment within landscapes even more.

In addition to these basic physical processes that still need to be resolved, this thesis shows that the common assumption of landscapes reaching either a topographic or flux steady-state with tectonic uplift does not hold true if changes in climate or vegetation cover shift the landscape into transient adjustments. This shows the need for studies that aim to draw conclusions about tectonic uplift rates by the means of analytically determination of erosion rates, to eventually correct for mismatches due to climatic and vegetational shifts.

5 Appendices

5.1 Data repositories

Paths to the data that was used for simulations and papers. All paths link to the specific directory that contains the data on the ESD-Group Fileserver.

Werner et al. 2018

- Simulations:
  /esd/esd02/data/old_users/mschmid/dissertation_data/simulations/werneretal2018
- Paper:
  /esd/esd02/data/old_users/mschmid/dissertation_data/papers/werneretal2018

Schmid et al. 2018

- Simulations:
  /esd/esd02/data/old_users/mschmid/dissertation_data/simulations/schmidetal2018
- Paper:
  /esd/esd02/data/old_users/mschmid/dissertation_data/papers/schmidetal2018

Schmid et at. - in prepraration

- Simulations:
  /esd/esd02/data/old_users/mschmid/dissertation_data/simulations/schmidetal-inprep
- Paper:
  /esd/esd02/data/old_users/mschmid/dissertation_data/papers/schmidetal-inprep

Source - Code for Landlab Model

- Source Code - Tarball:
  /esd/esd02/data/old_users/mschmid/dissertation_data/source

Dissertation LaTex source files

- Tex-Files and Source-Files:
  /esd/esd02/data/old_users/mschmid/dissertation_data/dissertation

References for Chapters 1, 2 and 4

F. S. Anselmetti, D. A. Hodell, D. Ariztegui, M. Brenner, and M. F. Rosenmeier. Quantification of soil erosion rates related to ancient Maya deforestation. *Geology*, 35:915 – 918, 2007. doi: 10.1130/G23834A.1.

A. Arneth, C. Brown, and M. D. A. Rounsevell. Global models of human decision-making for land-based mitigation and adaptation assessment. *Nature Climate Change*, 4:550–557, 2014. doi: 10.1038/nclimate2250.

G. P. Asner, A. J. Elmore, R. F. Hughes, A. S. Warner, and P. M. Vitousek. Ecosystem structure along bioclimatic gradients in Hawai'i from imaging spectroscopy. *Remote Sensing of Environment*, 96:497–508, 2005. doi: 10.1016/j.rse.2005.04.008.

S. D. Baets, D. Torri, J. Poesen, M. P. Salvador, and J. Meersmans. Modelling increased soil cohesion due to roots with EUROSEM. *Earth Surface Processes and Landforms*, 33: 1948–1963, 2008. doi: 10.1002/esp.1647.

T. Barigah, B. Saugier, M. Mousseau, J. Guittet, and R. Ceulemans. Photosynthesis, leaf area and productivity of 5 poplar clones during their establishment year. *Annales des Sciences Forestières*, 51:613–625, 1994. doi: 10.1051/forest:19940607.

J. Bosch and J. Hewlett. A review of catchment experiments to determine the effect of vegetation changes on water yield and evapotranspiration. *Journal of Hydrology*, 55:3–23, 1982. doi: 10.1016/0022-1694(82)90117-2.

E. O. Box. Plant functional types and climate at the global scale. *Journal of Vegetation Science*, 7:309–320, 1996. doi: 10.2307/3236274.

C. Brandt. The size distribution of throughfall drops under vegetation canopies. *CATENA*, 16:507–524, 1989. doi: 10.1016/0341-8162(89)90032-5.

D. W. Burbank, J. Leland, E. Fielding, R. S. Anderson, N. Brozovic, M. R. Reid, and C. Duncan. Bedrock incision, rock uplift and threshold hillslopes in the northwestern Himalayas. *Nature*, 379:505–510, 1996. doi: 10.1038/379505a0.

V. Chow. *Open-Channel Hydraulics*. New York, McGraw-Hill, 1959.

D. B. Clark, P. C. Olivas, S. F. Oberbauer, D. A. Clark, and M. G. Ryan. First direct landscape-scale measurement of tropical rain forest Leaf Area Index, a key driver of global

primary productivity. *Ecology Letters*, 11:163 – 172, 2007. doi: 10.1111/j.1461-0248.2007.01134.x.

D. B. G. Collins and R. L. Bras. Modeling the effects of vegetation-erosion coupling on landscape evolution. *Journal of Geophysical Research*, 109, 2004. doi: 10.1029/2003JF000028.

D. B. G. Collins and R. L. Bras. Climatic and ecological controls of equilibrium drainage density, relief, and channel concavity in dry lands. *Water Resources Research*, 46, 2010. doi: 10.1029/2009WR008615.

M. H. Costa and J. A. Foley. Water balance of the Amazon Basin: Dependence on vegetation cover and canopy conductance. *Journal of Geophysical Research: Atmospheres*, 102:23973–23989, 1997. doi: 10.1029/97JD01865.

S. J. Dadson, N. Hovius, H. Chen, W. B. Dade, M.-L. Hsieh, S. D. Willett, J.-C. Hu, M.-J. Horng, M.-C. Chen, C. P. Stark, D. Lague, and J.-C. Lin. Links between erosion, runoff variability and seismicity in the Taiwan orogen. *Nature*, 426:648–651, 2003. doi: 10.1038/nature02150.

K. Descheemaeker, J. Nyssen, J. Poesen, D. Raes, M. Haile, B. Muys, and S. Deckers. Runoff on slopes with restoring vegetation: A case study from the Tigray highlands, Ethiopia. *Journal of Hydrology*, 331:219–241, 2006. doi: 10.1016/j.jhydrol.2006.05.015.

W. E. Dietrich and J. T. Perron. The search for a topographic signature of life. *Nature*, 439:411–418, 2006. doi: 10.1038/nature04452.

J. C. Duckworth, M. Kent, and P. M. Ramsay. Plant functional types: An alternative to taxonomic plant community description in biogeography? *Progress in Physical Geography: Earth and Environment*, 24:515–542, 2000. doi: 10.1177/030913330002400403.

T. Dunne, W. Zhang, and B. F. Aubry. Effects of Rainfall, Vegetation, and Microtopography on Infiltration and Runoff. *Water Resources Research*, 27:2271–2285, 1991. doi: 10.1029/91WR01585.

T. Dunne, K. X. Whipple, and B. F. Aubry. Microtopography of hillslopes and initiation of channels by horton overland flow. *Geophysical Monograph Series*, 89:27–44, 1995. doi: 10.1029/GM089p0027.

T. Dunne, D. V. Malmon, and S. M. Mudd. A rain splash transport equation assimilating field and laboratory measurements. *Journal of Geophysical Research*, 115, 2010. doi: 10.1029/2009JF001302.

K. H. Eab, S. Likitlersuang, and A. Takahashi. Laboratory and modelling investigation of root-reinforced system for slope stabilisation. *Soils and Foundations*, 55:1270–1281, 2015. doi: 10.1016/j.sandf.2015.09.025.

K. Ebabu, A. Tsunekawa, N. Haregeweyn, E. Adgo, D. T. Meshesha, D. Aklog, T. Masunaga, M. Tsubo, D. Sultan, A. A. Fenta, and M. Yibeltal. Effects of land use and sustainable land management practices on runoff and soil loss in the Upper Blue Nile basin, Ethiopia. *Science of The Total Environment*, 648:1462–1475, 2019. doi: 10.1016/j.scitotenv.2018.08.273.

C.-C. Fan and C.-F. Su. Role of roots in the shear strength of root-reinforced soils with high moisture content. *Ecological Engineering*, 33:157–166, 2008. doi: 10.1016/j.ecoleng.2008.02.013.

M. Fattet, Y. Fu, M. Ghestem, W. Ma, M. Foulonneau, J. Nespoulous, Y. Le Bissonnais, and A. Stokes. Effects of vegetation type on soil resistance to erosion: Relationship between aggregate stability and shear strength. *CATENA*, 87:60–69, 2011. doi: 10.1016/j.catena.2011.05.006.

R. Ferguson. Estimating critical stream power for bedload transport calculations in gravel-bed rivers. *Geomorphology*, 70:33–41, 2005. doi: 10.1016/j.geomorph.2005.03.009.

R. Fisher, N. McDowell, D. Purves, P. Moorcroft, S. Sitch, P. Cox, C. Huntingford, P. Meir, and F. Ian Woodward. Assessing uncertainties in a second-generation dynamic vegetation model caused by ecological scale limitations. *New Phytologist*, 187:666–681, 2010. doi: 10.1111/j.1469-8137.2010.03340.x.

E. Foufoula-Georgiou, V. Ganti, and W. E. Dietrich. A nonlocal theory of sediment transport on hillslopes. *Journal of Geophysical Research: Earth Surface*, 115, 2010. doi: 10.1029/2009JF001280.

D. J. Furbish, E. M. Childs, P. K. Haff, and M. W. Schmeeckle. Rain splash of soil grains as a stochastic advection-dispersion process, with implications for desert plant-soil interactions and land-surface evolution. *Journal of Geophysical Research*, 114, 2009. doi: 10.1029/2009JF001265.

C. Geißler, P. Kühn, M. Böhnke, H. Bruelheide, X. Shi, and T. Scholten. Splash erosion potential under tree canopies in subtropical SE China. *CATENA*, 91:85–93, 2012. doi: 10.1016/j.catena.2010.10.009.

K. Gran and C. Paola. Riparian vegetation controls on braided stream dynamics. *Water Resources Research*, 37:3275–3283, 2001. doi: 10.1029/2000WR000203.

M. Grosjean, I. Cartajena, M. Geyh, and L. Nuñez. From proxy data to paleoclimate interpretation: The mid-Holocene paradox of the Atacama Desert, northern Chile. *Palaeogeography, Palaeoclimatology, Palaeoecology*, 194:247–258, 2003. doi: 10.1016/S0031-0182(03)00280-3.

P. B. Hairsine and C. W. Rose. Modeling water erosion due to overland flow using physical principles: 1. Sheet flow. *Water Resources Research*, 28:237–243, 1992. doi: 10.1029/91WR02380.

M.-A. Harel, S. Mudd, and M. Attal. Global analysis of the stream power law parameters based on worldwide 10 Be denudation rates. *Geomorphology*, 268:184–196, 2016. doi: 10.1016/j.geomorph.2016.05.035.

T. Hewawasam. Increase of human over natural erosion rates in tropical highlands constrained by cosmogenic nuclides. pages 597 – 600, 2003. doi: 10.1130/0091-7613(2003)031<0597:IOHONE>2.0.CO;2.

A. D. Howard. Badland Morphology and Evolution: Interpretation Using a Simulation Model. *Earth Surface Processes and Landforms*, 22:211–227, 1997. doi: 10.1002/(SICI)1096-9837(199703)22:33.0.CO;2-E.

A. D. Howard and G. Kerby. Channel changes in badlands. *GSA Bulletin*, 94:739 – 752, 1983. doi: https://doi.org/10.1130/0016-7606(1983)94<739:CCIB>2.0.CO;2.

A. D. Howard, W. E. Dietrich, and M. A. Seidl. Modeling fluvial erosion on regional to continental scales. *Journal of Geophysical Research: Solid Earth*, 99:13971–13986, 1994. doi: 10.1029/94JB00744.

E. Istanbulluoglu and R. Bras. Vegetation-modulated landscape evolution: Effects of vegetation on landscape processes, drainage density, and topography. *Journal of Geophysical Research*, 110, 2005. doi: 10.1029/2004JF000249.

E. Istanbulluoglu, D. G. Tarboton, R. T. Pack, and C. H. Luce. Modeling of the interactions between forest vegetation, disturbances, and sediment yields. *Journal of Geophysical Research: Earth Surface*, 109, 2004. doi: 10.1029/2003JF000041.

E. Istanbulluoglu, O. Yetemen, E. R. Vivoni, H. A. Gutiérrez-Jurado, and R. L. Bras. Eco-geomorphic implications of hillslope aspect: Inferences from analysis of landscape morphology in central New Mexico. *Geophysical Research Letters*, 35, 2008. doi: 10.1029/2008GL034477.

A. Jahn. The Soil Creep on Slopes in Different Altitudinal and Ecological Zones of Sudetes Mountains. *Geografiska Annaler. Series A, Physical Geography*, 71:161 – 170, 1989. doi: 10.2307/521387.

M. B. Jansson. A Global Survey of Sediment Yield. *Geografiska Annaler. Series A, Physical Geography*, 70:81 – 99, 1988. doi: 10.2307/521127.

J. Järvelä. Flow resistance of flexible and stiff vegetation: A flume study with natural plants. *Journal of Hydrology*, 269:44–54, 2002. doi: 10.1016/S0022-1694(02)00193-2.

J. Järvelä. Effect of submerged flexible vegetation on flow structure and resistance. *Journal of Hydrology*, 307:233–241, 2005. doi: 10.1016/j.jhydrol.2004.10.013.

X. Jiongxin. Precipitation–vegetation coupling and its influence on erosion on the Loess Plateau, China. *CATENA*, 64:103–116, 2005. doi: 10.1016/j.catena.2005.07.004.

D. K. C. Jones. The Evolution of Hillslope Processes. In D. L. Higgitt and E. M. Lee, editors, *Geomorphological Processes and Landscape Change*, pages 61–89. Blackwell Publishers Ltd, Oxford, UK, 2001. ISBN 978-0-470-71283-2 978-0-631-22273-6.

R. H. Kadlec. Overland Flow in Wetlands: Vegetation Resistance. *Journal of Hydraulic Engineering*, 116:691–706, 1990. doi: 10.1061/(ASCE)0733-9429(1990)116:5(691).

J. O. Kaplan, K. M. Krumhardt, and N. Zimmermann. The prehistoric and preindustrial deforestation of Europe. *Quaternary Science Reviews*, 28:3016–3034, 2009. doi: 10.1016/j.quascirev.2009.09.028.

J. T. Kerr and M. Ostrovsky. From space to species: Ecological applications for remote sensing. *Trends in Ecology & Evolution*, 18:299–305, 2003. doi: 10.1016/S0169-5347(03)00071-5.

N. K. Kokutse, A. G. T. Temgoua, and Z. Kavazović. Slope stability and vegetation: Conceptual and numerical investigation of mechanical effects. *Ecological Engineering*, 86: 146–153, 2016. doi: 10.1016/j.ecoleng.2015.11.005.

D. Kong, Q. Zhang, V. P. Singh, and P. Shi. Seasonal vegetation response to climate change in the Northern Hemisphere (1982–2013). *Global and Planetary Change*, 148:1–8, 2017. doi: 10.1016/j.gloplacha.2016.10.020.

J. Kramer and J. E. Weaver. Relative Efficiency of Roots and Tops of Plants in Protecting . the Soil from Erosion. *Science*, page 96, 1936. doi: 10.1126/science.82.2128.354.

D. Lague. The stream power river incision model: Evidence, theory and beyond. *Earth Surface Processes and Landforms*, 39:38–61, 2014. doi: 10.1002/esp.3462.

D. Lague, P. Davy, and A. Crave. Estimating uplift rate and erodibility from the area-slope relationship: Examples from Brittany (France) and numerical modelling. *Physics and Chemistry of the Earth, Part A: Solid Earth and Geodesy*, 25:543–548, 2000. doi: 10.1016/S1464-1895(00)00083-1.

D. Lal. Cosmic ray labeling of erosion surfaces: In situ nuclide production rates and erosion models. *Earth and Planetary Science Letters*, 104:424–439, 1991. doi: 10.1016/0012-821X(91)90220-C.

W. B. Langbein and S. A. Schumm. Yield of sediment in relation to mean annual precipitation. *Eos, Transactions American Geophysical Union*, 39:1076–1084, 1958. doi: 10.1029/TR039i006p01076.

I. J. Larsen and D. R. Montgomery. Landslide erosion coupled to tectonics and river incision. *Nature Geoscience*, 5:468–473, 2012. doi: 10.1038/ngeo1479.

J. Lavé and D. Burbank. Denudation processes and rates in the Transverse Ranges, southern California: Erosional response of a transitional landscape to external and anthropogenic forcing. *Journal of Geophysical Research: Earth Surface*, 109, 2004. doi: 10.1029/2003JF000023.

J. W. Leverenz and T. M. Hinckley. Shoot structure, leaf area index and productivity of evergreen conifer stands. *Tree Physiology*, 6:135–149, 1990. doi: 10.1093/treephys/6.2.135.

T. Liang, A. Bengough, J. Knappett, D. MuirWood, K. Loades, P. Hallett, D. Boldrin, A. Leung, and G. Meijer. Scaling of the reinforcement of soil slopes by living plants in a geotechnical centrifuge. *Ecological Engineering*, 109:207–227, 2017. doi: 10.1016/j.ecoleng.2017.06.067.

J. A. Ludwig, B. P. Wilcox, D. D. Breshears, D. J. Tongway, and A. C. Imeson. Vegetation patches and runoff-erosion as interacting ecohydrological processes in semiarid landscapes. *Ecology*, 86:288–297, 2005. doi: 10.1890/03-0569.

A. Maldonado and C. Villagrán. Climate variability over the last 9900 cal yr BP from a swamp forest pollen record along the semiarid coast of Chile. *Quaternary Research*, 66: 246–258, 2006. doi: 10.1016/j.yqres.2006.04.003.

R. Manning. On the flow of water in open channels and pipes. *Inst. Civil Engineers Trans.*, 20:161 – 207, 1891.

R. A. Marston. Geomorphology and vegetation on hillslopes: Interactions, dependencies, and feedback loops. *Geomorphology*, 116:206–217, 2010. doi: 10.1016/j.geomorph.2009.09.028.

K. Michaelides, D. Lister, J. Wainwright, and A. J. Parsons. Vegetation controls on small-scale runoff and erosion dynamics in a degrading dryland environment. *Hydrological Processes*, 23:1617–1630, 2009. doi: 10.1002/hyp.7293.

G. E. Moglen, E. A. B. Eltahir, and R. L. Bras. On the sensitivity of drainage density to climate change. *Water Resources Research*, 34:855–862, 1998. doi: 10.1029/97WR02709.

D. R. Montgomery and M. T. Brandon. Topographic controls on erosion rates in tectonically active mountain ranges. *Earth and Planetary Science Letters*, 201:481–489, 2002. doi: 10.1016/S0012-821X(02)00725-2.

A. B. Murray and C. Paola. Modelling the effect of vegetation on channel pattern in bedload rivers. *Earth Surface Processes and Landforms*, 28:131–143, 2003. doi: 10.1002/esp.428.

A. B. Murray, M. A. F. Knaapen, M. Tal, and M. L. Kirwan. Biomorphodynamics: Physical-biological feedbacks that shape landscapes. *Water Resources Research*, 44, 2008. doi: 10.1029/2007WR006410.

S. G. Mutz, T. A. Ehlers, M. Werner, G. Lohmann, C. Stepanek, and J. Li. Estimates of late Cenozoic climate change relevant to Earth surface processes in tectonically active orogens. *Earth Surface Dynamics*, 6:271–301, 2018. doi: 10.5194/esurf-6-271-2018.

M. Nachabe, N. Shah, M. Ross, and J. Vomacka. Evapotranspiration of Two Vegetation Covers in a Shallow Water Table Environment. *Soil Science Society of America Journal*, 69:492 – 499, 2005. doi: 10.2136/sssaj2005.0492.

V. Nikora, S. Larned, N. Nikora, K. Debnath, G. Cooper, and M. Reid. Hydraulic Resistance due to Aquatic Vegetation in Small Streams: Field Study. *Journal of Hydraulic Engineering*, 134:1326–1332, 2008. doi: 10.1061/(ASCE)0733-9429(2008)134:9(1326).

J. E. Norris, A. Stokes, S. B. Mickovski, E. Cammeraat, R. van Beek, B. C. Nicoll, and A. Achim, editors. *Slope Stability and Erosion Control: Ecotechnological Solutions*. Springer Netherlands, Dordrecht, 2008. ISBN 978-1-4020-6675-7. doi: 10.1007/978-1-4020-6676-4.

V. Operstein and S. Frydman. The influence of vegetation on soil strength. *Ground Improvement*, 4:81 – 89, 2000.

J. J. Owen, R. Amundson, W. E. Dietrich, K. Nishiizumi, B. Sutter, and G. Chong. The sensitivity of hillslope bedrock erosion to precipitation. *Earth Surface Processes and Landforms*, 36:117–135, 2011. doi: 10.1002/esp.2083.

Peng Gong, Ruiliang Pu, G. Biging, and M. Larrieu. Estimation of forest leaf area index using vegetation indices derived from hyperion hyperspectral data. *IEEE Transactions on Geoscience and Remote Sensing*, 41:1355–1362, 2003. doi: 10.1109/TGRS.2003.812910.

J. T. Perron. Climate and the Pace of Erosional Landscape Evolution. *Annual Review of Earth and Planetary Sciences*, 45:561–591, 2017. doi: 10/gdwrpm.

I. C. Prentice, M. T. Sykes, and W. Cramer. A simulation model for the transient effects of climate change on forest landscapes. *Ecological Modelling*, 65:51–70, 1993. doi: 10.1016/0304-3800(93)90126-D.

F. Preti and F. Giadrossich. Root reinforcement and slope bioengineering stabilization by Spanish Broom (Spartium junceum L.). *Hydrol. Earth Syst. Sci.*, 13:1713 – 1726, 2009.

I. P. Prosser and W. E. Dietrich. Field Experiments on Erosion by Overland Flow and Their Implication for a Digital Terrain Model of Channel Initiation. *Water Resources Research*, 31:2867–2876, 1995. doi: 10.1029/95WR02218.

M. M. Riestenberg and S. Sovonick-Dunford. The role of woody vegetation in stabilizing slopes in the Cincinnati area, Ohio. *GSA Bulletin*, 94:506 – 518, 1983. doi: 10.1130/0016-7606(1983)94<506:TROWVI>2.0.CO;2.

J. Robl, S. Hergarten, and G. Prasicek. The topographic state of fluvially conditioned mountain ranges. *Earth-Science Reviews*, 168:190–217, 2017. doi: 10.1016/j.earscirev.2017.03.007.

J. J. Roering, P. Almond, and P. Tonkin. Soil transport driven by biological processes over millennial time scales. 30:1115 – 1118, 2002. doi: 10.1130/0091-7613(2002)030<1115:STDBBP>2.0.CO;2.

J. J. Roering, K. M. Schmidt, J. D. Stock, W. E. Dietrich, and D. R. Montgomery. Shallow landsliding, root reinforcement, and the spatial distribution of trees in the Oregon Coast Range. *Canadian Geotechnical Journal*, 40:237–253, 2003. doi: 10.1139/t02-113.

J. J. Roering, J. T. Perron, and J. W. Kirchner. Functional relationships between denudation and hillslope form and relief. *Earth and Planetary Science Letters*, 264:245–258, 2007. doi: 10.1016/j.epsl.2007.09.035.

T. Saedi, M. Shorafa, M. Gorji, and B. Khalili Moghadam. Indirect and direct effects of soil properties on soil splash erosion rate in calcareous soils of the central Zagross, Iran: A laboratory study. *Geoderma*, 271:1–9, 2016. doi: 10.1016/j.geoderma.2016.02.008.

M. Schaller, T. Ehlers, K. Lang, M. Schmid, and J. Fuentes-Espoz. Addressing the contribution of climate and vegetation cover on hillslope denudation, Chilean Coastal Cordillera (26°–38°S). *Earth and Planetary Science Letters*, 489:111–122, 2018. doi: 10/gdgr8k.

M. Schmid, T. A. Ehlers, C. Werner, T. Hickler, and J.-P. Fuentes-Espoz. Effect of changing vegetation and precipitation on denudation – Part 2: Predicted landscape response to transient climate and vegetation cover over millennial to million-year timescales. *Earth Surface Dynamics*, 6:859–881, 2018. doi: 10.5194/esurf-6-859-2018.

M. Schmid, T. A. Ehlers, C. Werner, and T. Hickler. Effect of LGM to PD climatic change on landform vegetation cover and erosional feedbacks in the Chilean Coastal Cordillera. in prep.

A. Simon and A. J. C. Collison. Quantifying the mechanical and hydrologic effects of riparian vegetation on streambank stability. *Earth Surface Processes and Landforms*, 27: 527–546, 2002. doi: 10.1002/esp.325.

S. Sitch, B. Smith, I. C. Prentice, A. Arneth, A. Bondeau, W. Cramer, J. O. Kaplan, S. Levis, W. Lucht, M. T. Sykes, K. Thonicke, and S. Venevsky. Evaluation of ecosystem dynamics, plant geography and terrestrial carbon cycling in the LPJ dynamic global vegetation model. *Global Change Biology*, 9:161–185, 2003. doi: 10.1046/j.1365-2486.2003.00569.x.

B. Smith, I. C. Prentice, and M. T. Sykes. Representation of vegetation dynamics in the modelling of terrestrial ecosystems: Comparing two contrasting approaches within European climate space: Vegetation dynamics in ecosystem models. *Global Ecology and Biogeography*, 10:621–637, 2001. doi: 10.1046/j.1466-822X.2001.t01-1-00256.x.

N. P. Snyder, K. X. Whipple, G. E. Tucker, and D. J. Merritts. Channel response to tectonic forcing: Field analysis of stream morphology and hydrology in the Mendocino triple junction region, northern California. *Geomorphology*, 53:97–127, 2003. doi: 10.1016/S0169-555X(02)00349-5.

J. D. Stock and D. R. Montgomery. Geologic constraints on bedrock river incision using the stream power law. *Journal of Geophysical Research: Solid Earth*, 104:4983–4993, 1999. doi: 10.1029/98JB02139.

M. Stocking and H. Elwell. Vegetation and erosion: A review. *Scottish Geographical Magazine*, 92:4–16, 1976. doi: 10.1080/00369227608736322.

A. Stokes, J. E. Norris, L. P. H. van Beek, T. Bogaard, E. Cammeraat, S. B. Mickovski, A. Jenner, A. Di Iorio, and T. Fourcaud. How Vegetation Reinforces Soil on Slopes. In J. E. Norris, A. Stokes, S. B. Mickovski, E. Cammeraat, R. van Beek, B. C. Nicoll, and A. Achim, editors, *Slope Stability and Erosion Control: Ecotechnological Solutions*, pages 65–118. Springer Netherlands, Dordrecht, 2008. ISBN 978-1-4020-6675-7 978-1-4020-6676-4. doi: 10.1007/978-1-4020-6676-4_4.

G. E. Tucker and G. R. Hancock. Modelling landscape evolution. *Earth Surface Processes and Landforms*, 35:28–50, 2010. doi: 10.1002/esp.1952.

G. E. Tucker and R. L. Slingerland. Erosional dynamics, flexural isostasy, and long-lived escarpments: A numerical modeling study. *Journal of Geophysical Research: Solid Earth*, 99:12229–12243, 1994. doi: 10.1029/94JB00320.

R. van Dongen, D. Scherler, H. Wittmann, and F. von Blanckenburg. Cosmogenic 10Be in river sediment: Where grain size matters and why. *Earth Surface Dynamics*, 7:393–410, 2019. doi: 10.5194/esurf-7-393-2019.

W. Vannoppen, S. De Baets, J. Keeble, Y. Dong, and J. Poesen. How do root and soil characteristics affect the erosion-reducing potential of plant species? *Ecological Engineering*, 109:186–195, 2017. doi: 10.1016/j.ecoleng.2017.08.001.

F. von Blanckenburg. The control mechanisms of erosion and weathering at basin scale from cosmogenic nuclides in river sediment. *Earth and Planetary Science Letters*, 242: 224–239, 2006. doi: 10.1016/j.epsl.2005.11.017.

Q. Wang, S. Adiku, J. Tenhunen, and A. Granier. On the relationship of NDVI with leaf area index in a deciduous forest site. *Remote Sensing of Environment*, 94:244–255, 2005. doi: 10.1016/j.rse.2004.10.006.

C. Werner, M. Schmid, T. A. Ehlers, J. P. Fuentes-Espoz, J. Steinkamp, M. Forrest, J. Liakka, A. Maldonado, and T. Hickler. Effect of changing vegetation and precipitation on denudation – Part 1: Predicted vegetation composition and cover over the last 21 thousand years along the Coastal Cordillera of Chile. *Earth Surface Dynamics*, 6:829–858, 2018. doi: 10.5194/esurf-6-829-2018.

K. X. Whipple, E. Kirby, and S. H. Brocklehurst. Geomorphic limits to climate-induced increases in topographic relief. *Nature*, 401:39–43, 1999. doi: 10.1038/43375.

G. Willgoose. Mathematical Modeling of Whole Landscape Evolution. *Annual Review of Earth and Planetary Sciences*, 33:443–459, 2005. doi: 10.1146/annurev.earth.33.092203.122610.

A. M. Williams. Human Impact on the Nile Basin: Past, Present and Future. In *The Nile.*, Monographiae Biologicae, pages 771 – 779. 2009. ISBN 978-1-4020-9725-6.

Z. Xin, J. Xu, and W. Zheng. Spatiotemporal variations of vegetation cover on the Chinese Loess Plateau (1981–2006): Impacts of climate changes and human activities. *Science in China Series D: Earth Sciences*, 51:67–78, 2008. doi: 10.1007/s11430-007-0137-2.

S. Yang, H. Li, T. Ysebaert, T. Bouma, W. Zhang, Y. Wang, P. Li, M. Li, and P. Ding. Spatial and temporal variations in sediment grain size in tidal wetlands, Yangtze Delta:

On the role of physical and biotic controls. *Estuarine, Coastal and Shelf Science*, 77: 657–671, 2008. doi: 10.1016/j.ecss.2007.10.024.

O. Yetemen, E. Istanbulluoglu, and E. R. Vivoni. The implications of geology, soils, and vegetation on landscape morphology: Inferences from semi-arid basins with complex vegetation patterns in Central New Mexico, USA. *Geomorphology*, 116:246–263, 2010. doi: 10.1016/j.geomorph.2009.11.026.

F. Yu, K. P. Price, J. Ellis, and P. Shi. Response of seasonal vegetation development to climatic variations in eastern central Asia. *Remote Sensing of Environment*, 87:42–54, 2003. doi: 10.1016/S0034-4257(03)00144-5.

L. Zhang, W. R. Dawes, and G. R. Walker. Response of mean annual evapotranspiration to vegetation changes at catchment scale. *Water Resources Research*, 37:701–708, 2001. doi: 10.1029/2000WR900325.